TESIS DE LA UNIVERSIDAD DE ZARAGOZA

2021 299

Víctor Javier Llorente Lázaro

An Accurate and Robust Numerical Scheme for Transport Equations

Director/es
Pascau Benito, Antonio

ISSN 2254-7606

Prensas de la Universidad
Universidad Zaragoza

ISSN 2254-7606

Universidad Zaragoza
1542

Tesis Doctoral

AN ACCURATE AND ROBUST NUMERICAL SCHEME FOR TRANSPORT EQUATIONS

Autor

Víctor Javier Llorente Lázaro

Director/es

Pascau Benito, Antonio

UNIVERSIDAD DE ZARAGOZA
Escuela de Doctorado

Programa de Doctorado en Ingeniería Mecánica

2020

PhD thesis by

VÍCTOR JAVIER LLORENTE LÁZARO

Supervisor - Dr. ANTONIO PASCAU BENITO

An Accurate and Robust Numerical Scheme for Transport Equations

Universidad Zaragoza

Mechanical Engineering doctoral program, JULY 2020

Universidad Zaragoza

DOCTORAL THESIS

An accurate and robust numerical scheme for transport equations

Author:
Víctor Javier Llorente Lázaro

Supervisor:
Dr. Antonio Pascau Benito

A thesis submitted in fulfilment of the requirements
for the degree of PhD
in the

Mechanical Engineering doctoral program

UNIVERSITY OF ZARAGOZA

July 2020

Talking once with friends, one of them asked me *"What is CFD?"*. I aswered him *"CFD is the only powerful mathematical tool that turns a fully-qualified engineer into a five-year-old child drawing colours on his laptop screen"*.

Víctor Javier Llorente Lázaro

UNIVERSITY OF ZARAGOZA

Abstract

School of Engineering and Architecture (EINA)
Deparment of Science & Technology of Materials and Fluids
Computational Fluid Mechanics Group

PhD

An accurate and robust numerical scheme for transport equations

by Víctor Javier Llorente Lázaro

In this thesis, we present a novel discretization technique for transport equations in convection-diffusion problems across the whole range of Péclet numbers. The discretization employs the exact flux of a steady-state one-dimensional transport equation to derive a discrete equation with a three-point stencil in one-dimensional problems and a five-point stencil in two-dimensional ones. With "exact flux" it is meant that the exact solution can be obtained as a function of integrals of some fluid and flow parameters, even if these parameters are variable across a control volume. High-order quadratures are used to achieve numerical results close to machine-accuracy even with coarse grids.

As the discretization is essentially one-dimensional, getting the machine-accurate solution of multidimensional problems is not guaranteed even in cases where the integrals along each Cartesian coordinate have a primitive. In this regard, the main contribution of this thesis consists in a simple and elegant way of getting solutions in multidimensional problems while still using the one-dimensional formulation. Moreover, if the problem is such that the solution is machine-accurate in the one-dimensional problem along coordinate lines, it will also be for the multidimensional domain.

UNIVERSIDAD DE ZARAGOZA

Resumen

Escuela de Ingeniería y Arquitectura (EINA)
Departamento de Ciencia y Tecnología de Materiales y Fluidos
Grupo de Fluidodinamica Computacional

Doctor

An accurate and robust numerical scheme for transport equations

por Víctor Javier Llorente Lázaro

En esta tesis se presenta una nueva técnica de discretización para ecuaciones de transporte en problemas de convección-difusión para el rango completo de números de Péclet. La discretización emplea el flujo exacto de una ecuación de transporte unidimensional en estado estacionario para deducir una ecuación discreta de tres puntos en problemas unidimensionales y cinco puntos en problemas bidimensionales. Con "flujo exacto" se entiende que se puede obtener la solución exacta en función de integrales de algunos parámetros del fluido y flujo, incluso si estos parámetros son variables en un volumen de control. Las cuadraturas de alto orden se utilizan para lograr resultados numéricos cercanos a la precisión de la máquina, incluso con mallas bastas.

Como la discretización es esencialmente unidimensional, no está garantizada una solución con precisión de máquina para problemas multidimensionales, incluso en los casos en que las integrales a lo largo de cada coordenada cartesiana tienen una primitiva. En este sentido, la contribución principal de esta tesis consiste en una forma simple y elegante de obtener soluciones en problemas multidimensionales sin dejar de utilizar la formulación unidimensional. Además, si el problema es tal que la solución tiene precisión de máquina en el problema unidimensional a lo largo de las líneas coordenadas, también la tendrá para el dominio multidimensional.

Acknowledgements

I would like to start my thankfulness to my supervisor, Prof Antonio Pascau Benito, for giving me the chance to make my first move in research and to learn how amazing and odd can be this discrete world of Computational Fluid Dynamics.

Also, thanks to Profs Francisco Alcrudo, Esteban Calvo, Ignacio García and Luis Manuel Cerecedo for getting interested in my research and encouraging me to finish the thesis. Also to Müslüm Arıcı for his patience during the short stay at Unizar and reporting a positive mark of this thesis, and Chuan for all those days playing chess on our mobile phones.

Thanks to every person from the Computational Hydraulics Group and their warm atmosphere research: Profs Pilar García Navarro, Pilar Brufau and Javier Murillo, as well as its members that I have met during all those years: Mario, Javi, Daniel, Isabel, Eva, Jesus, Raúl and Pablo. Gratefulness to Geovanny for his happiness transmission and to Adrian with whom I shared a lot of interesting discussions about our thesis and encouraged me to go to my first conference living new experiences.

I want to thank especially Sergio for his valuable friendship. Above all for those squabbles on History, hiking-trails, trips, advice, support and for making me realise that when Aragonese go into a place we should move all the way into it and not get stuck in front of the door. I hope that in the future we will take many more memorable moments.

I don't forget to thank all CASA members who give me a cosy stay in Eindhoven, the Netherlands. In particular to Martijn and Jan who gave me remarks and comments for improving this thesis.

To all my friends especially Alberto, Andrea, Andrés and Roberto: thanks for being there, supporting me and being interested in my work and future. We learned a lot of life philosophy in Leiden.

Finally, I express my love to my parents and grandparents who have always helped in challenging times and wanted more than me to have this thesis finished.

Contents

List of Figures

List of Tables

Abbreviations

1D	one-**D**imensional
2D	two-**D**imensional
ADER	**A**rbitrary high-order **Der**ivative
ADI	**A**lternating **D**irection **I**mplicit
BC	**B**oundary **C**ondition
BVP	**B**oundary **V**alue **P**roblem
CDS	**C**entral-**D**ifferencing **S**cheme
CS	**C**ompact **S**cheme
CCS	**C**entral **C**ompact **S**cheme
CFD	**C**omputational **F**luid **D**ynamics
CIR	**C**ompact **I**ntegration **R**ules
CV	**C**onstants **V**ariation
DG	**D**iscontinuous **G**alerkin
DGSEM	**D**iscontinuous **G**alerkin **S**pectral **E**lement **M**ethod
ENATE	**E**nhanced **N**umerical **A**pproximation for a **T**ransport **E**quation
ENO	**E**ssentially **N**on-**O**scillatory
EoS	**E**quations **o**f **S**tate
FaP	**F**luxes **a**s **P**seudo-sources
FCT	**F**lux **C**orrected **T**ransport
FD	**F**inite **D**ifference
FE	**F**inite **E**lement
FV	**F**inite **V**olume
FV-CF	**F**inite **V**olume-**C**omplete **F**lux
GL	**G**auss-**L**egendre
IV	**I**nitial **V**alue
LHS	**L**eft-**H**and **S**ide
LOAD	**LO**cally **A**nalytic **D**ifferencing
MUSCL	**M**onotonic **U**pstream-centered **S**cheme for **C**onservation **L**aws
NFD	**N**on-standard **F**inite **D**ifference
NS	**N**avier-**S**tokes
NVD	**N**ormalized **V**ariable **D**iagram
ODE	**O**rdinary **D**ifferential **E**quation
PC	**P**redictor-**C**orrector
PDE	**P**artial **D**ifferential **E**quation
PECE	**P**redict-**E**valuate-**C**orrect-**E**valuate
PDMA	**P**enta-**D**iagonal **M**atrix **A**lgorithm
PG	**P**etrov-**G**alerkin
QUICK	**Q**uadratic **U**pstream **I**nterpolation for **C**onvective **K**inematics
REMEDIES	**R**apid **E**valuation of **M**ultidimensional **E**quations with **D**istinct **I**ntegrals as **E**xtra **S**ources
RHS	**R**ight-**H**and **S**ide
RK	**R**unge-**K**utta
SE	**S**pectral **E**lement

SFC	**S**tream-**F**unction **C**oordinates
SHARP	**S**imple **H**igh **A**ccuracy **R**esolution **P**rogram
SMART	**S**harp and **M**onotonic **A**lgorithm for **R**ealistic **T**ransport
SPH	**S**moothed **P**article **H**ydrodynamics
SUDS	**S**kew **U**pwind **D**ifferencing **S**cheme
TDMA	**T**ri-**D**iagonal **M**atrix **A**lgorithm or Thomas Algorithm
TE	**T**ransport **E**quation
TVD	**T**otal **V**ariation **D**isminishing
UC	**U**ndetermined **C**oefficient
VE	**V**irtual **E**lement
VoF	**V**olume **o**f **F**luid
WENO	**W**eighted **E**ssentially **N**on-**O**scillatory

Nomenclature

Symbol	Name or description	SI Units
a_i	coefficients of Hermite splines	-
a_k, a, b, c, d, e, g	coefficient in the RHS of CCS and CIR	-
A_C, $A_{x\,C}$	central influence coefficient in x direction	$\mathrm{kg\,m^{-2}\,s^{-1}}$
$A_{y\,C}$	central influence coefficient in y direction	$\mathrm{kg\,m^{-2}\,s^{-1}}$
A_W, A_E, A_S, A_N	west/east/south/north influence coefficient	$\mathrm{kg\,m^{-2}\,s^{-1}}$
b_C, $b_{x\,C}$, $b^n_{x\,C}$	discrete source term in x direction	$[\phi]\,\mathrm{kg\,m^{-2}\,s^{-1}}$
$b_{y\,C}$	discrete source term in y direction	$[\phi]\,\mathrm{kg\,m^{-2}\,s^{-1}}$
$b^n_{\eta\,C}$	discrete source term in η direction	$[\phi]\,\mathrm{kg\,m^{-2}\,s^{-1}}$
B, B_0	Bernoulli function	-
B_i	recurrence Bernoulli function	-
c	scaling factor	$\mathrm{m\,s^{-1}}$
$\mathcal{C}$	Burgers' constant	-
$C^\star_1$	first constant for nonlinear problems	-
$C^\star_2$	second constant for nonlinear problems	$\mathrm{kg^{-1}\,m\,s^2}$
C_o	constant of integration	-
$\overline{E}$	exponential factor	-
E_H	Hermite error	$[f]\,\mathrm{m^{-1}}$
f, g, h	generic functions	$[f]$, $[g]$, $[h]$
f_{E}	exponential function	-
F	inhomogeneous solution	-
$\mathcal{F}$, $\mathcal{F}_x$	flux in x direction	$[\phi]\,\mathrm{kg\,m^{-2}\,s^{-1}}$
$\mathcal{F}_y$	flux in y direction	$[\phi]\,\mathrm{kg\,m^{-2}\,s^{-1}}$
$\mathcal{F}_\eta$	flux in η direction	$[\phi]\,\mathrm{kg\,m^{-2}\,s^{-1}}$
$\mathcal{F}^\phi$	homogeneous flux	$[\phi]\,\mathrm{kg\,m^{-2}\,s^{-1}}$
$\mathcal{F}^S$	inhomogeneous flux	$[\phi]\,\mathrm{kg\,m^{-2}\,s^{-1}}$
$\mathcal{F}^\star_{x(1-2)}$	numerical flux in x direction at $\star$ time	$[\phi]\,\mathrm{kg\,m^{-2}\,s^{-1}}$
G	Green's function	-
H_m	Hermite polynomial	-
i, j, k, l, s	indexs	-
$\mathcal{J}$	Jacobian of the transformation	$[\mathcal{J}]$
l, q	order	-
m	Hermite order	-
m_1, m_2, q_1, q_2	lower/upper bounds in CCS and CIR	-
n	number of nodes in a line of a mesh	-
N_{nodes}	number of computed nodes	-
N_{lines}	number of lines in the mesh	-
$\mathcal{N}$	neighbour point set in 2D	-
$\mathcal{N}_x$	west and east point set	-
$\mathcal{N}_y$	south and north point set	-
p	number of points	-
P, P_x	Péclet number in x direction	-
P_0, $P_{x\,0}$	reference Péclet number in x direction	-

P_y	Péclet number in y direction	-
$P_{y\,0}$	reference Péclet number in y direction	-
r_a	aspect ratio of the mesh	-
r_f	flux derivative ratio	-
S, S_x	source term in x direction	$[\phi]\,\mathrm{kg\,m^{-3}\,s^{-1}}$
S_y	source term in y direction	$[\phi]\,\mathrm{kg\,m^{-3}\,s^{-1}}$
S_η	source term in η direction	$[\phi]\,\mathrm{kg\,m^{-3}\,s^{-1}}$
t	temporal dimension	s
u	velocity field in x direction	$\mathrm{m\,s^{-1}}$
v	velocity field in y direction	$\mathrm{m\,s^{-1}}$
w	IGE ratio	-
w_1, w_2	diffusion factors in nonlinear problems	-
w_i	Gauss weight	-
x, y	spatial dimensions	m
$\tilde{x}$, $\tilde{y}$	uniform mapping	m
$x_{\mathrm{N}\,1}$, $x_{\mathrm{N}\,2}$	principal axis of numerical diffusion	m
$x^\star$, $\xi^\star$	number somewhere between a and b	m
z	generic variable	$[z]$
α_k, α, β	coefficient in the LHS of CCS and CIR	-
β	redistribution function	$[\phi]\,\mathrm{kg\,m^{-3}\,s^{-1}}$
β_C^{ini}	initial value of β at a central node	$[\phi]\,\mathrm{kg\,m^{-3}\,s^{-1}}$
γ	angle between principal directions	rad
γ_1, γ_2	Hermite first stencil-coefficient	m
Γ	diffusion parameter	$\mathrm{kg\,m^{-1}\,s^{-1}}$
$\Gamma_{\mathrm{N}\,1}$, $\Gamma_{\mathrm{N}\,2}$	principal numerical diffusivities	$\mathrm{kg\,m^{-1}\,s^{-1}}$
$\Gamma_{\mathrm{N}\,1\,\mathrm{max}}$	first principal numerical diffusivity (maximum)	$\mathrm{kg\,m^{-1}\,s^{-1}}$
δ_1, δ_2	Hermite second stencil-coefficient	$\mathrm{m^2}$
Δx, Δy, $\Delta\eta$	interval size	m
$\Delta\phi$	ϕ-value difference at the interval edges	$[\phi]$
ΔP	Péclet number based on u varations	-
ΔP_0	reference Péclet number based on u varations	-
$\Delta\beta^\star$	increment of the β field at $\star$ time	$[\phi]\,\mathrm{kg\,m^{-3}\,s^{-1}}$
$\Delta\phi_2^\star$	increment of $\phi_2^\star$ at $\star$ time	$[\phi]$
ϵ_1, ϵ_2	Hermite third stencil-coefficient	$\mathrm{m^3}$
ϵ	tolerance	-
ζ_1, ζ_2	Hermite fourth stencil-coefficient	-
η	$(= ct)$ spatial dimension $(c = 1\,\mathrm{m/s})$	m
θ	angle of the convection vector	rad
θ_{00}, θ_{01}	auxiliary variable type zero for the a_i	-
θ_{10}, θ_{11}	auxiliary variable type first for the a_i	-
θ_{20}, θ_{21}	auxiliary variable type second for the a_i	-
θ_{30}, θ_{31}	auxiliary variable type third for the a_i	-
Θ	angle of the first principal direction	rad
λ	ratio between convection and diffusion	$\mathrm{m^{-1}}$
$\Lambda_s^{(i)}$	source removal function i	-
ξ, η	generic coordinates	m
Ξ	streching coefficient	-
Π_s	source number	-
ρ	density	$\mathrm{kg\,m^{-3}}$
ρ, σ	first and second characteristic polynomial	-

σ, ϵ	control parameter	$[\sigma]$, $[\epsilon]$
Σ_1, Σ_2	sumatories of Hermite splines	-
τ_i, τ	local/global truncation error in CCS and CIR	$[f]\,\mathrm{m}^{-1}$ or $[f]\,\mathrm{m}$
τ	characteristic time	s
ϕ	transport variable	$[\phi]$
$\overline{\phi}^N$	homogeneous solution	-
$\phi_1^\star$	solution in x direction at $\star$ time	$[\phi]$
$\phi_2^\star$	solution in y direction at $\star$ time	$[\phi]$
$\phi_i\vert_{\text{num.}}$	numerical result at the i point of the mesh	$[\phi]$
$\phi_i\vert_{\text{exact}}$	exact result at the i point of the mesh	$[\phi]$
φ	potencial-function	$\mathrm{kg\,m^{-1}\,s^{-1}}$
ψ, Ψ	stream-function	$\mathrm{kg\,m^{-1}\,s^{-1}}$
ω_ρ	curl of the convection vector	$\mathrm{kg\,m^{-3}\,s^{-1}}$
ω	vorticity perpendicular to the flow plane	s^{-1}
$\mathbf{A}$, $\mathbf{A}^n$	influence matrix	$\mathrm{kg\,m^{-2}\,s^{-1}}$
$\mathbf{b}$, $\mathbf{b}^n$	discrete source vector	$[\phi]\,\mathrm{kg\,m^{-2}\,s^{-1}}$
$\mathbf{B}$, $\mathbf{C}$	generic matrices	$[B]$, $[C]$
$\mathbf{C}^n$	diagonal matrix of ρc's	$\mathrm{kg\,m^{-2}\,s^{-1}}$
$\mathbf{e}_x$, $\mathbf{e}_y$	Cartesian basis	-
$\mathbf{e}_\varphi$, $\mathbf{e}_\psi$	curviliniar basis	-
$\mathbf{e}_{\mathrm{N}\,1}$, $\mathbf{e}_{\mathrm{N}\,2}$	principal numerical diffusivity basis	-
$\boldsymbol{\mathcal{F}}$	flux vector	$[\phi]\,\mathrm{kg\,m^{-2}\,s^{-1}}$
$\boldsymbol{\mathcal{F}}^{\mathrm{c}}$	convective flux vector	$[\phi]\,\mathrm{kg\,m^{-2}\,s^{-1}}$
$\boldsymbol{\mathcal{F}}^{\mathrm{d}}$	diffusive flux vector	$[\phi]\,\mathrm{kg\,m^{-2}\,s^{-1}}$
$\mathbf{g}^\varphi$, $\mathbf{g}^\psi$	contravariant basis	$\mathrm{kg\,m^{-2}\,s^{-1}}$
$\mathbf{H}$	Hermite matrix	-
$\mathbf{M}$, $\mathbf{Q}$	matrices for CCS and CIR	-
$\mathbf{P}^n$, $\widetilde{\mathbf{P}}^n$	unsteady influence matrices	$\mathrm{kg\,m^{-2}\,s^{-1}}$
$\mathbf{u}$	velocity vector field	$\mathrm{m\,s^{-1}}$
$\mathbf{v}$	general vector	$[\mathrm{v}]$
$\mathbf{v}_{\mathrm{N}\,1}$, $\mathbf{v}_{\mathrm{N}\,2}$	eigenvectors of $\boldsymbol{\Gamma}_{\mathrm{N}}$	-
$\mathbf{v}_{\boldsymbol{\phi}}^{\star\,n}$, $\mathbf{v}_{\boldsymbol{\beta}}^{\star\,n}$	reaction vector	-
$\mathbf{x}$	space vector	m
$\boldsymbol{\Gamma}_{\mathrm{N}}$	numerical diffusion tensor	$\mathrm{kg\,m^{-1}\,s^{-1}}$
$\boldsymbol{\Delta S_2^\star}$	vector of $\Delta S_2^\star$s	$[\phi]\,\mathrm{kg\,m^{-3}\,s^{-1}}$
$\boldsymbol{\Delta\beta^\star}$	vector of $\Delta\beta^\star$s	$[\phi]\,\mathrm{kg\,m^{-3}\,s^{-1}}$
$\boldsymbol{\Delta\phi_2^\star}$	vector of $\Delta\phi_2^\star$s	$[\phi]$
$\boldsymbol{\Delta x}$, $\boldsymbol{\Delta\eta}$	interval length vector	m
$\boldsymbol{\theta}$	vector of θ_{00}, θ_{01} and so on	-
$\boldsymbol{\phi}$	vector of ϕs	$[\phi]$
$\boldsymbol{\phi_1^\star}$	vector of $\phi_1^\star$s	$[\phi]$
$\boldsymbol{\phi_2^\star}$	vector of $\phi_2^\star$s	$[\phi]$
$\boldsymbol{\tau}$	error vector in CCS and CIR	$[f]\,\mathrm{m}^{-1}$ or $[f]\,\mathrm{m}$
d	total differential operator	-
∂	partial differential operator	-
∇	nabla operator	m^{-1}
$\partial/\partial t$	temporal operator	s^{-1}
z_{lb}	left boundary of z	$[z]$

z_{rb}	right boundary of z	$[z]$
z_{bb}	bottom boundary of z	$[z]$
z_{tb}	top boundary of z	$[z]$
$\widehat{z}$	normalized z	-
$\overline{P}$, $\overline{P}_x$	average Péclet number in x direction	-
$\overline{P}_y$	average Péclet number in y direction	-
$\widetilde{k}$, $\widetilde{k}_x$	k parameter in x direction	-
$\widetilde{k}_y$	k parameter in y direction	-
ILE, ILE_x	Integral of Lambda and E in x direction	-
ILE_y	Integral of Lambda and E in y direction	-
IGE, IGE_x	Integral of Gamma and E in x direction	-
IGE_y	Integral of Gamma and E in y direction	-
$\widetilde{IS}$	Integral of Source	-
IS, IS_x	Integral of Source in x direction	$[\phi]\mathrm{kg\,m^{-2}\,s^{-1}}$
IS_y	Integral of Source in y direction	$[\phi]\mathrm{kg\,m^{-2}\,s^{-1}}$
$\widetilde{ISGE}$	Integral of Source, Gamma and E	-
$ISGE$, IS_xGE_x	Integral of Source, Gamma and E in x direction	$[\phi]\mathrm{kg\,m^{-2}\,s^{-1}}$
IS_yGE_y	Integral of Source, Gamma and E in y direction	$[\phi]\mathrm{kg\,m^{-2}\,s^{-1}}$

Dedicated to my parents and grandparents

Chapter 1

Introduction

In many branches of engineering that involve fluid problems, Figure 1.1, one is interested in the values of some global variables for which it is fundamental to know the detailed fluid flow. For instance, in wind engineering aerodynamic drag is calculated in order to know the fuel consumption in aircraft or lorries [179]. Meanwhile, aerospace engineers may be engaged in determining the position and shape of shock waves during the atmospheric reentry of spacecraft [131]. Civil engineers focus their calculations on erosion and sedimentation in floods [129], or the design of hydraulic works for irrigation and navigation like the Aragon's Imperial Channel, one of the most important works in this field in 18th century Europe [40]. These are some examples where the detailed fluid flow is of interest in itself or as a prior step to calculate global parameters (functionals) of the flowfield.

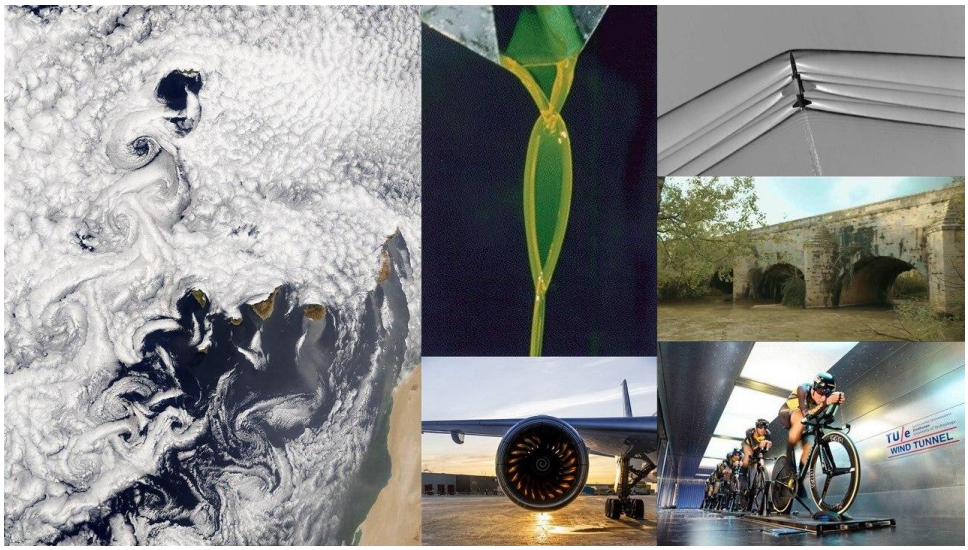

FIGURE 1.1: Examples in Fluid Mechanics. *Left*, Vortex street near Canary Islands [144]. *Middle top*, Fluid chains produced by obliquely intersecting viscous jets [184]. *Middle bottom*, Airbus Jet Engine [4]. *Right top*, shock wave from a USAF Test Pilot School T-38C aircraft [145]. *Right middle*, waterway canal-bridge [54]. *Right bottom*, Aerodynamic of a cyclist bunch in a wind tunnel [124].

From the 17th to 20th centuries, renowned physicists such as Bernoulli, Reynolds, Navier or Stokes, among others, could translate into mathematical language, what we nowadays know as Partial Differential Equations (PDEs), the motion of fluids. The Navier-Stokes equations describe a balance between the variations of the velocity under study and the forces that

elicit those variations. We define two types of variations. Phenomena that can change in time are expressed by the operator $\partial/\partial t$, with the spatial coordinate fixed. The operator ∇ represent changes in space, with the time coordinate fixed, and depends strictly on the coordinate base, see Simmonds [199]. Forces are diverse and can also be expressed in terms of variations of the velocities or other variables under study. Thus, if we want to understand the fluid behaviour and get some results to design devices or to predict atmospheric motion as in meteorology, the whole flow field has to be determined solving these PDEs.

It can be found in a basic course of Fluid Mechanics [202] that the mechanical problem is described by the conservation of mass and momentum transport,

$$\begin{aligned}
&\frac{\partial \rho}{\partial t} + \nabla \cdot (\rho \mathbf{u}) = 0, \\
&\frac{\partial \rho \mathbf{u}}{\partial t} + \nabla \cdot \left(\rho \mathbf{u} \otimes \mathbf{u} - \mu(\nabla \mathbf{u} + (\nabla \mathbf{u})^T)\right) = \rho \mathbf{f}_m - \nabla \left(p - \kappa \nabla \cdot \mathbf{u}\right),
\end{aligned}$$

and the thermal problem by the transport of internal energy,

$$\frac{\partial \rho e}{\partial t} + \nabla \cdot (\rho \mathbf{u} e - k \nabla T) = \rho \dot{q}_m - p(\nabla \cdot \mathbf{u}) + \Phi_V.$$

The system is closed with two equations of state (EoS): $p = p(\rho, T)$ and $e = e(\rho, T)$. The meaning of all terms will not be commented on, the purpose is to show that they have a similar structure. The previous PDEs are not unique and one could add more as their range of applicability is widespread. Let us see some examples. In combustion [105] each N species has a mass fraction Y_k that obeys

$$\frac{\partial \rho Y_k}{\partial t} + \nabla \cdot \left(\rho \left(\mathbf{u} + \mathbf{u}^c\right) Y_k - \rho D_k \frac{W_k}{W} \nabla Y_k\right) = \dot{\omega}_k,$$

and react through M chemical reactions, $\dot{\omega}_k = \sum_{j=1}^{M} \dot{\omega}_{kj}$. In turbulence [236], (U)RANS equations along with the $k - \varepsilon$ model are widely used in the industry to compute the mean velocity in turbulent flows. The turbulent kinetic energy k,

$$\frac{\partial \rho k}{\partial t} + \nabla \cdot \left(\rho \mathbf{u} k - \left(\mu + \frac{\mu_t}{\sigma_k}\right) \nabla k\right) = G - \rho \epsilon,$$

and dissipation ε,

$$\frac{\partial \rho \varepsilon}{\partial t} + \nabla \cdot \left(\rho \mathbf{u} \varepsilon - \left(\mu + \frac{\mu_t}{\sigma_\varepsilon}\right) \nabla \varepsilon\right) = \frac{\mathcal{C}_1 \varepsilon}{k} \left(G + \mathcal{C}_3 \frac{2}{3} k \nabla \cdot \mathbf{u}\right) - \mathcal{C}_2 \rho \frac{\varepsilon^2}{k},$$

links with the (U)RANS equations through the Reynolds stress tensor. In the physical sense, these turbulent variables intensify the molecular diffusion by adding some eddy viscosity, $\mu_t = \rho \mathcal{C}_\mu k^2/\varepsilon$. On the other hand, magnetohydrodynamics [38] couples the mechanical problem via the Lorentz force with the Maxwell equations to study the motion of an electrically-charged fluid in a magnetic field. The Maxwell equations can be combined

resulting in the induction magnetic equation,

$$\frac{\partial \mathbf{B}}{\partial t} + \nabla \cdot (\mathbf{u} \otimes \mathbf{B} - \eta \nabla \mathbf{B}) = \nabla \cdot (\mathbf{B} \otimes \mathbf{u}) \,.$$

Finally, in ventilation [50] not only is important to know the temperature of a room, but also the local mean age-of-air, $\overline{\tau}_a$, which is defined as the time that a particle has been in this room. Its equation writes

$$\frac{\partial \rho \overline{\tau}_a}{\partial t} + \nabla \cdot (\rho \mathbf{u} \overline{\tau}_a - \rho D_m \nabla \overline{\tau}_a) = 1.$$

If we look at all previous PDEs, we can realise that all of them are written with the same conservation law. This kind of PDE describes the transport of quantities carried by the fluid velocity and spread over the domain due to the existing gradients over the domain. In Fluid Mechanics, those problems are named as convection-diffusion problems and they are ruled by transport equations. The prototypical equation reads

$$\boxed{\frac{\partial \rho \phi}{\partial t} + \nabla \cdot (\rho \mathbf{u} \phi - \Gamma \nabla \phi) = S} \tag{1.1}$$

where ϕ is the transport variable, ρ the density, $\mathbf{u}$ the velocity vector field, Γ the diffusion coefficient and S the source term. Depending on the choice of ϕ, Γ and S, (1.1) can represent any of the former PDEs. The term inside brackets is named as flux, $\boldsymbol{\mathcal{F}}$, and is the sum of the convective flux, $\boldsymbol{\mathcal{F}}^{\mathrm{c}} := \rho \mathbf{u} \phi$, and the diffusive flux, $\boldsymbol{\mathcal{F}}^{\mathrm{d}} := -\Gamma \nabla \phi$. In this thesis Γ is treated like a scalar but it could also be a tensor, see e.g. Gómez [68]. The mathematical problem defined by the transport equation (1.1) is closed with boundary conditions (BC) and initial values (IV).

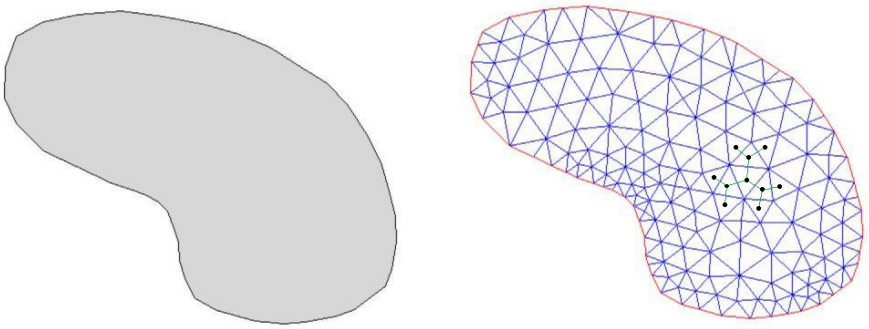

FIGURE 1.2: CFD outline. *Left*, continuum domain. *Right*, discrete domain split into cells (blue) with boundary (red) and a 10-point stencil or computational molecule (green lines with black nodes).

Only a very limited number of convection-diffusion problems can be solved exactly [139, 149, 157, 160, 246, 260], so in order to evaluate (1.1) numerical approximations are used to convert it to an algebraic system of equations. The branch of Fluid Mechanics that uses numerical analysis to compute the solution of transport phenomena is named "**C**omputational **F**luid **D**ynamics", CFD. Almost all methods in CFD usually have three-stages: first, the domain is broken down into small cells with an associated

node or point, then, the conservation law is discretized over the cells giving a p-point stencil, and finally, a system $\mathbf{A}\boldsymbol{\phi} = \mathbf{b}$ is solved with $\boldsymbol{\phi}$ a vector of ϕs at nodes. A stencil or computational molecule is a discrete region where several nodes link to each other, Fig. 1.2. The larger the computational molecule, the more accurate the method is. In addition, the size of the molecule affects the numerical performance of the system solver. A small stencil requires less special discretizations near boundaries.

Devising robust and accurate numerical methods is not at all a straightforward endeavour. Some guidelines should be followed:

- The computational molecule must be as small as possible while maintaining accuracy.
- Due to its good numerical properties the coefficient matrix $\mathbf{A}$ should be an M-matrix [237].
- The numerical scheme should preserve monotonicity and well-balancing [72, 81].
- It should provide smooth transition from the diffusion limit to strong convection.

In the following the most used techniques are summarized and the family to which the numerical approach described in this thesis belongs is described. If a reader is interested in a complete historical review about numerical techniques it is referred to Thomee [215].

1.1 Spatial Numerical Techniques

Spatial discretization methods could be classified as finite differences (FD), finite volumes (FV), finite elements (FE), spectral and meshless.

1.1.1 FD and FV method

In FD methods derivatives in the PDE at discrete points are approximated by algebraic relations obtained via Taylor series expansion, see the books [192, 214]. Those methods are conservative if the equations are discretized in conservative form. Indeed, this is a sufficient condition as interpolations for the fluxes can turn such methods into non-conservative. A drawback of FD is the requirement of cartesian meshes. In complex geometries FD may be combined with immersed boundary methods, see Pinelli *et al.* [161]. To illustrate FD we consider a semi-discrete form of a one-dimensional transport equation at a generic node i, i.e.

$$\frac{\mathrm{d}\rho_i\phi_i}{\mathrm{d}t} + \left.\frac{\partial \mathcal{F}}{\partial x}\right|_i = S_i.$$

The first standard idea for the discretized flux would be central differencing for the diffusive term and forward/backward differencing for convection. Assuming $u_i > 0$ and uniform spacing, this produces the discretized flux

$$\left.\frac{\partial \mathcal{F}}{\partial x}\right|_i \approx (\rho u)_i \frac{\phi_i - \phi_{i-1}}{\Delta x} - \Gamma_i \frac{\phi_{i-1} - 2\phi_i + \phi_{i+1}}{\Delta x^2}.$$

The reason to avoid central differencing to compute convective phenomena is the fact that the interpolation can generate spurious wiggles for strong convection, although it can still be used if corrections are applied. Later this idea will be further elaborated. If we want to increase the accuracy of the scheme, more nodes should be allowed in the expansion. Fornberg [57] provides an algorithm to calculate the weights for an FD formula with arbitrary spacing and several orders of accuracy. For instance, an eighth-order central difference will have a nine-point stencil that will increase the computational molecule and the storage requirements of the matrix.

Other option to achieve high-order accuracy but using fewer computational nodes is the family of compact schemes [108]. Now, the Taylor expansion serves to relate a linear combination of derivative values with values of variables at nodes, e.g

$$\frac{1}{4}\left.\frac{\partial\phi}{\partial x}\right|_{i-1} + \left.\frac{\partial\phi}{\partial x}\right|_{i} + \frac{1}{4}\left.\frac{\partial\phi}{\partial x}\right|_{i+1} = \frac{3}{2}\frac{\phi_{i+1}-\phi_{i-1}}{2\Delta x},$$

Finally, the idea is to obtain a tridiagonal system, in vectorial form, as follows

$$\mathbf{C}\frac{\mathrm{d}\boldsymbol{\phi}}{\mathrm{d}t} + \mathbf{A}\boldsymbol{\phi} = \mathbf{B}\mathbf{s},$$

in which $\boldsymbol{\phi}$ and $\mathbf{s}$ are the vectors of ϕ and S at nodes, respectively, and $\mathbf{A}$, $\mathbf{B}$ and $\mathbf{C}$ matrices from the discretization. The drawback is that compact schemes generate oscillations near shock or regions with strong gradients. In such cases numerical diffusion [32] or filters [37] are introduced. Anyway, a common discretization in the CFD community nowadays is the central difference based on values at half-way nodes. A second-order writes

$$\left.\frac{\partial\mathcal{F}}{\partial x}\right|_{i} \approx \frac{\mathcal{F}_{i+1/2}-\mathcal{F}_{i-1/2}}{\Delta x},$$

but any other order can be achieved expanding the stencil assigning different weights. Weight tables can be found in [57].

The FV method uses the integral form of the conservation law,

$$\frac{\mathrm{d}}{\mathrm{d}t}\int_{V_k}\rho\phi\,\mathrm{d}V + \oint_{A_k}\boldsymbol{\mathcal{F}}\cdot\mathbf{n}\,\mathrm{d}A = \int_{V_k}S\,\mathrm{d}V,$$

to aproximate the integrals by some quadratures from the balance over the control volumes V_k [3, 143]. Employing the same example as before a quadrature easy to handle is the midpoint rule for a one-dimensional problem. The volume integrals are evaluated around some node i with volume Δx and the surface integral is evaluated at the cell face center $i \pm 1/2$ over an unit area, i.e.

$$\frac{\mathrm{d}\rho_i\phi_i}{\mathrm{d}t} + \frac{\mathcal{F}_{i+1/2}-\mathcal{F}_{i-1/2}}{\Delta x} = S_i,$$

which is the same half-way FD scheme. This approximation results in a cell centered FV discretization but it could also be discretized by a cell vertex FV. Some comparisons of both can be found in [45, 46, 171, 205]. A consequence of the weak formulation is that FV is conservative by nature as

the flux balances are satisfied at two adjacent control volumes. Another advantage in comparison with FD is that FV can be applied in unstructured meshes employed for complex geometry.

The fluxes must be interpolated at mesh nodes for either FD or FV. For the diffusive flux, a central difference is widely used,

$$\mathcal{F}^{\mathrm{d}}_{i+1/2} = -\Gamma_{i+1/2} \left.\frac{\partial \phi}{\partial x}\right|_{i+1/2} \approx -\Gamma_{i+1/2} \frac{\phi_{i+1} - \phi_i}{\Delta x},$$

but for convection this discretization brings a dilemma. Although the scheme is second order, the numerical solution will be unstable in strong convection problems since the matrix is no longer an M-matrix. Physically speaking, the convection propagates ϕ in the direction of u and the information from downwind becomes negligible, so weighting the two contributions equally is not appropriate. Upwinding differences could apply

$$\mathcal{F}^{\mathrm{c}}_{i+1/2} = (\rho u)_{i+1/2}\, \phi_{i+1/2} \approx (\rho u)_{i+1/2} \begin{cases} \phi_i & \text{if} \quad u_{i+1/2} > 0, \\ \phi_{i+1} & \text{if} \quad u_{i+1/2} < 0, \end{cases}$$

guaranteeing stability although increasing the errors. This is a first-order scheme and adds artificial diffusion that in some cases is larger than the physical one. One way to reduce numerical diffusion is the use of some high-order linear scheme, e.g. QUICK [109]. van Leer [223] describes them as a family of κ-schemes:

$$\phi_{i+1/2} = \begin{cases} \phi_i + \dfrac{1+\kappa}{4}\left(\phi_{i+1} - \phi_i\right) + \dfrac{1-\kappa}{4}\left(\phi_i - \phi_{i-1}\right) & \text{if} \quad u_{i+1/2} > 0, \\ \phi_{i+1} + \dfrac{1+\kappa}{4}\left(\phi_i - \phi_{i+1}\right) + \dfrac{1-\kappa}{4}\left(\phi_{i+1} - \phi_{i+2}\right) & \text{if} \quad u_{i+1/2} < 0, \end{cases}$$

for some constant $\kappa \in [-1, 1]$. The drawback is that they are not bounded and tend to be dispersive near regions with strong gradients leading to over- or under-shoots. This result is due to Godunov's Theorem. Back in the 1950s, Godunov [67] proved that:

Theorem 1 (Godunov's order barrier)**.** *Linear monotone schemes are at most first-order accurate.*

Therefore, high-order schemes that preserve monotonicity need to be nonlinear. One way to generate nonlinear schemes is by using flux limiters, see book by LeVeque [112], which belong to the family of Total Variation Diminishing (TVD) schemes [77] and shock-capturing methods [163]. The first outline of flux limiters was introduced by Boris and Book [16] in their Flux Corrected Transport (FCT) algorithm. A generalization of a flux limiter [74] can be expressed as

$$\mathcal{F}^{\mathrm{c}}_{i+1/2} = \mathcal{F}^{\mathrm{c}\,L}_{i+1/2} + \Phi\left(r_{i+1/2}\right)\left[\mathcal{F}^{\mathrm{c}\,H}_{i+1/2} - \mathcal{F}^{\mathrm{c}\,L}_{i+1/2}\right],$$

where $\mathcal{F}^{\mathrm{c}\,L}_{i+1/2}$ and $\mathcal{F}^{\mathrm{c}\,H}_{i+1/2}$ are the low- and high-order fluxes, respectively, $\Phi = \Phi(r)$ is the limiter function and $r_{i+1/2}$ the smoothness indicator defined as $r_{i+1/2} \coloneqq (\phi_{i+1} - \phi_i)/(\phi_i - \phi_{i-1})$. For instance, a low-order flux can be the upwind flux and a high-order flux can be the second-order upwind flux.

Then the interpolator at cell face for $u_{i+1/2} > 0$ is given by

$$\phi_{i+1/2} = \phi_i + \frac{1}{2}\Phi\left(r_{i+1/2}\right)\left[\phi_i - \phi_{i-1}\right].$$

The idea behind limiters is that in smooth regions, $r_{i+1/2} \approx 1$, the interpolator becomes high-order, but near shocks or large gradient regions where $r_{i+1/2}$ is away from 1, low interpolation works adding some numerical diffusion [30]. The most relevant contribution of flux limiters is their monotone behaviour. Spekreijse [201] proves the next theorem:

Theorem 2. *If the limiter $\Phi(r)$ has the properties that there exist constants $C_1 \in (0, \infty)$, $C_2 \in [-2, 0]$ such that $C_2 \leq \Phi(r) \leq C_1$, $-C_1 \leq \Phi(r)/r \leq 2 + C_2$ for all $r \in \mathbb{R}$, then the scheme is monotone.*

For all second-order schemes, the monotone region is given by Sweby [206] and plotted in Figure 1.3a. An analysis of standard limiters can be found in [244, 251] on irregular grids [12] and some others more sophisticated in [23, 183, 247], mostly third order.

Another criterion for monotonicity is Gaskell and Lau's [62]. The interpolator formula is more straightforward to check under this criterion than under that from Spekreijse's theorem. They used the normalized variable diagram (NVD) that represents the mid-point value with respect to the upwind node in terms of normalized variables, $\widehat{\phi}_k = (\phi_k - \phi_{i-1})/(\phi_{i+1} - \phi_{i-1})$. They claimed that any characteristic line of a monotone scheme must lie in a specific region and contain the points $(0, 0)$ and $(1, 1)$, see Fig.1.3b. In addition Leonard [110] put forward a sufficient condition for a monotone scheme to be at most second-order: its characteristic must contain the point $(0.5, 0.75)$. If the slope at this point is 0.75, the scheme is at most third-order.

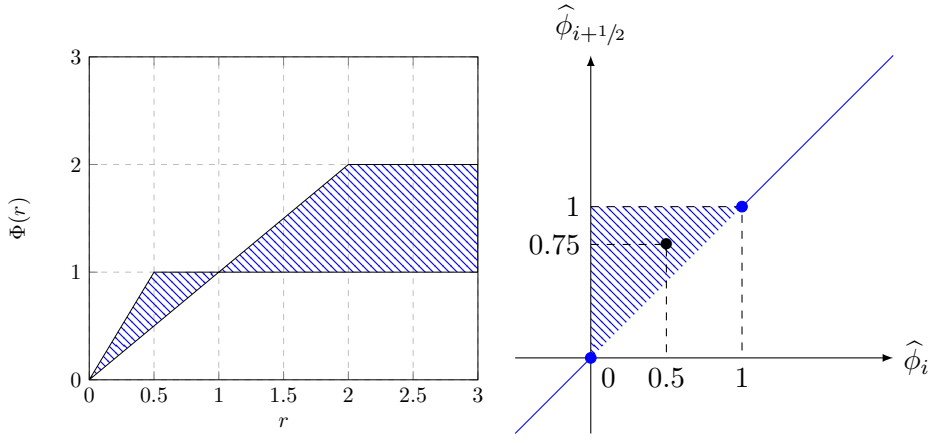

(A) Flux diagram (B) NVD

FIGURE 1.3: Monotone regions for flux limiter theory.

Another nonlinear interpolation is the family of (W)ENO schemes. The essentially non-oscillatory (ENO) reconstruction scheme was introduced by Harten and Osher [78] and extended by Harten *et al.* [79]. Some related schemes are the TVD Runge-Kutta + ENO by Shu and Osher [196, 197] or the enhanced ENO by Shu [198]. Hydrodynamic applications can be found

in Fatemi *et al.* [53]. As Zhang and Shu [255] pointed out, the ENO reconstruction adapts its computational molecule to avoid including, if possible, a stencil in a strong-gradient cell by comparing the local smoothness of the reconstruction polynomials, see Figure 1.4. Later, Liu, Osher and Chan [117] introduced the weighted ENO (WENO) reconstruction scheme that was standardized by Jiang and Shu [93]. In this sense, WENO approximates better in smooth regions, near regions with strong gradient reduces to ENO. The k-order WENO scheme reconstructs the value at the face cell in the form

$$\phi_{i+1/2} = \sum_{r=0}^{k-1} \tilde{\omega}_r \phi_{i+1/2}^{(r)},$$

where

$$\phi_{i+1/2}^{(r)} = \sum_{j=0}^{k-1} \mathcal{C}_{rj} \overline{\phi}_{i+r-j}, \quad r = 0, \ldots, k-1\,,$$

might represent a low-order interpolator for $\phi_{i+1/2}$ in each r-stencil. Note that the interpolation takes the value of the average ϕ at nodes. To link with nodal values is necessary to find, for each cell, a polynomial $p_r(x)$ of kth order accurate. Then,

$$\overline{\phi}_m = \frac{1}{\Delta x_m} \int_{x_{m-1/2}}^{x_{m+1/2}} p_r(x)\,\mathrm{d}x, \quad m = i-r, \ldots, i-r+k-1.$$

The weights $\tilde{\omega}_r$ in WENO are calculated as

$$\tilde{\omega}_r = \frac{\omega_r}{\sum_{s=0}^{k-1} \omega_s}, \quad \omega_r = \frac{d_r}{(\epsilon + \beta_r)^2}.$$

The parameter ϵ is introduced to avoid dividing by zero. The values of constants $\mathcal{C}_{rj}$ and d_r, and their calculations, can be found in [195]. Finally, the standard smoothness indicator β_r is defined as

$$\beta_r := \sum_{l=1}^{k-1} \int_{x_{i-1/2}}^{x_{i+1/2}} \Delta x^{2l-1} \left(\frac{\mathrm{d}^l p_r}{\mathrm{d}x^l} \right)^2 \mathrm{d}x,$$

but other indicators have been designed with different features [8, 83, 84, 240, 254]. Over the years several WENOs have been developed, a wide comparison was done by Zhao, Lardjane and Fedioun [256]. (W)ENO offers between third- and fifth-order monotone results, but for strong convection the computational molecule is large. For instance, a normal (W)ENO uses a five-point stencil resulting in a large sparse matrix.

Lastly, another option to increase the stability of numerical schemes are the deferred-correction methods. The best definition of such methods was given by Wesseling [235]: to improve a low-order discretization without having to solve for a high-order discretization. Thus, those methods are extremely flexible in order to make a correction up. As previously said, central differencing for the convective term is not such a good idea. However, as

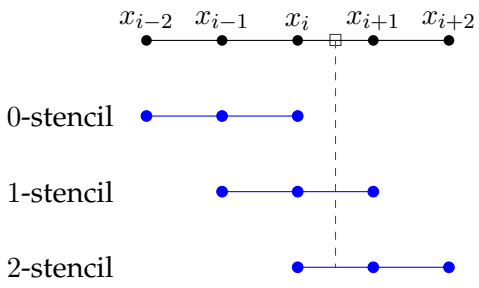

FIGURE 1.4: Computational molecule for the WENO reconstruction technique.

Khosla and Rubin pointed out [99], a central derivative can be understood as an upwind derivative plus an anti-diffusive term, i.e.

$$\frac{\phi_{i+1}-\phi_{i-1}}{2\Delta x}=\frac{\phi_i-\phi_{i-1}}{\Delta x}+\frac{\Delta x}{2}\frac{\phi_{i-1}-2\phi_i+\phi_{i+1}}{\Delta x^2}.$$

Upwinding is employed in the coefficient matrix and the anti-diffusion is evaluated with "old values" of ϕ in the source term. The converged solution will be second order and the method unconditionally stable. Deferred correction is, therefore, an iterative method in which values of a previous iteration level are used as "old values" in the source term.

The way to compute fluxes at cell faces, either convective or diffusive, is

$$\mathcal{F}_{i+1/2}=\mathcal{F}^L_{i+1/2}+\theta\left[\mathcal{F}^H_{i+1/2}-\mathcal{F}^L_{i+1/2}\right]^{\text{old}},$$

for some constant $\theta\in[0,1]$. When $\theta=0$ we have a purely *l*ow-order flux, if $\theta=1$ a *h*igh-order deferred flux. Otherwise, a mixture of both fluxes is employed. Since the low-order is in the coefficients we ensure that the matrix is an M-matrix, but stable oscillations can be developed during the iteration procedure if large gradients are at face cells. Another shortcoming of these corrections is the increase in computational time [55].

1.1.2 FE and spectral method

The FE method has its origin in the work of Turner *et al.* [219] as a generalization of the direct stiffness method to compute stress and strain in structural problems. The method belongs to the family of Galerkin's formulation to obtain a discrete counterpart from the continuous operator in PDEs. Insomuch as FE became more and more popular, it did not take long for it to be applied in fluid flows and heat transfer, see books [175, 259]. The FE approximation starts by multiplying the conservation law by a test function $W_k=W_k(\mathbf{x})$ and then integrating in each element, Ω_k, i.e.

$$\int_{\Omega_k}W_k\left[\frac{\partial\rho\phi}{\partial t}+\nabla\cdot\boldsymbol{\mathcal{F}}-S\right]\mathrm{d}\Omega=0.$$

The solution is a linear combination of shape functions $N_k=N_k(\mathbf{x})$ and ϕ values at nodes. These functions are defined to be 1 at node k and 0 at any node in the element. With the use of integration by parts the law is reduced

to the system

$$\mathbf{C}\frac{\mathrm{d}\boldsymbol{\phi}}{\mathrm{d}t} + \mathbf{A}\boldsymbol{\phi} = \mathbf{b},$$

where

$$\begin{aligned} C_{kl} &= \int_{\Omega_k} \rho W_k N_l \,\mathrm{d}\Omega, \\ A_{kl} &= \int_{\Omega_k} \Big[W_k \rho \mathbf{u} \cdot \nabla N_l + \Gamma \nabla W_k \cdot \nabla N_l \Big] \mathrm{d}\Omega, \\ b_k &= \int_{\Omega_k} W_k S \,\mathrm{d}\Omega - \int_{\partial\Omega_k} W_k \boldsymbol{\mathcal{F}}^{\mathrm{d}} \cdot \mathbf{n} \,\mathrm{d}(\partial\Omega). \end{aligned}$$

The matrix $\mathbf{A}$ is named the stiffness matrix. Legendre polynomials are usually chosen as shape functions although they can be taken arbitrarily. In 1D, linear (two-nodal element), quadratic (three-nodal element) or cubic (four-nodal element) can be employed, see Figure 1.5. In higher dimensions some extensions of these are appropriate. On the other hand, the test functions depend on the Galerkin formulation. In standard FE, $W_k = N_k$. The stiffness matrix will be symmetric iff $\rho\mathbf{u} = \mathbf{0}$. As the convection gets stronger, the matrix becomes more asymmetric and eventually the discrete equation will become unstable. For a 1D problem with linear shape function, constant convection and diffusion and equal size mesh, oscillations pop up for Péclet greater than 1. Petrov-Galerkin (PG) methods [73] provide stability taking $W_k = N_k + \alpha W_k^*$, where α is a parameter depending on the element Péclet number and W_k^* a perturbation function dependent on the convection direction [18, 43]. The integrals are approximated by Gauss-Legendre (GL) quadrature because of its higher accuracy.

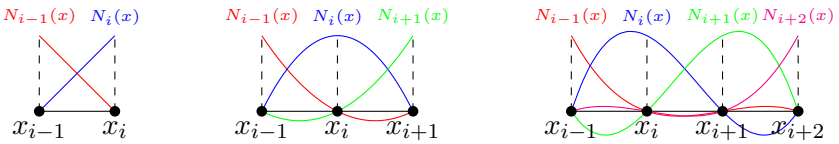

FIGURE 1.5: Linear (left), Quadratic (middle) and Cubic (right) shape functions on a 1D mesh.

A FE drawback has to do with the performance of the matrix solver that drops down when the matrix becomes more sparse, as happens with every numerical method dealing with unstructured meshes. Also, FE might face problems if the numerical solution is not sufficiently smooth [7]. In addition, FE is more sensitive to skinny faces or elements with small edges than the Virtual Element (VE) methods [35, 90, 91, 132] that can overcome these deficiencies. Other unsolved problems in FE methods are listed in Zienkiewicz [257].

In these methods the formulation is continuous, but there are others where the continuity requirement across element boundaries is relaxed: the so-called Discontinuous Galerkin (DG) methods, see books [44, 48]. From a geometrical point of view, the physical domain is divided into subdomains where the solution is approximated. This permits a compact computational molecule and flexibility to apply the method in a wide variety of fluid flows

with high-order results.

Spectral or Spectral Element (SE) methods are another type of discretization technique introduced by Canuto [24]. Zienkiewicz and Cheung [258] pointed out that SE methods may be viewed as a special case of PG methods. The main difference is that the shape functions are nonzero over the whole domain. Now, the solution is built up from Fourier series and, therefore, $N_k = \exp(\mathbf{i}k\mathbf{x})$. The test functions satisfy the biorthonormality condition giving $W_k = (1/2\pi)\exp(-\mathbf{i}k\mathbf{x})$. The main features of SE and DG method are combined in the "**D**iscontinuous **G**alerkin **S**pectral **E**lement **M**ethod", DGSEM [10, 63, 114, 191].

Regarding conservativeness, it is known that FE is at least globally conservative. However, Hughes *et al.* [86] proved that any continuous Galerkin formulation is locally conservative. Perot [158] suggested that this local conservation often follows from global conservation. SE methods can also be made conservative [15], although Giraldo and Restelli [66] indicated that they were at least globally. DG methods were both locally and globally.

1.1.3 Meshless

All previous methods are based on discretizations in a set of points connected with each other, what allows to obtain an approximation of spatial derivatives. However, there are other techniques to compute those derivatives based on the interactions of each node or particle with its neighbours rather than being connected with a mesh. These are the so-called meshless or meshfree methods. An application that makes those methods attractive is free-surface flows. Since FD, FV or FE use meshes, in each running time the procedure must know where the interface is inside a volume or an element. There are other techniques to deal with these flows such as the Volume of Fluid (VoF) method [170] or Shallow Water models [26].

One of the most famous and used meshless methods is the smoothed particle hydrodynamics (SPH) method, see books [113, 228]. SPH was invented in the '70s by Gingold and Monaghan [65] and Lucy [121] for astrophysical problems and later applied in Fluid Mechanics [140]. The basic idea in SPH is to take an integral representation of the transport variable or any variable as follows

$$\phi(\mathbf{x}) \simeq \int_V \phi(\mathbf{x}')K(\mathbf{x}-\mathbf{x}',h)\,\mathrm{d}V',$$

which is $\mathcal{O}(h^2)$. The kernel function K should be the Dirac delta as h goes to zero where h is the interaction radius with other particles. Then, the first derivative, after some mathematical manipulation, is given by

$$\nabla_{\mathbf{x}}\phi(\mathbf{x}) \simeq -\int_V \phi(\mathbf{x}')\nabla_{\mathbf{x}'}K(\mathbf{x}-\mathbf{x}',h)\,\mathrm{d}V',$$

or its discrete form

$$\nabla_n\phi \approx -\sum_m \phi_m \nabla_m K_{nm} V'_m,$$

which is $\mathcal{O}(h^{-1})$. Error estimation in SPH derivatives is assessed by Fatehi and Manzari [52]. For the kernel, there are several functions used in literature [11, 156, 169, 243]. The main problems in SPH are the accuracy and the particle clustering. The accuracy relates to the approximation of the integrals by sums of particles in the neighbourhood. The greater the number of particles is and the more uniformly are distributed, the more accurate the SPH method is. This requirement is not met near boundaries and empty areas can arise due to particle clustering. Those methods cluster particles by nature and, therefore, collisions models [102] must be programmed to avoid regions with high density of particles in the domain. A review in detail of meshless methods can be found in [59, 69]. Positiveness and the conditions under which the coefficient matrix of meshless methods is an M-matrix are studied by Seibold [189].

1.2 Time Numerical Techniques

Once equation (1.1) is spatially discretized with any of the above approximations, the result is a set of ODEs in the form of

$$\mathbf{C}\frac{\mathrm{d}\boldsymbol{\phi}}{\mathrm{d}t} = \mathcal{D}_s(\boldsymbol{\phi}, t),$$

where $\mathcal{D}_s(\boldsymbol{\phi}, t)$ is the spatial discretization of the convection-diffusion problem. The matrix $\mathbf{C}$ may appear due to techniques used in the spatial discretization. Finally, the time derivative is computed by time integration methods that can be classified as one-step, multi-step and others. In turn, the methods can be explicit, in which the solution depends on $\boldsymbol{\phi}$ at early times, or implicit, in which the current time is also considered. To illustrate time integration, we consider a single ODE, with $\mathbf{C}$ being the identity matrix. Further and complete information on time methods can be found in books [21, 71, 87, 130].

1.2.1 One-step methods

These methods consider ϕ at two timesteps. The midpoint method gives,

$$\frac{\phi_i^{n+1} - \phi_i^n}{\Delta t} = \mathcal{D}_s(\phi_i^{n+1/2}, t^{n+1/2}), \quad \phi_i^{n+1/2} := \frac{\phi_i^{n+1} + \phi_i^n}{2},$$

Euler method,

$$\begin{aligned} \frac{\phi_i^{n+1} - \phi_i^n}{\Delta t} &= \mathcal{D}_s(\phi_i^n, t^n), && \text{(Explicit)} \\ \frac{\phi_i^{n+1} - \phi_i^n}{\Delta t} &= \mathcal{D}_s(\phi_i^{n+1}, t^{n+1}), && \text{(Implicit)} \end{aligned}$$

and θ-method which is a linear combination of the previous two, i.e.

$$\frac{\phi_i^{n+1} - \phi_i^n}{\Delta t} = \theta\mathcal{D}_s(\phi_i^n, t^n) + (1-\theta)\mathcal{D}_s(\phi_i^{n+1}, t^{n+1}),$$

for some constant $\theta \in [0,1]$. If $\theta = 0$ we have the first-order implicit Euler, if $\theta = 1$, the first-order explicit and if $\theta = 1/2$, the Crank-Nicolson or trapezoidal rule which is expected to be second-order. Stability analysis shows that the explicit Euler may turn unstable for some time steps whereas the implicit Euler and the θ-method for $\theta \leq 1/2$ are unconditionally stable. An algorithm for reducing the computational cost to solve implicit schemes is a predictor-corrector (PC) method: in the prediction stage a value of ϕ is estimated for later improving the result by correcting the predicted value. For instance,

$$\frac{\widetilde{\phi}_i^{n+1} - \phi_i^n}{\Delta t} = \mathcal{D}_s(\phi_i^n, t^n), \qquad \text{(P stage)}$$
$$\frac{\phi_i^{n+1} - \phi_i^n}{\Delta t} = \frac{1}{2}\left[\mathcal{D}_s(\phi_i^n, t^n) + \mathcal{D}_s(\widetilde{\phi}_i^{n+1}, t^{n+1})\right], \qquad \text{(C stage)}$$

is Heun's method. Other improvements that require fewer time steps to achieve the same accuracy are the high-order Runge-Kutta (RK) methods. A classical one is the 4th-order RK. The method evaluates $\mathcal{D}_s$ at t^n, $t^{n+1/2}$ and t^{n+1}. With ϕ_i^n at the beginning it performs a ϕ-prediction with an explicit Euler and a ϕ-correction with an implicit Euler at midpoints, and finally a ϕ-correction with a midpoint method is done. RK averages these predictions/corrections with weights $1/6$ at the beginning and at the end, and $1/3$ at midpoints. The shortcoming of RKs lies in the great number of evaluations per time of $\mathcal{D}_s$ to achieve an accuracy comparable to multi-steps methods.

1.2.2 Multi-step methods

When more than two timesteps are considered, we have linear multistep methods. The general recurrence formula writes:

$$\frac{1}{\Delta t}\sum_{k=0}^{m} \lambda_k \phi_i^{n+k} = \sum_{k=0}^{m} \mu_k \mathcal{D}_s(\phi_i^{n+k}, t^{n+k}).$$

The method contains m steps and if $\mu_m \neq 0$ it is implicit. The coefficients depend on the chosen family of multistep methods and they are usually calculated by expanding ϕ and $\mathcal{D}_s$ via Taylor series in order to achieve a m-order method. For instance, a 4th-order Adams-Bashforth method gives:

$$\{\lambda_k | k = 0, \ldots, 4\} = \{0, 0, 0, -24, 24\},$$
$$\{\mu_k | k = 0, \ldots, 4\} = \{-9, 37, -59, 55, 0\},$$

and therefore it is explicit. One drawback of multistep methods is that they require several initial values to start running the scheme, e.g., in the previous Adams-Bashforth ϕ_i^0, ϕ_i^1, ϕ_i^2 and ϕ_i^3 are needed which are computed either with a low-order Adams-Bashforth or with 4th-order RK. The latter is more usual.

A surprising outcome related to multistep methods was found in the research related to this thesis. Some integrals of various functions are required in the numerical scheme on which this thesis is based, so a quadrature to compute integrals was devised. This quadrature can be cast as a linear multistep method. If the quadrature is written in terms of the usual

recurrence formula it is unstable, but if it is solved as a tridiagonal system, the results are more accurate than with traditional multistep methods. This is explained in Appendix D.

1.2.3 Others

In one-step methods one may notice that the time derivative was approximated by a forward difference. In doing so the number of time steps can be very large if the accuracy needs to be increased. For instance, the derivative

$$\frac{\mathrm{d}\phi_i}{\mathrm{d}t} \approx \frac{-3\phi_i^{n+4} + 16\phi_i^{n+3} - 36\phi_i^{n+2} + 48\phi_i^{n+1} - 25\phi_i^n}{12\Delta t}$$

is $\mathcal{O}(\Delta t^4)$. But again, this procedure suffers from the same problem as multistep methods as ϕ_i^0, ϕ_i^1, ϕ_i^2 and ϕ_i^3 should be provided to start off, not to mention stability.

ADER methods compute the time derivative by Taylor expansions in time, whose derivatives are later related to space derivatives. They are not time integration methods per se. First, we expand in time via Taylor series at a generic node:

$$\phi_i^{n+1} = \phi_i^n + \sum_{k=1}^{m} \frac{\Delta t^k}{k!} \left.\frac{\partial^k \phi}{\partial t^k}\right|_i^n .$$

If the transport equation is linear, e.g.

$$\frac{\partial \phi}{\partial t} + u\frac{\partial \phi}{\partial x} = 0 \Rightarrow \frac{\partial^k \phi}{\partial t^k} = (-u)^k \frac{\partial^k \phi}{\partial x^k}.$$

If is nonlinear, the Cauchy–Kowalewski [207] theorem is then applied. Spatial derivatives are discretized as before. ADER methods are user-friendly when the equation is hyperbolic but when the transport equation contains high-order derivatives and nonlinearities the task becomes tough.

1.3 Exponential schemes

As we have seen, all previous numerical techniques, either spatial or temporal, have strengths and weaknesses. The CFD community does not have a unique numerical method able to compute a wide range of transport phenomena keeping the size of the computational molecule small. Usually, if the convection is strong the required molecule size grows to maintain high accuracy. In addition, in singular perturbation problem [178], i.e. $0 < \Gamma \ll 1$, where the fluid flow exhibit boundary layers, numerical methods become unstable if numerical diffusion is not added. At this point, we should be able to construct a smooth interpolator covering from parabolic/elliptic flow to hyperbolic flow in order to have a robust numerical method. To overcome this "smooth transition" keeping high accuracy, the family of methods named *exponentially fitted*, *exponential fitting*, *exponential difference*, or just *exponential*, could be applied.

Exponential schemes form a group of discretization methods that have been around for a long time, used to discretize convection-diffusion problems. These schemes employ the analytical solution of a steady-state one-dimensional transport equation in a local boundary value problem in order to link the values of the variable at grid points. From this last point of view, exponential schemes may be considered as a subgroup of the so-called non-standard FD (NFD) methods introduced by Mickens [133]. There is no clear definition of an NFD method but some rules should be followed [134]. To illustrate, let us consider the transport equation

$$\frac{\mathrm{d}\phi}{\mathrm{d}x} - \frac{1}{\lambda}\frac{\mathrm{d}^2\phi}{\mathrm{d}x^2} = 0,$$

in which $\lambda = \rho u/\Gamma$ is a constant. The NFD derivatives would be:

$$\left.\frac{\mathrm{d}\phi}{\mathrm{d}x}\right|_i = \frac{\phi_i - \phi_{i-1}}{\Delta x \dfrac{\exp P - 1}{P \exp P}}, \qquad \left.\frac{\mathrm{d}^2\phi}{\mathrm{d}x^2}\right|_i = \frac{\phi_{i-1} - 2\phi_i + \phi_{i+1}}{\Delta x^2 \dfrac{(\exp P - 1)^2}{P^2 \exp P}},$$

as they give the exact solution of the ODE, i.e. $\phi_i = \exp(Px_i/\Delta x)$ with $P = \lambda \Delta x$. Further research on these methods are explored in [152, 186, 241, 252]

One of the first publications on exponential schemes comes from Allen and Southwell [39]. The motion of a viscous flow around a cylinder was calculated by the vorticity transport equation using the exact solution of the flow in order to discretize it by a central difference scheme. Later Il'in [89] developed a general exponential scheme for transport problems, and in the same line, Gartland [60] put forward a q-order compact exponential scheme in the '80s where the discrete equation is exact on the next set of functions:

$$\left\{1, x, \ldots, x^q, \exp\left(\int^x \lambda\,\mathrm{d}x'\right), x\exp\left(\int^x \lambda\,\mathrm{d}x'\right), \ldots, x^{q-1}\exp\left(\int^x \lambda\,\mathrm{d}x'\right)\right\}$$

This scheme was used by Costa do Amaral and Gonçalves dos Santos [47]. Back to the Il'in scheme, a similar approach was taken by Scharfetter and Gummel [188] for ionic flux models in semiconductors, see books [136, 162], and later extended to two-dimensional problems by Bank *et al.* [9]. On the other hand, Sacco [182] presented three families of exponential shape functions based on Scharfetter and Gummel in triangular elements with Galerkin formulation. The Scharfetter-Gummel scheme is very popular to calculate ionic transport in semiconductors at present [94, 100, 101, 153] and was the starting point for the development of exponential schemes in multidimensional flows for convection-diffusion problems in Fluid Mechanics, for instance the exponentially fitted technique of El-Mistikawy and Werle [49] employed to compute Falkner-Skan boundary-layer flows.

The first exponential scheme applied to fluid transport phenomena was designed by Spalding [200] and later included in the pioneer book of Patankar [150]. They assumed piecewise constant convection-diffusion parameters

in the one-dimensional sourceless transport equation. The discrete equation yielded a three-point stencil,

$$-\left.\frac{\rho u \exp P}{\exp P-1}\right|_{i-1/2}\phi_{i-1}+\left[\left.\frac{\rho u}{\exp P-1}\right|_{i-1/2}+\left.\frac{\rho u \exp P}{\exp P-1}\right|_{i+1/2}\right]\phi_i-\left.\frac{\rho u}{\exp P-1}\right|_{i+1/2}\phi_{i+1}=0,$$

where the influence coefficients were exponential functions of the Péclet number. The Péclet number contains the ratio between the convection and diffusion terms in a generic transport equation. An improvement over Patankar and Spalding is given by Thiart [212, 213]. Thiart's two-dimensional approach considers now a constant source over each control volume,

$$\text{Spalding-Patankar's stencil}=\Delta x\, S\left.\frac{(P-1)\exp P-2P+1}{P\,(\exp P-1)}\right|_{i-1/2}+\Delta x\, S\left.\frac{\exp P-P+1}{P\,(\exp P-1)}\right|_{i+1/2},$$

and it is used to formulate an algorithm for the pressure-velocity coupling. Thiart's scheme is similar to the locally analytic differencing (LOAD) scheme of Wong and Raithby [238]. LOAD assumes local one-dimensionality in treating fluxes what yields false diffusion at high Péclet numbers and in the presence of variable source term. Virag and Trincas [229] proposed some improvement of LOAD modifying both the discrete source terms and the interpolator at cell faces. Additionally, MacKinnon and Johnson [123] derived a fourth-order nine-point centred difference scheme with variable convective parameters for a 2D transport equation in nonconservative form. As Ramos [174] pointed out, those exponentially fitted methods work better than any numerical techniques in problems of exponential nature, such as boundary layers [85] or with steep gradients, and can be used with adaptive mesh refinements [173].

In the last few years, other authors have proposed more sophisticated exponential schemes. For instance, Tian and Yu [218] developed a high-order approach for unsteady one-dimensional transport equations but with constant convection and diffusion coefficients and no source. Neumann boundary conditions were considered by Fu, Tian and Liu [58]. Previously, Tian and Ge [217] developed a fourth-order exponential scheme for solving 2D unsteady convection-diffusion problems, and used in unsteady magnetohydrodynamics flows by Wu, Peng and Tian [239]. Extension to a three-dimensional case of the Tian-Dai's scheme [216] was done by Mohamed, Mohamed and Seddek [138]. Wang [232] gave a second-order exponential scheme for two-dimensional convection-diffusion problems with just a five-point stencil, changing to fourth-order if Richardson extrapolation was applied. Similar use of the Richardson extrapolation technique in a exponential scheme was done by Mishra and Yedida [137]. The effects of employing Richardson extrapolation in a CFD simulation are explored in [125]. Another second-order exponential scheme is proposed by Angermann and Wang [5] in a dual mesh. A modern exponential scheme is given by Cui [33, 34] where a Caputo time fractional model is presented for the unsteady transport equation. On the other hand, a complete integral representation of the flux is achieved as an extension of Thiart's by van't Hof, ten Thije Boonkkamp and Mattheij [225], and modified by ten Thije Boonkkamp and Anthonissen [209]. For reaction problems Luo, Dlugogorski, Moghtaderi and Kennedy [122] devised a family of one-dimensional exponential schemes

that give satisfactory results comparing with Spalding-Patankar's and conventional schemes. Finally, Polyakov [164, 165] designed a second-order exponential scheme with double integral transformation for one-dimensional modelling. This was extended and applied to a 2D electromagnetic water purification model by Polyakov, Karamzin, Kudryashova and Tsybulin [166].

Previous methods commonly use an alternating direction implicit method when they are extended to two- and three-dimensional problems. If these splitting techniques are not carried out correctly, the great accuracy in one dimension is lost. A completely and different way to circumvent this splitting issue was performed by Bianchini and Gosse [14] and Gosse [70]. They designed a genuinely 2D well-balanced exponential scheme based on an exact flux of a 2D steady-state transport equation with variable convection and no source in a disk of radius R. The scheme has a nine-point stencil overall and the coefficients are integral representations of Bessel functions.

In this thesis the exponential scheme established by Pascau will be studied and assessed. The first sketch of this scheme can be found in [146]. The exact solution in normalized variables is achieved by assuming piecewise-constant convection/diffusion and polynomial source, being later extended to arbitrary sources. An improvement of this scheme was given by Pascau and Arıcı [147] taking into account arbitrary convection and diffusion parameters. However, the scheme is one dimensional and its extension to multidimensional problems is the backbone of this doctoral work.

1.4 Outline of this thesis

The thesis is structured as follows:

Chapters

- Chapter 2: An introduction of the exponential scheme in 1D is provided, able to deal with nonlinear equations and arbitrarily varying coefficients and source.
- Chapter 3: The scheme is extended to cover steady two-dimensional problems. Three different approaches were developed.
- Chapter 4: The ideas of chapter 3 are applied to deal with unsteady one-dimensional problems.
- Chapter 5: Conclusions and future research. This chapter is later translated to spanish due to regulations of Zaragoza University.

Appendices

- Appendix A: An integral formulation of the exponential flux is presented.
- Appendix B: The coefficients of Hermite splines of different orders used to compute the basic integral of the scheme are provided.
- Appendix C: Some theoretical simplifications of the integrals are proposed and their features assessed.

- Appendix D: A review of the CIR quadrature is provided as well as its applications to time integration methods.
- Appendix E: How to obtain the coefficients of Central Compact Schemes for nonuniform meshes is explained.

Chapter 2

The first contact: one-dimensional ENATE

This chapter is based on two papers published by Pascau [146] and [147] with some extensions and new work.

Goals:

- To get the exact solution of a one-dimensional non-homogeneous transport equation
- To assemble it into a three-node algebraic equation
- To analyze their features, integration methods and boundary treatment
- To develop cases of nonlinear-convection and solutions with discontinuous derivatives

2.1 The dimensionless transport equation

Let us begin the chapter with the steady-state one-dimensional transport equation as a local boundary value problem (BVP) referred to an interval of length $\Delta x = x_{rb} - x_{lb}$,

$$\frac{\mathrm{d}}{\mathrm{d}x}\left(\rho u\phi - \Gamma\frac{\mathrm{d}\phi}{\mathrm{d}x}\right) = S, \qquad x_{lb} \leq x \leq x_{rb}, \tag{2.1a}$$

$$\phi(x_{lb}) = \phi_{lb}, \quad \phi(x_{rb}) = \phi_{rb}, \tag{2.1b}$$

with known variable coefficients: $\rho u = \rho(x)u(x)$, $\Gamma = \Gamma(x)$ and $S = S(x)$. The transported variable is named as $\phi = \phi(x)$. When working with equations such as the previous one it is sometimes convenient to make it nondimensional. When doing so, several dimensionless numbers come out, in particular the Péclet number which is defined as the ratio between transport by convection and by diffusion, i.e. $P \coloneqq \rho u \Delta x/\Gamma$. In the equations where momentum is transported the Péclet number becomes the Reynolds number. The ratio between the convective coefficient and the diffusive coefficient is the inverse of a characteristic length and will be called λ, i.e. $\lambda \coloneqq \rho u/\Gamma$. All variables will be normalized, see Figure 2.1, by using their values at the left boundary of the interval, marked as lb. The right boundary

will be marked as rb.

$$\widehat{\phi} \coloneqq \frac{\phi - \phi_{lb}}{\phi_{rb} - \phi_{lb}} = \frac{\phi - \phi_{lb}}{\Delta\phi}, \quad \widehat{\rho u} \coloneqq \frac{\rho u}{(\rho u)_{lb}}, \tag{2.2a}$$

$$\widehat{\Gamma} \coloneqq \frac{\Gamma}{\Gamma_{lb}}, \quad \widehat{\lambda} \coloneqq \frac{P}{P_0} = \frac{\widehat{\rho u}}{\widehat{\Gamma}}, \quad P_0 \coloneqq \frac{(\rho u)_{lb}\Delta x}{\Gamma_{lb}}. \tag{2.2b}$$

In addition, the space variable is rescaled to $\widehat{x} = (x - x_{lb})/(x_{rb} - x_{lb})$, thus $x = x_{lb} + \widehat{x}\Delta x$. Replacing the set (2.2) into equation (2.1a) and boundary conditions (2.1b), the normalized convection-diffusion problem becomes

$$\frac{\mathrm{d}}{\mathrm{d}\widehat{x}}\left(\widehat{\rho u}\widehat{\phi} - \frac{\widehat{\Gamma}}{P_0}\frac{\mathrm{d}\widehat{\phi}}{\mathrm{d}\widehat{x}}\right) = \Pi_s - \frac{\phi_{lb}}{\Delta\phi}\frac{\mathrm{d}\widehat{\rho u}}{\mathrm{d}\widehat{x}}, \qquad 0 \le \widehat{x} \le 1,$$
$$\widehat{\phi}(0) = 0, \quad \widehat{\phi}(1) = 1.$$

The Π_s-term is a dimensionless source, $\Pi_s = S\Delta x/(\rho u)_{lb}\Delta\phi$. Notice that in the previous equation normalization brings in a new source term as a result of the gradient of the convective term. The combination of both implies a net source, S^*, which exists even if there is no source in the original problem (2.1a), provided that the product $\phi_{lb}\mathrm{d}\rho u/\mathrm{d}x$ is not equal to zero.

$$\frac{\mathrm{d}}{\mathrm{d}\widehat{x}}\left(\widehat{\rho u}\widehat{\phi} - \frac{\widehat{\Gamma}}{P_0}\frac{\mathrm{d}\widehat{\phi}}{\mathrm{d}\widehat{x}}\right) = \Pi_s^*, \quad \Pi_s^* = \frac{S^*\Delta x}{(\rho u)_{lb}\Delta\phi}, \quad S^* = S - \frac{(\rho u)_{lb}\,\phi_{lb}}{\Delta x}\frac{\mathrm{d}\widehat{\rho u}}{\mathrm{d}\widehat{x}}.$$

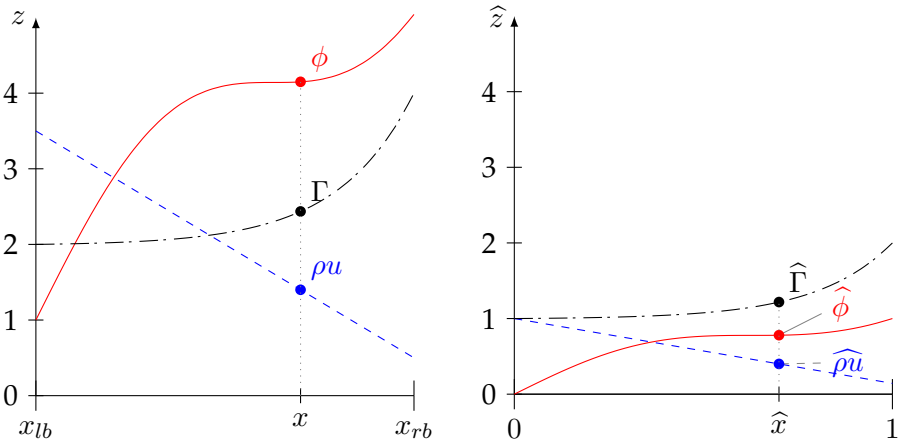

(A) Dimensional map (B) Normalized map

FIGURE 2.1: Sketching the main variables of equation (2.1a) in the normalized map.

2.1.1 The homogeneous exact solution

In the homogeneous case, that is $S = 0$, the normalized transport equation is

$$\frac{\mathrm{d}}{\mathrm{d}\widehat{x}}\left(\widehat{\rho u}\widehat{\phi} - \frac{\widehat{\Gamma}}{P_0}\frac{\mathrm{d}\widehat{\phi}}{\mathrm{d}\widehat{x}}\right) = -\frac{\phi_{lb}}{\Delta\phi}\frac{\mathrm{d}\widehat{\rho u}}{\mathrm{d}\widehat{x}}. \tag{2.4}$$

Thus, integrating between 0 and $\widehat{x}$,

$$\widehat{\rho u}\widehat{\phi} - \frac{\widehat{\Gamma}}{P_0}\frac{\mathrm{d}\widehat{\phi}}{\mathrm{d}\widehat{x}} + \frac{1}{P_0}\left.\frac{\mathrm{d}\widehat{\phi}}{\mathrm{d}\widehat{x}}\right|_0 = -\frac{\phi_{lb}}{\Delta\phi}\left(\widehat{\rho u} - 1\right),$$

the second-order ODE is reduced to first-order. The differential equation

$$\frac{\mathrm{d}\widehat{\phi}}{\mathrm{d}\widehat{x}} - P\widehat{\phi} = P_0\frac{\phi_{lb}}{\Delta\phi}\widehat{\lambda} + \frac{1}{\widehat{\Gamma}}\left[\left.\frac{\mathrm{d}\widehat{\phi}}{\mathrm{d}\widehat{x}}\right|_0 - P_0\frac{\phi_{lb}}{\Delta\phi}\right],$$

includes one unknown term, $(\mathrm{d}\widehat{\phi}/\mathrm{d}\widehat{x})_0$. The solution of this linear ODE with variable coefficients and source reads

$$\frac{\widehat{\phi}}{E} = \left[\left.\frac{\mathrm{d}\widehat{\phi}}{\mathrm{d}\widehat{x}}\right|_0 - P_0\frac{\phi_{lb}}{\Delta\phi}\right]\int^{\widehat{x}}\frac{\mathrm{d}\widehat{x}'}{\widehat{\Gamma}E} + P_0\frac{\phi_{lb}}{\Delta\phi}\int^{\widehat{x}}\frac{\widehat{\lambda}}{E}\mathrm{d}\widehat{x}' + C_o,$$

where the integrating factor $E = E(\widehat{x})$ is defined as $\exp\int^{\widehat{x}} P\,\mathrm{d}\widehat{x}'$, being $\widehat{x}'$ a dummy variable. The constant of integration C_o and $(\mathrm{d}\widehat{\phi}/\mathrm{d}\widehat{x})_0$ are determined making use of $\widehat{\phi}\,(0) = 0$ and $\widehat{\phi}\,(1) = 1$. The final solution is

$$\begin{aligned}\widehat{\phi} = \overline{E}\Bigg(&\int_0^{\widehat{x}}\frac{\mathrm{d}\widehat{x}'}{\widehat{\Gamma}\,\overline{E}}\Big/\int_0^1\frac{\mathrm{d}\widehat{x}'}{\widehat{\Gamma}\,\overline{E}} \\ &+ P_0\frac{\phi_{lb}}{\Delta\phi}\int_0^1\frac{\widehat{\lambda}}{\overline{E}}\mathrm{d}\widehat{x}'\left[\int_0^{\widehat{x}}\frac{\widehat{\lambda}}{\overline{E}}\mathrm{d}\widehat{x}'\Big/\int_0^1\frac{\widehat{\lambda}}{\overline{E}}\mathrm{d}\widehat{x}'\right. \\ &\left.- \int_0^{\widehat{x}}\frac{\mathrm{d}\widehat{x}'}{\widehat{\Gamma}\,\overline{E}}\Big/\int_0^1\frac{\mathrm{d}\widehat{x}'}{\widehat{\Gamma}\,\overline{E}}\right]\Bigg),\end{aligned} \tag{2.5}$$

where $\overline{E} = \overline{E}(\widehat{x})$ is defined as

$$\begin{aligned}\overline{E} \coloneqq \frac{E(\widehat{x})}{E(1)} &= \exp\left(\int^{\widehat{x}} P\,\mathrm{d}\widehat{x}'\right)\exp\left(-\int^1 P\,\mathrm{d}\widehat{x}'\right) \\ &= \exp\left(-\int_{\widehat{x}}^1 P\,\mathrm{d}\widehat{x}'\right).\end{aligned}$$

Equation (2.5) could be handled in a more convenient way with the integrals renamed as follows:

$$\widehat{\phi} = \overline{E}\left(\frac{IGE_{0\widehat{x}}}{IGE_{01}} + P_0\frac{\phi_{lb}}{\Delta\phi}ILE_{01}\left[\frac{ILE_{0\widehat{x}}}{ILE_{01}} - \frac{IGE_{0\widehat{x}}}{IGE_{01}}\right]\right), \tag{2.6a}$$

$$ILE_{0\widehat{x}} \coloneqq \int_0^{\widehat{x}}\frac{\widehat{\lambda}}{\overline{E}}\mathrm{d}\widehat{x}', \quad IGE_{0\widehat{x}} \coloneqq \int_0^{\widehat{x}}\frac{1}{\widehat{\Gamma}\overline{E}}\mathrm{d}\widehat{x}', \tag{2.6b}$$

$$ILE_{01} \coloneqq \int_0^1\frac{\widehat{\lambda}}{\overline{E}}\mathrm{d}\widehat{x}', \quad IGE_{01} \coloneqq \int_0^1\frac{1}{\widehat{\Gamma}\overline{E}}\mathrm{d}\widehat{x}', \tag{2.6c}$$

where $ILE_{0\widehat{x}}$ stands for **I**ntegral of **L**ambda and **E** from 0 to $\widehat{x}$ and $IGE_{0\widehat{x}}$, **I**ntegral of **G**amma and **E** from 0 to $\widehat{x}$. The only difference between $ILE_{0\widehat{x}}$ and ILE_{01} or $IGE_{0\widehat{x}}$ and IGE_{01} lies in the integration limits. The integral formula (2.6a) is the exact solution of equation (2.4). The dimensional

variable value is recovered straightforwardly as $\phi = \phi_{lb} + \widehat{\phi}\Delta\phi$. In many instances it is unlikely that the integrals of the above expression be evaluated exactly. Only $ILE_{0\widehat{x}}$ could be evaluated by using the exponential derivative rule: $\mathrm{d}\left(\exp u\right)/\mathrm{d}x = \mathrm{d}u/\mathrm{d}x \exp u$, since $\widehat{\lambda}$ and $\overline{E}$ are functions of Péclet, P,

$$\begin{aligned} ILE_{0\widehat{x}} = \int_0^{\widehat{x}} \frac{\widehat{\lambda}}{\overline{E}} \mathrm{d}\widehat{x}' &= \int_0^{\widehat{x}} \frac{P}{P_0}\frac{1}{\overline{E}} \mathrm{d}\widehat{x}' \\ &= -\frac{1}{P_0}\int_0^{\widehat{x}} \frac{\mathrm{d}}{\mathrm{d}\widehat{x}'}\left(\frac{1}{\overline{E}}\right)\mathrm{d}\widehat{x}' \\ &= \frac{1}{P_0}\left(\frac{1}{\overline{E}(0)} - \frac{1}{\overline{E}(\widehat{x})}\right) \\ &= \frac{1}{P_0}\left(\exp\overline{P} - \exp\int_{\widehat{x}}^1 P\,\mathrm{d}\widehat{x}'\right). \end{aligned} \tag{2.7}$$

Even so, this evaluation of ILE is only of some use if the integral of Péclet, $\int_{\widehat{x}}^1 P\,\mathrm{d}\widehat{x}'$, is known. The average Péclet, $\overline{P}$, is defined as $\int_0^1 P\,\mathrm{d}\widehat{x}$. Consequently, in a general problem involving integrands with no primitives some kind of interpolator will be needed for the integrands. In Sections 2.2 and 2.3 this idea will be recovered and extended.

There are some particular solutions of eqn.(2.6a). On the one hand, when ρu is constant, $\widehat{\rho u} = 1$ and $\widehat{\lambda} = 1/\widehat{\Gamma}$. Therefore $ILE_{0\widehat{x}} = IGE_{0\widehat{x}}$, as well as $ILE_{01} = IGE_{01}$, then the term in square brackets vanishes and the final solution is

$$\begin{aligned} \widehat{\phi} = \overline{E}\frac{IGE_{0\widehat{x}}}{IGE_{01}} &= \exp\left(-\int_{\widehat{x}}^1 P\,\mathrm{d}\widehat{x}'\right)\frac{\exp\overline{P} - \exp\int_{\widehat{x}}^1 P\,\mathrm{d}\widehat{x}'}{\exp\overline{P} - 1} \\ &= \frac{\exp\int_0^{\widehat{x}} P\,\mathrm{d}\widehat{x}' - 1}{\exp\overline{P} - 1}. \end{aligned}$$

Besides, if Γ is also constant, the Péclet number is easy to integrate and the solution is the standard one,

$$\widehat{\phi} = \frac{\exp P\widehat{x} - 1}{\exp P - 1}, \tag{2.8}$$

covered in a great number of books, for instance Ferziger *et al.* [55]. A last particular solution is that with equal boundary values, that is $\phi_{lb} = \phi_{rb}$. Multiplying both sides of eqn.(2.6a) by $\Delta\phi$ and using $\Delta\phi = 0$, the first term in brackets vanishes. Then dividing by ϕ_{lb}, the dimensionless solution is achieved,

$$\frac{\phi}{\phi_{lb}} = 1 + \overline{E}P_0 ILE_{01}\left[\frac{ILE_{0\widehat{x}}}{ILE_{01}} - \frac{IGE_{0\widehat{x}}}{IGE_{01}}\right].$$

With no source and fulfilling mass conservation, i.e. $\mathrm{d}\rho u/\mathrm{d}x = 0$, necessarily $ILE = IGE$ and, therefore, the term in brackets is identically zero. The final solution, $\phi = \phi_{lb} = \phi_{rb}\ \forall x$, satisfies the maximum principle [104, p. 91].

2.1.2 The complete exact solution

In this section the normalized equation is considered for the case $S \neq 0$,

$$\frac{\mathrm{d}}{\mathrm{d}\widehat{x}}\left(\widehat{\rho u}\widehat{\phi} - \frac{\widehat{\Gamma}}{P_0}\frac{\mathrm{d}\widehat{\phi}}{\mathrm{d}\widehat{x}}\right) = \Pi_s - \frac{\phi_{lb}}{\Delta\phi}\frac{\mathrm{d}\widehat{\rho u}}{\mathrm{d}\widehat{x}}. \tag{2.9}$$

The method of Undetermined Coefficients (UC) and Constants Variation (CV) are two well known techniques to obtain the particular solution of an ODE. However, UC only works for differential equations with constant coefficients if the right-hand side of eqn.(2.9) is a constant, polynomial, exponential or trigonometric function, or a linear combination of them. On the other hand, and although CV is a generalization of UC, replacing the arbitrary constants of the homogeneous solution by unknown functions to be determined in a system of differential equations may turn tough. Hence, the aim of this subsection is to figure out the way of removing the source Π_s from ODE (2.9) in order to transform it to the homogeneous case (2.4) whose solution is already known.

Let us assume for now that ρu, Γ and S are constants[1]. Under these assumptions, equation (2.9) reads

$$\frac{\mathrm{d}}{\mathrm{d}\widehat{x}}\left(\widehat{\phi} - \frac{1}{P}\frac{\mathrm{d}\widehat{\phi}}{\mathrm{d}\widehat{x}}\right) = \Pi_{s0}, \tag{2.10}$$

where Π_{s0} is a constant. Making up a new variable as $\overline{\phi}^{(0)} = \widehat{\phi} - \Pi_{s0}\widehat{x}$, the new transport equation is

$$\frac{\mathrm{d}}{\mathrm{d}\widehat{x}}\left(\overline{\phi}^{(0)} - \frac{1}{P}\frac{\mathrm{d}\overline{\phi}^{(0)}}{\mathrm{d}\widehat{x}}\right) = 0, \tag{2.11}$$

which is sourceless but with a new set of boundary values: $\overline{\phi}^{(0)}(0) = \widehat{\phi}(0) = 0$ and $\overline{\phi}^{(0)}(1) = \widehat{\phi}(1) - \Pi_{s0} = 1 - \Pi_{s0}$. We can construct a normalized $\overline{\phi}^{N}(\widehat{x}) = \overline{\phi}^{(0)}(\widehat{x})/\overline{\phi}^{(0)}(1)$ to have $\overline{\phi}^{N}(1) = 1$ as

$$\overline{\phi}^{N} = \frac{\widehat{\phi} - \Pi_{s0}\widehat{x}}{1 - \Pi_{s0}},$$

because in this way, although the normalization does not change the equation (2.11), $\overline{\phi}^{N}$ has the same boundary values as the homogeneous solution $\widehat{\phi}$ and hence, the same exact solution (2.8), i.e.

$$\overline{\phi}^{N} = \frac{\exp P\widehat{x} - 1}{\exp P - 1} \Longrightarrow \widehat{\phi} = \Pi_{s0}\widehat{x} + (1 - \Pi_{s0})\frac{\exp P\widehat{x} - 1}{\exp P - 1}. \tag{2.12}$$

This expression has been obtained previously, Thiart [212] and Wang *et al.* [233], following different paths. Here, by integrating the constant source and inserting it in the transformed $\widehat{\phi}$ has been easy to get an homogeneous

[1] Recall that in that case $\widehat{\rho u} = 1$ and $\widehat{\Gamma} = 1$ what implies $\widehat{\lambda} = 1$ and $P_0 = P$

differential equation with known solution. What if Π_s is now a linear polynomial? The transport equation becomes

$$\frac{\mathrm{d}}{\mathrm{d}\widehat{x}}\left(\widehat{\phi}-\frac{1}{P}\frac{\mathrm{d}\widehat{\phi}}{\mathrm{d}\widehat{x}}\right)=\Pi_{s1}\widehat{x}+\Pi_{s0}, \tag{2.13}$$

being Π_{s0} and Π_{s1} constants. Therefore, working out the integral of the polynomial source and again inserting it in $\overline{\phi}^{(0)}$, the equation

$$\frac{\mathrm{d}}{\mathrm{d}\widehat{x}}\left(\overline{\phi}^{(0)}-\frac{1}{P}\frac{\mathrm{d}\overline{\phi}^{(0)}}{\mathrm{d}\widehat{x}}\right)=\frac{1}{P}\Pi_{s1},$$

with $\overline{\phi}^{(0)}=\widehat{\phi}-\Pi_{s1}(\widehat{x}^2/2)-\Pi_{s0}\widehat{x}$, is a transport equation with a constant source term similar to (2.10). In order to get rid of this constant source, the process is as before by using $\overline{\phi}^{(1)}=\overline{\phi}^{(0)}-(\Pi_{s1}/P)\widehat{x}$. Then, the normalized $\overline{\phi}^{N}$ with the same boundary values as $\widehat{\phi}$ is

$$\overline{\phi}^{N}=\frac{\widehat{\phi}-\Pi_{s1}\dfrac{\widehat{x}^2}{2}-\left(\Pi_{s0}+\dfrac{1}{P}\Pi_{s1}\right)\widehat{x}}{1-\Pi_{s1}\left(\dfrac{1}{2}+\dfrac{1}{P}\right)-\Pi_{s0}}=\frac{\exp P\widehat{x}-1}{\exp P-1},$$

and the exact solution of eqn.(2.13) is

$$\begin{aligned}\widehat{\phi}=&\Pi_{s1}\frac{\widehat{x}^2}{2}+\left(\Pi_{s0}+\frac{1}{P}\Pi_{s1}\right)\widehat{x}\\&+\left(1-\Pi_{s1}\left(\frac{1}{2}+\frac{1}{P}\right)-\Pi_{s0}\right)\frac{\exp P\widehat{x}-1}{\exp P-1}.\end{aligned}$$

It can be realized that for arbitrary source polynomials this procedure reduces them one degree whenever the transport equation is transformed. It can be repeated over and over again until achieving a sourceless equation. In a general case where ρu, Γ and S are arbitrary function of x this approach can be generalized. Unless otherwise indicated, these coefficients are smooth, of class C^{∞}.

Let us define the function $\Lambda_s^{(0)}=\Lambda_s^{(0)}(\widehat{x})$ as

$$\frac{\mathrm{d}}{\mathrm{d}\widehat{x}}\left(\widehat{\rho u}\Lambda_s^{(0)}\right):=\Pi_s\Longrightarrow\Lambda_s^{(0)}=\frac{1}{\widehat{\rho u}}\int_0^{\widehat{x}}\Pi_s\mathrm{d}\widehat{x}', \tag{2.14}$$

assuming $\Lambda_s^{(0)}(0)=0$. This Λ function is used to formulate the new variable $\overline{\phi}^{(0)}=\widehat{\phi}-\Lambda_s^{(0)}$. So, the transport equation associated to this variable is

$$\frac{\mathrm{d}}{\mathrm{d}\widehat{x}}\left(\widehat{\rho u}\overline{\phi}^{(0)}-\frac{\widehat{\Gamma}}{P_0}\frac{\mathrm{d}\overline{\phi}^{(0)}}{\mathrm{d}\widehat{x}}\right)=-\frac{\phi_{lb}}{\Delta\phi}\frac{\mathrm{d}\widehat{\rho u}}{\mathrm{d}\widehat{x}}+\frac{\mathrm{d}}{\mathrm{d}\widehat{x}}\left(\frac{\widehat{\Gamma}}{P_0}\frac{\mathrm{d}\Lambda_s^{(0)}}{\mathrm{d}\widehat{x}}\right). \tag{2.15}$$

Although there is a second source term that turns up in eqn.(2.15), it can be taken out in the same way by looking for a function $\Lambda_s^{(1)}$ that satisfies:

$$\frac{\mathrm{d}}{\mathrm{d}\widehat{x}}\left(\widehat{\rho u}\Lambda_s^{(1)}\right) := \frac{\mathrm{d}}{\mathrm{d}\widehat{x}}\left(\frac{\widehat{\Gamma}}{P_0}\frac{\mathrm{d}\Lambda_s^{(0)}}{\mathrm{d}\widehat{x}}\right) \Rightarrow \Lambda_s^{(1)} = \frac{1}{\widehat{\rho u}}\left(\frac{\widehat{\Gamma}}{P_0}\frac{\mathrm{d}\Lambda_s^{(0)}}{\mathrm{d}\widehat{x}} + C_o\right).$$

The constant of integration C_o is written so as not to loose generality and it can be estimated by taking $\Lambda_s^{(1)}(0) = \Lambda_s^{(0)}(0) = 0$ what leads to $C_o = -(\mathrm{d}\Lambda_s^{(0)}/\mathrm{d}\widehat{x})_0/P_0$, as $\widehat{\Gamma}(0) = 1$. Then, $\Lambda_s^{(1)}$ together with $\overline{\phi}^{(0)}$ makes $\overline{\phi}^{(1)} = \overline{\phi}^{(0)} - \Lambda_s^{(1)} = \widehat{\phi} - (\Lambda_s^{(0)} + \Lambda_s^{(1)})$ whose transport equation is similar to (2.15) where $\Lambda_s^{(0)}$ is replaced by $\Lambda_s^{(1)}$. If one goes on adding up Λ functions,

$$\Lambda_s^{(i)} = \frac{1}{\widehat{\rho u}P_0}\left(\widehat{\Gamma}\frac{\mathrm{d}\Lambda_s^{(i-1)}}{\mathrm{d}\widehat{x}} - \left.\frac{\mathrm{d}\Lambda_s^{(i-1)}}{\mathrm{d}\widehat{x}}\right|_0\right) \quad \forall i = 1, 2, 3, \ldots, \tag{2.16}$$

the final variable reads

$$\overline{\phi}^{(\infty)} = \widehat{\phi} - \sum_{i=0}^{\infty}\Lambda_s^{(i)}, \tag{2.17}$$

and the process ends up with a transport equation where Π_s has disappeared. An important remark is the relationship between the $\Lambda_s^{(i)}$ function and the Péclet number. As each $\Lambda_s^{(i)}$ is built with $\Lambda_s^{(i-1)}$ and $\Lambda_s^{(1)}$ is inversely proportional to Péclet then $\Lambda_s^{(i)} \propto P_0^{-i}$. So in cases where Péclet number is very high, $\Lambda_s^{(0)}$ is the dominant factor and it will only be necessary to perform one integration.

Further, the variable (2.17) is normalized in order to achieve the same boundary values as $\widehat{\phi}$,

$$\overline{\phi}^N(\widehat{x}) = \frac{\widehat{\phi}(\widehat{x}) - \sum_{i=0}^{\infty}\Lambda_s^{(i)}(\widehat{x})}{1 - \sum_{i=0}^{\infty}\Lambda_s^{(i)}(1)} =: \frac{\widehat{\phi}(\widehat{x}) - F(\widehat{x})}{1 - F(1)}. \tag{2.18}$$

To fulfil $\overline{\phi}^N(0) = \widehat{\phi}(0) = 0$, then $F(0) = 0$. Therefore, $\overline{\phi}^N$ is governed by the transport equation

$$\frac{\mathrm{d}}{\mathrm{d}\widehat{x}}\left(\widehat{\rho u}\overline{\phi}^N - \frac{\widehat{\Gamma}}{P_0}\frac{\mathrm{d}\overline{\phi}^N}{\mathrm{d}\widehat{x}}\right) = -\Phi\frac{\mathrm{d}\widehat{\rho u}}{\mathrm{d}\widehat{x}}, \quad \Phi := \frac{1}{1 - F(1)}\frac{\phi_{lb}}{\Delta\phi},$$

whose solution is already highlighted in eqn.(2.6a), given by

$$\overline{\phi}^N = \overline{E}\left(\frac{IGE_{0\widehat{x}}}{IGE_{01}} + P_0\Phi ILE_{01}\left[\frac{ILE_{0\widehat{x}}}{ILE_{01}} - \frac{IGE_{0\widehat{x}}}{IGE_{01}}\right]\right). \tag{2.19}$$

So, the complete solution of the non-homogeneous transport equation (2.9) is taken from (2.18) as

$$\widehat{\phi} = F + (1 - F(1))\,\overline{\phi}^N, \tag{2.20}$$

and is made up of the particular solution F and the normalized function $\widehat{\phi}^N$ corresponding to the homogeneous part of the dimensional equation. The factor $1 - F(1)$ appears in (2.20) to satisfy the boundary values of $\widehat{\phi}$ mentioned before. Finally, if the $\Lambda_s^{(i)}$ functions (2.16) and (2.14) are summed up,

$$\sum_{i=0}^{\infty} \Lambda_s^{(i)} = \frac{1}{\widehat{\rho u}} \int_0^{\widehat{x}} \Pi_s \mathrm{d}\widehat{x}' + \frac{1}{\widehat{\rho u} P_0} \left(\widehat{\Gamma} \frac{\mathrm{d}}{\mathrm{d}\widehat{x}} \sum_{i=0}^{\infty} \Lambda_s^{(i)} - \frac{\mathrm{d}}{\mathrm{d}\widehat{x}} \sum_{i=0}^{\infty} \Lambda_s^{(i)} \bigg|_0 \right),$$

taking $F \coloneqq \sum_{i=0}^{\infty} \Lambda_s^{(i)}$, a nonhomogeneous first order differential equation with variable coefficient is procured,

$$\frac{\mathrm{d}F}{\mathrm{d}\widehat{x}} - PF = -\frac{P_0}{\widehat{\Gamma}} \int_0^{\widehat{x}} \Pi_s \mathrm{d}\widehat{x}' + \frac{1}{\widehat{\Gamma}} \frac{\mathrm{d}F}{\mathrm{d}\widehat{x}} \bigg|_0 . \tag{2.21}$$

It is remarked that a family of ODE arises as solution, owing to the arbitrary value of $(\mathrm{d}F/\mathrm{d}\widehat{x})_0$. This derivative is not fixed and the particular solution of (2.21) is a one-parameter family of solutions. For algebraic reasons it is better to characterize the family with the parameter $F(1)$ which, based on the differential equation, is directly linked to $(\mathrm{d}F/\mathrm{d}\widehat{x})_0$. Therefore, the set of F solutions is given by the $F(1)$-parameter family as follows:

$$\begin{aligned} F = \overline{E} \Bigg(& F(1) \int_0^{\widehat{x}} \frac{\mathrm{d}\widehat{x}'}{\widehat{\Gamma}\,\overline{E}} \Big/ \int_0^1 \frac{\mathrm{d}\widehat{x}'}{\widehat{\Gamma}\,\overline{E}} \\ & - P_0 \int_0^1 \frac{\int_0^{\widehat{x}'} \Pi_s \mathrm{d}\widehat{x}''}{\widehat{\Gamma}\overline{E}} \mathrm{d}\widehat{x}' \left[\int_0^{\widehat{x}} \frac{\int_0^{\widehat{x}'} \Pi_s \mathrm{d}\widehat{x}''}{\widehat{\Gamma}\overline{E}} \mathrm{d}\widehat{x}' \Big/ \int_0^1 \frac{\int_0^{\widehat{x}'} \Pi_s \mathrm{d}\widehat{x}''}{\widehat{\Gamma}\overline{E}} \mathrm{d}\widehat{x}' \right. \\ & \left. - \int_0^{\widehat{x}} \frac{\mathrm{d}\widehat{x}'}{\widehat{\Gamma}\,\overline{E}} \Big/ \int_0^1 \frac{\mathrm{d}\widehat{x}'}{\widehat{\Gamma}\,\overline{E}} \right] \Bigg) . \end{aligned} \tag{2.22}$$

Rewriting equation (2.22) with integral terms already defined and some new ones,

$$F = \overline{E} \left(F(1) \frac{IGE_{0\widehat{x}}}{IGE_{01}} - P_0 \widetilde{ISGE}_{01} \left[\frac{\widetilde{ISGE}_{0\widehat{x}}}{\widetilde{ISGE}_{01}} - \frac{IGE_{0\widehat{x}}}{IGE_{01}} \right] \right), \tag{2.23a}$$

$$\widetilde{ISGE}_{0\widehat{x}} \coloneqq \int_0^{\widehat{x}} \frac{1}{\widehat{\Gamma}\overline{E}} \left[\int_0^{\widehat{x}'} \Pi_s \mathrm{d}\widehat{x}'' \right] \mathrm{d}\widehat{x}', \quad \widetilde{IS}_{0\widehat{x}} \coloneqq \int_0^{\widehat{x}} \Pi_s \mathrm{d}\widehat{x}', \tag{2.23b}$$

$$\widetilde{ISGE}_{01} \coloneqq \int_0^1 \frac{1}{\widehat{\Gamma}\overline{E}} \left[\int_0^{\widehat{x}} \Pi_s \mathrm{d}\widehat{x}' \right] \mathrm{d}\widehat{x}, \quad \widetilde{IS}_{01} \coloneqq \int_0^1 \Pi_s \mathrm{d}\widehat{x}, \tag{2.23c}$$

where $\widetilde{ISGE}_{0\widehat{x}}$ stands for **I**ntegral of **S**ource, **G**amma and **E** between 0 and $\widehat{x}$. $\widetilde{IS}_{0\widehat{x}}$ is the **I**ntegral of **S**ource between 0 and $\widehat{x}$. Therefore, $\widetilde{ISGE}_{01}$ and $\widetilde{IS}_{01}$ are evaluated in the whole interval. Note that integrals (2.23b) and

(2.23c) are written in a dimensionless form but they can be made dimensional on multiplying by $(\rho u)_{lb}\Delta\phi$,

$$ISGE_{0\widehat{x}} \coloneqq (\rho u)_{lb}\Delta\phi\widetilde{ISGE}_{0\widehat{x}} = \int_0^{\widehat{x}} \frac{\Delta x}{\widehat{\Gamma}\overline{E}}\left[\int_0^{\widehat{x}'} S\,\mathrm{d}\widehat{x}''\right]\mathrm{d}\widehat{x}', \tag{2.24a}$$

$$IS_{0\widehat{x}} \coloneqq (\rho u)_{lb}\Delta\phi\widetilde{IS}_{0\widehat{x}} = \Delta x\int_0^{\widehat{x}} S\,\mathrm{d}\widehat{x}' \equiv \int_{x_{lb}}^{x} S\,\mathrm{d}x', \tag{2.24b}$$

$$ISGE_{01} \coloneqq (\rho u)_{lb}\Delta\phi\widetilde{ISGE}_{01} = \int_0^{1} \frac{\Delta x}{\widehat{\Gamma}\overline{E}}\left[\int_0^{\widehat{x}} S\,\mathrm{d}\widehat{x}'\right]\mathrm{d}\widehat{x}, \tag{2.24c}$$

$$IS_{01} \coloneqq (\rho u)_{lb}\Delta\phi\widetilde{IS}_{01} = \Delta x\int_0^{1} S\,\mathrm{d}\widehat{x} \equiv \int_{x_{lb}}^{x_{rb}} S\,\mathrm{d}x. \tag{2.24d}$$

When assembling the final equation $F(1)$ will disappear of the $\widehat{\phi}$ expression as shown below.

$$\begin{aligned}
\widehat{\phi} =& F + (1-F(1))\,\overline{\phi}^N \\
=& \overline{E}\left(F(1)\frac{IGE_{0\widehat{x}}}{IGE_{01}} - P_0\,\widetilde{ISGE}_{01}\left[\frac{\widetilde{ISGE}_{0\widehat{x}}}{\widetilde{ISGE}_{01}} - \frac{IGE_{0\widehat{x}}}{IGE_{01}}\right]\right) \\
&+ (1-F(1))\,\overline{E}\left(\frac{IGE_{0\widehat{x}}}{IGE_{01}} + P_0\frac{1}{1-F(1)}\frac{\phi_{lb}}{\Delta\phi}ILE_{01}\left[\frac{ILE_{0\widehat{x}}}{ILE_{01}} - \frac{IGE_{0\widehat{x}}}{IGE_{01}}\right]\right), \\
=& \overline{E}\left(\frac{IGE_{0\widehat{x}}}{IGE_{01}} + P_0\frac{\phi_{lb}}{\Delta\phi}ILE_{01}\left[\frac{ILE_{0\widehat{x}}}{ILE_{01}} - \frac{IGE_{0\widehat{x}}}{IGE_{01}}\right]\right. \\
&\left. - P_0\,\widetilde{ISGE}_{01}\left[\frac{\widetilde{ISGE}_{0\widehat{x}}}{\widetilde{ISGE}_{01}} - \frac{IGE_{0\widehat{x}}}{IGE_{01}}\right]\right).
\end{aligned} \tag{2.25}$$

An estimation of $F(1)$ is not required anymore. It is easy to check that the complete solution (2.25) satisfies the ODE (2.9). $\widehat{\phi}$ is assembled with equation (2.20) together with (2.19) and (2.23a). Table 2.1 summarizes all integral formulae and solutions derived so far.

As an example, take the first case in this subsection: ρu, Γ and S constants, what leads to $\widehat{\Gamma} = \widehat{\rho u} = \widehat{\lambda} = 1$ and P, Π_s constants. The integral formulae can be calculated in a straightforward manner as

$$\begin{aligned}
\overline{E} &= \exp\left(P(\widehat{x}-1)\right), \\
ILE_{0\widehat{x}} = IGE_{0\widehat{x}} &= \frac{\exp P - \exp\left(P(1-\widehat{x})\right)}{P}, \\
\widetilde{IS}_{0\widehat{x}} &= \Pi_s\widehat{x}, \\
\widetilde{ISGE}_{0\widehat{x}} &= \Pi_s\frac{\exp P - (1+P\widehat{x})\exp\left(P(1-\widehat{x})\right)}{P^2},
\end{aligned}$$

then, they can be plugged into equations (2.19) and (2.23a). After some mathematical manipulation, the homogeneous and particular solutions read

$$\begin{aligned}
\overline{\phi}^N &= \frac{\exp P\widehat{x} - 1}{\exp P - 1}, \\
F &= \Pi_s\widehat{x} + (F(1) - \Pi_s)\frac{\exp P\widehat{x} - 1}{\exp P - 1}.
\end{aligned}$$

The complete solution is made up of the combination of both solutions and yields the same result as (2.12). In this case if one goes back to equation (2.10) when $\Pi_s = \text{const.}$, only one-step integration of the source term is required to get $F = \Pi_s \widehat{x}$ and achieve a homogeneous solution.

The assembled exact solution (2.25) is a general formula in which Péclet number plays a fundamental role. If $P = 0$, $\rho u = 0$ and $\overline{E} = 1 \, \forall \widehat{x} \in [0, 1]$, the complete solution becomes

$$\widehat{\phi} = \frac{IGE_{0\widehat{x}}}{IGE_{01}} - \frac{\Delta x}{\Gamma_{lb} \Delta \phi} \, ISGE_{01} \left[\frac{ISGE_{0\widehat{x}}}{ISGE_{01}} - \frac{IGE_{0\widehat{x}}}{IGE_{01}} \right].$$

When $|P| \to \infty$ because of $\Gamma \to 0$ the homogeneous component, $\overline{\phi}^N$, will come from a first-order ODE and $F = \Lambda_s^{(0)}$. Thus, the complete solution could be written down as follows:

$$\widehat{\phi} = \frac{\widetilde{IS}_{0\widehat{x}}}{\widehat{\rho u}} + \frac{\phi_{lb}}{\Delta \phi} \left(\frac{1}{\widehat{\rho u}} - 1 \right).$$

Transport Equation	
Dimensional	Normalized
$\dfrac{\mathrm{d}}{\mathrm{d}x}\left(\rho u\phi - \Gamma\dfrac{\mathrm{d}\phi}{\mathrm{d}x}\right) = S, \qquad x_{lb} \le x \le x_{rb}$ $\phi(x_{lb}) = \phi_{lb}, \quad \phi(x_{rb}) = \phi_{rb}$	$\dfrac{\mathrm{d}}{\mathrm{d}\widehat{x}}\left(\widehat{\rho u}\widehat{\phi} - \dfrac{\widehat{\Gamma}}{P_0}\dfrac{\mathrm{d}\widehat{\phi}}{\mathrm{d}\widehat{x}}\right) = \Pi_s - \dfrac{\phi_{lb}}{\Delta\phi}\dfrac{\mathrm{d}\widehat{\rho u}}{\mathrm{d}\widehat{x}}, \qquad 0 \le \widehat{x} \le 1$ $\widehat{\phi}(0) = 0, \quad \widehat{\phi}(1) = 1$
$\widehat{\phi} = \dfrac{\phi - \phi_{lb}}{\Delta\phi}, \quad \widehat{x} = \dfrac{x - x_{lb}}{\Delta x}, \quad \widehat{\rho u} = \dfrac{\rho u}{(\rho u)_{lb}}, \quad \widehat{\Gamma} = \dfrac{\Gamma}{\Gamma_{lb}}, \quad P = \dfrac{\rho u \Delta x}{\Gamma}, \quad P_0 = \dfrac{(\rho u)_{lb}\Delta x}{\Gamma_{lb}}, \quad \widehat{\lambda} = \dfrac{\widehat{\rho u}}{\widehat{\Gamma}} = \dfrac{P}{P_0}, \quad \Pi_s = \dfrac{S\Delta x}{(\rho u)_{lb}\Delta\phi}$	
The complete solution, $\widehat{\phi}(\widehat{x})$	$F(\widehat{x}) + (1 - F(1))\,\overline{\phi}^N(\widehat{x})$
The homogeneus solution, $\overline{\phi}^N(\widehat{x})$	$\overline{E}(\widehat{x})\left(\dfrac{IGE_{0\widehat{x}}}{IGE_{01}} + P_0\Phi ILE_{01}\left[\dfrac{ILE_{0\widehat{x}}}{ILE_{01}} - \dfrac{IGE_{0\widehat{x}}}{IGE_{01}}\right]\right)$
The particular solution, $F(\widehat{x})$	$\overline{E}(\widehat{x})\left(F(1)\dfrac{IGE_{0\widehat{x}}}{IGE_{01}} - P_0\,\widetilde{ISGE}_{01}\left[\dfrac{\widetilde{ISGE}_{0\widehat{x}}}{\widetilde{ISGE}_{01}} - \dfrac{IGE_{0\widehat{x}}}{IGE_{01}}\right]\right)$
Integration factor, $\overline{E}(\widehat{x})$	$\exp\left(-\displaystyle\int_{\widehat{x}}^{1} P\mathrm{d}\widehat{x}'\right)$
Integral of Lambda and E, $ILE_{0\widehat{x}}$	$\displaystyle\int_0^{\widehat{x}} \frac{\widehat{\lambda}}{\overline{E}}\mathrm{d}\widehat{x}' = \frac{1}{P_0}\left(\exp\overline{P} - \frac{1}{\overline{E}(\widehat{x})}\right), \qquad \overline{P} = \int_0^1 P\mathrm{d}\widehat{x}$
Integral of Gamma and E, $IGE_{0\widehat{x}}$	$\displaystyle\int_0^{\widehat{x}} \frac{1}{\widehat{\Gamma}\overline{E}}\mathrm{d}\widehat{x}'$
Integral of Source, $IS_{0\widehat{x}}$	$\Delta x\displaystyle\int_0^{\widehat{x}} S\,\mathrm{d}\widehat{x}', \qquad \widetilde{IS}_{0\widehat{x}} = \frac{IS_{0\widehat{x}}}{(\rho u)_{lb}\Delta\phi}$
Integral of Source, Gamma and E, $ISGE_{0\widehat{x}}$	$\displaystyle\int_0^{\widehat{x}}\left[\frac{\Delta x}{\widehat{\Gamma}\overline{E}}\int_0^{\widehat{x}'} S\,\mathrm{d}\widehat{x}''\right]\mathrm{d}\widehat{x}', \qquad \widetilde{ISGE}_{0\widehat{x}} = \dfrac{ISGE_{0\widehat{x}}}{(\rho u)_{lb}\Delta\phi}$

TABLE 2.1: Overview of the exact solution of a one-dimensional nonhomogeneous convection-diffusion problem with variable coefficients. Other useful parameters and relations are $\Delta\phi = \phi_{rb} - \phi_{lb}$, $\Delta x = x_{rb} - x_{lb}$ and $\Phi(1 - F(1)) = \phi_{lb}/\Delta\phi$.

2.2 The nodal equation

An exact solution of a transport equation with variable coefficients and source term in a given interval has been put forward. Such a solution requires integrals whose estimation is accurate as long as the integrand is interpolated appropriately. The larger any domain is, the more difficult it will be to find good interpolators, so the traditional alternative is to split up the whole domain in intervals wherein the solution is known. To connect two adjacent intervals the continuity of diffusion flux is enforced at a generic point x_C belonging to both. The whole discretization is named "**E**nhanced **N**umerical **A**pproximation of a **T**ransport **E**quation", ENATE.

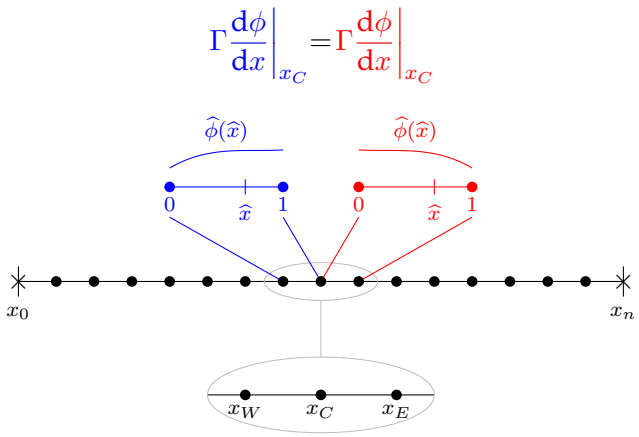

FIGURE 2.2: ENATE discretization: (×) Boundary points; (•) Internal points. Two generic intervals: one from *W*est node to *C*entral node and the other from *C*entral to *E*ast

The diffusion flux on the normalized map reads

$$\Gamma\frac{\mathrm{d}\phi}{\mathrm{d}x} = \Gamma\frac{\Delta\phi}{\Delta x}\frac{\mathrm{d}\widehat{\phi}}{\mathrm{d}\widehat{x}} = \frac{\rho u\Delta\phi}{P}\frac{\mathrm{d}\widehat{\phi}}{\mathrm{d}\widehat{x}} = \rho u\Delta\phi\left[\frac{1}{P}\frac{\mathrm{d}F}{\mathrm{d}\widehat{x}} + (1-F(1))\frac{1}{P}\frac{\mathrm{d}\overline{\phi}^N}{\mathrm{d}\widehat{x}}\right], \tag{2.26}$$

where the derivatives of the homogeneous and particular solutions are

$$\frac{\mathrm{d}\overline{\phi}^N}{\mathrm{d}\widehat{x}} = P\left[\overline{\phi}^N + \frac{\widetilde{k}}{\widehat{\rho u}} + \Phi\left(1 - \frac{1}{\widehat{\rho u}}\frac{ILE_{01}}{IGE_{01}}\right)\right], \tag{2.27a}$$

$$\frac{\mathrm{d}F}{\mathrm{d}\widehat{x}} = P\left[F + \frac{F(1)\widetilde{k}}{\widehat{\rho u}} - \frac{1}{\widehat{\rho u}}\left(\widetilde{IS}_{0\widehat{x}} - \frac{\widetilde{ISGE}_{01}}{IGE_{01}}\right)\right], \tag{2.27b}$$

being $\widetilde{k} \coloneqq 1/(P_0 IGE_{01})$. Equation (2.26) is associated to a reference interval that goes from 0 to 1, either blue or red in Figure 2.2. The value of a variable at a node depends on the interval where it is located. For instance, if the reference Péclet over an interval, P_0, is required, it is calculated as

$$P_0 = P(0) = \begin{cases} \dfrac{(\rho u)_W \Delta x_{WC}}{\Gamma_W}, & \text{if } \widehat{x} \text{ is within } WC \\ \dfrac{(\rho u)_C \Delta x_{CE}}{\Gamma_C}, & \text{if } \widehat{x} \text{ is within } CE \end{cases}$$

Equation (2.26) is thus applied to both intervals, $[x_W, x_C]$ and $[x_C, x_E]$, in the discretized domain. The interval lengths $\Delta x_{WC} = x_C - x_W$ and $\Delta x_{CE} = x_E - x_C$ could be the same, as in Figure 2.2, or different, if a non-uniform mesh is employed. The Péclet number will be affected by the different lengths. On the other hand, integrals such as ILE, IGE, IS, $ISGE$ must be found in all intervals using the available information at nodes. In Subsection 2.3 this will be further detailed.

The Central node, the end point of the interval $[x_W, x_C]$, $\widehat{x} = 1$ in the reference interval, is the same as the start point of the next one $[x_C, x_E]$, $\widehat{x} = 0$ in the reference interval. Linking the diffusion fluxes yields:

$$
\begin{aligned}
&(\rho u)_C \, \Delta\phi_{WC} \left[\frac{1}{P_1} \frac{\mathrm{d}F}{\mathrm{d}\widehat{x}}\bigg|_1 + (1 - F_C) \, \frac{1}{P_1} \frac{\mathrm{d}\overline{\phi}^N}{\mathrm{d}\widehat{x}}\bigg|_1 \right] \\
&= (\rho u)_C \, \Delta\phi_{CE} \left[\frac{1}{P_0} \frac{\mathrm{d}F}{\mathrm{d}\widehat{x}}\bigg|_0 + (1 - F_E) \, \frac{1}{P_0} \frac{\mathrm{d}\overline{\phi}^N}{\mathrm{d}\widehat{x}}\bigg|_0 \right],
\end{aligned}
\tag{2.28}
$$

where $\Delta\phi_{WC} = \phi_C - \phi_W$, $\Delta\phi_{CE} = \phi_E - \phi_C$ and $F_C = F(1)|_{WC}$, $F_E = F(1)|_{CE}$. Finally, the factors that have to be calculated at the edges of the intervals are

$$
\begin{aligned}
\frac{1}{P_0} \frac{\mathrm{d}\overline{\phi}^N}{\mathrm{d}\widehat{x}}\bigg|_0 &= \widetilde{k}_{CE} + \Phi_{CE} \left[1 - \frac{ILE_{01}}{IGE_{01}}\bigg|_{CE} \right], \\
\frac{1}{P_1} \frac{\mathrm{d}\overline{\phi}^N}{\mathrm{d}\widehat{x}}\bigg|_1 &= 1 + \frac{\widetilde{k}_{WC}}{\widehat{\rho u}_C} + \Phi_{WC} \left[1 - \frac{1}{\widehat{\rho u}_C} \frac{ILE_{01}}{IGE_{01}}\bigg|_{WC} \right], \\
\frac{1}{P_0} \frac{\mathrm{d}F}{\mathrm{d}\widehat{x}}\bigg|_0 &= F_E \widetilde{k}_{CE} + \frac{\widetilde{ISGE}_{01}}{IGE_{01}}\bigg|_{CE}, \\
\frac{1}{P_1} \frac{\mathrm{d}F}{\mathrm{d}\widehat{x}}\bigg|_1 &= F_C \left[1 + \frac{\widetilde{k}_{WC}}{\widehat{\rho u}_C} \right] - \frac{1}{\widehat{\rho u}_C} \left[\widetilde{IS}_{01}\Big|_{WC} - \frac{\widetilde{ISGE}_{01}}{IGE_{01}}\bigg|_{WC} \right],
\end{aligned}
$$

together with the following parameters:

$$
\begin{aligned}
&\widetilde{k}_{CE} = \frac{1}{P_0 IGE_{01}}\bigg|_{CE}, \quad \widetilde{k}_{WC} = \frac{1}{P_0 IGE_{01}}\bigg|_{WC}, \\
&\Phi_{CE} = \frac{1}{1 - F_E} \frac{\phi_C}{\Delta\phi_{CE}}, \quad \Phi_{WC} = \frac{1}{1 - F_C} \frac{\phi_W}{\Delta\phi_{WC}}, \\
&\widetilde{ISGE}_{01}\Big|_{CE} = \frac{ISGE_{01}|_{CE}}{(\rho u)_C \Delta\phi_{CE}}, \quad \widetilde{ISGE}_{01}\Big|_{WC} = \frac{ISGE_{01}|_{WC}}{(\rho u)_W \Delta\phi_{WC}}, \\
&\widetilde{IS}_{01}\Big|_{WC} = \frac{IS_{01}|_{WC}}{(\rho u)_W \Delta\phi_{WC}}, \quad \widehat{\rho u}_C = \widehat{\rho u}(1)|_{WC} = \frac{(\rho u)_C}{(\rho u)_W}.
\end{aligned}
$$

Introducing previous factors and parameters into equation (2.28), the inner nodal equation takes the following expression:

$$\begin{aligned}
&-(\rho u)_W \left(\widetilde{k}_{WC} + \left. \frac{ILE_{01}}{IGE_{01}} \right|_{WC} \right) \phi_W + \left[(\rho u)_W \widetilde{k}_{WC} \right. \\
&\left. + (\rho u)_C \left(\widetilde{k}_{CE} + \left. \frac{ILE_{01}}{IGE_{01}} \right|_{CE} \right) \right] \phi_C - (\rho u)_C \widetilde{k}_{CE} \, \phi_E \\
&= IS_{01}|_{WC} + \left(\left. \frac{ISGE_{01}}{IGE_{01}} \right|_{CE} - \left. \frac{ISGE_{01}}{IGE_{01}} \right|_{WC} \right).
\end{aligned} \tag{2.29}$$

Although the integrals, now applied at each interval, have been defined in (2.6c), (2.24d) and (2.24c), and set forth in Table 2.1, will be rewritten here as a reminder.

$$\begin{aligned}
ILE_{01} &= \int_0^1 \frac{\widehat{\lambda}}{\overline{E}} \mathrm{d}\widehat{x} = \frac{\exp \overline{P} - 1}{P_0}, \quad \overline{P} = \int_0^1 P \, \mathrm{d}\widehat{x}, \\
IGE_{01} &= \int_0^1 \frac{1}{\widehat{\Gamma}\overline{E}} \mathrm{d}\widehat{x}, \quad \widetilde{k} = \frac{1}{P_0 IGE_{01}}, \\
IS_{01} &= \Delta x \int_0^1 S \, \mathrm{d}\widehat{x}, \quad ISGE_{01} = \int_0^1 \frac{\Delta x}{\widehat{\Gamma}\overline{E}} \left[\int_0^{\widehat{x}} S \, \mathrm{d}\widehat{x}' \right] \mathrm{d}\widehat{x}.
\end{aligned}$$

Identifying the coefficients that multiply each ϕ_i, equation (2.29) can be written in the form

$$-A_W \phi_W + A_C \phi_C - A_E \phi_E = b_C, \tag{2.30}$$

with the influence coefficients,

$$A_C \coloneqq (\rho u)_W \widetilde{k}_{WC} + (\rho u)_C \left(\widetilde{k}_{CE} + \left. \frac{ILE_{01}}{IGE_{01}} \right|_{CE} \right), \tag{2.31a}$$

$$A_W \coloneqq (\rho u)_W \left(\widetilde{k}_{WC} + \left. \frac{ILE_{01}}{IGE_{01}} \right|_{WC} \right), \tag{2.31b}$$

$$A_E \coloneqq (\rho u)_C \widetilde{k}_{CE}, \tag{2.31c}$$

and discrete source,

$$b_C \coloneqq IS_{01}|_{WC} + \left(\left. \frac{ISGE_{01}}{IGE_{01}} \right|_{CE} - \left. \frac{ISGE_{01}}{IGE_{01}} \right|_{WC} \right). \tag{2.32}$$

Some algebraic relations can be extracted form the result derived. The equation (2.29) can be arranged as follows:

$$\begin{aligned}
&-(\rho u)_W \widetilde{k}_{WC} \, \phi_C + (\rho u)_W \left(\widetilde{k}_{WC} + \left. \frac{ILE_{01}}{IGE_{01}} \right|_{WC} \right) \phi_W + IS_{01}|_{WC} - \left. \frac{ISGE_{01}}{IGE_{01}} \right|_{WC} = \\
&-(\rho u)_C \widetilde{k}_{CE} \, \phi_E + (\rho u)_C \left(\widetilde{k}_{CE} + \left. \frac{ILE_{01}}{IGE_{01}} \right|_{CE} \right) \phi_C - \left. \frac{ISGE_{01}}{IGE_{01}} \right|_{CE}.
\end{aligned}$$

The total flux $\mathcal{F} = \mathcal{F}(x) \coloneqq \rho u\phi - \Gamma \mathrm{d}\phi/\mathrm{d}x$, defined by the transport equation (2.1a), can be written within a reference interval[2],

$$\mathcal{F}(\widehat{x}) = -(\rho u)_0 \widetilde{k}\,\phi_1 + (\rho u)_0 \left(\widetilde{k} + \frac{ILE_{01}}{IGE_{01}}\right)\phi_0 + IS_{0\widehat{x}} - \frac{ISGE_{01}}{IGE_{01}}.$$

The discrete equation (2.29) becomes

$$\mathcal{F}(1)|_{WC} = \mathcal{F}(0)|_{CE}\,.$$

The former expression just says that $\mathcal{F}$ leaving the interval $[x_W, x_C]$ is equal to that entering the interval $[x_C, x_E]$ or roughly speaking, the discrete solution guarantees the continuity of $\mathcal{F}$. This comes as no surprise as the term $\rho u\phi$ is supposed to be continuous at node x_C and $\mathcal{F}$ is also continuous on matching the diffusive flux. $\mathcal{F}$ can only be discontinuous if the source is a Dirac-delta. In Section 2.5 a case with discontinuous coefficients but with continuous flux will be assessed with ENATE scheme.

The algebraic relation (2.30) is akin to other Finite Volume (FV) methods, although some differences arise. In traditional FV methods, numerical tools are employed to approximate the integral balances of an ODE or PDE with values interpolated at cell faces. This gives a connection between nodes in the discrete domain, with coefficients related to all these approximations. By contrast, ENATE is a numerical scheme whose coefficients (2.31) are related to integrals of the convective, diffusive and source terms and whose accuracy can be as high as desired by using better interpolations without modifying the computational molecule.

In Table 2.4, on page 46, all formulae that are used to compute the numerical solution of a convection-diffusion problem are summarized.

2.2.1 A low-order approximation

As mentioned before ILE_{01}, IGE_{01}, $ISGE_{01}$ and IS_{01} should be approximated to get a numerical solution. A simplification could be carried out with the assumption that ρu, Γ and S are constant between nodes, with their values taken at the interval midpoint, e.g., $\rho u = (\rho u)_w$ if $x_W \le x \le x_C$; $\rho u = (\rho u)_e$ if $x_C \le x \le x_E$. Here w denotes the midpoint of $[x_W, x_C]$ and e that of $[x_C, x_E]$. So, the integrals in a generic interval are

$$ILE_{01} = IGE_{01} = \frac{1}{B(P_{1/2})}, \quad \widetilde{k} = \frac{B(P_{1/2})}{P_{1/2}},$$
$$IS_{01} = S_{1/2}\Delta x, \quad \frac{ISGE_{01}}{IGE_{01}} = IS_{01}W(P_{1/2}),$$

where the $B(z)$ and $W(z)$ functions are defined as

$$B(z) \coloneqq \frac{z}{\exp z - 1}, \quad W(z) \coloneqq \frac{\exp z - z - 1}{z\,(\exp z - 1)}.$$

[2]For further information on the deduction of the flux (2.33) see Appendix A.

Finally the influence coefficients and discrete source now read

$$
\begin{aligned}
&A_C = A_W + A_E + \left[(\rho u)_e - (\rho u)_w\right], \\
&A_W = \frac{\Gamma_w}{\Delta x_{WC}} B(-P_w), \quad A_E = \frac{\Gamma_e}{\Delta x_{CE}} B(P_e), \\
&b_C = S_w \Delta x_{WC} \left[1 - W(P_w)\right] + S_e \Delta x_{CE} W(P_e),
\end{aligned}
$$

with the western and eastern Péclet calculated as

$$
P_w = \frac{(\rho u)_w \, \Delta x_{WC}}{\Gamma_w}, \quad P_e = \frac{(\rho u)_e \, \Delta x_{CE}}{\Gamma_e}.
$$

This discretization leads to the second order accurate scheme of Thiart [212]. All in all, ENATE is a global exponential scheme that can be particularized to known schemes by taking different approximations to the integrals that are involved in the influence coefficients and discrete source. In *Numerical Tests* section, ENATE will be compared to a scheme closer than Thiart's: the exponential scheme of ten Thije Boonkkamp [209]. The coefficients in this subsection are identical to those in ten Thije Boonkkamp *et al.* but the quadrature employed is different, normally a trapezoidal rule. In [6] a GL quadrature was occasionally implemented. The coefficients equality was demonstrated in a paper where the FV-CF scheme and ENATE were already compared for linear source terms [224].

2.2.2 Fundamental discretization-properties

The ENATE scheme ends up solving a system of algebraic equations that in matrix form is

$$
\mathbf{A}\boldsymbol{\phi} = \mathbf{b}, \tag{2.33}
$$

where $\mathbf{A}$ is a tridiagonal matrix, $\boldsymbol{\phi}$ is the vector of the discrete transported variable, and $\mathbf{b}$ the discrete source vector.

$$
\mathbf{A} = \begin{pmatrix}
\circ & \circ & & & & \\
\circ & \circ & \circ & & & \\
 & \circ & \circ & \circ & & \\
 & & \circ & \circ & \circ & \\
 & & & \circ & \circ
\end{pmatrix}, \quad
\boldsymbol{\phi} = \begin{pmatrix} \circ \\ \circ \\ \circ \\ \circ \\ \circ \end{pmatrix}, \quad
\mathbf{b} = \begin{pmatrix} \circ \\ \circ \\ \circ \\ \circ \\ \circ \end{pmatrix}.
$$

Blue circles symbolize the inner region of the domain. Red circles are the special treatment of eqn.(2.30) at boundaries which is provided in Subsection 2.2.3. As solving (2.33) with a direct method requires a notable amount of work and computer storage, iterative methods are normally used. Their features are studied by numerical analysis. However, not only does it matter the numerical behaviour in terms of stability, also the solution must be in accordance with physical reality and violation of physical laws such as casual loss/gain of mass, non-physical oscillations or shock moving at wrong speed should not be allowed. Therefore, to give realistic results a numerical scheme in CFD should satisfy some properties summarized in Table 2.2, see Versteeg *et al.* [227], and Schäfer [187].

Transportiveness is the ability of a numerical scheme to reproduce by itself in what direction the information of ϕ is being transported. In a

Numerical analysis	CFD
Convergence	Transportiveness
Consistency	Conservativeness
Stability	Boundedness

TABLE 2.2: Properties of a CFD scheme related to those studied in numerical analysis

diffusion-dominated problem ($P \to 0$), ϕ is spread over the whole domain with a non-preferred direction. In the opposite case, in a convection-dominated problem ($|P| \to \infty$), ϕ only depends on upstream values or rather, the information is totally transported in the sense marked by the sign of u velocity.

When Péclet is zero in ENATE, $\overline{E}(\widehat{x}) = 1 \ \forall \widehat{x}$ and $ILE_{01} = 0$. Since the exponential factor is no longer considered in IGE_{01} and $ISGE_{01}$, the integrals are renamed as

$$IGE_{01} \to IG_{01} \coloneqq \int_0^1 \frac{\mathrm{d}\widehat{x}}{\widehat{\Gamma}},$$
$$ISGE_{01} \to ISG_{01} \coloneqq \int_0^1 \frac{\Delta x}{\widehat{\Gamma}} \left[\int_0^{\widehat{x}} S \, \mathrm{d}\widehat{x}' \right] \mathrm{d}\widehat{x}.$$

The product of the convective term and the parameter $\widetilde{k}$ is rearranged as

$$\begin{aligned}(\rho u)_C \, \widetilde{k}_{CE} &= (\rho u)_C \left. \frac{1}{P_0 IG_{01}} \right|_{CE} \\ &= \cancel{(\rho u)_C} \frac{1}{\dfrac{\cancel{(\rho u)_C} \Delta x_{CE}}{\Gamma_C} \, IG_{01}|_{CE}} \\ &= \frac{\Gamma_C}{\Delta x_{CE}} \frac{1}{IG_{01}|_{CE}}.\end{aligned}$$

Thus, the pure-diffusion nodal equation writes

$$-A_W \phi_W + A_C \phi_C - A_E \phi_E = b_C, \tag{2.34a}$$
$$A_W = \frac{\Gamma_W}{\Delta x_{WC}} \frac{1}{IG_{01}|_{WC}}, \quad A_E = \frac{\Gamma_C}{\Delta x_{CE}} \frac{1}{IG_{01}|_{CE}}, \tag{2.34b}$$
$$A_C = A_W + A_E, \tag{2.34c}$$
$$b_C = IS_{01}|_{WC} + \left(\left. \frac{ISG_{01}}{IG_{01}} \right|_{CE} - \left. \frac{ISG_{01}}{IG_{01}} \right|_{WC} \right). \tag{2.34d}$$

The discrete equation (2.34a) corresponds to the 1D Poisson equation and shows up a transportive behaviour: ϕ at x_C is influenced by x_W and x_E. Note that A_W and A_E contain the harmonic average of Γ if $1/\Gamma$ is linear in their respective intervals. Moreover, if a uniform mesh is set up and Γ is constant, $IG_{01} = 1$, the influence coefficients are the same and ϕ tends to be influenced equally by upwind and downwind directions.

As Péclet increases and goes to plus infinity, ϕ_W contribution becomes more and more important as compared to that of ϕ_C. When Péclet goes to minus infinity, ϕ_E is dominant. The case where ρu is positive will be

discussed, with convective information travelling from left to right within the domain. Integrals such as IGE and $ISGE$ must be approximated for this Péclet regime. Similarly to ILE (2.7) we can obtain a simplified version for the Integral of Gamma and E,

$$\begin{aligned} IGE_{01} &= \int_0^1 \frac{1}{\widehat{\Gamma}\overline{E}}\mathrm{d}\widehat{x} \\ &= \int_0^1 \frac{1}{\widehat{\rho u}}\frac{\widehat{\lambda}}{\overline{E}}\mathrm{d}\widehat{x} \\ &= -\frac{1}{P_0}\int_0^1 \frac{1}{\widehat{\rho u}}\frac{\mathrm{d}}{\mathrm{d}\widehat{x}}\left(\frac{1}{\overline{E}}\right)\mathrm{d}\widehat{x} \\ &\overset{(a)}{=} -\frac{1}{P_0}\int_0^1 \frac{\mathrm{d}}{\mathrm{d}\widehat{x}}\left(\frac{1}{\widehat{\rho u}\overline{E}}\right)\mathrm{d}\widehat{x} \\ &= \frac{1}{P_0}\left(\exp\int_0^1 P\,\mathrm{d}\widehat{x} - \frac{1}{\widehat{\rho u}(1)}\right), \end{aligned}$$

and for the Integral of Source, Gamma and E,

$$\begin{aligned} ISGE_{01} &= \int_0^1 \left[\frac{\Delta x}{\widehat{\Gamma}\overline{E}}\int_0^{\widehat{x}} S\,\mathrm{d}\widehat{x}'\right]\mathrm{d}\widehat{x} \\ &= -\frac{1}{P_0}\int_0^1 \left[\frac{\Delta x}{\widehat{\rho u}}\frac{\mathrm{d}}{\mathrm{d}\widehat{x}}\left(\frac{1}{\overline{E}}\right)\int_0^{\widehat{x}} S\,\mathrm{d}\widehat{x}'\right]\mathrm{d}\widehat{x} \\ &\overset{(b)}{=} -\frac{1}{P_0}\int_0^1 \frac{\mathrm{d}}{\mathrm{d}\widehat{x}}\left(\frac{\Delta x}{\widehat{\rho u}\overline{E}}\int_0^{\widehat{x}} S\,\mathrm{d}\widehat{x}'\right)\mathrm{d}\widehat{x} \\ &= -\frac{\Delta x}{P_0\widehat{\rho u}(1)}\int_0^1 S\,\mathrm{d}\widehat{x}. \end{aligned}$$

Both simplifications can be employed if the inequality (a),

$$\begin{aligned} &\left|\frac{1}{\overline{E}}\frac{\mathrm{d}}{\mathrm{d}\widehat{x}}\left(\frac{1}{\widehat{\rho u}}\right)\right| \ll \left|\frac{1}{\widehat{\rho u}}\frac{\mathrm{d}}{\mathrm{d}\widehat{x}}\left(\frac{1}{\overline{E}}\right)\right| \\ &\left|\frac{\mathrm{d}}{\mathrm{d}\widehat{x}}\left(\frac{1}{\widehat{\rho u}}\right)\right| \ll \left|\frac{1}{\widehat{\rho u}}P\right| \\ &\left|\frac{\mathrm{d}}{\mathrm{d}\widehat{x}}\left(\ln\widehat{\rho u}\right)\right| \ll |P|, \end{aligned}$$

and inequality (b),

$$\begin{aligned} &\left|\frac{1}{\overline{E}}\frac{\mathrm{d}}{\mathrm{d}\widehat{x}}\left(\frac{\Delta x}{\widehat{\rho u}}\int_0^{\widehat{x}} S\,\mathrm{d}\widehat{x}'\right)\right| \ll \left|\frac{\Delta x}{\widehat{\rho u}}\frac{\mathrm{d}}{\mathrm{d}\widehat{x}}\left(\frac{1}{\overline{E}}\right)\int_0^{\widehat{x}} S\,\mathrm{d}\widehat{x}'\right|, \\ &\left|\frac{\mathrm{d}}{\mathrm{d}\widehat{x}}\left(\frac{\Delta x}{\widehat{\rho u}}\right)\int_0^{\widehat{x}} S\,\mathrm{d}\widehat{x}' + \frac{\Delta x\,S}{\widehat{\rho u}}\right| \ll \left|\frac{\Delta x\,P}{\widehat{\rho u}}\int_0^{\widehat{x}} S\,\mathrm{d}\widehat{x}'\right|, \\ &\left|\frac{\mathrm{d}}{\mathrm{d}\widehat{x}}\left(\ln\widehat{\rho u}\right)\right| + \frac{1}{\left|\frac{1}{S}\int_0^{\widehat{x}} S\,\mathrm{d}\widehat{x}'\right|} \ll |P|, \end{aligned}$$

are satisfied. These inequalities will now be used to estimate the values of $\widetilde{k}$ and the ratios ILE_{01}/IGE_{01} and $ISGE_{01}/IGE_{01}$ when Péclet is very high. These are

$$\widetilde{k} = \frac{1}{\exp \int_0^1 P \,\mathrm{d}\widehat{x} - \dfrac{1}{\widehat{\rho u}(1)}}, \tag{2.35a}$$

$$\frac{ILE_{01}}{IGE_{01}} = \frac{\exp \int_0^1 P \,\mathrm{d}\widehat{x} - 1}{\exp \int_0^1 P \,\mathrm{d}\widehat{x} - \dfrac{1}{\widehat{\rho u}(1)}}, \tag{2.35b}$$

$$\frac{ISGE_{01}}{IGE_{01}} = -\frac{\Delta x \int_0^1 S \,\mathrm{d}\widehat{x}}{\widehat{\rho u}(1) \exp \int_0^1 P \,\mathrm{d}\widehat{x} - 1}. \tag{2.35c}$$

It is clear that when taking the limit as Péclet goes to infinity, the exponential dominates to make the ratio (2.35b) go to 1, whereas the ratio (2.35c) and parameter (2.35a) become negligible. In Figure 2.3 the tendency of all these functions is displayed. Finally, the pure-convection nodal equation reads

$$-A_W \phi_W + A_C \phi_C = b_C, \tag{2.36a}$$

$$A_C = (\rho u)_C\,, \quad A_W = (\rho u)_W\,, \tag{2.36b}$$

$$b_C = IS_{01}|_{WC}\,, \tag{2.36c}$$

assuming $\rho u > 0$. Notice ϕ at x_C is only bound to x_W as the convective information only comes from the upwind side. In case that $P \to -\infty$ the resulting equation gives

$$A_C \phi_C - A_E \phi_E = b_C, \tag{2.37a}$$

$$A_C = -(\rho u)_C\,, \quad A_E = -(\rho u)_E\,, \tag{2.37b}$$

$$b_C = IS_{01}|_{CE}\,. \tag{2.37c}$$

Therefore, ENATE fulfills transportiveness for any Péclet number regime.

Conservativeness is the ability of a numerical scheme to represent the conservation principle at the discrete level whatever the grid size, or in other words, preserves $\mathcal{F}$ at the edge between two adjacent intervals. This is easy to check with a generic interval, for instance, $[x_W, x_C]$. Working out the

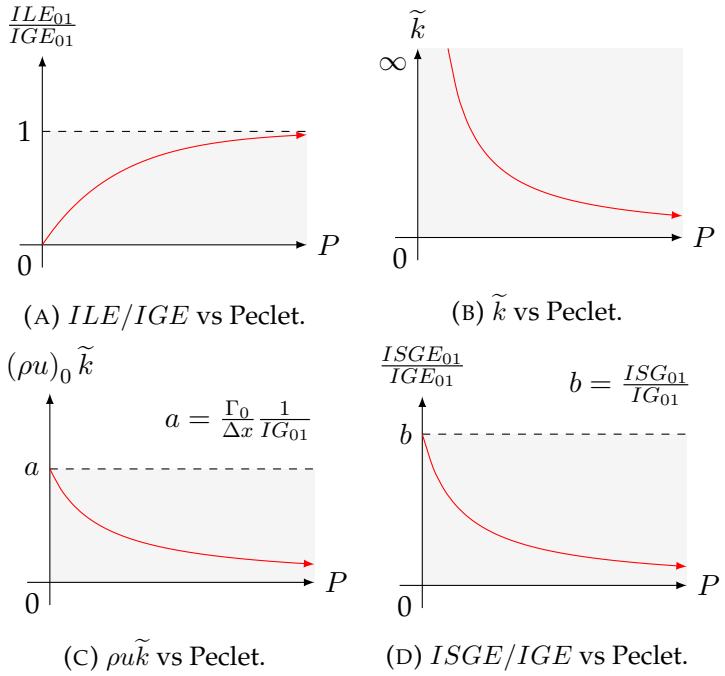

(A) ILE/IGE vs Peclet.

(B) $\widetilde{k}$ vs Peclet.

(C) $\rho u\widetilde{k}$ vs Peclet.

(D) $ISGE/IGE$ vs Peclet.

FIGURE 2.3: Trends for the ratios and parameters of the equation (2.29) with increasing Péclet. Gray areas mean the ranges over which those functions can vary. $\widetilde{k}$ is an unbounded function at $P = 0$.

total flux $\mathcal{F}$ at both nodes,

$$\begin{aligned}
\mathcal{F}_C = \mathcal{F}(1)|_{WC} = &- (\rho u)_W \widetilde{k}_{WC}\,\phi_C \\
&+ (\rho u)_W \left(\widetilde{k}_{WC} + \left.\frac{ILE_{01}}{IGE_{01}}\right|_{WC}\right)\phi_W \\
&+ IS_{01}|_{WC} - \left.\frac{ISGE_{01}}{IGE_{01}}\right|_{WC}, \\
\mathcal{F}_W = \mathcal{F}(0)|_{WC} = &- (\rho u)_W \widetilde{k}_{WC}\,\phi_C \\
&+ (\rho u)_W \left(\widetilde{k}_{WC} + \left.\frac{ILE_{01}}{IGE_{01}}\right|_{WC}\right)\phi_W \\
&- \left.\frac{ISGE_{01}}{IGE_{01}}\right|_{WC},
\end{aligned}$$

and,

$$\mathcal{F}_C - \mathcal{F}_W = IS_{01}|_{WC} = \int_{x_W}^{x_C} S\,\mathrm{d}x.$$

The left-hand side can be defined as the integral from x_W to x_C of the $\mathcal{F}$ variation. The final result,

$$\int_{x_W}^{x_C} \left(\frac{\mathrm{d}\mathcal{F}}{\mathrm{d}x} - S\right)\mathrm{d}x = 0,$$

gives the integral form of the conservation law (2.1a) valid in a single interval as in the whole domain. ENATE is thus a conservative approach.

Finally, *Boundedness* relates to the fact that in the absence of sources the value of ϕ within an interval should lie between the values at the edges. From a physical point of view some transport quantities must be bounded to certain limits, the thermodynamic temperature cannot be negative for instance. Since the continuous transport equation must fulfil a maximum principle, as we proved for the homogeneous solution on page 22, the discrete equation does satisfy monotonicity. This CFD property is basically related to the matrix of (2.33) being an M-matrix. The matrix $\mathbf{A}$ is an M-matrix if:

1. The off-diagonal elements of $\mathbf{A}$ are negative,
2. $\mathbf{A}$ is regular (nonsingular),
3. $\mathbf{A}^{-1} \geq 0$.

These items ensure positivity but criteria 2 and 3 are tricky to check. Authors such as Fiedler [56] or Horn and Johnson [82] gave a list of equivalent conditions that are sufficient but sometimes not necessary. In this group it is included the condition that the matrix is diagonally dominant [226, p. 92], what can be expressed as

$$|A_C| \geq \sum_{i \in \mathcal{N}_x} |A_i| \,, \tag{2.38}$$

with $\mathcal{N}_x = \{W, E\}$. When the case of pure diffusion, ϕ is absolutely bounded. In a general case, A_C is not equal to $\sum_i A_i$ considering that

$$A_C = A_W + A_E + \left[(\rho u)_C \left. \frac{ILE_{01}}{IGE_{01}} \right|_{CE} - (\rho u)_W \left. \frac{ILE_{01}}{IGE_{01}} \right|_{WC} \right].$$

In 1D mass conservation implies $\mathrm{d}\rho u/\mathrm{d}x = 0$, that is ρu constant. The term in square brackets is identically zero and ϕ is bounded. In other cases, such as multidimensions or an injection/extraction of mass $\mathrm{d}\rho u/\mathrm{d}x = \dot{m}$ where $\dot{m}$ is the arbitrary mass flux, the term in brackets could be equal, less or greater than zero, and therefore, the condition (2.38) can be met or not. It should be mentioned that the solution could converge even if the diagonal is not dominant.

Another essential criterion, see Patankar [150], is that the influence coefficients (2.31) must always have the same sign, either positive or negative. Take the steady-state 1D heat conduction equation,

$$\frac{\mathrm{d}}{\mathrm{d}x} \left(-k \frac{\mathrm{d}T}{\mathrm{d}x} \right) = 0,$$

with variable thermal conductivity $k = k(x)$. Since the problem is free of heat sources, the temperature must be within the range of the boundary values. Applying $k = \exp(100\,x)$, $T(0) = 0$ and $T(1) = 1$ the exact solution is $T(x) = (1 - \exp(-100x))/(1 - \exp(-100))$. Let the problem be discretized uniformly by a central difference scheme in conservative form,

$$-k_w\, T_W + (k_w + k_e)\, T_C - k_e\, T_E = 0, \tag{2.39}$$

and in non-conservative form,

$$-\left(1-\frac{\dot{k}_C\Delta x}{2\,k_C}\right)T_W+2\,T_C-\left(1+\frac{\dot{k}_C\Delta x}{2\,k_C}\right)T_E=0. \tag{2.40}$$

Thermal conductivities k_e and k_w are evaluated at interfaces of the control volume and $\dot{k}$ is the spatial derivative of k. In the scheme (2.39) the temperature at x_C is calculated with the weighted average of their neighbour nodes at x_W and x_E and hence limited, while in the scheme (2.40) an increase of T_E leads to a decrease of T_C, giving a non-realistic physics displayed in Figure 2.4. Therefore, this criterion could be a better tool to catch whether a numerical scheme is bounded or not.

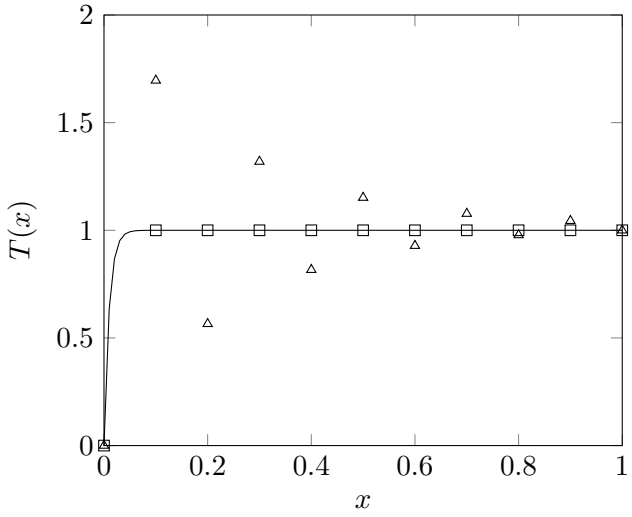

FIGURE 2.4: Numerical solutions for the schemes (2.39) (□) and (2.40) (△) compared with the exact solution (-).

The ENATE coefficients can be summarized by the next expression:

$$A_i=(1-\delta_{ij})\left[(\rho u)_j\widetilde{k}_{ji}\right]+(1-\delta_{il})\left[(\rho u)_i\left(\widetilde{k}_{il}+\frac{ILE_{01}}{IGE_{01}}\bigg|_{il}\right)\right], \tag{2.41}$$

being δ_{ij} and δ_{il} Kronecker deltas,

$$\delta_{ab}=\begin{cases}1, & \text{if } a=b,\\ 0, & \text{if } a\neq b.\end{cases}$$

The indices i, j, and l are given in Table below.

i	W	C	E
j	W	W	C
l	C	E	E

TABLE 2.3: Index specification

As an example, if A_E is sought, then $i\equiv E$ and $j\equiv C$ and $l\equiv E$. That makes $\delta_{EC}=0$ and $\delta_{EE}=1$ which results is $(\rho u)_C\widetilde{k}_{CE}$. Same for the other coefficients.

In expression (2.41) there are two fundamental terms: $(\rho u)_{lb}\widetilde{k}$ and $(\rho u)_{lb}(\widetilde{k}+ ILE_{01}/IGE_{01})$. The main idea is that if it is shown that both terms have the same sign, the sign of A_i will be the same for the three coefficients of (2.30). To do so, it is essential to seek the sign of the integrals and variables that make up the coefficients. By definition, the diffusion variable Γ is always positive what makes $\widehat{\Gamma}$ positive as well. The factor $\overline{E}$ is positive since it is an exponential function, and as IGE_{01} is an integral by combination of both parameters, is also positive. Therefore, the A_i sign depends on the convective sign. $\widetilde{k}$ contains $(\rho u)_{lb}$ in P_0, and ILE_{01} in P.

If $(\rho u)_{lb} \geq 0$ all coefficients have the same sign. If $(\rho u)_{lb} < 0$ we will work with the modulus, $(\rho u)_{lb} = -\left|(\rho u)_{lb}\right|$. In the first term,

$$-\left|(\rho u)_{lb}\right|\widetilde{k} = \cancel{-}\left|(\rho u)_{lb}\right| \frac{1}{\cancel{-}\left|P_0\right| IGE_{01}} > 0,$$

the sign cancels out so it remains positive, whereas the second one could be rearranged by using the simple form of ILE_{01} as follows:

$$\begin{aligned}
-\left|(\rho u)_{lb}\right|\left(\widetilde{k}+\frac{ILE_{01}}{IGE_{01}}\right) &= -\left|(\rho u)_{lb}\right|\left(\frac{1}{-\left|P_0\right| IGE_{01}}+\frac{ILE_{01}}{IGE_{01}}\right) \\
&= \frac{-\left|(\rho u)_{lb}\right|}{IGE_{01}}\left(-\frac{1}{\left|P_0\right|}+ILE_{01}\right) \\
&= \frac{-\left|(\rho u)_{lb}\right|}{IGE_{01}}\left(-\frac{1}{\left|P_0\right|}+\frac{\exp\int_0^1 -\left|P\right|\mathrm{d}\widehat{x}-1}{-\left|P_0\right|}\right) \\
&= \frac{\left|(\rho u)_{lb}\right|}{\left|P_0\right| IGE_{01}}\exp\int_0^1 -\left|P\right|\mathrm{d}\widehat{x} > 0,
\end{aligned}$$

which is also positive. ENATE thus meets the physical requirement that all coefficients must be of the same sign.

2.2.3 Boundary value problem

The mathematical modelling of the physical world by PDEs requires a set of conditions at the boundaries of the domain of interest that determine a unique solution of the mathematical problem. Then, it is said that one has a *boundary value problem*.

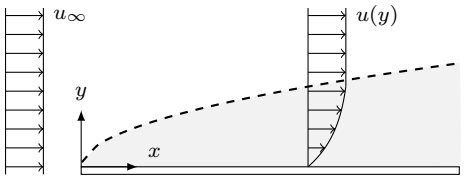

FIGURE 2.5: Boundary layer around a flat plate

See for instance Figure 2.5. At large distances from the plate a frictionless fluid could be assumed to model the flow, giving reasonable predictions. But around the plate viscous stresses become essential since the fluid velocity changes quickly within a thin layer, gray area, as the fluid does not slip on the surface. The boundary condition for this problem is $u(x,0) = 0$.

Sorting out such boundaries there are three classic conditions used: Dirichlet, Neumann, and Robin. All of them have some importance in fluid mechanics. For instance, in the illustration above the value of the fluid velocity imposed on the body wall is a *Dirichlet Condition* for the velocity equation. The *Neumann Condition* deals with the gradient of a variable and could be used as condition of fluid outlet, in a symmetry axis of the domain or as a given heat flux. A *Robin Condition* imposes the value of the flux $\mathcal{F}$ on the boundary and models, for instance, the heat transmission between a wall and a fluid by Newton's law of cooling, see Powers [167]. Other sophisticated conditions such as *periodic boundary condition* and *mixed boundary condition* are a special case of the former three.

We will describe how to apply them with the ENATE scheme.

Dirichlet condition or *fixed boundary problem*

(A) Left boundary (B) Right boundary

FIGURE 2.6: Boundary zones in a one-dimensional domain. The circles at edges correspond to known values with Dirichlet BC.

The boundary condition of the first type sets the value of the dependent variable, ϕ. Thus, the nodal equation (2.30) can be handled in the following way. For the left boundary, Figure 2.6a, West node matches up with x_{B1} what leads to the same influence coefficients $A_{B1} \equiv A_W$, $A_{C1} \equiv A_C$, $A_{E1} \equiv A_E$ and discrete source term $b_{C1} \equiv b_C$. As in that case $\phi(x_{B1}) = \phi_{B1}$ is the known value, it is included along with b_{C1} in a new source. Finally, the system of equations (2.33) is partially closed by the left-boundary equation as follows:

$$A_{C1}\phi_{C1} - A_{E1}\phi_{E1} = b'_{C1}, \tag{2.42a}$$

$$b'_{C1} \coloneqq b_{C1} + A_{B1}\phi_{B1}. \tag{2.42b}$$

Similar procedure is employed for the right boundary, Figure 2.6b. The right-boundary equation reads as follows:

$$-A_{W2}\phi_{W2} + A_{C2}\phi_{C2} = b'_{C2}, \tag{2.43a}$$

$$b'_{C2} \coloneqq b_{C2} + A_{B2}\phi_{B2}, \tag{2.43b}$$

where $A_{W2} \equiv A_W$, $A_{C2} \equiv A_C$, $A_{B2} \equiv A_E$ and $b_{C2} \equiv b_C$. The problem contains $n-1$ equations with $n-1$ unknowns.

Neumann condition

The second type of boundary condition (Neumann BC) fixes the value of the gradient at the edge of the domain. It is not as straightforward to implement as the previous condition. If a relation between the gradient and

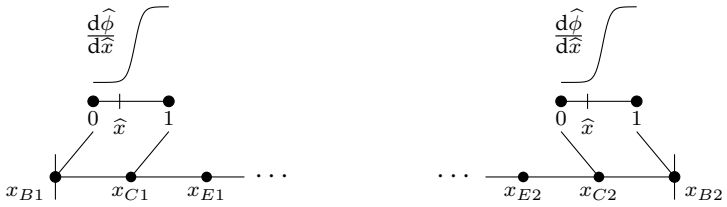

(A) Left boundary (B) Right boundary

FIGURE 2.7: Boundary zones in a one-dimensional domain. Values of ϕ at edge points are unknown.

the edge value is formulated by first-order finite differences:

$$\left.\frac{\mathrm{d}\phi}{\mathrm{d}x}\right|_{x_{B1}} \approx \frac{\phi_{C1}-\phi_{B1}}{x_{C1}-x_{B1}},$$

and

$$\left.\frac{\mathrm{d}\phi}{\mathrm{d}x}\right|_{x_{B2}} \approx \frac{\phi_{B2}-\phi_{C2}}{x_{B2}-x_{C2}},$$

the accuracy of the method could be impaired. However, as ENATE works with the exact solution the gradient can also be evaluated exactly. ENATE uses a reference interval, $\widehat{x}$, for each interval of the dimensional x domain. For the left boundary, Figure 2.7a, x_{B1} matches up with $\widehat{x}=0$ and x_{C1} with $\widehat{x}=1$. In case of the right boundary, Figure 2.7b, x_{C2} matches up with $\widehat{x}=0$ and x_{B2} with $\widehat{x}=1$. Then the gradients $\mathrm{d}\phi/\mathrm{d}x$ read

$$\begin{aligned}
\frac{\Gamma_{B1}}{(\rho u)_{B1}}\left.\frac{\mathrm{d}\phi}{\mathrm{d}x}\right|_{B1} &= \Delta\phi_{B1C1}\left[\frac{1}{P_0}\left.\frac{\mathrm{d}F}{\mathrm{d}\widehat{x}}\right|_0 + (1-F_{C1})\frac{1}{P_0}\left.\frac{\mathrm{d}\overline{\phi}^N}{\mathrm{d}\widehat{x}}\right|_0\right],\\
\frac{\Gamma_{B2}}{(\rho u)_{B2}}\left.\frac{\mathrm{d}\phi}{\mathrm{d}x}\right|_{B2} &= \Delta\phi_{C2B2}\left[\frac{1}{P_1}\left.\frac{\mathrm{d}F}{\mathrm{d}\widehat{x}}\right|_1 + (1-F_{B2})\frac{1}{P_1}\left.\frac{\mathrm{d}\overline{\phi}^N}{\mathrm{d}\widehat{x}}\right|_1\right],
\end{aligned}$$

with $\overline{\phi}^N$ and F derivatives at edges

$$\begin{aligned}
\frac{1}{P_0}\left.\frac{\mathrm{d}\overline{\phi}^N}{\mathrm{d}\widehat{x}}\right|_0 &= \widetilde{k}_{B1C1} + \frac{1}{1-F_{C1}}\frac{\phi_{B1}}{\Delta\phi_{B1C1}}\left[1-\left.\frac{ILE_{01}}{IGE_{01}}\right|_{B1C1}\right],\\
\frac{1}{P_0}\left.\frac{\mathrm{d}F}{\mathrm{d}\widehat{x}}\right|_0 &= F_{C1}\widetilde{k}_{B1C1} + \left.\frac{1}{(\rho u)_{B1}\Delta\phi_{B1C1}}\frac{ISGE_{01}}{IGE_{01}}\right|_{B1C1},
\end{aligned}$$

and

$$\begin{aligned}
\frac{1}{P_1}\left.\frac{\mathrm{d}\overline{\phi}^N}{\mathrm{d}\widehat{x}}\right|_1 =& 1 + \frac{\widetilde{k}_{C2B2}}{\widehat{\rho u}_{B2}} + \frac{1}{1-F_{B2}}\frac{\phi_{C2}}{\Delta\phi_{C2B2}}\left[1-\left.\frac{1}{\widehat{\rho u}_{B2}}\frac{ILE_{01}}{IGE_{01}}\right|_{C2B2}\right],\\
\frac{1}{P_1}\left.\frac{\mathrm{d}F}{\mathrm{d}\widehat{x}}\right|_1 =& F_{B2}\left[1+\frac{\widetilde{k}_{C2B2}}{\widehat{\rho u}_{B2}}\right]\\
&- \frac{1}{\widehat{\rho u}_{B2}}\frac{1}{(\rho u)_{C2}\Delta\phi_{C2B2}}\left[IS_{01}|_{C2B2} - \left.\frac{ISGE_{01}}{IGE_{01}}\right|_{C2B2}\right],
\end{aligned}$$

being $F_{C1} = F(1)|_{B1C1}$, $F_{B2} = F(1)|_{C2B2}$, $\widehat{\rho u}_{B2} = (\rho u)_{B2} / (\rho u)_{C2}$, $\Delta\phi_{B1C1} = \phi_{C1} - \phi_{B1}$, and $\Delta\phi_{C2B2} = \phi_{B2} - \phi_{C2}$. After some mathematical manipulation, the left-boundary equation becomes

$$A_{B1}\phi_{B1} - A_{C1}\phi_{C1} = b_{B1}, \tag{2.45a}$$

$$A_{B1} \coloneqq (\rho u)_{B1} \left(\widetilde{k}_{B1C1} + \left. \frac{ILE_{01}}{IGE_{01}} \right|_{B1C1} \right) - (\rho u)_{B1}\,, \tag{2.45b}$$

$$A_{C1} \coloneqq (\rho u)_{B1}\, \widetilde{k}_{B1C1}, \tag{2.45c}$$

$$b_{B1} \coloneqq \left. \frac{ISGE_{01}}{IGE_{01}} \right|_{B1C1} - \Gamma_{B1} \left. \frac{\mathrm{d}\phi}{\mathrm{d}x} \right|_{B1}, \tag{2.45d}$$

whereas the right-boundary equation becomes

$$-A_{C2}\phi_{C2} + A_{B2}\phi_{B2} = b_{B2}, \tag{2.46a}$$

$$A_{B2} \coloneqq (\rho u)_{B2} + (\rho u)_{C2}\, \widetilde{k}_{C2B2}, \tag{2.46b}$$

$$A_{C2} \coloneqq (\rho u)_{C2} \left(\widetilde{k}_{C2B2} + \left. \frac{ILE_{01}}{IGE_{01}} \right|_{C2B2} \right), \tag{2.46c}$$

$$b_{B2} \coloneqq IS_{01}|_{C2B2} - \left. \frac{ISGE_{01}}{IGE_{01}} \right|_{C2B2} + \Gamma_{B2} \left. \frac{\mathrm{d}\phi}{\mathrm{d}x} \right|_{B2}, \tag{2.46d}$$

The system (2.33) is made up of $n+1$ equations with $n+1$ unknowns if both boundaries are of *Neumann* type.

Robin condition or *convective boundary problem*

A *Robin* condition works with the flux as known value:

$$\mathcal{F}_{B1} = (\rho u)_{B1}\, \phi_{B1} - \Gamma_{B1} \left. \frac{\mathrm{d}\phi}{\mathrm{d}x} \right|_{B1},$$

and

$$\mathcal{F}_{B2} = (\rho u)_{B2}\, \phi_{B2} - \Gamma_{B2} \left. \frac{\mathrm{d}\phi}{\mathrm{d}x} \right|_{B2}.$$

As $\Gamma \mathrm{d}\phi/\mathrm{d}x$ and $\mathcal{F}$ are related to each other, those diffusion terms could be replaced in the source term (2.45d) and (2.46d) by the total fluxes. This results in the left-boundary equation

$$A_{B1}\phi_{B1} - A_{C1}\phi_{C1} = b_{B1}, \tag{2.47a}$$

$$A_{B1} \coloneqq (\rho u)_{B1} \left(\widetilde{k}_{B1C1} + \left. \frac{ILE_{01}}{IGE_{01}} \right|_{B1C1} \right), \tag{2.47b}$$

$$A_{C1} \coloneqq (\rho u)_{B1}\, \widetilde{k}_{B1C1}, \tag{2.47c}$$

$$b_{B1} \coloneqq \left. \frac{ISGE_{01}}{IGE_{01}} \right|_{B1C1} + \mathcal{F}_{B1}, \tag{2.47d}$$

and the right-boundary equation

$$-A_{C2}\phi_{C2} + A_{B2}\phi_{B2} = b_{B2}, \tag{2.48a}$$

$$A_{B2} \coloneqq (\rho u)_{C2}\, \widetilde{k}_{C2B2}, \tag{2.48b}$$

$$A_{C2} \coloneqq (\rho u)_{C2} \left(\widetilde{k}_{C2B2} + \left.\frac{ILE_{01}}{IGE_{01}}\right|_{C2B2} \right), \tag{2.48c}$$

$$b_{B2} \coloneqq IS_{01}|_{C2B2} - \left.\frac{ISGE_{01}}{IGE_{01}}\right|_{C2B2} - \mathcal{F}_{B2}. \tag{2.48d}$$

As before, the system is made up of $n+1$ equations with $n+1$ unknowns if both boundaries are of *Robin* type.

Discussion on the Neumann condition

A *Dirichlet* condition does not affect the global scheme (2.29) because the influence coefficients are the same as those of the inner part. Hence, it is expected to have the same boundedness behaviour. However, a *Neumann* condition modifies some coefficients by incorporating an extra convective term that could endanger satisfying the constraint of equal signs. Recall that $(\rho u)_{lb}\widetilde{k}$ and $(\rho u)_{lb}(\widetilde{k} + ILE_{01}/IGE_{01})$ are always positive whatever the convection sign. A *Robin* condition removes this problem and the scheme is bounded. In consequence, *Robin* BC is suitable as, unlike *Neumann* BC, it is guarantee of boundedness.

So, if *Neumann* BC is used and the coefficients (2.45b) and (2.46b) could change the sign, it is recommended to take this extra convective term to the source as a value from the old iteration. The left- and right-boundary equations are

$$\begin{aligned} A_{B1}\phi_{B1} - A_{C1}\phi_{C1} &= b'_{B1}, \\ -A_{C2}\phi_{C2} + A_{B2}\phi_{B2} &= b'_{B2}, \end{aligned}$$

with

$$\begin{aligned} b'_{B1} &\coloneqq b_{B1} + (\rho u)_{B1}\, \phi^{\text{old}}_{B1}, \\ b'_{B2} &\coloneqq b_{B2} - (\rho u)_{B2}\, \phi^{\text{old}}_{B2}, \end{aligned}$$

where A_{B1} and A_{B2} do not contain $(\rho u)_{B1}$ and $(\rho u)_{B2}$.

Nodal Equation	
Tridiagonal System	$-A_W\phi_W + A_C\phi_C - A_E\phi_E = b_C$

Influence coefficients and Discrete source				
Contribution	General Formula	$P = 0$	$P \to +\infty$	$P \to -\infty$
West node, A_W	$(\rho u)_W \left(\widetilde{k}_{WC} + \dfrac{ILE_{01}}{IGE_{01}}\Big\vert_{WC}\right)$	$\dfrac{\Gamma_W}{\Delta x_{WC}} \dfrac{1}{IG_{01}\vert_{WC}}$	$(\rho u)_W$	0
Central node, A_C	$(\rho u)_W \widetilde{k}_{WC} + (\rho u)_C \left(\widetilde{k}_{CE} + \dfrac{ILE_{01}}{IGE_{01}}\Big\vert_{CE}\right)$	$A_W + A_E$	$(\rho u)_C$	$-(\rho u)_C$
East node, A_E	$(\rho u)_C \widetilde{k}_{CE}$	$\dfrac{\Gamma_C}{\Delta x_{CE}} \dfrac{1}{IG_{01}\vert_{CE}}$	0	$-(\rho u)_E$
Source, b_C	$IS_{01}\vert_{WC} + \left(\dfrac{ISGE_{01}}{IGE_{01}}\Big\vert_{CE} - \dfrac{ISGE_{01}}{IGE_{01}}\Big\vert_{WC}\right)$	$IS_{01}\vert_{WC} + \left(\dfrac{ISG_{01}}{IG_{01}}\Big\vert_{CE} - \dfrac{ISG_{01}}{IG_{01}}\Big\vert_{WC}\right)$	$IS_{01}\vert_{WC}$	$IS_{01}\vert_{CE}$

Integrals over a generic interval
$ILE_{01} = \dfrac{\exp \overline{P} - 1}{P_0}, \quad \overline{P} = \displaystyle\int_0^1 P \,\mathrm{d}x,$
$IGE_{01} = \displaystyle\int_0^1 \frac{1}{\widehat{\Gamma}\overline{E}} \mathrm{d}\widehat{x}, \quad \widetilde{k} = \dfrac{1}{P_0 IGE_{01}},$
$IS_{01} = \Delta x \displaystyle\int_0^1 S \,\mathrm{d}\widehat{x}, \quad ISGE_{01} = \int_0^1 \frac{\Delta x}{\widehat{\Gamma}\overline{E}} \left[\int_0^{\widehat{x}} S \,\mathrm{d}\widehat{x}'\right] \mathrm{d}\widehat{x},$
$IG_{01} = \displaystyle\int_0^1 \frac{\mathrm{d}\widehat{x}}{\widehat{\Gamma}}, \quad ISG_{01} = \int_0^1 \frac{\Delta x}{\widehat{\Gamma}} \left[\int_0^{\widehat{x}} S \,\mathrm{d}\widehat{x}'\right] \mathrm{d}\widehat{x}.$

TABLE 2.4: Overview of the inner algebraic equation of ENATE. Boundary equations (2.42), (2.45) and (2.47) for left BC and (2.43), (2.46) and (2.48) for right BC are obtained by taking $A_C\phi_C - \sum A_i\phi_i = b_C$ together with the As formulae, and applying the corresponding known data either to ϕ, $\mathrm{d}\phi/\mathrm{d}x$ or $\mathcal{F}$.

2.3 Integration methods I

The ENATE scheme provides an algebraic relation of a three-point stencil. Its accuracy relies on the way the numerical integrals are worked out in each interval. If the domain is cut off into n intervals with $n+1$ points $(x_0, x_1, \cdots, x_n)$, n integrals must be solved. If the integrand does not have a primitive an interpolating function has to be chosen in order to evaluate the integrals. As integrands with no primitive are most common, in this section two numerical approaches to calculate integrals such as ILE_{01}, IGE_{01}, $ISGE_{01}$ and IS_{01}, are developed: Hermite splines and GL quadrature. In Section 2.6, both interpolators will be compared.

2.3.1 Hermite splines

A fundamental background of Hermite interpolation can be found in the book [20], among others. This interpolation for quadratures is employed in this thesis.

On the whole a *Hermite spline* is an interpolation tool that matches the target function $f(x)$ given a dataset of its values and derivatives up to q-order at $p+1$ points, as read below.

x_0	x_1	x_2	$\cdots$	x_p
$f(x_0)$	$f(x_1)$	$f(x_2)$	$\cdots$	$f(x_p)$
$\mathrm{d}f(x_0)$	$\mathrm{d}f(x_1)$	$\mathrm{d}f(x_2)$	$\cdots$	$\mathrm{d}f(x_p)$
$\mathrm{d}^2f(x_0)$	$\mathrm{d}^2f(x_1)$	$\mathrm{d}^2f(x_2)$	$\cdots$	$\mathrm{d}^2f(x_p)$
$\vdots$	$\vdots$	$\vdots$	$\ddots$	$\vdots$
$\mathrm{d}^qf(x_0)$	$\mathrm{d}^qf(x_1)$	$\mathrm{d}^qf(x_2)$	$\cdots$	$\mathrm{d}^qf(x_p)$

Note: $\mathrm{d}^q f = \mathrm{d}^q f/\mathrm{d}x^q$

Consequently, the total number of data that Hermite requires is $(p+1)(q+1)$. By the theory of the interpolation, the integral within $[x_0, x_p]$, and interval length $\Delta = (x_p - x_0)/p$, could be written as

$$\int_{x_0}^{x_p} f(x)\mathrm{d}x \approx \Delta \sum_{i=0}^{p} w_{i0} f(x_i) + \sum_{j=1}^{q} \left(\Delta^{j+1} \sum_{i=0}^{p} w_{ij} \left. \frac{\mathrm{d}^j f}{\mathrm{d}x^j} \right|_{x_i} \right), \tag{2.49}$$

with the error given by

$$E_H(x; f) = \int_{x_0}^{x_p} \frac{1}{r!} \left. \frac{\mathrm{d}^r f}{\mathrm{d}x^r} \right|_{x^\star} \prod_{i=0}^{p} (x - x_i)^{1+q} \, \mathrm{d}x, \quad x_0 \leqslant x^\star \leqslant x_p,$$

and $r = (p+1)(q+1)$. Thus, the quadrature would be exact if the polynomial is of degree $r-1$. The error formula has been obtained by integrating the error term of Hermite interpolation. Regarding the integral (2.49), the dimensionless weights, w_{ij}, are calculated as follows. Take $f(x) = x^k$ for all k values that meet $E_H\left(x; x^k\right) = 0$. To reduce complexity throughout the calculation rename the variables as

$$\begin{array}{lccl} \text{Domain :} & [x_0, x_p] & \longrightarrow & [0, p] \\ \text{Continuum :} & x & \longrightarrow & t = (x - x_0)/\Delta \\ \text{Discrete :} & x_i & \longrightarrow & t_i = i \end{array}$$

A linear equation system is obtained whose solution gives unique weights,

$$\sum_{\substack{j=0\\ j\le k}}^{q}\sum_{i=0}^{p}\frac{k!}{(k-j)!}i^{k-j}w_{ij}=\frac{p^{k+1}}{k+1},\quad k=0,1,...,r-1. \tag{2.50}$$

Some rules and tips should be followed in the above equation: 1) Start off with the k-index, go on with the j-index and end up with the i-index; 2) When the term i^{k-j} becomes the indeterminate form 0^0, change it to 1.

The value of the influence coefficients (2.31) and discrete source (2.32) depends on integrals in each interval within the split-up domain, see Figure 2.2. Those integrals can be calculated straightaway in the domain $[0,1]$, due to the mapping. So, it all comes down to applying (2.50) with two points, $p=1$, at the edges of the normalized interval. The degree of accuracy relates to the order of employed derivatives of the function to be interpolated. For instance, the simplest Hermite spline, also named as Cubic Hermite, has the first derivatives, $q=1$,

$$\int_0^1 f(\widehat{x})\mathrm{d}\widehat{x}\approx\frac{1}{2}\left(f_1+f_0\right)+\frac{1}{12}\left(\left.\frac{\mathrm{d}f}{\mathrm{d}\widehat{x}}\right|_0-\left.\frac{\mathrm{d}f}{\mathrm{d}\widehat{x}}\right|_1\right), \tag{2.51}$$

whereas a Quintic Hermite uses up to the second derivative, $q=2$,

$$\begin{aligned}\int_0^1 f(\widehat{x})\mathrm{d}\widehat{x}\approx\frac{1}{2}\left(f_1+f_0\right)&+\frac{1}{10}\left(\left.\frac{\mathrm{d}f}{\mathrm{d}\widehat{x}}\right|_0-\left.\frac{\mathrm{d}f}{\mathrm{d}\widehat{x}}\right|_1\right)\\&+\frac{1}{120}\left(\left.\frac{\mathrm{d}^2f}{\mathrm{d}\widehat{x}^2}\right|_0+\left.\frac{\mathrm{d}^2f}{\mathrm{d}\widehat{x}^2}\right|_1\right).\end{aligned} \tag{2.52}$$

Finally, if the third derivative is included, $q=3$, a Septic Hermite is obtained,

$$\begin{aligned}\int_0^1 f(\widehat{x})\mathrm{d}\widehat{x}\approx\frac{1}{2}\left(f_1+f_0\right)&+\frac{3}{28}\left(\left.\frac{\mathrm{d}f}{\mathrm{d}\widehat{x}}\right|_0-\left.\frac{\mathrm{d}f}{\mathrm{d}\widehat{x}}\right|_1\right)\\&+\frac{1}{84}\left(\left.\frac{\mathrm{d}^2f}{\mathrm{d}\widehat{x}^2}\right|_0+\left.\frac{\mathrm{d}^2f}{\mathrm{d}\widehat{x}^2}\right|_1\right)\\&+\frac{1}{1680}\left(\left.\frac{\mathrm{d}^3f}{\mathrm{d}\widehat{x}^3}\right|_0-\left.\frac{\mathrm{d}^3f}{\mathrm{d}\widehat{x}^3}\right|_1\right).\end{aligned} \tag{2.53}$$

The splines above could work fine with slowly varying functions, but, with ILE_{01}, IGE_{01}, and $ISGE_{01}$ depending on the exponential of Péclet, $\overline{E}$, they could give rise to large errors and even blow up the method when Péclet is high. Let us evaluate the integral

$$\int_0^1\frac{\mathrm{d}\widehat{x}}{\overline{E}}\quad\text{with}\quad\overline{E}(\widehat{x})=\exp\left(-P\left(1-\widehat{x}\right)\right), \tag{2.54}$$

in three numerical regimes: a low-Péclet, $P=0.1$, a medium-Péclet, $P=1$, and a high-Péclet, $P=10$. It is observed in Table 2.5 that errors increase significantly for high values of Péclet what caused by the splines being unable to fit the integrand, $1/\overline{E}$. These discrepancies have their origin in the sharp slope of the exponential within $[0,1]$, the integrand is $\exp P$ at $\widehat{x}=0$

and 1 at $\widehat{x} = 1$. When Péclet is high $\exp P \gg 1$.

P	0.1	1	10
Exact	1.051709180	1.718281828	2202.546579480
Cubic	1.051709(034)	1.71(5950761)	-7340.821931602
Quintic	1.051709180	1.7182(98413)	7344.488598269
Septic	1.051709180	1.718281(762)	527.796804638

TABLE 2.5: Comparison between exact and numerical values of the integral (2.54) using the splines (2.51) to (2.53)

It is observed that all splines provide results far from the correct ones for $P = 10$. The cubic spline even gives a negative value which is mathematically wrong as the integral (2.54) is a monotonically increasing function of Péclet. Taking as an example the Cubic spline,

$$\int_0^1 \frac{\mathrm{d}\widehat{x}}{\overline{E}} \approx \frac{1}{2}\left(1 + \frac{1}{\overline{E}(0)}\right) + \frac{P}{12}\left(1 - \frac{1}{\overline{E}(0)}\right).$$

The derivative with respect to Péclet is

$$\frac{\mathrm{d}}{\mathrm{d}P}\left[\int_0^1 \frac{\mathrm{d}\widehat{x}}{\overline{E}}\right] \approx \frac{1}{12}\left(1 + \frac{5-P}{\overline{E}(0)}\right).$$

For $P > 5.0070$ it is found that the approximation of the integral starts decreasing. A similar procedure reveals that Quintic provides a monotonically increasing integral for the whole range of Péclet, $P \in [0, \infty)$, and Septic displays a Cubic-like behaviour when $P > 9.5780$. This monotonic behaviour is crucial in the splines approximation. A negative value could change the signs of the influence coefficients and the numerical scheme will not work. With Cubic the integral is negative when $P \geq 6.0290$ and Septic when $P \geq 10.4730$. In Figure 2.8 the spline approximation is shown and a white circle displays where the curve stops being monotonically increasing. The color circle represents the point where the integral becomes negative.

In a general case, when $P = P(\widehat{x})$, it is difficult to determine the mean Péclet number for which the integral evaluation goes wrong. From the point of view of obtaining a robust scheme it is fundamental to seek another formulation of Hermite that keeps good results in low-, medium-Péclet while diminishing the errors for high Péclet. Consider an integrand with an exponential factor, $f_{\mathrm{E}} = f_{\mathrm{E}}(\widehat{x}) := g(\widehat{x})/\overline{E}(\widehat{x})$ for some specific function $g = g(\widehat{x})$ that depends on the integral to evaluate,

$$\int_0^1 f_{\mathrm{E}}\,\mathrm{d}\widehat{x} = \int_0^1 \frac{g}{\overline{E}}\mathrm{d}\widehat{x}, \quad g = \begin{cases} \widehat{\lambda}, & \text{for } ILE_{01} \\ \dfrac{1}{\widehat{\Gamma}}, & \text{for } IGE_{01} \\ \dfrac{IS_{0\widehat{x}}}{\widehat{\Gamma}}, & \text{for } ISGE_{01} \end{cases}. \tag{2.55}$$

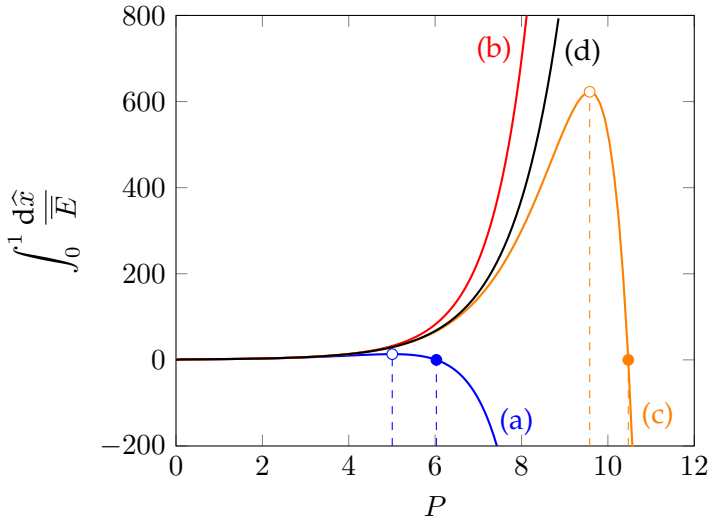

FIGURE 2.8: Behaviours of the cubic (a), quintic (b), and septic (c) fitting in relation to the exact integral (d)

The factor $1/\overline{E}$ is modified by using a reference Péclet, $P^\dagger$, as an arbitrary constant, and a change of integral limits as follows:

$$\begin{aligned}
\frac{1}{\overline{\overline{E}}} &= \exp\left(\int_{\widehat{x}}^1 P\mathrm{d}\widehat{x}'\right) \\
&= \exp\left(\int_{\widehat{x}}^1 P^\dagger \mathrm{d}\widehat{x}'\right) \exp\left(\int_{\widehat{x}}^1 (P-P^\dagger)\mathrm{d}\widehat{x}'\right) \\
&= \exp\left(P^\dagger(1-\widehat{x})\right) \exp\left(\int_0^1 (P-P^\dagger)\mathrm{d}\widehat{x}\right) \exp\left(-\int_0^{\widehat{x}} (P-P^\dagger)\mathrm{d}\widehat{x}'\right) \\
&= \exp\left(P^\dagger(1-\widehat{x})\right) \exp\left(\overline{P}-P^\dagger\right) \exp\left(-\int_0^{\widehat{x}} (P-P^\dagger)\mathrm{d}\widehat{x}'\right).
\end{aligned}$$

If $P^\dagger$ is chosen as the average Péclet, $\overline{P}$, then the above factor becomes

$$\frac{1}{\overline{\overline{E}}} = \exp\left(\overline{P}\,(1-\widehat{x})\right) \exp\left(-\int_0^{\widehat{x}} \left(P-\overline{P}\right)\mathrm{d}\widehat{x}'\right). \tag{2.56}$$

The reason for this transformation (2.56) lies in the second exponential which is smoother than $\exp\int_{\widehat{x}}^1 P\mathrm{d}\widehat{x}'$. It starts and ends with the same value, 1, and hence, it is more suitable for an accurate interpolation, contrary to the original one that varies from $\exp\overline{P}$ to 1.

The interpolator $H_m = H_m(\widehat{x})$ is defined as the m-th Hermite spline

$$H_m := \sum_{i=0}^{m} a_i \widehat{x}^i, \quad m = 1+2q,$$

that interpolates the set of functions which multiplies $\exp\left(\overline{P}\,(1-\widehat{x})\right)$ in the factor (2.56) once it is replaced into the integral (2.55), i.e.,

$$\begin{aligned}\int_0^1 f_{\mathrm{E}}\,\mathrm{d}\widehat{x} &= \int_0^1 \frac{g}{\overline{E}}\mathrm{d}\widehat{x}\\ &= \int_0^1 g\,\exp\left(-\int_0^{\widehat{x}}\left(P-\overline{P}\right)\mathrm{d}\widehat{x}'\right)\exp\left(\overline{P}\,(1-\widehat{x})\right)\mathrm{d}\widehat{x}\\ &\approx \int_0^1 H_m\,\exp\left(\overline{P}\,(1-\widehat{x})\right)\mathrm{d}\widehat{x}\\ &= \int_0^1 \sum_{i=0}^{m} a_i\widehat{x}^i\,\exp\left(\overline{P}\,(1-\widehat{x})\right)\mathrm{d}\widehat{x}\\ &= \sum_{i=0}^{m} a_i \int_0^1 \widehat{x}^i\,\exp\left(\overline{P}\,(1-\widehat{x})\right)\mathrm{d}\widehat{x}.\end{aligned}$$

In this way the integrals in the previous expression can be calculated exactly, see Jeffrey [92, p. 176], giving as final result

$$\int_0^1 f_{\mathrm{E}}\,\mathrm{d}\widehat{x} \approx \frac{\exp\overline{P}}{\overline{P}}\sum_{i=0}^{m} a_i\frac{i!}{\overline{P}^i} - \frac{1}{\overline{P}}\sum_{i=0}^{m}\left(a_i\sum_{j=0}^{i}\frac{i!}{\overline{P}^j(i-j)!}\right). \tag{2.57}$$

The determination of the coefficients $\{a_0, a_1, a_2, \ldots, a_m\}$ is carried out by matching the values and derivatives of both the Hermite polynomial H_m and the function to be interpolated, up to order q at the edges of the reference interval. The function is $g\,\exp h$, with $h \coloneqq -\int_0^{\widehat{x}}\left(P-\overline{P}\right)\mathrm{d}\widehat{x}'$.

$$H_m(0) = g(0), \tag{2.58a}$$

$$H_m(1) = g(1), \tag{2.58b}$$

$$\left.\frac{\mathrm{d}^k H_m}{\mathrm{d}\widehat{x}^k}\right|_{\{0,1\}} = \sum_{l=0}^{k}\binom{k}{l}\left.\frac{\mathrm{d}^{k-l}g}{\mathrm{d}\widehat{x}^{k-l}}\right|_{\{0,1\}}\left.\frac{\mathrm{d}^l\exp h}{\mathrm{d}\widehat{x}^l}\right|_{\{0,1\}},\quad k=1,2,\cdots,q. \tag{2.58c}$$

For instance, a Cubic Hermite spline, $q=1$, uses a third degree polynomial, $m = 1+2\cdot 1 = 3$, given by $H_3 = a_0 + a_1\widehat{x} + a_2\widehat{x}^2 + a_3\widehat{x}^3$. By applying conditions (2.58), the system written in matrix form is

$$\begin{pmatrix}1&0&0&0\\1&1&1&1\\0&1&0&0\\0&1&2&3\end{pmatrix}\begin{pmatrix}a_0\\a_1\\a_2\\a_3\end{pmatrix} = \begin{pmatrix}g(0)\\g(1)\\(\mathrm{d}g/\mathrm{d}\widehat{x})_0 - g(0)\,\left(P(0)-\overline{P}\right)\\(\mathrm{d}g/\mathrm{d}\widehat{x})_1 - g(1)\,\left(P(1)-\overline{P}\right)\end{pmatrix}. \tag{2.59}$$

In the case of Quintic Hermite spline, $q=2$, the polynomial is of fifth degree, $m=5$, whereas in Septic Hermite spline, $q=3$, is of seventh degree, $m=7$. The set of a_i coefficients are listed in Appendix B.

On calculating the integral of $1/\overline{E}$ when $P=$ const., the coefficients become $a_0=1$ and $a_1,\ldots,a_m=0$. Therefore, the integral (2.57) is calculated as $(\exp P-1)/P$, getting the exact solution of the example. If a linear Péclet is tested the Table 2.6 shows that the errors of the high-Péclet case are much reduced.

	α	0.1	1	10
	Exact	1.087927463	2.517182609	$3.010062626{\cdot}10^5$
Cubic	(2.51)	1.0879(01860)	2.5(34037112)	$-1.089670290{\cdot}10^6$
	(2.57)/$m=3$	1.087(882373)	2.5(07667597)	$2.808933031{\cdot}10^5$
Quintic	(2.52)	1.0879274(03)	2.517(675628)	$8.172600931{\cdot}10^5$
	(2.57)/$m=5$	1.087927(303)	2.51(6848424)	$2.967137221{\cdot}10^5$
Septic	(2.53)	1.087927463	2.51718(9383)	$2.724298048{\cdot}10^5$
	(2.57)/$m=7$	1.087927463	2.5171(73425)	$3.0(01935044){\cdot}10^5$

TABLE 2.6: Comparison between exact and numerical values of the integral (2.55) with $g(\widehat{x})=1$ and $P(\widehat{x})=\alpha(1+\widehat{x})$ using different Hermite splines.

In a nutshell: Using the splines (2.51) to (2.53) to calculate smooth functions such as IS_{01}, or $\overline{P}$ will work well while ILE_{01}, IGE_{01}, and $ISGE_{01}$ should be tackled with the spline (2.57).

2.3.2 Gauss–Legendre Quadrature

Other option to compute integrals, instead of Hermite, is a GL quadrature. This kind of p-point quadrature manages to integrate exactly a polynomial of $(2p-1)$th degree by picking optimal points which are the roots of the Legendre polynomial, and evaluating the integrand in those points multiplied by a weight. The modifed GL quadrature for the ENATE integrals can be written as

$$\int_0^1 f(\widehat{x})\mathrm{d}\widehat{x} \approx \frac{1}{2}\sum_{i=1}^{p} w_i f(\widehat{x}_i).$$

Number of points, p	Points, $\widehat{x}_i$	Weights, w_i
3	$1/2$	$8/9$
	$1/2\left(1\pm\sqrt{3/5}\right)$	$5/9$
4	$1/2\left(1\pm\sqrt{3/7-2/7\sqrt{6/5}}\right)$	$\left(18+\sqrt{30}\right)/36$
	$1/2\left(1\pm\sqrt{3/7+2/7\sqrt{6/5}}\right)$	$\left(18-\sqrt{30}\right)/36$

TABLE 2.7: Localization of points and weights for different number of points in GL quadrature

In Table 2.7, the key information is summarized. For the integrals ILE_{01}, IGE_{01}, and $ISGE_{01}$ the quadrature gives the next approximations:

$$ILE_{01} \approx \frac{1}{2}\sum_{i=1}^{p} w_i \frac{\widehat{\lambda}(\widehat{x}_i)}{\overline{E}(\widehat{x}_i)}, \tag{2.60a}$$

$$IGE_{01} \approx \frac{1}{2}\sum_{i=1}^{p} w_i \frac{1}{\widehat{\Gamma}(\widehat{x}_i)\overline{E}(\widehat{x}_i)}, \tag{2.60b}$$

$$ISGE_{01} \approx \frac{1}{2}\sum_{i=1}^{p} w_i \frac{IS_{0\widehat{x}_i}}{\widehat{\Gamma}(\widehat{x}_i)\overline{E}(\widehat{x}_i)}. \tag{2.60c}$$

However, $\overline{E}(\widehat{x}_i)$ and $IS_{0\widehat{x}_i}$ contain integrals whose integration does not go from 0 to 1 as it depends on $\widehat{x}_i$. In such case the GL quadrature becomes

$$\int_a^b f(\widehat{x})\mathrm{d}\widehat{x} \approx \frac{b-a}{2}\sum_{k=1}^{p} w_k f\left(b\,\widehat{x}_k + a(1-\widehat{x}_k)\right).$$

Notice that if the limits are $a = 0$ and $b = 1$ we recover the GL quadrature at the beginning of this subsection. Since either a or b depends on $\widehat{x}_i$, $k = i$. For the exponential factor $a = \widehat{x}_i$ and $b = 1$,

$$\overline{E}(\widehat{x}_i) \approx \exp\left(-\frac{1-\widehat{x}_i}{2}\sum_{k=1}^{p} w_k P\left(\widehat{x}_k + \widehat{x}_i - \widehat{x}_i\widehat{x}_k\right)\right),$$

and for the integral of the source $a = 0$ and $b = \widehat{x}_i$,

$$IS_{0\widehat{x}_i} \approx \Delta x\frac{\widehat{x}_i}{2}\sum_{k=1}^{p} w_k S\left(\widehat{x}_i\widehat{x}_k\right).$$

Contrary to Hermite, the GL quadrature provides a monotonically increasing integration since it consists of a sum of positive terms. Some numerical tests similar to those in the previous subsection are displayed in Table 2.8.

Constant Peclet, $P = \alpha$

α	0.1	1	10
Exact	1.051709180	1.718281828	2202.546579480
3-point	1.051709180	1.718281(00)	2409.190973573
4-point	1.051709180	1.71828182(7)	2187.328913256

Linear Peclet, $P = \alpha(1+\widehat{x})$

α	0.1	1	10
Exact	1.087927463	2.517182609	$3.010062626{\cdot}10^5$
3-point	1.08792746(7)	2.5171(57428)	$2.789135221{\cdot}10^5$
4-point	1.08792746(4)	2.517182(706)	$3.0(01353937){\cdot}10^5$

TABLE 2.8: Comparison between exact and numerical values of the integral (2.55) with $g(\widehat{x}) = 1$ for two Péclet cases using the GL quadrature

However, the Gauss points are within $[0, 1]$ and, therefore, the quadrature is not suitable for functions not given analytically as it will require interpolation. In addition, the calculation of ILE_{01} by (2.60a) and IGE_{01} by (2.60b) involves a total of $\left(p^2 - 2p + 6\right)$-points, see Figure 2.9. Similarly, $ISGE_{01}$ by (2.60c) is evaluated with a total of $\left(p^2 + 2p\right)$-points. So, the GL quadrature needs more information than the Hermite splines.

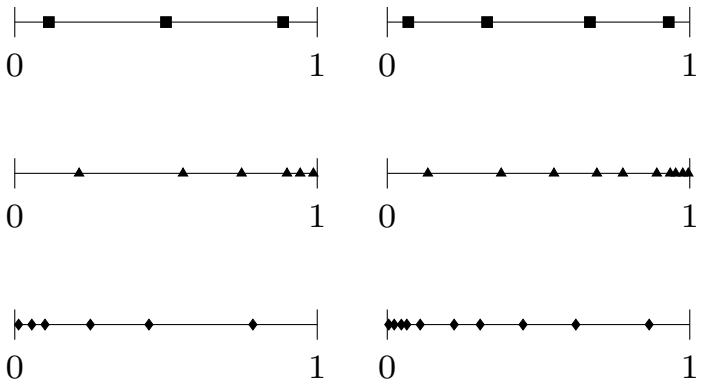

(A) Taking $p = 3$ (B) Taking $p = 4$

FIGURE 2.9: Localization of Gauss' points in a reference interval for $\widehat{\lambda}$ or $\widehat{\Gamma}$ (■), P (▲), and S (♦) using different GL quadratures.

2.4 Nonlinear ENATE

So far, in sections 2.1 and 2.2 an algebraic equation has been derived for linear convection-diffusion problems and the exact solution has been obtained. What if the transported variable is the velocity, $\phi = u$? In such a case, one deals with the equation

$$\frac{\mathrm{d}}{\mathrm{d}x}\left(\rho u u - \Gamma \frac{\mathrm{d}u}{\mathrm{d}x}\right) = S.$$

If $\Gamma = 0$, a recurrence nodal equation can be written as follows:

$$u_C = \pm\sqrt{\frac{\rho_W}{\rho_C} u_W^2 + \frac{1}{\rho_C}\int_{x_W}^{x_C} S\,\mathrm{d}x}.$$

We only consider solutions with $u^2 > 0$.

In a general case with diffusion one could use the derivation for linear problems to compute the solution of a nonlinear one. To do so, ENATE becomes a numerical iterative procedure:

1. Start off with guessed values of u, u^{old}
2. First evaluation of ILE_{01}, IGE_{01} and $ISGE_{01}$
3. Substitute u in the convective term, ρu^{old}
4. Calculate the integrals ILE_{01}, IGE_{01} and $ISGE_{01}$ by Hermite (2.57)

5. Update u by using the algebraic equation (2.29), u^{new}
6. If $|u^{\text{old}} - u^{\text{new}}|_\infty \leq \epsilon$ stop, if not, $u^{\text{old}} \leftarrow u^{\text{new}}$ and go to point 3

The parameter ϵ is the tolerance. As with the linear problems, at some point of Hermite calculations the values of $\mathrm{d}^k P/\mathrm{d}\widehat{x}^k$ $(k = 1, 2, 3)$ are required. However, this evaluation is not straightforward since u within the Péclet number is unknown a priori. To calculate these values the normalized velocity is defined as

$$\widehat{u} = \frac{u - u_{lb}}{u_{rb} - u_{lb}} = \frac{u - u_{lb}}{\Delta u}.$$

In nonlinear problems we could distinguish three types of Péclet numbers. $\rho u \Delta x/\Gamma$ is the local Péclet, P, whereas

$$\Delta P = \frac{\rho \Delta u \Delta x}{\Gamma}, \quad \Delta P_0 = \frac{\rho \Delta u \Delta x}{\Gamma_{lb}},$$

are the Péclet number based on u variation and the reference Péclet number based on u variation, respectively. So, the first derivative of Péclet is

$$\begin{aligned} \frac{\mathrm{d}P}{\mathrm{d}\widehat{x}} &= \frac{\mathrm{d}}{\mathrm{d}\widehat{x}}\left(\frac{\rho u \Delta x}{\Gamma}\right) \\ &= \frac{\rho \Delta x}{\Gamma}\frac{\mathrm{d}u}{\mathrm{d}\widehat{x}} + \rho u \Delta x \frac{\mathrm{d}}{\mathrm{d}\widehat{x}}\left(\frac{1}{\Gamma}\right) \\ &= \Delta P \frac{\mathrm{d}\widehat{u}}{\mathrm{d}\widehat{x}} - \frac{P}{\widehat{\Gamma}}\frac{\mathrm{d}\widehat{\Gamma}}{\mathrm{d}\widehat{x}}, \end{aligned} \tag{2.61}$$

assuming ρ constant. From equation (2.20) it is deduced that

$$\frac{\mathrm{d}\widehat{u}}{\mathrm{d}\widehat{x}} = \frac{\mathrm{d}F}{\mathrm{d}\widehat{x}} + (1 - F(1))\frac{\mathrm{d}\overline{u}^N}{\mathrm{d}\widehat{x}}.$$

Substituting derivatives (2.27a) and (2.27b) above, the derivative of the velocity is

$$\frac{\mathrm{d}\widehat{u}}{\mathrm{d}\widehat{x}} = P\frac{u}{\Delta u} + \frac{1 - P_0\dfrac{u_{lb}}{\Delta u} ILE_{01}}{\widehat{\Gamma}\, IGE_{01}} - \frac{\Delta x}{\Gamma \Delta u}\left(IS_{0\widehat{x}} - \frac{ISGE_{01}}{IGE_{01}}\right).$$

Finally, if this is inserted into (2.61), the Péclet derivative is

$$\frac{\mathrm{d}P}{\mathrm{d}\widehat{x}} = P^2 + w_1\left(C_1^\star - C_2^\star IS_{0\widehat{x}}\right) - w_2 P,$$

where the constants are defined as

$$C_1^\star \coloneqq \frac{\Delta P_0 - P_0^2 ILE_{01}}{IGE_{01}} + C_2^\star \frac{ISGE_{01}}{IGE_{01}}, \quad C_2^\star \coloneqq \rho\left(\frac{\Delta x}{\Gamma_{lb}}\right)^2,$$

and the factors related to diffusion by

$$w_1 \coloneqq \frac{1}{\widehat{\Gamma}^2}, \quad w_2 \coloneqq \frac{\mathrm{d}}{\mathrm{d}\widehat{x}}\left(\ln\widehat{\Gamma}\right), \quad \frac{\mathrm{d}w_1}{\mathrm{d}\widehat{x}} = -2w_1 w_2. \tag{2.62}$$

Thus, its second derivative reads

$$\begin{aligned}\frac{\mathrm{d}^2P}{\mathrm{d}\widehat{x}^2} =& 2P\frac{\mathrm{d}P}{\mathrm{d}\widehat{x}} - 2w_2\left(\frac{\mathrm{d}P}{\mathrm{d}\widehat{x}} - P^2 + w_2P\right)\\ &- \frac{\mathrm{d}}{\mathrm{d}\widehat{x}}\left(w_2P\right) - C_2^\star w_1 S\,\Delta x,\end{aligned}$$

and the third is

$$\begin{aligned}\frac{\mathrm{d}^3P}{\mathrm{d}\widehat{x}^3} =& 2\left(\frac{\mathrm{d}P}{\mathrm{d}\widehat{x}}\right)^2 + 2P\frac{\mathrm{d}^2P}{\mathrm{d}\widehat{x}^2}\\ &- 2\left(2w_2^2 + \frac{\mathrm{d}w_2}{\mathrm{d}\widehat{x}}\right)\left(\frac{\mathrm{d}P}{\mathrm{d}\widehat{x}} - P^2 + w_2P\right)\\ &- 4w_2\left(\frac{\mathrm{d}^2P}{\mathrm{d}\widehat{x}^2} - P^2 + w_2P\right) - C_2^\star w_1\frac{\mathrm{d}S}{\mathrm{d}\widehat{x}}\Delta x.\end{aligned}$$

In the limit case when Γ is constant, the previous calculations convert into

$$\begin{aligned}\frac{\mathrm{d}P}{\mathrm{d}\widehat{x}} =& P^2 + C_1^\star - C_2^\star I S_{0\widehat{x}},\\ \frac{\mathrm{d}^2P}{\mathrm{d}\widehat{x}^2} =& 2P^3 + 2P\left(C_1^\star - C_2^\star I S_{0\widehat{x}}\right) - C_2^\star S\,\Delta x,\\ \frac{\mathrm{d}^3P}{\mathrm{d}\widehat{x}^3} =& 6P^4 + 8P^2\left(C_1^\star - C_2^\star I S_{0\widehat{x}}\right)\\ &+ 2\left(C_1^\star - C_2^\star I S_{0\widehat{x}}\right)^2 - C_2^\star\Delta x\left(2PS - \frac{\mathrm{d}S}{\mathrm{d}\widehat{x}}\right).\end{aligned}$$

Sometimes an initial estimation of ILE_{01}, IGE_{01} and $ISGE_{01}$ is required to start the iterative procedure. The derivatives of P depend on those integrals. The starting Péclet can be assumed to be the average Péclet over the interval, and the source taken as the source value at the left node of the interval, then

$$\begin{aligned}ILE_{01} &= \frac{\exp\overline{P} - 1}{P_0}, \quad IGE_{01} = \frac{\exp\overline{P} - 1}{\overline{P}},\\ ISGE_{01} &= S_0\Delta x\frac{\exp\overline{P} - \overline{P} - 1}{\overline{P}^2}.\end{aligned}$$

2.5 ENATE with discontinuous coefficients and source

Extensions of ENATE to more complex problems will now be commented on. In multiphase flows with geometrically complex physical interfaces either density or viscosity have jumps where they could vary several orders of magnitude, see e.g. Brennen [17]. In electromagnetic applications both permittivity and permeability show discontinuous behaviour when either a charged or magnetic material is within an electromagnetic field.

In order to simplify the problem in ENATE, the domain will have a discontinuity at x_D, see Figure 2.10, where

$$\lim_{x\to x_D}\phi_i^+ = \lim_{x\to x_D}\phi_i^- = \phi_D.$$

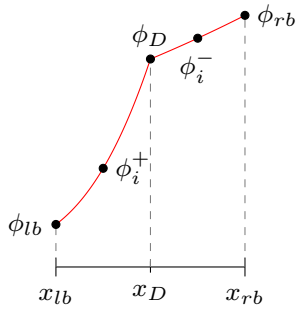

FIGURE 2.10: Representation of a two-zone problem

The coefficients ρu and Γ are assumed to be piecewise continuous,

$$\rho u = \begin{cases} \rho u^+(x), & \text{for } x \in [x_{lb}, x_D] \\ \rho u^-(x), & \text{for } x \in [x_D, x_{rb}] \end{cases},$$
$$\Gamma = \begin{cases} \Gamma^+(x), & \text{for } x \in [x_{lb}, x_D] \\ \Gamma^-(x), & \text{for } x \in [x_D, x_{rb}] \end{cases},$$

as well as the source term,

$$S = \begin{cases} S^+(x), & \text{for } x \in [x_{lb}, x_D] \\ S^-(x), & \text{for } x \in [x_D, x_{rb}] \end{cases}.$$

Note that when the discretization is applied, one grid-point must lie at x_D to link upstream and downstream solutions. In each zone, ϕ_i^+ and ϕ_i^-, the algebraic equation is (2.29) with the corresponding coefficients and source. So, the compatibility condition at the discontinuity is of Robin type,

$$\mathcal{F}(1)|_{WD}^{+} = \mathcal{F}(0)|_{DE}^{-}.$$

Then, replacing the total flux $\mathcal{F}$ of appendix A, the expression

$$\begin{aligned} &-(\rho u)_W^+ \left(\widetilde{k}_{WD}^+ + \frac{ILE_{01}}{IGE_{01}}\bigg|_{WD}^{+} \right) \phi_W^+ + \left[(\rho u)_W^+ \widetilde{k}_{WD}^+ \right. \\ &\left. +(\rho u)_D^- \left(\widetilde{k}_{DE}^- + \frac{ILE_{01}}{IGE_{01}}\bigg|_{DE}^{-} \right) \right] \phi_D - (\rho u)_D^- \widetilde{k}_{DE}^- \, \phi_E^- \\ &= IS_{01}|_{WD}^{+} + \left(\frac{ISGE_{01}}{IGE_{01}}\bigg|_{DE}^{-} - \frac{ISGE_{01}}{IGE_{01}}\bigg|_{WD}^{+} \right), \end{aligned} \tag{2.63}$$

is the discretized equation at x_D. If there is more than one discontinuity, equation (2.63) will be implemented at each one. In the special case of ρu, Γ and S being piecewise constant, the equation reads

$$\begin{aligned} &-\rho u^+ (1 + \widetilde{k}^+) \phi_W^+ + \left[\rho u^+ \widetilde{k}^+ + \rho u^- (1 + \widetilde{k}^-) \right] \phi_D - \rho u^- \widetilde{k}^- \phi_E^- \\ &= S^+ \Delta x^+ + S^+ \Delta x^+ \left(\widetilde{k}^+ - \frac{1}{P^+} \right) - S^- \Delta x^- \left(\widetilde{k}^- - \frac{1}{P^-} \right). \end{aligned}$$

2.6 Numerical Examples

All numerical tests but one that are evaluated in this section have an exact solution. In order to know how well or poorly ENATE resolves any of them the l_2-norm of the error vector will be used as monitor and calculated as

$$||\phi_{\text{num.}} - \phi_{\text{exact}}||_2 := \sqrt{\frac{1}{N_{\text{nodes}}} \sum_{i=0}^{N_{\text{nodes}}} (\phi_i|_{\text{num.}} - \phi_i|_{\text{exact}})^2},$$

being N_{nodes} the number of computed nodes, $\phi_i|_{\text{num.}}$ the numerical result at the i point of the mesh and $\phi_i|_{\text{exact}}$ the exact solution at the same point. Numerical examples from Pascau *et al.* [147] are included first, since the initial work of this thesis was the coding of both a central-differencing scheme (CDS) and a compact scheme (CS) proposed by Sen [190] that later were compared with ENATE. Next, a study where ENATE is compared with a high-order scheme is discussed. This study was published in Llorente *et al.* [119]. Finally, some work performed during a short stay in the Department of Mathematics and Computer Science of the Eindhoven University of Technology, The Netherlands, is shown, in which ENATE was compared with the FV-CF scheme.

TDMA (TriDiagonal Matrix Algorithm) was used as solver of the system of equations. The TDMA solver is based on LU-descomposition, a direct method to evaluate the matrix. In all cases a uniform mesh was employed.

2.6.1 Case with variable diffusion

Tian and Dai case [216] case is a traditional test employed to assess the accuracy of CFD schemes. The transport equation with BC is

$$\frac{\mathrm{d}}{\mathrm{d}x}\left(\rho u\phi - \Gamma\frac{\mathrm{d}\phi}{\mathrm{d}x}\right) = e^x\left(1-\epsilon(1+x)\right), \quad x \in [0,1]$$
$$\phi(0) = 1 + \frac{1}{2^{1/\epsilon}}, \quad \phi(1) = 2 + e,$$

where $\rho u = \rho(1+\epsilon)$ and $\Gamma = \epsilon(1+x)$. So, the factor ϵ controls both convection and diffusion terms and therefore, the Péclet number. ρ is set to 1. The solution, that develops a boundary layer near $x = 1$ for small ϵ see Fig. 2.11, is given by

$$\phi(x) = e^x + (1+x)\left(\frac{1+x}{2}\right)^{1/\epsilon}.$$

The l_2-norm is plotted in Fig. 2.12a for interval sizes within $[10^{-4}, 10^{-1}]$ and $\epsilon = 10^{-2}$. The results obtained indicate that a Septic Hermite spline behaves as a seventh-order scheme for Δx around 10^{-1} and a eighth-order for $\Delta x < 5 \cdot 10^{-2}$. Machine accuracy is obtained with 101 nodes. Quintic has the same convergence in those intervals: fifth- and sixth-order, whereas Cubic is fourth-order over a wide range of Δx. Convergence of three- and four-point Gauss is similar to those of Quintic and Septic. Also, the l_2-norm of CDS is plotted given second-order accuracy and CS fourth-order.

Changing ϵ to 10^{-4}, the rates of convergence are displayed in Fig. 2.12b. Hermite splines show similar behaviour to the previous case. Septic reaches machine accuracy for 201 nodes. Regarding GL quadrature, the three- and four-point quadratures produce two regions that are likely related to the approximation of the exponential. Errors could be magnified by GL quadrature if large values of the interval size are used due to its inability to integrate exponentials of large Péclet. The central and compact schemes, CDS and CS, have converged in a small stable region. The stability limit for CDS is $P < 2$ and for CS, $P < 8/3$.

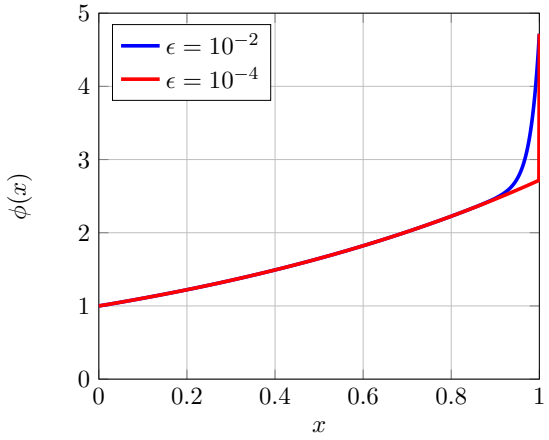

FIGURE 2.11: Example *Case with variable diffusion*, exact solution for two values of ϵ.

2.6.2 Case with variable convection

The test below solves the ODE with BC [142, p. 147],

$$\frac{\mathrm{d}}{\mathrm{d}x}\left(\rho u\phi - \Gamma\frac{\mathrm{d}\phi}{\mathrm{d}x}\right) = \frac{S_{\max}}{1 + S_{\max}(2x-1)^2}, \quad x \in [0,1]$$
$$\phi(0) = 0, \quad \left.\frac{\mathrm{d}\phi}{\mathrm{d}x}\right|_1 = 0.$$

The flow velocity is $u = (1+x)^3$ whereas the kinematic diffusion $\Gamma/\rho = \epsilon$ remains constant. ρ is set to 1. The BC at $x = 1$ is of Neumann type. The parameter $S_{\max}$ controls the source that takes a value of $S_{\max}/(S_{\max}+1)$ at the edges of the domain and raises to $S_{\max}$ at $x = 0.5$. As a result, the solution displays a steep layer at $x = 0.5$ where $S_{\max}$ regulates its top value. Since the previous ODE does not have an analytic solution, a reference solution is used with Septic Hermite and 10 001 nodes taking $\epsilon \in \{10^{-2}, 10^{-4}\}$ and $S_{max} \in \{10^2, 10^3\}$. As an example the reference solution for $\epsilon = 10^{-2}$ is plotted in Figure 2.13.

In the case of $\epsilon = 10^{-2}$, the results for the convergence rates are plotted in Figure 2.14. When $S_{\max} = 10^2$, Cubic Spline gets a third order scheme, Quintic, fifth order and Septic, seventh order. In the regime of high-Péclet Hermite mimics the theoretical tendency as shown in Figure 2.3. On the whole, Hermite works better than a GL quadrature as the large exponentials are poorly resolved with the latter for high Péclet. For instance, the

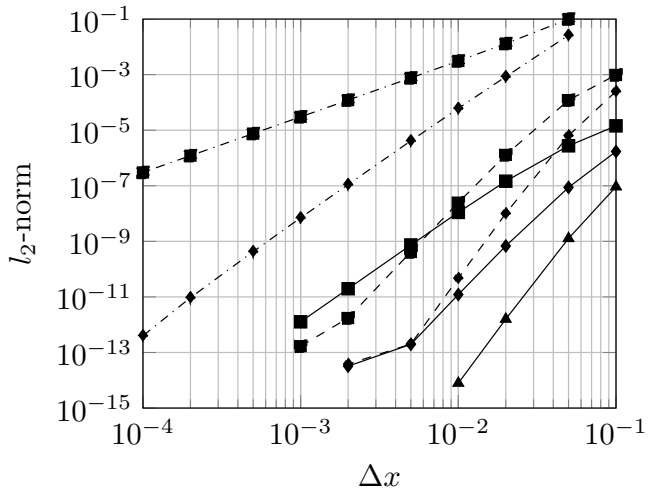

(A) Test with $\epsilon = 10^{-2}$

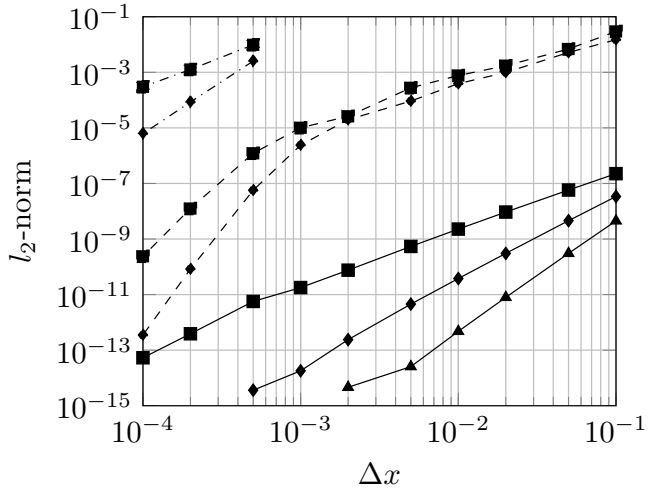

(B) Test with $\epsilon = 10^{-4}$

FIGURE 2.12: Example *Case with variable diffusion*, the l_2-norm of the error for the ENATE scheme. Solid lines represent Hermite spline: Cubic (■), Quintic (⧫) and Septic (▲). Dashed lines are Gauss quadrature: 3-point (■) and 4-point (⧫). Dash-dotted lines: central scheme (■) and central compact scheme (⧫).

ratio ILE_{01}/IGE_{01} did not get a value of one as it should be. Similar residuals and behaviours were achieved with $S_{\max} = 10^3$.

For $\epsilon = 10^{-4}$, results are plotted in Figure 2.15. In that case the residuals are two orders of magnitude better than for $\epsilon = 10^{-2}$. However, Cubic Spline performs like a second-order scheme, Quintic is third-order and Septic, fourth-order. Regarding the GL quadrature, two regions showed up before and after $\Delta x = 10^{-3}$. Initially it is a first-order scheme and then it moves closer to the order of Quintic and Septic.

In the four cases, neither CDS nor CS show a stable numerical solution and, therefore, they were substituted by an upwind scheme.

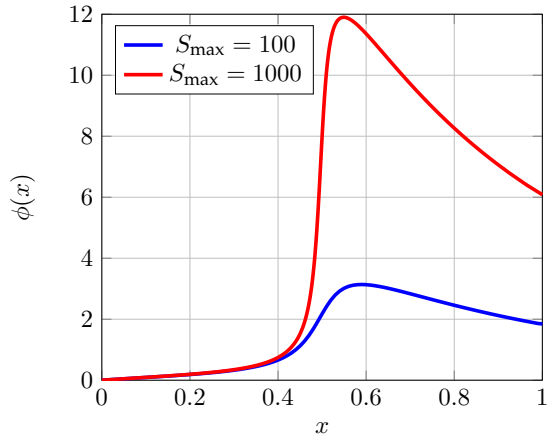

FIGURE 2.13: Example *Case with variable convection*, exact solution for $\Gamma = 10^{-2}$.

2.6.3 Nonlinear case: the 1D Burgers' equation

To assess a nonlinear convection-diffusion problem, the nonhomogeneous Burgers' equation with constant diffusion,

$$\frac{\mathrm{d}}{\mathrm{d}x}\left(\frac{1}{2}u^2 - \Gamma\frac{\mathrm{d}u}{\mathrm{d}x}\right) = 0, \quad x \in [0,1]$$
$$u(0) = 1, \quad u(1) = 0,$$

is employed. This ODE has an exact solution, drawn in Fig. 2.16,

$$u(x) = \mathcal{C}\tanh\left(\frac{\mathcal{C}}{2\Gamma}(1-x)\right) \quad \text{with} \quad 1 = \mathcal{C}\tanh\left(\frac{\mathcal{C}}{2\Gamma}\right).$$

This solution shows two zones: a boundary layer near $x = 1$, thinner as diffusion decreases, and a region where u remains constant and very close to one.

The tests proposed were with $\Gamma = 0.04$ and $\Gamma = 0.01$. In Figure 2.17a a similar behaviour to previous numerical cases is depicted. Septic Hermite has an l_2-norm of $1.19 \cdot 10^{-14}$ with 100 nodes, its convergence is somewhat worse than eighth-order, in contrast to Quintic, which is a bit better than sixth-order. Cubic spline is fourth-order. As we pointed out on page 54, the GL quadrature requires the value of the integrands within the interval. Due to the nonlinearity of the problem, the solution u participates in

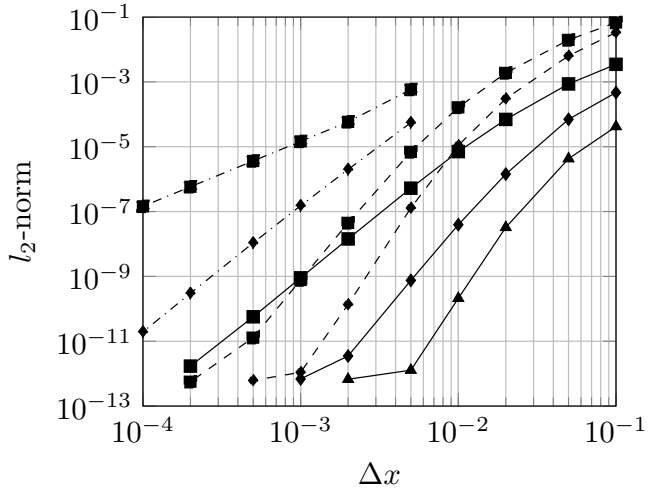

(A) Test with $S_{max} = 100$

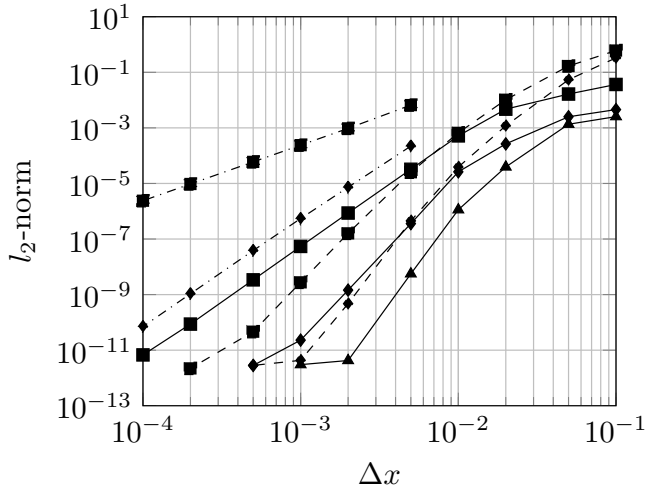

(B) Test with $S_{max} = 1000$

FIGURE 2.14: Example *Case with variable convection* and $\epsilon = 10^{-2}$, the l_2-norm of the error for the ENATE scheme. Solid lines represent ENATE: Cubic (■), Quintic (⧫) and Septic (▲). Dashed lines are Gauss quadrature: 3-point (■) and 4-point (⧫). Dash-dotted lines: central scheme (■) and central compact scheme (⧫).

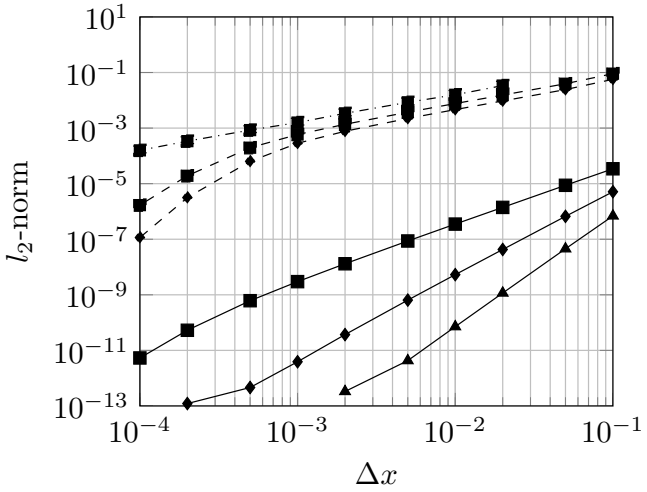

(A) Test with $S_{max} = 100$

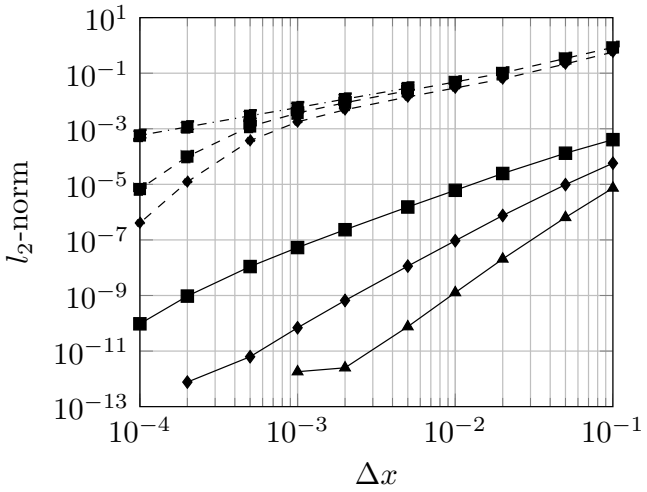

(B) Test with $S_{max} = 1000$

FIGURE 2.15: Example *Case with variable convection* and $\epsilon = 10^{-4}$, the l_2-norm of the error for the ENATE scheme. Same symbols as Fig. 2.14 except dash-dotted lines: upwind scheme (■).

the integrand and must be interpolated, adding complexity and numerical errors. Moreover, according to the numerical results presented before Hermite achieved better l_2-norms than GL. For all these reasons GL is no longer used.

The smaller the contribution of the diffusion is, the thinner the boundary layer is. This is the case with $\Gamma = 0.01$ where the convergence rates are plotted in Fig. 2.17b. It is seen that for large interval size, some Hermite did not converge. Also Septic needed fine grids to reach machine accuracy, $2.84 \cdot 10^{-13}$ with 500 nodes. Orders of Hermite, CDS and CS were as expected.

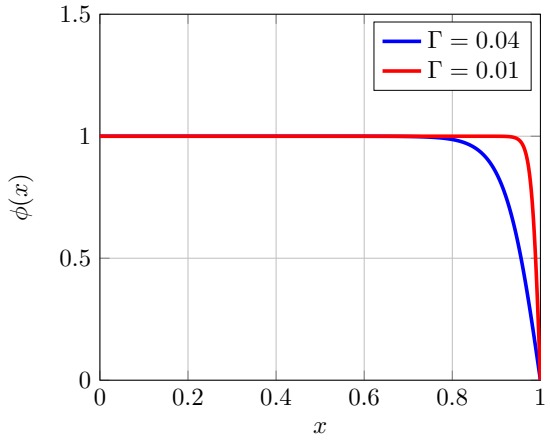

FIGURE 2.16: Example *Nonlinear case*, exact solution for two values of diffusion.

2.6.4 Case with discontinuities in the coefficients and source

A fourth numerical test deals with a solution with discontinuous derivative at $x = 0.5$ induced by a piecewise Gamma. The transport equation with BC is defined as,

$$\frac{\mathrm{d}}{\mathrm{d}x}\left(\rho u\phi - \Gamma\frac{\mathrm{d}\phi}{\mathrm{d}x}\right) = S, \quad x \in [0,1]$$
$$\phi(0) = 2, \quad \phi(1) = 0,$$

where $\rho u = 10^3$, $\Gamma(x) = 0.1(1+x)^2$ if $0 \leq x \leq 0.5$ and $\Gamma(x) = 0.0231(2-x)^2$ if $0.5 < x \leq 1$. The $S(x)$ term was such that the manufactured solution depicted in Figure 2.18 gave

$$\phi(x) = \begin{cases} 3 - 2^{2x}, & \text{If } x \in [0, 0.5] \\ 20x^2 - 32x + 12, & \text{If } x \in [0.5, 1] \end{cases}.$$

The values were chosen to set up a moderate jump in the derivative at 0.5 where the diffusion coefficient and the source vary in almost one order of magnitude. In Figure 2.19 the convergence rates are plotted. It can be seen that Hermite splines get fourth-order accuracy with Cubic, sixth-order for Quintic, eighth-order for Septic. With this last spline, l_2-norm was around 10^{-10} with ten intervals.

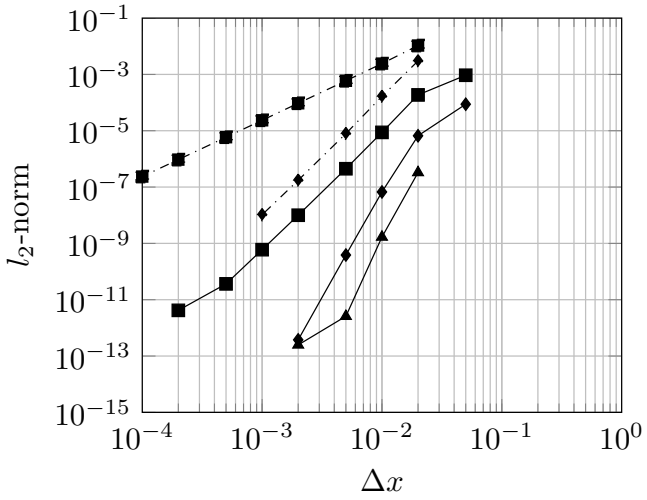

(A) Test with $\Gamma = 0.04$

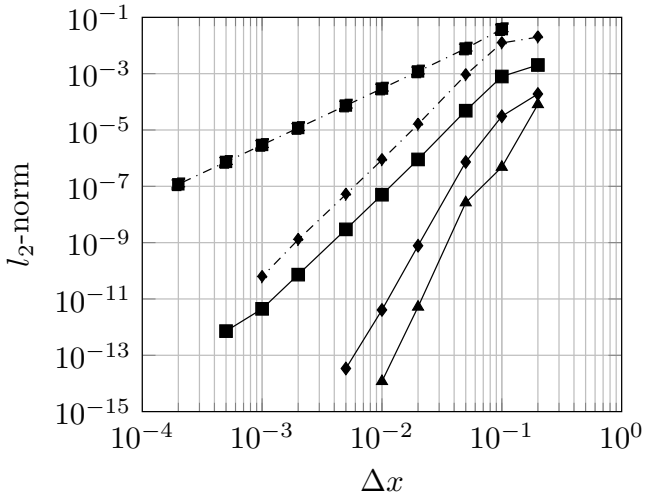

(B) Test with $\Gamma = 0.01$

FIGURE 2.17: Example *Nonlinear case,* the l_2-norm of the error for the ENATE scheme with two values of Γ. Solid lines correspond to Cubic Hermite (■), Quintic Hermite (⧫) and Septic Hermite (▲). Dash-dotted lines: CD (■) and CS (⧫).

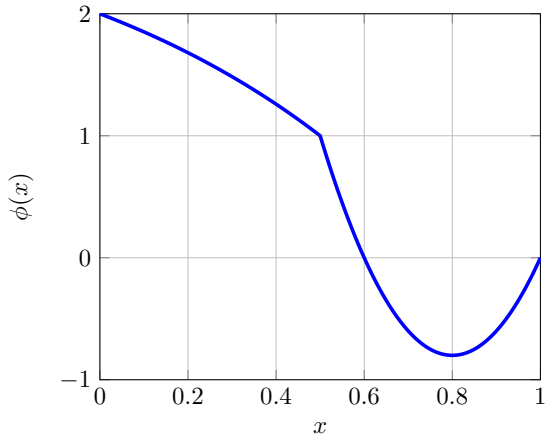

FIGURE 2.18: Example *Case with discontinuities in the coefficients and source*, exact solution.

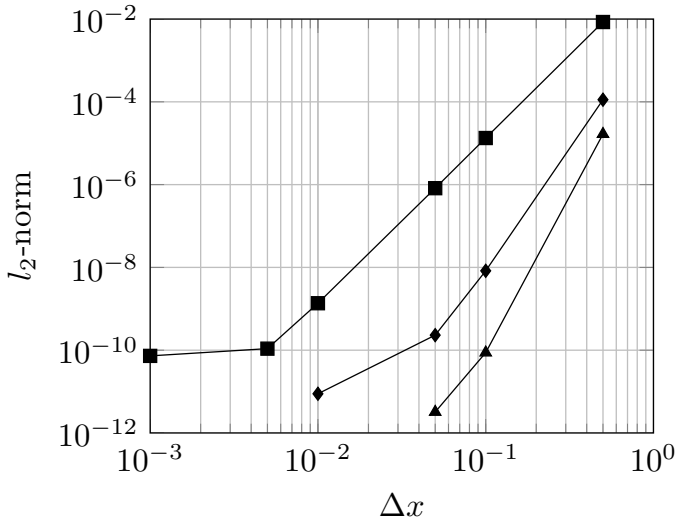

FIGURE 2.19: Example *Case with discontinuities in the coefficients and source*, the l_2-norm of the error for the ENATE scheme. Cubic Hermite (■), Quintic Hermite (⧫) and Septic Hermite (▲).

2.6.5 ENATE vs DGSEM

A comparison between ENATE and a well established numerical scheme, the Discontinuous Galerkin Spectral Element Method (DGSEM) was carried out within a collaboration with the Applied Mathematics and Statistics Department, Polytechnical University of Madrid. The DGSEM data were obtained with an in-house code of Madrid group.

The DG approach was introduced more than 40 years ago for the neutron distibution in a nuclear reactor [176]. This approach binds the flux balance in FV with the weak formulation in FE. The extra feature in DG lies in the fact that there is no continuity at the interfaces of adjacent elements. SE uses high-order discontinuous Lagrangian interpolants as bases and GL quadrature to approximate the integrals. Further information on one-dimension DGSEM formulation can be found in Llorente *et.al.* [119].

Since the 1D Burgers' equation was checked and reported good results for ENATE, it was decided to use this nonlinear equation for the purpose of comparison. DGSEM was run with fourth-degree and ninth-degree polynomials for each element.

As a first test, an inviscid Burgers' equation with source was tested.

$$\begin{aligned}&\frac{\mathrm{d}}{\mathrm{d}x}\left(\frac{1}{2}uu\right) = 20\frac{\tanh(20x+15)}{\cosh^2(20x+15)}, \quad x\in[-1,1]\\ &u(-1)=\tanh(-5), \quad u(1)=\tanh(35).\end{aligned}$$

The solution of the ODE, $u(x) = \tanh(20x + 15)$, contains a steep layer near the left boundary, Fig. 2.20. The approximation by DGSEM is given in Figure 2.21. The test is of paramount importance to show that DGSEM does not work well if sharp variations occur within an element, whatever order the polynomials may have. With ENATE the result was the exact one as the source has a primitive. However, one could use Hermite to approximate the source integral. If this is done, the l_2-norm with $\Delta x = 10^{-1}$ gets $8.32 \cdot 10^{-3}$ for Cubic, it is $4.05 \cdot 10^{-3}$ for Quintic and $6.69 \cdot 10^{-3}$ for Septic. None of the Hermite splines was able to reproduce the steep slope of the solution due to the poor resolution of the source and the l_2-norm is pretty much the same for all splines. It is expected that a nonuniform mesh would alleviate this problem.

In a second test, the diffusion is activated with $\Gamma = 0.1$ and $5 \cdot 10^{-3}$ whereas the source is removed. The former provides a smooth solution whilst the latter presents an abrupt drop at the end of the domain, Fig.2.22. The exact solution is

$$u(x) = \mathcal{C}\tanh\left(\frac{\mathcal{C}}{2\Gamma}(1-x)\right) \quad \text{with} \quad 1 = \mathcal{C}\tanh\left(\frac{\mathcal{C}}{2\Gamma}\right).$$

The constant $\mathcal{C}$, calculated to fix $u(0) = 1$, and BCs are those in the Table below.

The l_2-norm for ENATE and DGSEM with $\Gamma = 0.1$ is plotted in Figure 2.23a. As can be seen, both methods converge with their theoretical rates. However, a Cubic spline gets a lower order and less accuracy than DGSEM with a $4th$-degree polynomial. A norm of 10^{-6} is achieved with six elements in Galerkin and a slightly lower one with ten intervals in ENATE. Figure 2.23b shows norms for $\Gamma = 5 \cdot 10^{-3}$. For large Δx, ENATE could not

Γ	$\mathcal{C}$	$u(-1)$	$u(1)$
0.1	1.000090688	1.000090683	0
$5 \cdot 10^{-3}$	1	1	0

TABLE 2.9: Key parameters for the second test ENATE vs DGSEM.

achieve a solution and DGSEM has low accuracy. In medium and fine Δx the convergence and orders are correct, but Galerkin does not reproduce the steep layer near the right boundary whereas ENATE gives good results with higher accuracy.

Finally, a nonhomogeneous convection-diffusion case is presented. The source was chosen in such a way that the manufactured solution was $u(x) = 2 - A\sin(\sigma x\pi)$, $-1 \leq x \leq 1$, picture in Figure 2.24. Similarly, BCs are obtained from the exact solution. Two cases were run with $\sigma = 1$ and 5. The parameter σ represents the wavelength of the sine wave and A the amplitude, that is set to 1. For large wavelength problems, both ENATE and DGSEM reach the asymptotic slope with few nodes, see Figure 2.25a. A fourth-degree polynomial DGSEM has the same order as a Quintic spline, showing DGSEM a better performance. When the wavelength is one fifth of the whole domain, both show similar behaviour in convergence rates, see Figure 2.25b. DGSEM is showing better accuracy, e.g., with fifteen elements the l_2-norm is 10^{-8} and ENATE provides the same norm with forty.

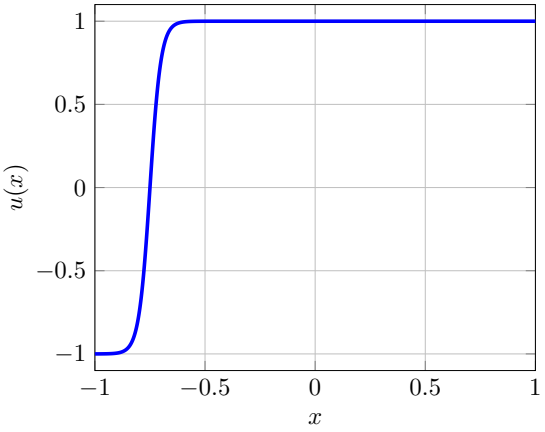

FIGURE 2.20: Example *ENATE vs DGSEM*, exact solution for the first test case.

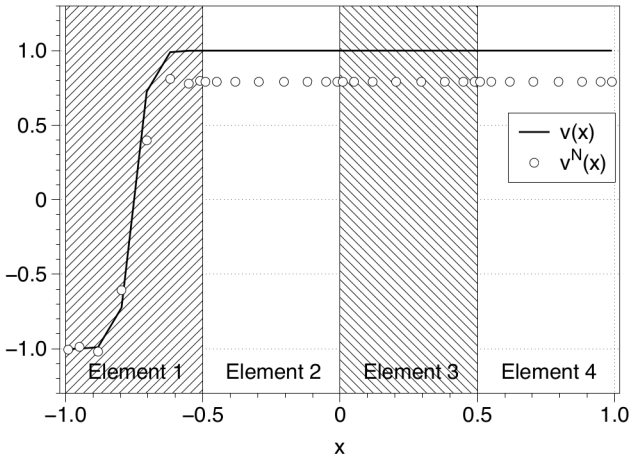

FIGURE 2.21: Solid line correspond to the exact solution and white dots to the DGSEM approximation [181].

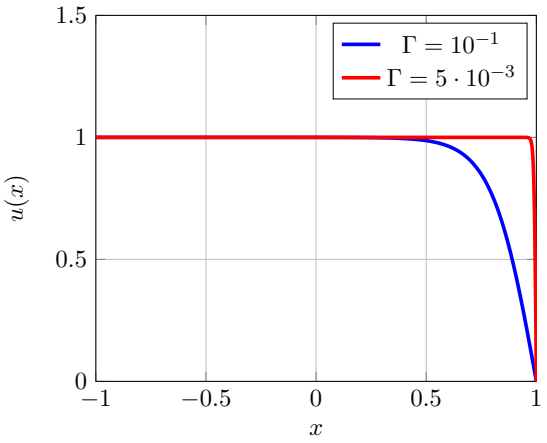

FIGURE 2.22: Example *ENATE vs DGSEM*, exact solution for the second test case.

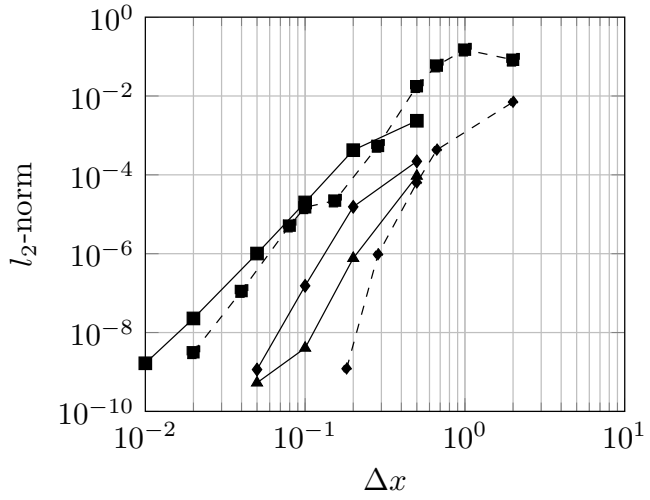

(A) $\Gamma = 0.1$

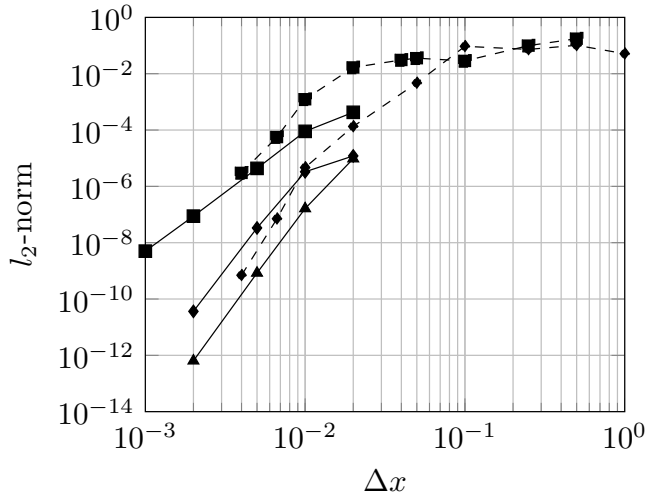

(B) $\Gamma = 0.005$

FIGURE 2.23: Example *ENATE vs DGSEM*, the l_2-norm of the error for two values of Γ. Solid lines represent ENATE: Cubic (■), Quintic (♦) and Septic (▲). Dashed lines are DGSEM: 4th degree polynomial (■) and 9th degree polynomial (♦).

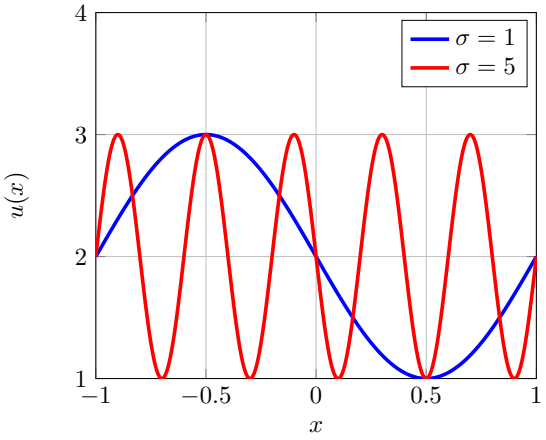

FIGURE 2.24: Example *ENATE vs DGSEM*, exact solution for the third test case.

2.6.6 Analysis with another modern exp-scheme

In recent years, the exponential scheme named "**F**inite **V**olume-**C**omplete **F**lux", FV-CF [209], has been developed in the Department of Mathematics and Computer Science of Eindhoven University of Technology, The Netherlands. This numerical procedure solves transport equations in a similar way to ENATE with some differences that are detailed in [120]. The first difference is that the control volume of ENATE goes between nodes and that of FV-CF between interfaces, as drawn in Figure 2.26. Secondly, in the FV-CF scheme some integrals that appear in the coefficients have the lower limit of integration at the interfaces and others at nodes, e.g.,

$$\Lambda = \int_{x_e}^{x} \lambda \, \mathrm{d}x', \quad \mathcal{S} = \int_{x_e}^{x} S \, \mathrm{d}x', \quad \langle a, b \rangle = \int_{x_C}^{x_E} ab \, \mathrm{d}x,$$

whereas ENATE the integration limits are always from nodes. The ENATE integrals can be linked with the FV-CF ones as follows:

$$\overline{P} \equiv \langle \lambda, 1 \rangle, \quad \frac{\overline{E}_{1/2}}{\overline{E}} \equiv e^{-\Lambda}, \quad IS_{0\widehat{x}} - IS_{01/2} \equiv \mathcal{S},$$
$$P_0 \overline{E}_{1/2} \, ILE_{01} \equiv \langle \lambda, e^{-\Lambda} \rangle, \quad \frac{P_0 \overline{E}_{1/2}}{(\rho u)_{lb}} \, IGE_{01} \equiv \langle \Gamma^{-1}, e^{-\Lambda} \rangle$$
$$\frac{P_0 \overline{E}_{1/2}}{(\rho u)_{lb}} \, ISGE_{01} \equiv \langle \mathcal{S}\,\Gamma^{-1}, e^{-\Lambda} \rangle + IS_{01/2} \langle \Gamma^{-1}, e^{-\Lambda} \rangle.$$

where $\overline{E}_{1/2} = \overline{E}(1/2)$. If the total flux in FV-CF is broken down in the homogeneous and inhomogeneous fluxes

$$\mathcal{F}_e = \mathcal{F}_e^{\phi} + \mathcal{F}_e^{S},$$
$$\mathcal{F}_e^{\phi} = \frac{\langle \lambda, e^{-\Lambda} \rangle / \langle \lambda, 1 \rangle}{\langle \Gamma^{-1}, e^{-\Lambda} \rangle} \left[\frac{-\langle \lambda, 1 \rangle}{\exp(-\langle \lambda, 1 \rangle) - 1} \phi_C - \frac{\langle \lambda, 1 \rangle}{\exp(\langle \lambda, 1 \rangle) - 1} \phi_E \right],$$
$$\mathcal{F}_e^{S} = -\frac{\langle \mathcal{S}\,\Gamma^{-1}, e^{-\Lambda} \rangle}{\langle \Gamma^{-1}, e^{-\Lambda} \rangle},$$

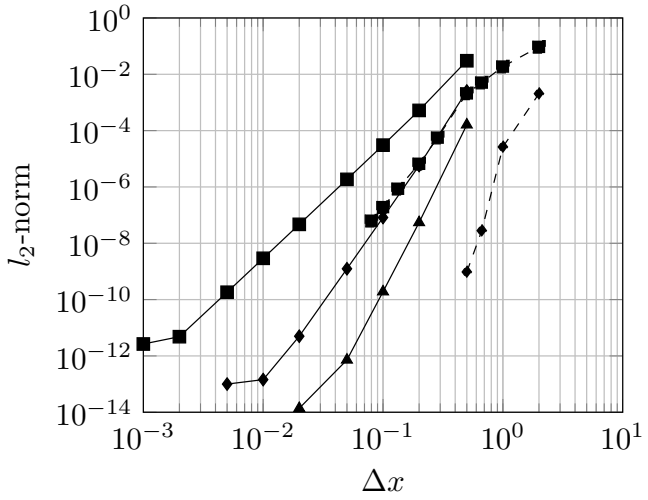

(A) Wave with $\sigma = 1$

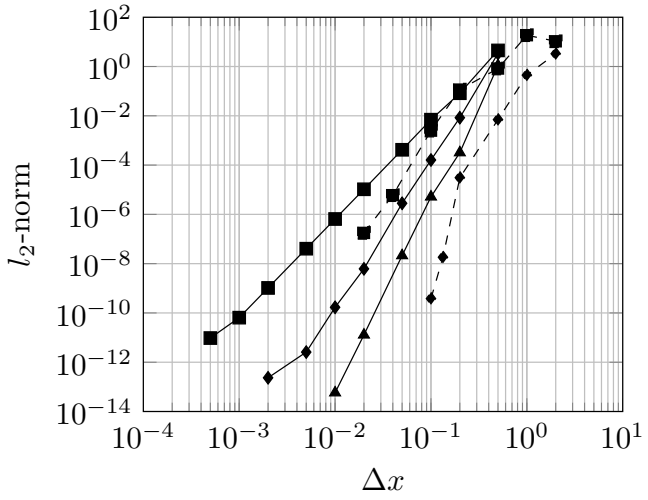

(B) Wave with $\sigma = 5$

FIGURE 2.25: Example *ENATE vs DGSEM*, the l_2-norm of the error for two values of σ. Same legend as in Figure 2.23.

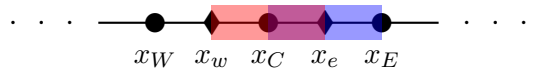

FIGURE 2.26: Control volume for FV-CF (red box) and ENATE (blue box). Grid-points (•), Interfaces (⧫).

and compared with the ENATE flux, as done in Appendix A, it is concluded that both homogeneous ($\mathcal{F}^\phi$) and inhomogeneous ($\mathcal{F}^S$) fluxes at the interfaces are the same. The difference comes from the method chosen to numerically calculate the integrals. The FV-CF scheme uses second-order approximations in the calculations of the integrals whereas ENATE uses high-order splines to do the same.

In order to compare them let us assume a transport equation with constant convection and diffusion,

$$\frac{\mathrm{d}}{\mathrm{d}x}\left(\rho u\phi - \Gamma\frac{\mathrm{d}\phi}{\mathrm{d}x}\right) = S, \qquad 0 \leq x \leq a,$$

where the source and BCs are those that give as solution

$$\phi(x) = 2\frac{\rho u x}{\Gamma}\exp\left(-\frac{\rho u x^2}{\Gamma a}\right).$$

The exact solution is pictured in Fig. 2.27. The smaller the diffusion is, the bigger is the contribution of the source in the left boundary. In Table 2.10 the l_2-norm is displayed in three meshes. Clearly, ENATE reduces the norm very quickly on increasing the number of intervals, much more than FV-CF with a second-order approximation. In fact, from 10 to 100 nodes, FV-CF is a second-order scheme and ENATE is fourth-, sixth- and eighth-order. With $\Gamma = 10^{-2}$, Septic achieves machine accuracy with 100 nodes and requires ten times more nodes with $\Gamma = 10^{-3}$. In contrast, the FV-CF gets the same accuracy with 1000 nodes as Septic with 10 nodes in both diffusion regimes.

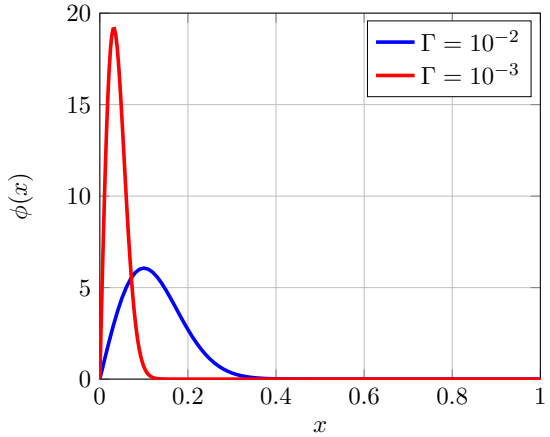

FIGURE 2.27: Example *Analysis with another modern exp-scheme*, exact solution for two values of diffusion taken $a = 1$ and $\rho u = 0.5$

$\Gamma = 10^{-2}$

N_{nodes}	Δx	FV-CF	ENATE		
			Cubic	Quintic	Septic
10	0.1	$6.4737 \cdot 10^{-1}$	$3.4219 \cdot 10^{-2}$	$1.6612 \cdot 10^{-3}$	$5.8206 \cdot 10^{-5}$
50	0.02	$7.1589 \cdot 10^{-3}$	$3.5051 \cdot 10^{-5}$	$6.0070 \cdot 10^{-8}$	$7.6507 \cdot 10^{-11}$
100	0.01	$2.5418 \cdot 10^{-3}$	$2.2344 \cdot 10^{-6}$	$9.5419 \cdot 10^{-10}$	$3.0428 \cdot 10^{-13}$
500	0.002	$1.2916 \cdot 10^{-4}$	$3.5970 \cdot 10^{-9}$	$6.2685 \cdot 10^{-14}$	$3.9511 \cdot 10^{-15}$
1000	0.001	$3.3134 \cdot 10^{-5}$	$2.2478 \cdot 10^{-10}$	$1.4890 \cdot 10^{-13}$	$1.5556 \cdot 10^{-13}$

$\Gamma = 10^{-3}$

N_{nodes}	Δx	FV-CF	ENATE		
			Cubic	Quintic	Septic
10	0.1	$4.1300 \cdot 10^{+1}$	$1.4243 \cdot 10^{-1}$	$2.4309 \cdot 10^{-3}$	$6.9036 \cdot 10^{-4}$
50	0.02	$3.2521 \cdot 10^{-1}$	$6.6915 \cdot 19^{-3}$	$1.0452 \cdot 10^{-4}$	$1.2338 \cdot 10^{-6}$
100	0.01	$6.2289 \cdot 10^{-2}$	$4.1856 \cdot 10^{-4}$	$1.9207 \cdot 10^{-6}$	$6.4660 \cdot 10^{-9}$
500	0.002	$1.2628 \cdot 10^{-3}$	$6.2217 \cdot 10^{-7}$	$1.0604 \cdot 10^{-10}$	$1.3431 \cdot 10^{-14}$
1000	0.001	$4.5417 \cdot 10^{-4}$	$3.9670 \cdot 10^{-8}$	$1.7128 \cdot 10^{-12}$	$1.9204 \cdot 10^{-13}$

TABLE 2.10: Example *Analysis with another modern exp-scheme*, the l_2-norm of the error for ENATE and FV-CF.

2.7 In Closing

In this chapter, a complete formulation of the numerical solution of a one-dimensional steady-state transport equation with ENATE was carried out. The procedure allows an algebraic equation between three nodes to be formulated by ensuring the continuity of the diffusion fluxes at the central one. BCs of different type are easily implemented. A complete analysis of classical properties of schemes used in CFD shows ENATE to be a robust 1D scheme. In addition, ENATE can be used to solve linear and non-linear cases with continuous and discontinuous variable coefficients.

Numerical results for several tests were provided, showing that the best option was Hermite spline interpolation. On the other hand, a comparison study was done with another high-order scheme, DGSEM, with good outcomes for both. Also, the comparison with another exponential scheme, FV-CF, in which the assembly of the algebraic equation is the same, highlights the fact that the source treatment is of paramount importance for the global accuracy.

Some issues arise when extensions and generalizations to multidimensions are required in the problem, as one-dimensional cases are very simplistic. In chapters to follow, a multidimensional ENATE will be drawn up to achieve similar accuracy to the one-dimensional scheme.

Chapter 3

Climbing the challenge: two-dimensional ENATE

Goals:

- To carry over to two dimensions the procedure devised for one-dimensional non-homogeneous transport equation.
- To compare different treatments of the sources.
- To develop a case on nonuniform mesh.

3.1 Overview of the difficulties related to exponential schemes

Exponential schemes work properly with steady-state one-dimensional flows. The treatment of the source is also fundamental. Yet, many important flows are multidimensional and unsteady so the practical applications of exponential schemes as originally devised are reduced to a very large extent. In the '90s, Leonard published an article [111] where he gave some reasons why exponential schemes should not be used for practical calculations, considering that they were devised under the following restrictions:

1. Steady one-dimensional problems,
2. Convection/diffusion coefficients constant over control volumes,
3. Sources negligible or weak enough,

and flows of interest never satisfy these constraints. The main problem of these schemes is associated to the existence of a large numerical diffusion superimposed to the physical one. This makes the results overly diffusive. Along the same line, Roos [177] claimed that although one can extend these schemes to high dimensions, the convergence and the accuracy level will be affected. Contrary to this claim, different approaches of ENATE for multidimensional problems will be derived in this chapter, specifically in two dimensions, keeping similar convergence rates to one dimension. As will be explained, two paths can be taken, either to reduce the dimensionality of the PDE, or to set a system of pseudo-1D convection-diffusion problems that considers somehow the influence of the other dimension via the source term. A correct numerical treatment of either approach will be required.

3.2 Streamline approach

Let us start with a convection-only equation,

$$\nabla \cdot (\rho \mathbf{u} \phi) = S, \tag{3.1}$$

where $\mathbf{u} = (u, v)^T \neq \mathbf{0}$. If the fluid flows along the x-direction, ϕ values at north and south of a generic point in the grid are unconnected and the solution may have layers with strong gradients between them. When flow is skewed with respect to the coordinate lines, flow along unconnected layers will also appear. In order to solve the 2D equation there is a transformation that turns it into an ordinary differential equation along each layer. The transformation will be based on the streamline geometry of the given velocity field.

The history of stream-function coordinates (SFC) goes back to 1927 with the boundary layer theory [168] and von Mises' work [231]. SFC formulation was used for potential and viscous flows in curved geometries, multiphase flows, airfoils, tubomachinery, porous media and many others [22, 28, 76, 97]. On the whole, there are two types of formulations:

- von Mises transformation considers a mapping between Cartesian coordinates (x, y) and curvilinear coordinates (x, ψ) where the variable ψ is the stream-function,
- Martin's approach [127, 128] turns (x, y) into (φ, ψ) where the iso-φ are taken arbitrarily.

The preference for any new system of coordinates varies. In this work it was decided to use (φ, ψ) as an orthogonal curvilinear space. $\psi = \psi(x, y)$ is the stream-function defined such that

$$\nabla \psi \cdot \rho \mathbf{u} = 0,$$

and the potential function $\varphi = \varphi(x, y)$ is defined by

$$\nabla \psi \cdot \nabla \varphi = 0.$$

A possible solution to the previous PDE system could be

$$\frac{\partial \psi}{\partial x} = -\rho v, \qquad \frac{\partial \psi}{\partial y} = \rho u, \tag{3.2a}$$

$$\frac{\partial \varphi}{\partial x} = \Xi \rho u, \qquad \frac{\partial \varphi}{\partial y} = \Xi \rho v, \tag{3.2b}$$

where $\Xi = \Xi(x, y)$, similar to Keller [97], is a stretching coefficient for rotational flows. This coefficient will be defined later. On the other hand, we write the curvilinear basis vectors as $\mathbf{e}_\varphi$ and $\mathbf{e}_\psi$. The base is an orthonormal set, $|\mathbf{e}_\varphi| = |\mathbf{e}_\psi| = 1$ and $\mathbf{e}_\varphi \cdot \mathbf{e}_\psi = 0$. $\mathbf{e}_\varphi$ is the unitary vector aligned with the direction of the flow. The transformation between the map (x, y) and (φ, ψ), Figure 3.1, is given by

$$\mathbf{e}_x = \mathbf{R}(\theta)\, \mathbf{e}_\varphi, \quad \mathbf{e}_y = \mathbf{R}(\theta)\, \mathbf{e}_\psi, \quad \mathbf{R}(\theta) := \begin{pmatrix} \cos\theta & \sin\theta \\ -\sin\theta & \cos\theta \end{pmatrix},$$

where $\mathbf{R}(\theta)$ is the rotation matrix being θ the angle between $\mathbf{e}_x$ and $\mathbf{e}_\varphi$ which may depend on the position:

$$\cos\theta = \frac{\rho u}{|\rho\mathbf{u}|}, \quad \sin\theta = \frac{\rho v}{|\rho\mathbf{u}|}, \quad |\rho\mathbf{u}|^2 = (\rho u)^2 + (\rho v)^2.$$

As a result, the convection vector is $\rho\mathbf{u} = |\rho\mathbf{u}|\mathbf{e}_\varphi$. The next step is to describe the divergence in the curvilinear space (φ, ψ). A formulation for the differential operators in generalized coordinates is found in [242]. Taking the changes (3.2a) and (3.2b), the contravariant basis is

$$\mathbf{g}^\varphi := \nabla\varphi = \Xi|\rho\mathbf{u}|\mathbf{e}_\varphi, \quad \mathbf{g}^\psi := \nabla\psi = |\rho\mathbf{u}|\mathbf{e}_\psi.$$

On the other hand, the Jacobian of the transformation reads

$$\mathcal{J} := \left|\frac{\partial(\varphi,\psi)}{\partial(x,y)}\right| = \Xi|\rho\mathbf{u}|^2. \tag{3.3}$$

Note that the mapping $(x, y) \to (\varphi, \psi)$ is valid provided that $\Xi \neq 0$. Given the new basis, a general vector $\mathbf{v}$ could be written with their covariant components as follows:

$$\begin{aligned}\mathbf{v} &= \mathrm{v}_\varphi\mathbf{g}^\varphi + \mathrm{v}_\psi\mathbf{g}^\psi \\ &= |\rho\mathbf{u}|\left(\Xi\mathrm{v}_\varphi\mathbf{e}_\varphi + \mathrm{v}_\psi\mathbf{e}_\psi\right).\end{aligned}$$

Finally, the divergence of $\mathbf{v}$ is defined by

$$\begin{aligned}\nabla\cdot\mathbf{v} &= \mathcal{J}\frac{\partial}{\partial\varphi}\left(\frac{\mathbf{g}^\varphi\cdot\mathbf{v}}{\mathcal{J}}\right) + \mathcal{J}\frac{\partial}{\partial\psi}\left(\frac{\mathbf{g}^\psi\cdot\mathbf{v}}{\mathcal{J}}\right) \\ &= \Xi|\rho\mathbf{u}|^2\left[\frac{\partial}{\partial\varphi}\left(\Xi\mathrm{v}_\varphi\right) + \frac{\partial}{\partial\psi}\left(\frac{\mathrm{v}_\psi}{\Xi}\right)\right].\end{aligned}$$

In the problem at hand, $\mathbf{v} = \rho\mathbf{u}\phi$ then $\mathrm{v}_\varphi = \phi/\Xi$ and $\mathrm{v}_\psi = 0$. So, the purely convective transport equation on streamlines writes

$$\frac{\partial\phi}{\partial\varphi} = \frac{S}{\Xi|\rho\mathbf{u}|^2}. \tag{3.4}$$

The great achievement of this transformation is that it allows a reduction in the dimensionality of the convective terms. The new coordinate is pointed out in the direction of the flow and that is why ϕ changes only with φ. The direction of the φ coordinate is the flow direction whereas ψ coordinate is orthogonal to it, owing to the definition of a streamline. In consequence, ψ remains constant along it.

The procedure with ENATE keeps the discretization of (3.4) very simple. What is needed is to cut the streamline into intervals as in Figure 3.1 and then to calculate ϕ at a Central node with the help of ϕ at an Upstream node by

$$\phi_C = \phi_U + \int_{\varphi_U}^{\varphi_C}\frac{S}{\Xi|\rho\mathbf{u}|^2}\mathrm{d}\varphi, \quad \text{on } \psi = \text{const.} \ . \tag{3.5}$$

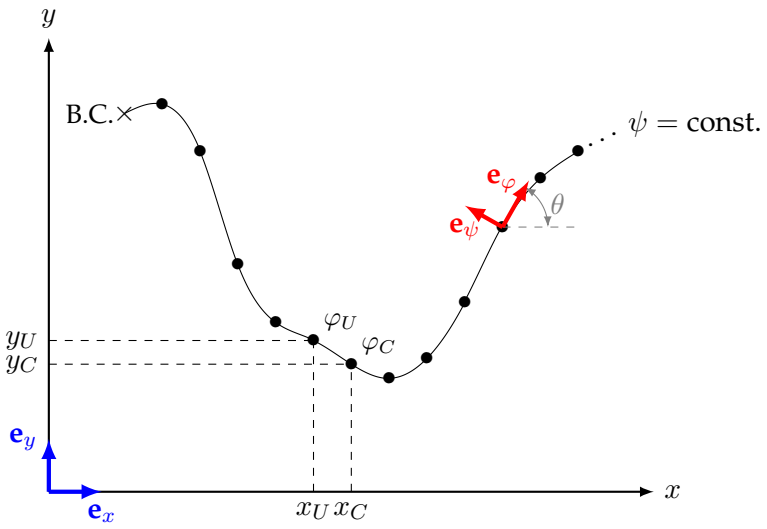

FIGURE 3.1: Discretization on a streamline. Boundary Condition: cross node. Black points: inner nodes. Cartesian basis: blue arrows. Curvilinear basis: red arrows.

The previous equation is recurrently applied for every streamline drawn over the domain. The integral of $S/\Xi|\rho\mathbf{u}|^2$ could be split up as

$$\begin{aligned}\int_{\varphi_U}^{\varphi_C} \frac{S}{\Xi|\rho\mathbf{u}|^2}\mathrm{d}\varphi &= \int_{x_U}^{x_C} \frac{S}{\Xi|\rho\mathbf{u}|^2}\frac{\partial\varphi}{\partial x}\mathrm{d}x + \int_{y_U}^{y_C} \frac{S}{\Xi|\rho\mathbf{u}|^2}\frac{\partial\varphi}{\partial y}\mathrm{d}y \\ &= \int_{x_U}^{x_C} S\frac{\rho u}{|\rho\mathbf{u}|^2}\mathrm{d}x + \int_{y_U}^{y_C} S\frac{\rho v}{|\rho\mathbf{u}|^2}\mathrm{d}y.\end{aligned}$$

Since the integrals are performed over a streamline, i.e. $\rho v\mathrm{d}x = \rho u\mathrm{d}y$, then

$$\int_{\varphi_U}^{\varphi_C} \frac{S}{\Xi|\rho\mathbf{u}|^2}\mathrm{d}\varphi = \int_{x_U}^{x_C} \frac{S}{\rho u}\mathrm{d}x = \int_{y_U}^{y_C} \frac{S}{\rho v}\mathrm{d}y.$$

3.2.1 Change of variables

As seen above, this approach requires the curvilinear geometry of streamlines and, therefore, a mesh oriented to the flow in the whole domain, see Figure 3.2. This entails knowing the change of variables $(\varphi(x,y), \psi(x,y))$ in

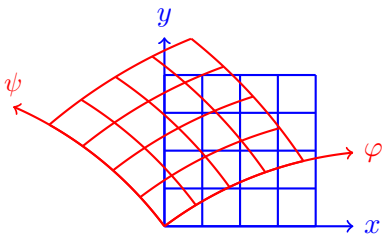

FIGURE 3.2: Cartesian mesh (blue) vs Curvilinear mesh (red)

the domain. An option would be to solve the next set of Poisson equations,

$$\nabla^2\varphi = \rho\mathbf{u}\cdot\nabla\Xi,$$
$$\nabla^2\psi = -\mathbf{e}_z\cdot\nabla\times(\rho\mathbf{u}),$$

what gives the φ, ψ fields to calculate the isolines. The expression for $\nabla^2\varphi$ is valid provided that $\nabla\cdot(\rho\mathbf{u}) = 0$. On the other hand, the unit vector $\mathbf{e}_z$ is perpendicular to the plane. For simplicity, $\nabla^2\psi$ is defined in terms of the variable

$$\omega_\rho \coloneqq \mathbf{e}_z\cdot\nabla\times(\rho\mathbf{u}) = \frac{\partial\rho v}{\partial x} - \frac{\partial\rho u}{\partial y}.$$

If ρ is constant, then $\omega_\rho = \rho\omega$ where ω is the z-component of the vorticity. Another way to calculate the $\psi = \text{const.}$ lines is by taking the total derivative of ψ,

$$\mathrm{d}\psi = -\rho v\,\mathrm{d}x + \rho u\,\mathrm{d}y.$$

The isoline satisfies $\mathrm{d}\psi = 0$. So, the former equation is an exact differential equation if and only if $\partial\rho u/\partial x = -\partial\rho v/\partial y$ or $\nabla\cdot(\rho\mathbf{u}) = 0$ which is the mass conservation. The solution can be obtained integrating the first equation of (3.2a) with respect to x, i.e.

$$\psi(x,y) = -\int_0^x \rho v\,\mathrm{d}x' + a(y),$$

where $a(y)$ is an arbitrary function of integration. Substituting in the second equation of (3.2a),

$$-\int_0^x \frac{\partial\rho v}{\partial y}\mathrm{d}x' + \frac{\mathrm{d}a}{\mathrm{d}y} = \rho u,$$

the function a is found by integrating with respect to y. The arbitrary constant of integration can be set to zero if $\psi(0,0) = 0$. The result is

$$\psi = -\int_0^x \rho v\,\mathrm{d}x' + \int_0^y \rho u\,\mathrm{d}y' + \int_0^y\int_0^x \frac{\partial\rho v}{\partial y'}\mathrm{d}x'\mathrm{d}y', \tag{3.6}$$

Similarly, the total derivative of φ,

$$\mathrm{d}\varphi = \Xi\rho u\,\mathrm{d}x + \Xi\rho v\,\mathrm{d}y,$$

allows to formulate the φ-field as

$$\varphi = \int_0^x \Xi\rho u\,\mathrm{d}x' + \int_0^y \Xi\rho v\,\mathrm{d}y' - \int_0^y\int_0^x \frac{\partial\,(\Xi\rho u)}{\partial y'}\mathrm{d}x'\mathrm{d}y', \tag{3.7}$$

if $\partial(\Xi\rho v)/\partial x = \partial(\Xi\rho u)/\partial y$ or $\nabla\times(\Xi\rho\mathbf{u}) = \mathbf{0}$ is valid. If the flow was irrotational with constant density , then $\Xi(x,y) = \Xi_0$ being Ξ_0 an arbitrary constant. In a general case, a solution can be obtained by the method of characteristics [261, p. 432]. Write $\nabla\times(\Xi\rho\mathbf{u}) = \mathbf{0}$ in the form of a PDE,

$$\rho v\frac{\partial\Xi}{\partial x} - \rho u\frac{\partial\Xi}{\partial y} = -\Xi\omega_\rho.$$

The total differentiation of Ξ with respect to the characteristic s is

$$\frac{\mathrm{d}\Xi}{\mathrm{d}s} = \frac{\partial \Xi}{\partial x}\frac{\mathrm{d}x}{\mathrm{d}s} + \frac{\partial \Xi}{\partial y}\frac{\mathrm{d}y}{\mathrm{d}s}.$$

Comparing both equations, one takes

$$\frac{\mathrm{d}\Xi}{\mathrm{d}s} = -\Xi\omega_\rho, \tag{3.8a}$$

$$\frac{\mathrm{d}x}{\mathrm{d}s} = \rho v, \quad \frac{\mathrm{d}y}{\mathrm{d}s} = -\rho u. \tag{3.8b}$$

Assuming $\Xi(s=0) = \Xi_0 = 1$, the ODE (3.8a) leads to a stretching coefficient

$$\Xi(s) = \exp\left(-\int_0^s \omega_\rho \,\mathrm{d}s'\right) \tag{3.9}$$

along the path described by the system (3.8b), which are in this case curves orthogonal to the streamlines. Since $\Xi > 0$, then $\mathcal{J} \neq 0$ and the transformation is valid.

3.2.2 Skewed flow at 45^o

A special case could be considered when $\rho u = \rho v$. In such a case, some simplifications can be done. Firstly, the stretching coefficient (3.9) becomes $\Xi = 1/\rho u$ and the Jacobian of the transformation (3.3) now writes $\mathcal{J} = 2\rho u$. Secondly, the convective terms could be taken out in the iso-ψ and iso-φ equations and the mapping (3.6) and (3.7) yields

$$(\varphi, \psi)^T = (y + x, y - x)^T.$$

Streamlines are just straight lines with unity slope. The grid has rotated $\alpha = \pi/4$ and the derivatives of ρu in the curvilinear coordinates are

$$\frac{\partial \rho u}{\partial \varphi^i} = \frac{\partial x^j}{\partial \varphi^i}\frac{\partial \rho u}{\partial x^j} \longrightarrow \begin{cases} \dfrac{\partial \rho u}{\partial \varphi} = \dfrac{1}{2}\nabla \cdot (\rho \mathbf{u}) = 0, \\ \dfrac{\partial \rho u}{\partial \psi} = -\dfrac{1}{2}\omega_\rho. \end{cases}$$

These calculations say that ρu is going to be a function of ψ and if $\omega_\rho = 0$, then ρu in the (φ, ψ)-space is constant. This allows to simplify the recurrence equation (3.5) to

$$\phi_C = \phi_U + \frac{1}{2\rho u}\int_{\varphi_U}^{\varphi_C} S \,\mathrm{d}\varphi \quad \text{on} \quad \psi = \text{const.} \ .$$

3.3 Cross-flux approach

A convection-diffusion problem is written as

$$\nabla \cdot \boldsymbol{\mathcal{F}} = S, \tag{3.10}$$

where the total flux $\boldsymbol{\mathcal{F}}$ writes

$$\begin{aligned} \boldsymbol{\mathcal{F}} &= \rho \mathbf{u}\phi - \Gamma \nabla \phi \\ &= \left(\rho u\phi - \Gamma \frac{\partial \phi}{\partial x}, \rho v\phi - \Gamma \frac{\partial \phi}{\partial y} \right)^T = (\mathcal{F}_x, \mathcal{F}_y)^T . \end{aligned} \tag{3.11}$$

The previous section referred to convection-only problems. With diffusion the streamline approach does not make much sense. Diffusion processes tend to spread information, so it is expected that a ϕ value on a streamline depends on adjacent streamlines. Moreover, although this is not a major problem, the transformation (φ, ψ) turns the problem into one with anisotropic diffusion,

$$\begin{aligned} \nabla \cdot (\Gamma \nabla \phi) =& \mathcal{J} \frac{\partial}{\partial \varphi} \left(\frac{\mathbf{g}^\varphi \cdot \mathbf{g}^\varphi}{\mathcal{J}} \Gamma \frac{\partial \phi}{\partial \varphi} \right) + \mathcal{J} \frac{\partial}{\partial \varphi} \left(\cancel{\frac{\mathbf{g}^\varphi \cdot \mathbf{g}^\psi}{\mathcal{J}}} \Gamma \frac{\partial \phi}{\partial \psi} \right) \\ &+ \mathcal{J} \frac{\partial}{\partial \psi} \left(\cancel{\frac{\mathbf{g}^\psi \cdot \mathbf{g}^\varphi}{\mathcal{J}}} \Gamma \frac{\partial \phi}{\partial \varphi} \right) + \mathcal{J} \frac{\partial}{\partial \psi} \left(\frac{\mathbf{g}^\psi \cdot \mathbf{g}^\psi}{\mathcal{J}} \Gamma \frac{\partial \phi}{\partial \psi} \right) \\ =& \Xi |\rho \mathbf{u}|^2 \left[\frac{\partial}{\partial \varphi} \left(\Gamma \Xi \frac{\partial \phi}{\partial \varphi} \right) + \frac{\partial}{\partial \psi} \left(\frac{\Gamma}{\Xi} \frac{\partial \phi}{\partial \psi} \right) \right], \end{aligned}$$

for orthogonal curvilinear coordinates.

Another alternatives should be considered. An option to deal with a 2D convection-diffusion problem is the Alternating Direction Implicit (ADI) method. The ADI method is a splitting operator method where the variables are separately solved along each coordinate of the domain. Those kinds of schemes are used widespread in CFD techniques such as projection methods [75]. In a nutshell, given a 1D transport equation,

$$\mathrm{L}_x \phi \coloneqq a_x(x) \frac{\mathrm{d}\phi}{\mathrm{d}x} - b_x(x) \frac{\mathrm{d}^2 \phi}{\mathrm{d}x^2} = c(x),$$

the symbolic discrete equation can be written as follows:

$$\mathrm{A}_x \phi_i = \mathrm{B}_x c_i \quad \Longrightarrow \quad \mathrm{B}_x^{-1} \mathrm{A}_x \phi_i = c_i,$$

being A_x and B_x the finite differential operators of the discrete technique and $\mathrm{B}_x^{-1}\mathrm{A}_x$ the operator that mimics L_x. So, the approximation of a 2D transport equation,

$$\mathrm{L}_x \phi + \mathrm{L}_y \phi = c(x, y),$$

would be given by

$$\mathrm{B}_x^{-1} \mathrm{A}_x \phi_{ij} + \mathrm{B}_y^{-1} \mathrm{A}_y \phi_{ij} = c_{ij},$$

or cancelling out the inverses,

$$(\mathrm{B}_y\mathrm{A}_x + \mathrm{B}_x\mathrm{A}_y)\,\phi_{ij} = \mathrm{B}_x\mathrm{B}_y c_{ij},$$

if B_x and B_y commute, i.e. $[\mathrm{B}_x, \mathrm{B}_y] = \mathrm{B}_x\mathrm{B}_y - \mathrm{B}_y\mathrm{B}_x = 0$. The previous approach can achieve high-order accuracy and stability via some witty factorization of the operators, as many authors have shown [19, 36, 64, 95, 96, 234, 250], for both unsteady and steady problems. However, this procedure might not fulfil some basic properties in CFD, e.g., conservativeness.

As ENATE is basically a one-dimensional scheme, the operator splitting idea is very appealing. After the splitting ENATE can be applied to the particular equation along each coordinate. The difference with ADI is that the splitting is made over the original 2D differential equation and not over the algebraic relation.

The first strategy followed in this thesis is to move the derivatives along the other coordinate to the right-hand side as a new additional source [238]. Thus, the convection-diffusion problem in x-direction writes

$$\frac{\partial}{\partial x}\left(\rho u\phi - \Gamma\frac{\partial\phi}{\partial x}\right) = S - \frac{\partial \mathcal{F}_y}{\partial y} =: S_x, \qquad x_{lb} \le x \le x_{rb}, \tag{3.12a}$$

$$\phi(x_{lb}, y) = \phi_{lb}, \quad \phi(x_{rb}, y) = \phi_{rb}, \qquad y = \text{const.}, \tag{3.12b}$$

whereas in y-direction is

$$\frac{\partial}{\partial y}\left(\rho v\phi - \Gamma\frac{\partial\phi}{\partial y}\right) = S - \frac{\partial \mathcal{F}_x}{\partial x} =: S_y, \qquad y_{bb} \le y \le y_{tb}, \tag{3.13a}$$

$$\phi(x, y_{bb}) = \phi_{bb}, \quad \phi(x, y_{tb}) = \phi_{tb}, \qquad x = \text{const.} \tag{3.13b}$$

The subscripts bb and tb stand for bottom boundary and top boundary, respectively. Next, ENATE scheme is employed in both 1D equations. The horizontal and vertical intervals are shown in Figure 3.3. The two discretized equations are now summed up to provide the algebraic equation

$$A_C\phi_C - \sum_{i\in\mathcal{N}} A_i\phi_i = b_C, \tag{3.14}$$

being $\mathcal{N}$ the neighbour points: West, East, South and North. $\mathcal{N} = \mathcal{N}_x \cup \mathcal{N}_y$, $\mathcal{N}_x = \{W, E\}$ and $\mathcal{N}_y = \{S, N\}$. The influence coefficients are

$$A_C = A_{x\,C} + A_{y\,C}, \tag{3.15a}$$

$$A_{x\,C} = (\rho u)_W \widetilde{k}_{x\,WC} + (\rho u)_C \left(\widetilde{k}_{x\,CE} + \left.\frac{ILE_{x\,01}}{IGE_{x\,01}}\right|_{CE}\right), \tag{3.15b}$$

$$A_{y\,C} = (\rho v)_S \widetilde{k}_{y\,SC} + (\rho v)_C \left(\widetilde{k}_{y\,CN} + \left.\frac{ILE_{y\,01}}{IGE_{y\,01}}\right|_{CN}\right), \tag{3.15c}$$

$$A_W = (\rho u)_W \left(\widetilde{k}_{x\,WC} + \left.\frac{ILE_{x\,01}}{IGE_{x\,01}}\right|_{WC}\right), \tag{3.15d}$$

$$A_E = (\rho u)_C \widetilde{k}_{x\,CE}, \tag{3.15e}$$

$$A_S = (\rho v)_S \left(\widetilde{k}_{y\,SC} + \left.\frac{ILE_{y\,01}}{IGE_{y\,01}}\right|_{SC}\right), \tag{3.15f}$$

$$A_N = (\rho v)_C \widetilde{k}_{y\,CN}, \tag{3.15g}$$

and the discrete source is

$$b_C = b_{x\,C} + b_{y\,C}, \tag{3.16a}$$

$$b_{x\,C} = IS_{x\,01}|_{WC} + \left(\left.\frac{IS_xGE_{x\,01}}{IGE_{x\,01}}\right|_{CE} - \left.\frac{IS_xGE_{x\,01}}{IGE_{x\,01}}\right|_{WC} \right), \tag{3.16b}$$

$$b_{y\,C} = IS_{y\,01}|_{SC} + \left(\left.\frac{IS_yGE_{y\,01}}{IGE_{y\,01}}\right|_{CN} - \left.\frac{IS_yGE_{y\,01}}{IGE_{y\,01}}\right|_{SC} \right). \tag{3.16c}$$

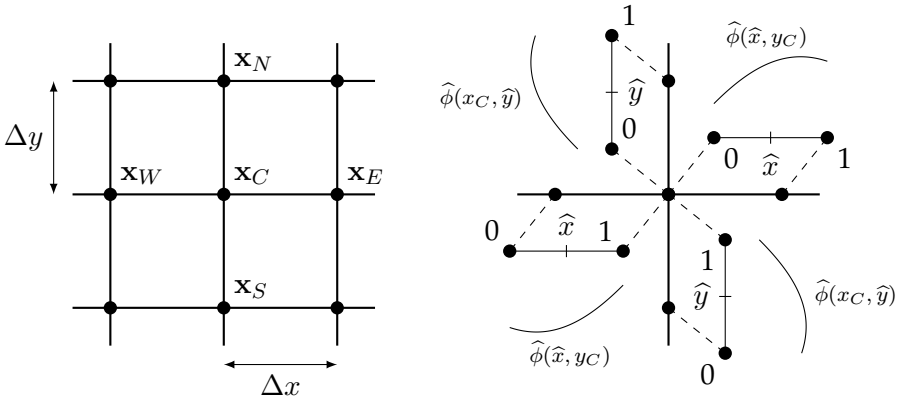

FIGURE 3.3: A five-point stencil in a structured mesh for two-dimensional ENATE. Nodes are located at $\mathbf{x}_C = (x_C, y_C)^T$, $\mathbf{x}_W = (x_W, y_C)^T$, $\mathbf{x}_E = (x_E, y_C)^T$, $\mathbf{x}_N = (x_C, y_N)^T$ and $\mathbf{x}_S = (x_C, y_S)^T$.

All these expressions are just extensions of the 1D formulation. If we define $\xi = x$ or $\xi = y$, $\rho u_x = \rho u$ and $\rho u_y = \rho v$, then the Péclet number and related integrals are

$$P_\xi = \frac{\rho u_\xi \Delta\xi}{\Gamma}, \quad P_{\xi\,0} = \frac{(\rho u_\xi)_0\,\Delta\xi}{\Gamma_0}, \quad \overline{P}_\xi = \int_0^1 P_\xi \,\mathrm{d}\widehat{\xi}, \tag{3.17a}$$

$$\overline{E}_\xi = \exp\left(-\overline{P}_\xi(1-\widehat{\xi})\right) \exp\left(\int_0^{\widehat{\xi}} \left(P_\xi - \overline{P}_\xi\right) \mathrm{d}\widehat{\xi}' \right), \tag{3.17b}$$

$$ILE_{\xi\,01} = \frac{\exp \overline{P}_\xi - 1}{P_{\xi\,0}}, \quad IGE_{\xi\,01} = \int_0^1 \frac{\mathrm{d}\widehat{\xi}}{\widehat{\Gamma}\overline{E}_\xi}, \quad \widetilde{k}_\xi = \frac{1}{P_{\xi\,0} IGE_{\xi\,01}}, \tag{3.17c}$$

$$IS_{\xi\,01} = \Delta\xi \int_0^1 S_\xi \,\mathrm{d}\widehat{\xi}, \quad IS_\xi GE_{\xi\,01} = \int_0^1 \frac{\Delta\xi}{\widehat{\Gamma}\overline{E}_\xi} \left[\int_0^{\widehat{\xi}} S_\xi \,\mathrm{d}\widehat{\xi}' \right] \mathrm{d}\widehat{\xi}. \tag{3.17d}$$

In section *Numerical Examples* this approach will be named as "**F**luxes **a**s **P**seudo-sources", FaP. Regarding the CFD properties, the extension to 2D contains the same features as the 1D counterpart. The discrete equation (3.14) keeps *transportiveness*, that is, in a diffusive problem ϕ_C links with $\{\phi_W, \phi_E, \phi_S, \phi_N\}$, whereas in convective processes ϕ_C links with ϕ_W and ϕ_S if $\rho u, \rho v > 0$. On the other hand, all influence coefficients are positive providing a diagonally dominant matrix in most cases, which makes ENATE a *bounded* scheme. If the flux balance is done over horizontal lines,

$y = \text{const.}$,

$$\mathcal{F}_{x\,C} - \mathcal{F}_{x\,W} = \int_{x_W}^{x_C} S_x \,\mathrm{d}x,$$
$$\int_{x_W}^{x_C} \frac{\partial \mathcal{F}_x}{\partial x}\mathrm{d}x = \int_{x_W}^{x_C} \left(S - \frac{\partial \mathcal{F}_y}{\partial y} \right) \mathrm{d}x,$$
$$\int_{x_W}^{x_C} \left(\frac{\partial \mathcal{F}_x}{\partial x} + \frac{\partial \mathcal{F}_y}{\partial y} - S \right) \mathrm{d}x = 0,$$

and vertical lines, $x = \text{const.}$,

$$\mathcal{F}_{y\,C} - \mathcal{F}_{y\,S} = \int_{y_S}^{y_C} S_y \,\mathrm{d}y,$$
$$\int_{y_S}^{y_C} \frac{\partial \mathcal{F}_y}{\partial y}\mathrm{d}y = \int_{y_S}^{y_C} \left(S - \frac{\partial \mathcal{F}_x}{\partial x} \right) \mathrm{d}y,$$
$$\int_{y_S}^{y_C} \left(\frac{\partial \mathcal{F}_x}{\partial x} + \frac{\partial \mathcal{F}_y}{\partial y} - S \right) \mathrm{d}y = 0,$$

ENATE recovers the conservation law in each direction of the problem, so *conservativeness* is ensured. That was the point in setting $\partial \mathcal{F}_{\{x,y\}}/\partial\{x,y\}$ in the source, to ensure this basic property. The numerical treatment of this derivative and its integral is crucial for determining the order of the scheme.

Finally, a mention of the solver of the matrix is needed. Now the matrix of the scheme $\mathbf{A}$ contains elements far off the diagonal, so the tridiagonal algorithm cannot be used.

$$\mathbf{A} = \begin{pmatrix}
\circ & \circ & & \circ & & & & & \\
\circ & \circ & \circ & & \circ & & & & \\
 & \circ & \circ & & & \circ & & & \\
\circ & & & \circ & \circ & & \circ & & \\
 & \circ & & \circ & \circ & \circ & & \circ & \\
 & & \circ & & \circ & \circ & & & \circ \\
 & & & \circ & & & \circ & \circ & \\
 & & & & \circ & & \circ & \circ & \circ \\
 & & & & & \circ & & \circ & \circ
\end{pmatrix}.$$

The algorithm employed in this thesis for two-dimensional problems solves a tridiagonal system sweeping from south to north of the domain taking the old (previous level) values of neighbour lines as a source-like term. Since it is not known which boundary is important and how they spread the information in a convection-diffusion problem, another sweep from north to south is done, see Patankar [150, p. 64]. For lines of y constant,

$$-A_W\phi_W + A_C\phi_C - A_E\phi_E = A_S\phi_S^{\text{old}} + A_N\phi_N^{\text{old}} + b_C,$$

and in the other direction,

$$-A_S\phi_S + A_C\phi_C - A_N\phi_N = A_W\phi_W^{\text{old}} + A_E\phi_E^{\text{old}} + b_C,$$

it sweeps from left to right and then from right to left. In a convection-dominant problem, only one sweep is required in the direction of convection. A TDMA will be applied in each case, see Figure 3.4.

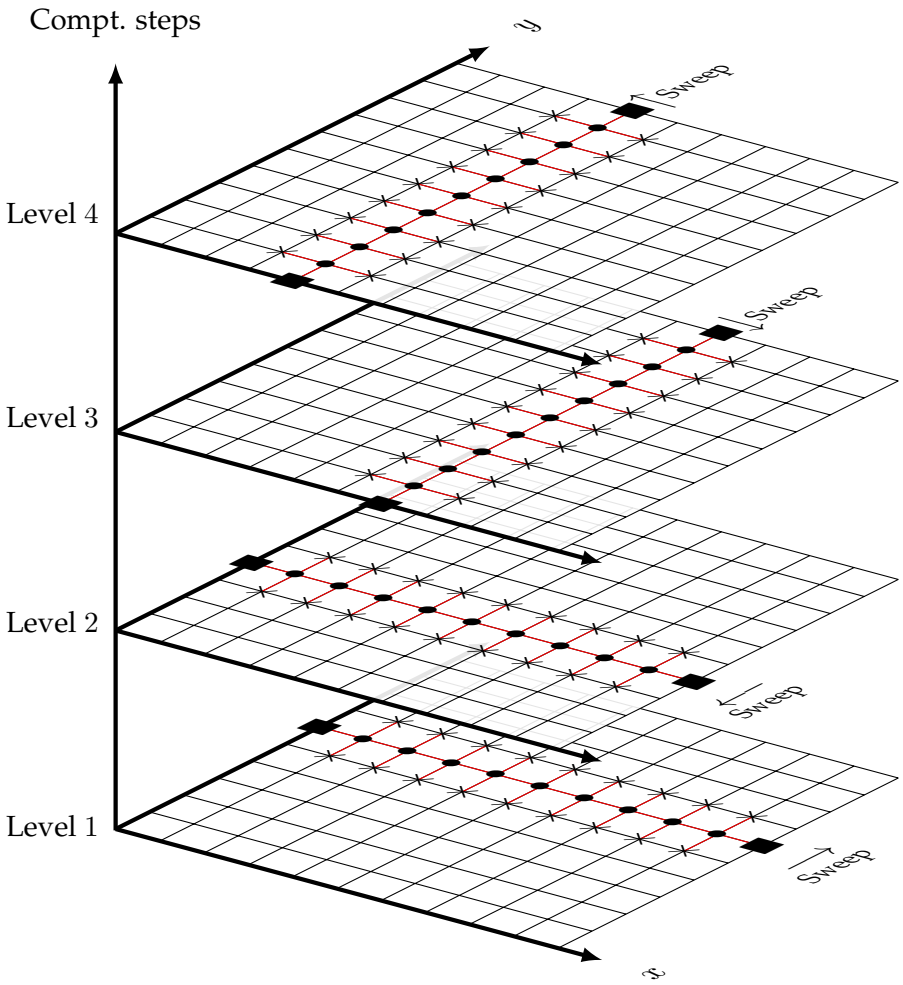

FIGURE 3.4: Iterative process to solve the discrete equation by a line-by-line TDMA. Symbols: •, points where the Thomas algorithm calculates; ■, boundary value points; ×, points whose contribution is considered as source.

3.3.1 Additional sources and start-off of the method

Hermite polynomials are used again as the method for the interpolation of the integrals, further information is in Section 2.3 and Appendix B. These integrals contain non-analytical sources as in

$$\begin{aligned} IS_{x\,01} &= \Delta x \int_0^1 S_x \,\mathrm{d}\widehat{x}, \\ &= \Delta x \int_0^1 S \,\mathrm{d}\widehat{x} - \Delta x \int_0^1 \left(\frac{\partial \mathcal{F}_y}{\partial y}\right)^{\text{old}} \mathrm{d}\widehat{x}, \end{aligned}$$

and

$$\begin{aligned} IS_x GE_{x\,01} &= \int_0^1 \frac{\Delta x}{\widehat{\Gamma}\overline{E}_x} \left[\int_0^{\widehat{x}} S_x \,\mathrm{d}\widehat{x}'\right] \mathrm{d}\widehat{x}, \\ &= \int_0^1 \frac{\Delta x}{\widehat{\Gamma}\overline{E}_x} \left[\int_0^{\widehat{x}} S \,\mathrm{d}\widehat{x}'\right] \mathrm{d}\widehat{x} - \int_0^1 \frac{\Delta x}{\widehat{\Gamma}\overline{E}_x} \left[\int_0^{\widehat{x}} \left(\frac{\partial \mathcal{F}_y}{\partial y}\right)^{\text{old}} \mathrm{d}\widehat{x}'\right] \mathrm{d}\widehat{x}, \end{aligned}$$

which should be calculated accurately. With Hermite, the knowledge of the integrand and its derivatives at mesh points are required. Neither $\partial\phi/\partial\{x,y\}$ nor $\partial\mathcal{F}_{\{x,y\}}/\partial\{x,y\}$, nor their derivatives, are directly available at the start of the numerical procedure. To estimate those derivatives at each point and in each direction, ENATE applies the "**C**entral **C**ompact **S**cheme", CCS, originally proposed by Lele [108], although other authors had proposed similar schemes earlier [31, 159, 180].

Let us consider a generic coordinate ξ and a function $f = f(\xi, \eta = \text{const.})$ that could be either ϕ or $\mathcal{F}_{\{x,y\}}$. A compact differentiation scheme consists of a linear combination of first derivatives and values at nodes, i.e.

$$\sum_{k=-m_1}^{m_2} \alpha_k \left.\frac{\partial f}{\partial \xi}\right|_{i+k} = \frac{1}{\Delta\xi} \sum_{k=-q_1}^{q_2} a_k f_{i+k} + \tau_i.$$

The relations between the coefficients $\{a_k\}$ and $\{\alpha_k\}$ are derived by matching the Taylor series coefficients of $\partial f/\partial\xi|_{i+k}$ and f_{i+k} to the desired order. The first unmatched coefficient determines the local truncation error, τ_i. Notice that the previous scheme is valid at inner and boundary points. If we want a left-boundary scheme, for instance, we set $m_1 = q_1 = 0$ and $i = 0$. The stencil sizes of left- and right-hand side are $1+m_1+m_2$, $m_{1,2} \in \mathbb{N}_0$, and $1 + q_1 + q_2$, $q_{1,2} \in \mathbb{N}_0$, respectively. Hence, a compact scheme ends up by solving the system

$$\mathbf{M}\frac{\partial \mathbf{f}}{\partial \xi} = \frac{1}{\Delta\xi}\mathbf{Q}\mathbf{f} + \boldsymbol{\tau}, \tag{3.18}$$

where $\mathbf{M}, \mathbf{Q} \in \mathbb{R}^{(n+1)\times(n+1)}$ are banded matrices and

$$\mathbf{f} \coloneqq (f_0, \ldots, f_{i-q_1}, \ldots, f_{i+q_2}, \ldots, f_n)^T, \tag{3.19a}$$

$$\frac{\partial \mathbf{f}}{\partial \xi} \coloneqq \left(\left.\frac{\partial f}{\partial \xi}\right|_0, \ldots, \left.\frac{\partial f}{\partial \xi}\right|_{i-m_1}, \ldots, \left.\frac{\partial f}{\partial \xi}\right|_{i+m_1}, \ldots, \left.\frac{\partial f}{\partial \xi}\right|_n\right)^T, \tag{3.19b}$$

are the discrete vectors of the scheme in $\mathbb{R}^{n+1}$, with $\boldsymbol{\tau}$ the error vector. Lele's

CCS assume that $m_1 = m_2$ and $q_1 = q_2$. In this thesis a $4th$ order CCS has been employed, where

$$\mathbf{M} \coloneqq \begin{pmatrix} 1 & 3 & & & \\ 1/4 & 1 & 1/4 & & \\ & \ddots & \ddots & \ddots & \\ & & 1/4 & 1 & 1/4 \\ & & & 3 & 1 \end{pmatrix},$$

$$\mathbf{Q} \coloneqq \begin{pmatrix} -17/6 & 3/2 & 3/2 & -1/6 & \\ -3/4 & 0 & 3/4 & & \\ & \ddots & \ddots & \ddots & \\ & & -3/4 & 0 & 3/4 \\ & 1/6 & -3/2 & -3/2 & 17/6 \end{pmatrix},$$

and a $6th$ order CCS

$$\mathbf{M} \coloneqq \begin{pmatrix} 1 & 5 & & & & & \\ 1/8 & 1 & 3/4 & & & & \\ & 1/3 & 1 & 1/3 & & & \\ & & \ddots & \ddots & \ddots & & \\ & & & 1/3 & 1 & 1/3 & \\ & & & & 3/4 & 1 & 1/8 \\ & & & & & 5 & 1 \end{pmatrix},$$

$$\mathbf{Q} \coloneqq \begin{pmatrix} -197/60 & -5/12 & 5 & -5/3 & 5/12 & -1/20 & \\ -43/96 & -5/6 & 9/8 & 1/6 & -1/96 & & \\ -1/36 & -7/9 & 0 & 7/9 & 1/36 & & \\ & \ddots & \ddots & \ddots & \ddots & \ddots & \\ & & -1/36 & -7/9 & 0 & 7/9 & 1/36 \\ & & 1/96 & -1/6 & -9/8 & 5/6 & 43/96 \\ & 1/20 & -5/12 & 5/3 & -5 & 5/12 & 197/60 \end{pmatrix}.$$

A complete analysis of those schemes can be found in [220], and different configurations of the stencils in [51, 115, 116], among others. Just to show the numerical behaviour of system (3.18) CCS is compared with an upwind and an explicit central scheme for a case where $f = \xi + 0.5 + 0.02 \ln(2\cosh(50(\xi - 0.5)))$ and $\partial f/\partial \xi = 1 + \tanh(50(\xi - 0.5))$, Figure 3.5. Although the elapsed CPU time in CCS is twice the time of upwind or central, CCS fits better the derivative around $\xi = 0.5$.

In order to calculate $\partial\phi/\partial\{x, y\}$, the process just sweeps in both directions, see Figure 3.6, solving tridiagonal systems with TDMA. What about $\partial\mathcal{F}_{\{x,y\}}/\partial\{x, y\}$? Is it better to calculate them in a non-conservative form requiring a second-derivative CCS for $\partial^2\phi/\partial\{x, y\}^2$, or in a conservative form applying twice the system (3.18)? As Visbal and Gaitonde [230] showed, there are hardly any numerical differences in both treatments, and the conservative form is very efficient. Furthermore, a CCS for $\partial^2\phi/\partial\{x, y\}^2$ needs a spatial filtering that damps the smallest wave length of the solution because it does not provide good numerical stability by itself [230]. So, in this thesis the system (3.18) will be applied in each direction as many times as required by the derivative order.

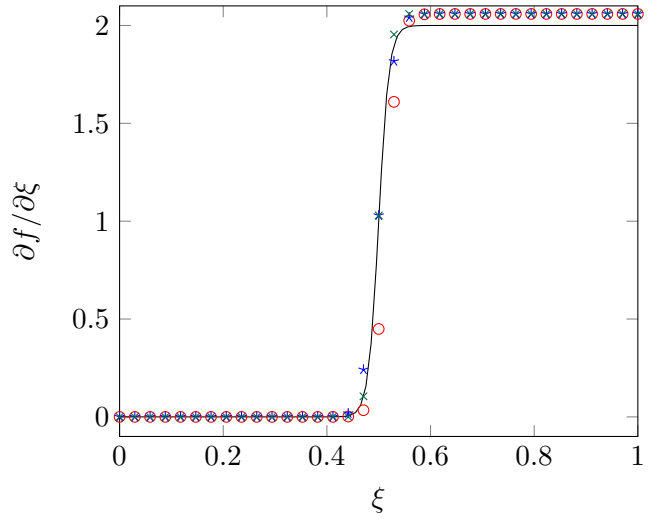

FIGURE 3.5: Numerical example for the calculation of $\partial f/\partial\xi$. Solid line, exact derivative. Red circle, Upwind. Blue star, Central. Green cross, fourth-order CCS.

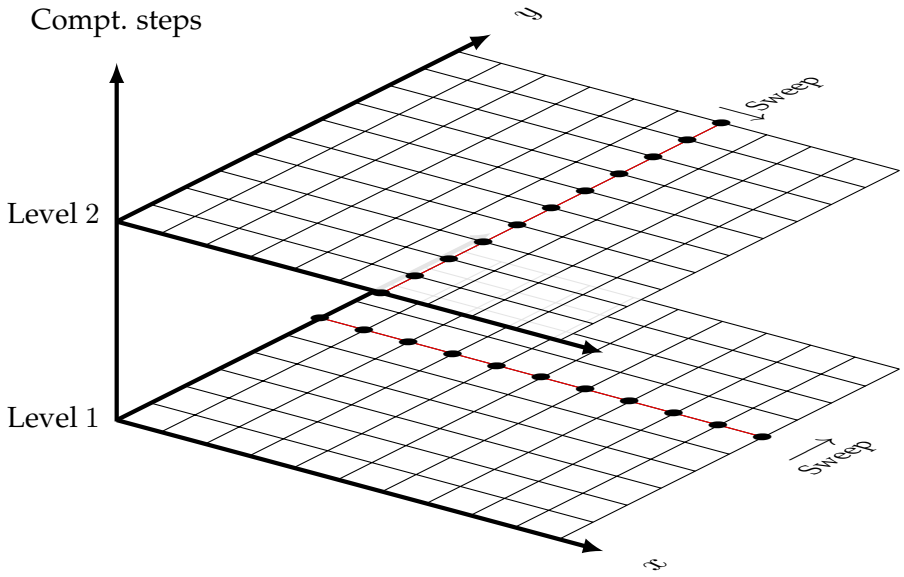

FIGURE 3.6: Iterative process for calculating derivatives. Symbol: •, points where TDMA calculates. In level 1 derivative with respect to x is solved; level 2, derivative with respect to y.

The iterative sequence to calculate the pseudo-sources in both directions is summarized below:

1. Calculate ϕ with the algebraic equation (3.14) setting $S_{\{x,y\}} = S$,
2. Calculate $\partial\phi/\partial\{x,y\}$ with CCS and then $\mathcal{F}_{\{x,y\}}$. In convection-only problems this step is not needed,
3. Calculate $\partial\mathcal{F}_{\{x,y\}}/\partial\{x,y\}$ with CCS and then $S_{(x,y)} = S - \partial\mathcal{F}_{\{y,x\}}/\partial\{y,x\}$,

4. Apply CCS to $S_{\{x,y\}}$ to obtain as many derivatives as required by the polynomial order of the interpolant,
5. Calculate b_C (3.16) by computing the integrals with Hermite polynomials,
6. Update ϕ solving the equation (3.14),
7. Back to second step until convergence.

3.3.2 Numerical diffusion

A key point in the use of high-order methods lies in the fact that they can reduce the numerical dissipation caused by discretization errors. Within this category the second-order upwind, SUDS [172], QUICK [109], MUSCL [222], SHARP [110], SMART [62] are widely used, among others. An analytical way to calculate these errors is via the modified equation. Let us start with the basic transport equation

$$\frac{\partial\left(\rho u\phi\right)}{\partial x}+\frac{\partial\left(\rho v\phi\right)}{\partial y}=0, \tag{3.20}$$

being ρu and ρv functions of x and y that meet mass conservation, i.e. $\partial\rho u/\partial x+\partial\rho v/\partial y=0$. The ENATE scheme will discretize this PDE as

$$\begin{aligned}\left(\rho u+\rho v\right)_C\phi_C=&\left(\rho u\right)_W\phi_W+\left(\rho v\right)_S\phi_S\\&-\int_{x_W}^{x_C}\left(\frac{\partial\left(\rho v\phi\right)}{\partial y}\right)^{\text{old}}\mathrm{d}x-\int_{y_S}^{y_C}\left(\frac{\partial\left(\rho u\phi\right)}{\partial x}\right)^{\text{old}}\mathrm{d}y.\end{aligned} \tag{3.21}$$

Omitting the superscript old, the previous equation can be rearranged with the definition of the flux, i.e $\mathcal{F}_x=\rho u\phi$ and $\mathcal{F}_y=\rho v\phi$, as follows:

$$\mathcal{F}_{x\,C}+\mathcal{F}_{y\,C}=\mathcal{F}_{x\,W}+\mathcal{F}_{y\,S}-\int_{x_W}^{x_C}\frac{\partial\mathcal{F}_y}{\partial y}\mathrm{d}x-\int_{y_S}^{y_C}\frac{\partial\mathcal{F}_x}{\partial x}\mathrm{d}y. \tag{3.22}$$

Taking into account the location of nodes in Figure 3.3, the Taylor series for the fluxes at west and south about the central node are

$$\mathcal{F}_{x\,W}=\mathcal{F}_{x\,C}-\Delta x\left.\frac{\partial\mathcal{F}_x}{\partial x}\right|_C+\frac{\Delta x^2}{2!}\left.\frac{\partial^2\mathcal{F}_x}{\partial x^2}\right|_C+\mathcal{O}(\Delta x^3), \tag{3.23}$$

$$\mathcal{F}_{x\,S}=\mathcal{F}_{x\,C}-\Delta y\left.\frac{\partial\mathcal{F}_y}{\partial y}\right|_C+\frac{\Delta y^2}{2!}\left.\frac{\partial^2\mathcal{F}_y}{\partial y^2}\right|_C+\mathcal{O}(\Delta y^3). \tag{3.24}$$

Also, the integrals of the fluxes are evaluated in Taylor expansions over the intervals as

$$\int_{y_S}^{y_C}\frac{\partial\mathcal{F}_x}{\partial x}\mathrm{d}y=\Delta y\left.\frac{\partial\mathcal{F}_x}{\partial x}\right|_C-\frac{\Delta y^2}{2!}\left.\frac{\partial^2\mathcal{F}_x}{\partial x\partial y}\right|_C+\mathcal{O}(\Delta y^3),$$

$$\int_{x_W}^{x_C}\frac{\partial\mathcal{F}_y}{\partial y}\mathrm{d}x=\Delta x\left.\frac{\partial\mathcal{F}_y}{\partial y}\right|_C-\frac{\Delta x^2}{2!}\left.\frac{\partial^2\mathcal{F}_y}{\partial x\partial y}\right|_C+\mathcal{O}(\Delta x^3).$$

In the following subscript C is removed. Plugging those Taylor expansions in the discrete equation and using the mass conservation, the modified equation is given by

$$\frac{\partial(\rho u\phi)}{\partial x}+\frac{\partial(\rho v\phi)}{\partial y}=\frac{\partial}{\partial x}\left(\frac{\rho u\Delta x}{2(1+r_a)}\frac{\partial\phi}{\partial x}+\frac{\rho v\Delta x}{2(1+r_a)}\frac{\partial\phi}{\partial y}\right)+\frac{\partial}{\partial y}\left(\frac{\rho v\Delta y\, r_a}{2(1+r_a)}\frac{\partial\phi}{\partial y}+\frac{\rho u\Delta y\, r_a}{2(1+r_a)}\frac{\partial\phi}{\partial x}\right)+HOT,$$

being $r_a \coloneqq \Delta y/\Delta x$ the aspect ratio of the mesh. The right-hand side of the equation contains the leading error terms and show that the ENATE scheme is essentially dissipative in nature. Higher-order terms (HOT) are collected in the next compact formula:

$$HOT=\sum_{k=3}^{\infty}\frac{(-1)^k}{k!}\left(\Delta x^{k-1}\frac{1}{1+r_a}\left(\frac{\partial^k\mathcal{F}_x}{\partial x^k}+\frac{\partial^k\mathcal{F}_y}{\partial x^{k-1}\partial y}\right)+\Delta y^{k-1}\frac{r_a}{1+r_a}\left(\frac{\partial^k\mathcal{F}_x}{\partial x\partial y^{k-1}}+\frac{\partial^k\mathcal{F}_y}{\partial y^k}\right)\right).$$

Neglecting those terms, the equation that the scheme is actually solving in vectorial form reads

$$\nabla\cdot(\rho\mathbf{u}\phi-\mathbf{\Gamma}_{\mathrm{N}}\nabla\phi)\simeq 0, \tag{3.25}$$

where

$$\mathbf{\Gamma}_{\mathrm{N}}=\begin{pmatrix}\Gamma_{\mathrm{N}xx} & \Gamma_{\mathrm{N}xy}\\ \Gamma_{\mathrm{N}yx} & \Gamma_{\mathrm{N}yy}\end{pmatrix}\coloneqq\begin{pmatrix}\frac{\rho u\Delta x}{2(1+r_a)} & \frac{\rho v\Delta x}{2(1+r_a)}\\ \frac{\rho u\Delta y\, r_a}{2(1+r_a)} & \frac{\rho v\Delta y\, r_a}{2(1+r_a)}\end{pmatrix}, \tag{3.26}$$

is the 2×2 numerical diffusion tensor. This tensor and the local flux vector, $-\mathbf{\Gamma}_{\mathrm{N}}\nabla\phi$, have an analogy in heat conduction in anisotropic media. Carslaw and Jaeger [25] considered two measurable thermal conductivities to construct the conductivity tensor what causes the normal of an isothermal not to be necessarily parallel to the local heat flux. From this analogy, de Vahl Davies and Mallinson [41] calculated an approximate expression for the numerical diffusion of the upwind scheme. Later, Hwang [88] applied it for higher-order exponential schemes or any generic thirteen-point stencil scheme.

Let us analyze the previous tensor considering that $\Gamma_{\mathrm{N}xy}\neq\Gamma_{\mathrm{N}yx}$. The diagonalization of $\mathbf{\Gamma}_{\mathrm{N}}$ gives the set of eigenvalues, called *principal numerical diffusivities*,

$$\Gamma_{\mathrm{N}1,2}=\frac{1}{2}\left[\mathrm{tr}(\mathbf{\Gamma}_{\mathrm{N}})\pm\sqrt{\mathrm{tr}(\mathbf{\Gamma}_{\mathrm{N}})^2-4\det(\mathbf{\Gamma}_{\mathrm{N}})}\right],$$

where $\mathrm{tr}(\mathbf{\Gamma}_{\mathrm{N}})$ and $\det(\mathbf{\Gamma}_{\mathrm{N}})$ are the trace and the determinant of (3.26) respectively. $\Gamma_{\mathrm{N}1}$ is chosen with the positive sign. The eigenvectors,

$$\mathbf{v}_{\mathrm{N}1,2}=\left(\frac{\Gamma_{\mathrm{N}1,2}-\Gamma_{\mathrm{N}yy}}{\Gamma_{\mathrm{N}yx}},1\right)^T,$$

allows to make up the basis for the *principal axis of numerical diffusion* $x_{\mathrm{N}1}$ and $x_{\mathrm{N}2}$. Since the tensor is non-symmetric, the eigenvectors are nonorthogonal. The angle between each other is

$$\cos\gamma = \frac{\mathbf{v}_{\mathrm{N}1}\cdot\mathbf{v}_{\mathrm{N}2}}{|\mathbf{v}_{\mathrm{N}1}||\mathbf{v}_{\mathrm{N}2}|} = \frac{\Gamma_{\mathrm{N}yx}(\Gamma_{\mathrm{N}yx}-\Gamma_{\mathrm{N}xy})}{\sqrt{\left[(\Gamma_{\mathrm{N}1}-\Gamma_{\mathrm{N}yy})^2+\Gamma_{\mathrm{N}yx}^2\right]\left[(\Gamma_{\mathrm{N}2}-\Gamma_{\mathrm{N}yy})^2+\Gamma_{\mathrm{N}yx}^2\right]}}.$$

The angle between the principal axis x_1 and the x-axis is

$$\cos\Theta = \frac{\mathbf{v}_{\mathrm{N}1}\cdot\mathbf{e}_x}{|\mathbf{v}_{\mathrm{N}1}||\mathbf{e}_x|} = \frac{\Gamma_{\mathrm{N}1}-\Gamma_{\mathrm{N}yy}}{\sqrt{(\Gamma_{\mathrm{N}1}-\Gamma_{\mathrm{N}yy})^2+\Gamma_{\mathrm{N}yx}^2}}.$$

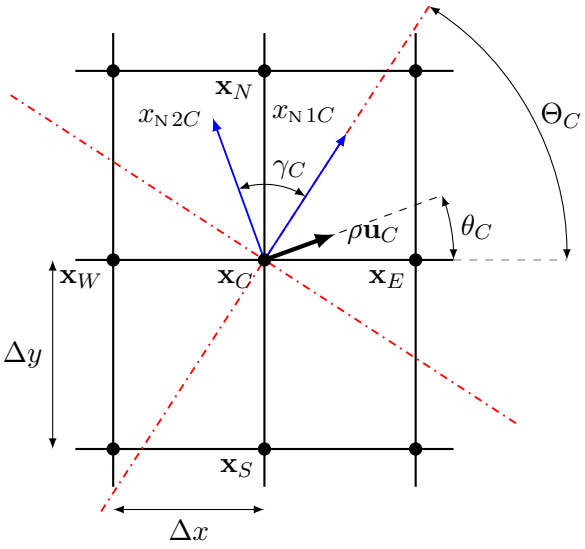

FIGURE 3.7: Representation of the principal axis at Central point. One red line is a direction free of numerical diffusion when the local velocity vector is pointing in the other red line.

For the cross-flux approach, $\Gamma_{\mathrm{N}xy} = \Gamma_{\mathrm{N}yy}/r_a^2$ and $\Gamma_{\mathrm{N}yx} = \Gamma_{\mathrm{N}xx}r_a^2$. So, the principal numerical diffusivities are

$$\Gamma_{\mathrm{N}1} = |\rho\mathbf{u}|\frac{\cos\theta\Delta x + \sin\theta\Delta y r_a}{2(1+r_a)}, \quad \Gamma_{\mathrm{N}2} = 0,$$

where θ is the angle between the convection vector and the x-axis. The principal basis become

$$\mathbf{e}_{\mathrm{N}1} = \frac{\mathbf{v}_{\mathrm{N}1}}{|\mathbf{v}_{\mathrm{N}1}|} = \left(\frac{1}{\sqrt{1+r_a^4}}, \frac{r_a^2}{\sqrt{1+r_a^4}}\right)^T, \quad \mathbf{e}_{\mathrm{N}2} = \frac{\mathbf{v}_{\mathrm{N}2}}{|\mathbf{v}_{\mathrm{N}2}|} = (-\sin\theta, \cos\theta)^T,$$

and the angles are

$$\cos\gamma = \frac{r_a^2\cos\theta - \sin\theta}{\sqrt{1+r_a^4}}, \quad \cos\Theta = \frac{1}{\sqrt{1+r_a^4}}.$$

From those results, the principal numerical diffusivity $\Gamma_{\mathrm{N}2}$ in the direction

of $\mathbf{e}_{\mathrm{N}\,2}$ is zero. Another consequence, $\mathbf{e}_{\mathrm{N}\,2}$ is perpendicular to the local velocity vector and, therefore, $\Theta + \gamma = \theta + \pi/2$, see Figure 3.7. As for the principal numerical diffusivity $\Gamma_{\mathrm{N}\,1}$ is zero when $\tan\theta = -r_a^{-2}$ ($\cos\gamma = 1$) and maxima when $\tan\theta = r_a^2$ ($\cos\gamma = 0$) with a value of

$$\Gamma_{\mathrm{N}\,1\,\mathrm{max}} = \frac{|\rho\mathbf{u}|\sqrt{\Delta x \Delta y}}{2} \frac{1}{\sqrt{r_a(1+r_a^4)}}.$$

Hence, when the velocity vector is either perpendicular or parallel to $\mathbf{e}_{\mathrm{N}\,1}$, the numerical diffusion normal to the convection direction would disappear. On the other hand, the diffusivity in x direction, $\Gamma_{\mathrm{N}\,1}(\theta = 0)$, and in y direction, $\Gamma_{\mathrm{N}\,1}(\theta = \pi/2)$, are less than that of the upwind scheme, $\Gamma_{\mathrm{N}\,x\,\mathrm{upwind}} = \rho u \Delta x/2$ and $\Gamma_{\mathrm{N}\,y\,\mathrm{upwind}} = \rho v \Delta y/2$, see Figure 3.8. In fact, in a uniform mesh ($r_a = 1$) the numerical diffusion is half of that of upwind scheme.

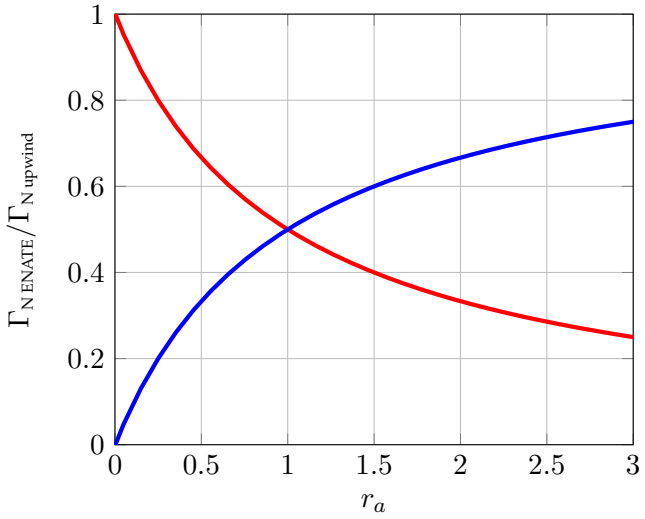

FIGURE 3.8: Normalized numerical diffusion for ENATE with the cross-flux approach in x direction (red line) and y direction (blue line).

3.4 Redistribution coefficient approach

In the approach just shown the discretization is applied independently to each coordinate and the computation is carried out sequentially one coordinate after another with an extra-source. However, one drawback that the cross-flux approach might have is the significant increase in the computational time due to the number of side calculations in the discrete source and consequent slowness of convergence. Bear in mind that the TDMA algorithm requires $\mathcal{O}(N_{\mathrm{nodes}})$ operations, and looking at Table 3.1 each sweep consists of N_{lines} solved by TDMA. Do not forget that the number of sweeps in the matrix solver is optional and one could take more sweeps than one if numerical instabilities occur around boundaries. To reduce the computational burden and speed up the convergence, another approach to reduce the extra calculations will be put forward in this section.

Hermite	Compute		Matrix solver(minimum)	Total
	$\partial\mathcal{F}_{\{x,y\}}/\partial\{x,y\}$	$\partial^{a+b}S_{\{x,y\}}/\partial x^a\partial y^b$		
Cubic	4	2	4	10
Quintic	4	4	4	12
Septic	4	6	4	14

TABLE 3.1: Total number of sweeps for each interpolation spline of Hermite.

Let us consider the next coordinate splitting,

$$\frac{\partial}{\partial x}\left(\rho u\phi - \Gamma\frac{\partial\phi}{\partial x}\right) = \frac{1}{2}S + \beta, \tag{3.27a}$$

$$\frac{\partial}{\partial y}\left(\rho v\phi - \Gamma\frac{\partial\phi}{\partial y}\right) = \frac{1}{2}S - \beta. \tag{3.27b}$$

This idea was put forward by Lee and Kim [107] where it was named as *axial splitting*. Instead of the pseudo-sources, this alternative introduces a scalar field, named $\beta = \beta(x,y)$, that represents the extra source to be redistributed between coordinates with respect to an equally distributed source. The solution of the set (3.27) will also be solution of the original convection-diffusion problem (3.10). The nature of β is unknown. On dividing eqn.(3.27a) by eqn.(3.27b) we can get with a bit of algebra the ratio between β and S,

$$\frac{\beta}{S} = \frac{1}{2} - \frac{r_f}{1+r_f}, \quad r_f := \frac{\partial\mathcal{F}_y/\partial y}{\partial\mathcal{F}_x/\partial x}, \tag{3.28}$$

the field β is bounded by the source when $r_f \geq 0$.

Remark. *If* $\mathrm{sgn}(\partial\mathcal{F}_x/\partial x) = \mathrm{sgn}(\partial\mathcal{F}_y/\partial y)$, *then* $-1/2 \leq \beta/S \leq 1/2$.

However, no more information about this ratio can be extracted. β does not have a PDE of its own. It will also form part of the iterative process to find ϕ.

Consider that in an iteration the scalar field is $\beta^\star$. If $\beta^\star$ is not the correct β the solution of both equations will be different. Defining $\phi_1^\star$ and $\phi_2^\star$ as the solution of ϕ in both directions, these solutions are ruled by the following ODEs:

$$\frac{\partial}{\partial x}\left(\rho u\phi_1^\star - \Gamma\frac{\partial\phi_1^\star}{\partial x}\right) = \frac{1}{2}S + \beta^\star =: S_x, \tag{3.29a}$$

$$\frac{\partial}{\partial y}\left(\rho v\phi_2^\star - \Gamma\frac{\partial\phi_2^\star}{\partial y}\right) = \frac{1}{2}S - \beta^\star =: S_y, \tag{3.29b}$$

along y-constant and x-constant lines, respectively, as many as those employed to mesh the 2D domain. The purpose is to reach the solution given in equations (3.27) via successive iterations. Defining the differences between the current values and the correct ones as

$$\Delta\beta^\star := \beta - \beta^\star, \quad \Delta\phi_1^\star := \phi - \phi_1^\star, \quad \Delta\phi_2^\star := \phi - \phi_2^\star,$$

the equations for the increments, eqns.(3.27) − eqns.(3.29), are

$$\frac{\partial}{\partial x}\left(\rho u\Delta\phi_1^\star - \Gamma\frac{\partial\Delta\phi_1^\star}{\partial x}\right) = \Delta\beta^\star, \tag{3.30a}$$

$$\frac{\partial}{\partial y}\left(\rho v\Delta\phi_2^\star - \Gamma\frac{\partial\Delta\phi_2^\star}{\partial y}\right) = -\Delta\beta^\star, \tag{3.30b}$$

provided that S and Γ are independent of ϕ. On page 96, the case when S depends on ϕ will be developed. Since the final solutions should be common to both equations upon convergence, i.e., $\phi = \phi_1^\star + \Delta\phi_1^\star = \phi_2^\star + \Delta\phi_2^\star$, both increments are linked, that is, $\Delta\phi_1^\star = \Delta\phi_2^\star - (\phi_1^\star - \phi_2^\star)$. The two equations for $\Delta\phi_2^\star$ are given by

$$\frac{\partial}{\partial x}\left(\rho u\Delta\phi_2^\star - \Gamma\frac{\partial\Delta\phi_2^\star}{\partial x}\right) = \Delta\beta^\star + \frac{\partial\mathcal{F}^\star_{x(1-2)}}{\partial x}, \tag{3.31a}$$

$$\frac{\partial}{\partial y}\left(\rho v\Delta\phi_2^\star - \Gamma\frac{\partial\Delta\phi_2^\star}{\partial y}\right) = -\Delta\beta^\star. \tag{3.31b}$$

where

$$\mathcal{F}^\star_{x(1-2)} = \rho u(\phi_1^\star - \phi_2^\star) - \Gamma\frac{\partial(\phi_1^\star - \phi_2^\star)}{\partial x},$$

can be interpreted as a numerical flux in x-direction due to the differences in the solution for both coordinates. Note that if we knew the correct $\Delta\beta^\star$ both equations would give the same answer at a generic node x_C.

How do we numerically solve the previous equations without affecting the order of convergence? The discretization of equations (3.29) controls the accuracy of the method and the good or bad resolution of $\Delta\beta^\star$ and $\Delta\phi_2^\star$ is not crucial as long as the final solution is $\phi_1^\star = \phi_2^\star$. These are computed with the discrete equations in one-dimensional modelling, from eqn.(2.30) to eqn.(2.32) on page 32, substituting ρu or ρv in the influence coefficients and $S/2 + \beta^\star$ or $S/2 - \beta^\star$ in the source integrals as appropriate. On the other hand, the set (3.31) looks similar to (3.12a) − (3.13a) and, therefore, its two-dimensional discrete equation is

$$\begin{aligned} A_C\Delta\phi^\star_{2\,C} - \sum_{i\in\mathcal{N}} A_i\Delta\phi^\star_{2\,i} = b_C &+ A_{x\,C}(\phi^\star_{1\,C} - \phi^\star_{2\,C}) \\ &- A_W(\phi^\star_{1\,W} - \phi^\star_{2\,W}) \\ &- A_E(\phi^\star_{1\,E} - \phi^\star_{2\,E}), \end{aligned} \tag{3.32}$$

where the As are the same as the coefficients (3.15) and the b_C term is (3.16) setting $S_x = \Delta\beta^\star$ and $S_y = -\Delta\beta^\star$, i.e.

$$\begin{aligned} b_C = \Delta x\int_0^1 \Delta\beta^\star\,\frac{IGE_{x\,0\widehat{x}}}{IGE_{x\,01}}\mathrm{d}\widehat{x}\bigg|_{WC} + \Delta x\int_0^1 \Delta\beta^\star\left[1 - \frac{IGE_{x\,0\widehat{x}}}{IGE_{x\,01}}\right]\mathrm{d}\widehat{x}\bigg|_{CE} \\ - \Delta y\int_0^1 \Delta\beta^\star\,\frac{IGE_{y\,0\widehat{y}}}{IGE_{y\,01}}\mathrm{d}\widehat{y}\bigg|_{SC} - \Delta y\int_0^1 \Delta\beta^\star\left[1 - \frac{IGE_{y\,0\widehat{y}}}{IGE_{y\,01}}\right]\mathrm{d}\widehat{y}\bigg|_{CN}. \end{aligned}$$

This reformulation of the source integrals is explained in Appendix C. The remaining terms are the discretization of $\partial\mathcal{F}^\star_{x(1-2)}/\partial x$. Two issues must be taken into account. First, the problem has two unknowns, namely, $\Delta\phi_2^\star$ and $\Delta\beta^\star$, and one discrete equation. Thus, some assumptions to calculate both are clearly needed. Under the assumption of $\Delta x = \Delta y$, an obvious

simplification is to consider $\Delta\beta^\star$ contribution negligible in comparison to the other source term in equation (3.32). It must be noticed that the source terms related to $\Delta\beta^\star$ have positive and negative coefficients so the error made in neglecting them is likely to be small, i.e. $b_C \approx 0$. This hypothesis is consistent with the solution sought because, if $\phi^\star_{1\,C} \to \phi^\star_{2\,C}$ then $\Delta\phi^\star_{2\,C} \to 0$ and the iterative process would be near the solution of (3.27). Second, when $\Delta x \neq \Delta y$, the algebraic equation in the x-direction can be multiplied by $\Delta y/\Delta x$ to have $\Delta\beta^\star$ contribution of the same order in both coordinates that will produce smaller errors on being neglected. Summarizing, the discrete equation for $\Delta\phi^\star_2$ is given by

$$A'_C\Delta\phi^\star_{2\,C} - \sum_{i\in\mathcal{N}} A'_i\Delta\phi^\star_{2\,i} = A'_{x\,C}(\phi^\star_{1\,C} - \phi^\star_{2\,C}) - \sum_{i\in\mathcal{N}_x} A'_i(\phi^\star_{1\,i} - \phi^\star_{2\,i}), \tag{3.33}$$

where

$$\begin{aligned} A'_C &= A'_{x\,C} + A^y_C, & A'_{x\,C} &= r_a A_{x\,C}, \\ A'_W &= r_a A_W, & A'_E &= r_a A_E, \\ A'_S &= A_S, & A'_N &= A_N, \end{aligned}$$

and

$$r_a \coloneqq \frac{\max\{\Delta y_{SC}, \Delta y_{CN}\}}{\max\{\Delta x_{WC}, \Delta x_{CE}\}}.$$

The discrete equation to update $\Delta\beta^\star$ is going to be eqn.(3.31b) with ENATE, i.e.

$$\begin{aligned} &\Delta y \int_0^1 -\Delta\beta^\star \frac{IGE_{y\,0\widehat{y}}}{IGE_{y\,01}} \mathrm{d}\widehat{y}\Big|_{SC} + \Delta y \int_0^1 -\Delta\beta^\star \left[1 - \frac{IGE_{y\,0\widehat{y}}}{IGE_{y\,01}}\right] \mathrm{d}\widehat{y}\Big|_{CN} \\ &= -A_S\Delta\phi^\star_{2\,S} + A_{y\,C}\Delta\phi^\star_{2\,C} - A_N\Delta\phi^\star_{2\,N}. \end{aligned}$$

The coefficients of the right-hand side are those on page 82. How to extract $\Delta\beta^\star$ at grid points? It must be realized that the integral evaluation of sources is being accomplished with ENATE knowing the nodal values of the source field but obtaining the field from the integrals is not easy. If the field in the RHS was exact, one would strive for seeking a manner of obtaining the $\Delta\beta^\star$ field with the complete left-hand side, but as this field is approximate, one can get away with a much simpler calculation. The simplest estimation employed is the usual one in the finite-volume approach: constant source around a node. Thus, the $\Delta\beta^\star$ field is calculated as

$$\Delta\beta^\star_C = \frac{A_S\Delta\phi^\star_{2\,S} - A_{y\,C}\Delta\phi^\star_{2\,C} + A_N\Delta\phi^\star_{2\,N}}{\Delta}, \tag{3.34}$$

where $\Delta \coloneqq (\Delta y_{SC} + \Delta y_{CN})/2$. This formula will be applied to every x-constant line in the discrete domain. Other alternatives such as assuming $\Delta\beta^\star$ linear and constant Péclet number in each interval were considered but did not provide good results. Although the starting point was the same as in [107], Lee and Kim employed some very drastic simplifications for the β calculation that reduced the order of accuracy.

The iterative sequence to calculate both ϕ and β is summarized below:

1. Initialize the scalar field β, named β^{old},
2. Calculate ϕ_1^{old} and ϕ_2^{old} in the ODEs (3.29) via the one-dimensional ENATE in Chapter 2.

3. Calculate $\Delta\phi_2^{\text{old}}$ with the equation (3.33). A line-by-line TDMA procedure is used,
4. Calculate the target ϕ, i.e. $\phi = \phi_2^{\text{old}} + \Delta\phi_2^{\text{old}}$. This step is only needed if the source depends on the solution. It is used to update the source,
5. Calculate $\Delta\beta^{\text{old}}$ with the equation (3.34) on vertical lines,
6. Update β, i.e. $\beta^{\text{new}} = \beta^{\text{old}} + \Delta\beta^{\text{old}}$,
7. Do $\beta^{\text{old}} \leftarrow \beta^{\text{new}}$ and go to second step till $\max_i\{|\phi_{1\,i}^{\text{old}} - \phi_{2\,i}^{\text{old}}|\} < \epsilon$ where ϵ is the tolerance.

This approach has been named "**R**apid **E**valuation of **M**ultidimensional **E**quations with **D**istinct **I**ntegrals as **E**xtra **S**ources", REMEDIES. "Distinct Integrals" refer to the fact that $+\beta$ integral is in the x coordinate and $-\beta$ in the y coordinate. It is appropriate to stress that this procedure is not exclusive of ENATE, coefficients and other parameters of equations (3.33) and (3.34) can be obtained by any other alternative discretization.

3.4.1 Reaction problem

When the source depends on the solution, i.e. $S = S(\phi(x,y))$, a special treatment of the schemes must be adopted to update the source in every iteration. Such problems are called reaction problems [61, 141, 204]. In the *cross-flux approach* nothing is modified in the discrete equation but for REMEDIES the equations (3.30) contain in this case an extra source that can be split in two. Defining $\Delta S_1^\star := S - S(\phi_1^\star)$ and $\Delta S_2^\star := S - S(\phi_2^\star)$, then

$$\frac{\partial}{\partial x}\left(\rho u\Delta\phi_1^\star - \Gamma\frac{\partial\Delta\phi_1^\star}{\partial x}\right) = \frac{1}{2}\Delta S_1^\star + \Delta\beta^\star, \tag{3.35a}$$

$$\frac{\partial}{\partial y}\left(\rho v\Delta\phi_2^\star - \Gamma\frac{\partial\Delta\phi_2^\star}{\partial y}\right) = \frac{1}{2}\Delta S_2^\star - \Delta\beta^\star. \tag{3.35b}$$

Doing the same simplifications for $\Delta\beta^\star$, the discrete equation (3.32) becomes

$$A'_C\Delta\phi_{2\,C}^\star - \sum_{i\in\mathcal{N}} A'_i\Delta\phi_{2\,i}^\star = \overline{\Delta S_2^\star}^x + \overline{\Delta S_2^\star}^y + A'_{x\,C}(\phi_{1\,C}^\star - \phi_{2\,C}^\star) - \sum_{i\in\mathcal{N}_x} A'_i(\phi_{1\,i}^\star - \phi_{2\,i}^\star), \tag{3.36}$$

where

$$\overline{\Delta S_2^\star}^x := \frac{\Delta x}{2}\int_0^1 \Delta S_2^\star \frac{IGE_{x\,0\widehat{x}}}{IGE_{x\,01}}\mathrm{d}\widehat{x}\bigg|_{WC} + \frac{\Delta x}{2}\int_0^1 \Delta S_2^\star\left[1 - \frac{IGE_{x\,0\widehat{x}}}{IGE_{x\,01}}\right]\mathrm{d}\widehat{x}\bigg|_{CE},$$

$$\overline{\Delta S_2^\star}^y := \frac{\Delta y}{2}\int_0^1 \Delta S_2^\star \frac{IGE_{y\,0\widehat{y}}}{IGE_{y\,01}}\mathrm{d}\widehat{y}\bigg|_{SC} + \frac{\Delta y}{2}\int_0^1 \Delta S_2^\star\left[1 - \frac{IGE_{y\,0\widehat{y}}}{IGE_{y\,01}}\right]\mathrm{d}\widehat{y}\bigg|_{CN},$$

are again average quantities. The new term in (3.36) has been obtained assuming $\phi_1^\star = \phi_2^\star$ so $\Delta S_1^\star = \Delta S_2^\star$. This last assumption was taken in order to have the same solution-dependent source in both equations (3.35). Finally, the calculation of $\Delta\beta_C^\star$ is modified as

$$\Delta\beta_C^\star = \frac{\overline{\Delta S_2^\star}^x_{SC} + \overline{\Delta S_2^\star}^y_{CN}}{\Delta} + \frac{A_S\Delta\phi_{2\,S}^\star - A_{y\,C}\Delta\phi_{2\,C}^\star + A_N\Delta\phi_{2\,N}^\star}{\Delta},$$

3.4.2 Application of boundary conditions

In order to calculate the numerical solution of a convection-diffusion problem, REMEDIES needs a correct implementation of the boundary conditions. Regular domains will be employed. Since REMEDIES should end up with $\phi = \phi_1^\star = \phi_2^\star$ in the whole domain, the BC for the discrete equation (3.33) is,

$$\Delta\phi_{2\,Bl}^\star = 0, \quad l \in \{1,2,3,4\} \tag{3.37}$$

at the boundaries. For equations (3.27), ϕ values at the boundaries should be employed. β must be calculated at the boundaries and its calculation depends on the boundary type. When ϕ is fixed on the boundary, i.e. Dirichlet BC, equation (3.27a) is used to compute β along horizontal boundary lines and (3.27b) in vertical boundary lines. In Neumann BC, $\partial\phi/\partial\{x,y\}$ is known. Thus, in each iteration ϕ at boundary needs to be updated to calculate β again with equations (3.27). In Robin BC, what is known is $\rho\mathbf{u}\phi - \Gamma\nabla\phi$ at boundaries and therefore β is fixed. As always, CCS is used in all calculations involving derivatives.

Finally, β should be initialized within the domain, Figure 3.9. A weighted average that takes into account the distance from the boundaries to the central point is employed, i.e.

$$\beta_C^{\text{ini}} = \frac{\displaystyle\sum_{l=1}^{4} \frac{\beta_{Bl}}{|\mathbf{x}_C - \mathbf{x}_{Bl}|}}{\displaystyle\sum_{l=1}^{4} \frac{1}{|\mathbf{x}_C - \mathbf{x}_{Bl}|}}.$$

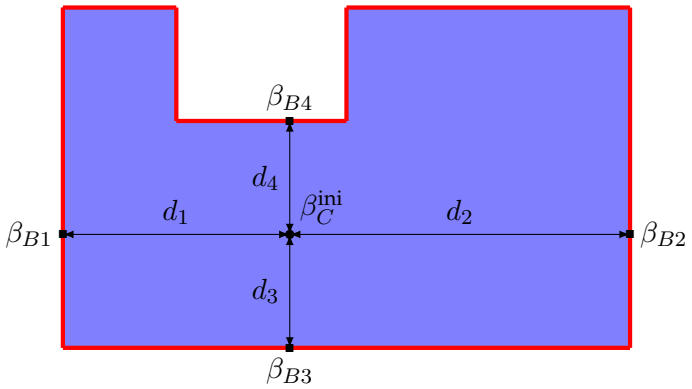

FIGURE 3.9: Schematic representation for the initialization of β where $d_l := |\mathbf{x}_C - \mathbf{x}_{Bl}|$ is the euclidean distance from the Central point to the Boundary l.

3.5 Integration methods II

In Chapter 2, page 47, two quadratures were proposed to compute the integrals from the matrix of the scheme and the discrete-source vector, being the Hermite splines the optimal one in all numerical tests coded. The drawback was that the variable derivatives at grid points had to be computed as required by the Hermite interpolant.

In two-dimensional modelling, all numerical Hermite calculations either along vertical lines, $\xi = y$ and $x =$ const., or along horizontal lines, $\xi = x$ and $y =$ const., will require two basic integrals: the average Péclet number, $\overline{P}_\xi$, or the integral of the source, $IS_{\xi\,01}$. For instance, taking the formula (2.57), the a_i from Cubic Hermite that interpolate $IS_\xi GE_{\xi\,01}$ are

$$
\begin{aligned}
a_0 &= 0,\\
a_1 &= \Delta\xi\, S_{\xi 0},\\
a_2 &= \left(\frac{3 + P_{\xi 1} - \overline{P}_\xi}{\Gamma_0/\Gamma_1} + \frac{1}{\Gamma_0}\left.\frac{\partial\Gamma}{\partial\widehat{\xi}}\right|_0\right) IS_{\xi\,01} - \Delta\xi\left(2S_{\xi 0} - \frac{S_{\xi 1}}{\Gamma_0/\Gamma_1}\right),\\
a_3 &= \left(\frac{-2 - P_{\xi 1} + \overline{P}_\xi}{\Gamma_0/\Gamma_1} - \frac{1}{\Gamma_0}\left.\frac{\partial\Gamma}{\partial\widehat{\xi}}\right|_0\right) IS_{\xi\,01} + \Delta\xi\left(S_{\xi 0} + \frac{S_{\xi 1}}{\Gamma_0/\Gamma_1}\right).
\end{aligned}
$$

Instead of computing $\overline{P}_\xi$ and $IS_{\xi\,01}$ via, e.g., spline (2.51), one may wonder if there are any other alternative quadrature for such smooth functions that is free of derivatives, only using the values of the integrand at mesh nodes, whatever order of accuracy is sought. A first idea could reside in taking nodes outside the interval where the integral is calculated. For example,

$$
\int_{\xi_{i-1}}^{\xi_i} f\,\mathrm{d}\xi \approx \frac{\Delta\xi}{192}\left[3f_{i-3} - 25f_{i-2} + 137f_{i-1} + 77f_i\right],
$$

its error is proportional to $\Delta\xi^5$, so it is of fifth order. The higher the order of the rule is, the larger the stencil is. A way to avoid a large set of points while still having the same order is to calculate the integral over an interval with its neighbor integrals, that is

$$
\frac{1}{10}\int_{\xi_{i-2}}^{\xi_{i-1}} f\,\mathrm{d}\xi + \int_{\xi_{i-1}}^{\xi_i} f\,\mathrm{d}\xi + \frac{1}{10}\int_{\xi_i}^{\xi_{i+1}} f\,\mathrm{d}\xi \approx \frac{3\Delta\xi}{5}\left[f_{i-1} + f_i\right].
$$

This quadrature generalization is named "**C**ompact **I**ntegration **R**ules", CIR [118], and results in an implicit numerical integration method. The previous rule is just one out of many where a general CIR centered at (ξ_{i-1}, ξ_i) is given by

$$
\sum_{k=-m_1}^{m_2} \alpha_k \int_{\xi_{i+k-1}}^{\xi_{i+k}} f\,\mathrm{d}\xi = \Delta\xi \sum_{k=-q_1}^{q_2} a_k f_{i+k} + \tau_i,
$$

or in matrix form,

$$
\mathbf{M}\int \mathbf{f}\mathrm{d}\xi = \Delta\xi\,\mathbf{Q}\mathbf{f} + \boldsymbol{\tau}, \tag{3.39}
$$

where $\mathbf{M} \in \mathbb{R}^{n\times n}$, $\mathbf{Q} \in \mathbb{R}^{n\times(n+1)}$ are banded matrices and

$$
\int \mathbf{f}\mathrm{d}\xi := \left(\int_{\xi_0}^{\xi_1} f\,\mathrm{d}\xi, \int_{\xi_1}^{\xi_2} f\,\mathrm{d}\xi, \ldots, \int_{\xi_{N-1}}^{\xi_N} f\,\mathrm{d}\xi\right)^T,
$$

the discrete solution vector in $\mathbb{R}^n$. The vector $\mathbf{f}$ is defined on page 86. It is easy to see that CIR is an analogy of CCS. The set $\{a_k\}$ links with the $\{\alpha_k\}$

set when matching the Taylor series coefficients until the desired order of accuracy. The first unmatched coefficient determines the local truncation error, τ_i and $\boldsymbol{\tau}$. In Appendix D is explained in detail how to determine the coefficients α_k and a_k.

If $\mathbf{M}$ is diagonal, $m_1 = m_2 = 0$, the rule is explicit. If not, a system of equations must be solved. We assume $m_1 = m_2$ and $q_1 = q_2$. The order of any rule is named as local if it is referred to the integral within an interval whereas it will be named as global if it is referred to the whole domain. The global order is one order of accuracy less than the local one due to the pile-up of local truncation errors, see details in [118]. In this thesis a global $4th$ order CIR was applied where

$$\mathbf{M} \coloneqq \begin{pmatrix} 1 & 1 & & & \\ 1/10 & 1 & 1/10 & & \\ & \ddots & \ddots & \ddots & \\ & & 1/10 & 1 & 1/10 \\ & & & 1 & 1 \end{pmatrix},$$

$$\mathbf{Q} \coloneqq \begin{pmatrix} 1/3 & 4/3 & 1/3 & & & \\ & 3/5 & 3/5 & & & \\ & & \ddots & \ddots & & \\ & & & 3/5 & 3/5 & \\ & & & 1/3 & 4/3 & 1/3 \end{pmatrix},$$

and a global $6th$ order CIR

$$\mathbf{M} \coloneqq \begin{pmatrix} 1 & 27/11 & & & \\ 11/38 & 1 & 11/38 & & \\ & \ddots & \ddots & \ddots & \\ & & 11/38 & 1 & 11/38 \\ & & & 27/11 & 1 \end{pmatrix},$$

$$\mathbf{Q} \coloneqq \begin{pmatrix} 281/990 & 1028/495 & 196/165 & -52/495 & 1/90 & & & \\ 3/38 & 27/38 & 27/38 & 3/38 & & & & \\ & \ddots & \ddots & \ddots & \ddots & & & \\ & & & 3/38 & 27/38 & 27/38 & 3/38 & \\ & & 1/90 & -52/495 & 196/165 & 1028/495 & 281/990 \end{pmatrix}.$$

Similarly to CCS, TDMA was used for solving the system (3.39).

3.6 Numerical Examples

In this section some numerical tests will be presented in order to compare both approaches. Most of them have an exact solution so the l_2-norm defined on page 58 is calculated. In the last one also the l_1-norm is computed, defined as

$$||\phi_{\text{num.}} - \phi_{\text{exact}}||_1 \coloneqq \frac{1}{N_{\text{nodes}}} \sum_{i=1}^{N_{\text{nodes}}} |\, \phi_i|_{\text{num.}} - \phi_i|_{\text{exact}}\,|,$$

and the l_∞-norm,

$$||\phi_{\text{num.}} - \phi_{\text{exact}}||_\infty \coloneqq \max_{1\leq i\leq N_{\text{nodes}}} \left(|\ \phi_i|_{\text{num.}} - \phi_i|_{\text{exact}}\ |\right).$$

where N_{nodes} is the number of nodes in the mesh. If the exact solution is unknown, as in the fifth test, the order of the scheme can be estimated by Richardson extrapolation [27]. According to this theory and once the simulations are in the convergence region, the approximation of ϕ_i at a given point in a Δx-size mesh, termed $\phi_{\Delta x}$, could be expressed as

$$\phi_i|_{\text{exact}} = \phi_{\Delta x} + C\Delta x^p.$$

Using three mesh configurations: a coarse (Δx), a medium ($\Delta x/2$) and a fine ($\Delta x/4$), the Richardson factor is defined by

$$RF_{\Delta x} \coloneqq 2^p = \frac{\phi_{\Delta x/2} - \phi_{\Delta x}}{\phi_{\Delta x/4} - \phi_{\Delta x/2}},$$

with p the order of convergence, different for each point.

3.6.1 2D machine-accurate solution

The equation solved in this case corresponds to a manufactured problem that represents the transport of temperature in a fluid with variable velocity. The BVP is

$$\begin{cases} \dfrac{\partial}{\partial x}\left(\rho c_p u T - k\dfrac{\partial T}{\partial x}\right) + \dfrac{\partial}{\partial y}\left(\rho c_p v T - k\dfrac{\partial T}{\partial y}\right) = S, & (x,y)\in(0,1)\times(0,1), \\ T(x,0) = 0, \quad T(x,1) = 1-x, & 0\leq x\leq 1, \\ T(0,y) = y, \quad T(1,y) = 0, & 0\leq y\leq 1, \end{cases}$$

where ρ is the density and c_p is the specific heat at constant pressure, both are constant. The actual equation solved is

$$\frac{\partial}{\partial x}\left(uT - \alpha\frac{\partial T}{\partial x}\right) + \frac{\partial}{\partial y}\left(vT - \alpha\frac{\partial T}{\partial y}\right) = S^*,$$

with $\alpha = k/\rho c_p$ and $S^* = S/\rho c_p$. The velocity is variable and given by $u = y$ and $v = -x$. Two cases were run for $\alpha \in \{10^{-2}, 10^{-4}\}$. The source is $S^*(x,y) = x^2 + y^2 - x$, such that the solution is $T = y(1-x)$, see Figure 3.10.

With cubic Hermite and just one node in the center of the square domain the difference between the computed solution and the exact one is of the order of 10^{-16}. In fact, this manufactured test case was especially chosen to show the capability of ENATE to obtain a machine-accurate solution for any number of grid points in a test case with analytic integrals. In the following it will be explained why the machine-accurate solution is obtained.

For this particular case the integrating factors included in the integrals of the coefficients are

$$\exp\int_{\widehat{x}}^{1} P_x\,\mathrm{d}\widehat{x}' = \exp\left(P_x(1-\widehat{x})\right), \quad \exp\int_{\widehat{y}}^{1} P_y\,\mathrm{d}\widehat{y}' = \exp\left(P_y(1-\widehat{y})\right),$$

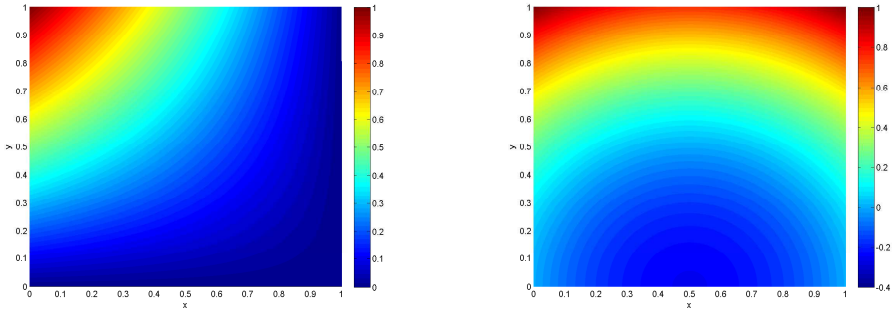

(A) Temperature field, $T(x, y)$. (B) Source field, $S^*(x, y)$.

FIGURE 3.10: Example *2D machine-accurate solution*, Manufactured problem for the energy equation in fluid mechanics.

as $P_x = (u\Delta x)/\alpha$ depends only on y through u and $P_y = (v\Delta y)/\alpha$ depends only on x through v. The IGEs ratios can be calculated exactly. For instance,

$$IGE_{x\,0\widehat{x}} = \int_0^{\widehat{x}} \exp(P_x(1-\widehat{x}'))\mathrm{d}\widehat{x}' = \frac{1-\exp(-P_x\widehat{x})}{P_x\exp(-P_x)},$$
$$IGE_{x\,01} = \frac{1-\exp(-P_x)}{P_x\exp(-P_x)},$$

and, therefore,

$$\frac{IGE_{x\,0\widehat{x}}}{IGE_{x\,01}} = \frac{1-\exp(-P_x\widehat{x})}{1-\exp(-P_x)},$$

similarly in the other direction. Thus, $IGE_{\{x,y\}01}$ makes all coefficients, A_W, A_E, A_S, A_N and A_C, exact in 2D.

The source and pseudo-sources are quadratic in x and y, so any polynomial of second degree or higher may approximate it exactly along one coordinate, in particular a third-degree Hermite polynomial (cubic Hermite), $S^*(\widehat{x}, y_C) = \sum_{k=0}^{3} a_k\widehat{x}^k$. After interpolating the integrand, all source contribution reduces to calculating integrals of the type $\int x^n \exp(-P_x x)\,\mathrm{d}x$. These integrals have primitives that have been included in the code. In conclusion, whatever number of intervals is used the result of the integrals of both sources and pseudo-sources is exact. As both coefficients and source integrals are exact, the code with ENATE scheme provides for this example a machine-accurate solution for any number of grid points. The computer program turned over machine-accurate results in all cases with cubic, quintic or septic Hermite polynomials and just one node at any position in the domain. It must be stressed that this case was run with the general-purpose code, no previous calculation was done by hand to be later coded.

3.6.2 Nonlinear convection-only problem

Let us briefly consider the 2D pure convection case [181],

$$\begin{cases} u\dfrac{\partial u}{\partial x} + u\dfrac{\partial u}{\partial y} = S, & (x,y) \in (0,1)\times(0,1), \\ u(x,0) = a + \sin\left(x - 0.5\right), & 0 \leq x \leq 1, \\ u(0,y) = b + \tanh\left(\sigma\left(y - 0.5\right)\right), & 0 \leq y \leq 1, \end{cases}$$

where $a = 2 + \tanh\left(-0.5\sigma\right)$ and $b = 2 + \sin\left(-0.5\right)$ to enforce continuity of u in the origin. This is a 2D steady Burgers' equation in which the velocity components are the same, so there is only one PDE to solve. A manufactured source is employed,

$$\begin{aligned} S(x,y) = &\left(2 + \sin\left(x - 0.5\right) + \tanh\left(\sigma\left(y - 0.5\right)\right)\right)\cos\left(x - 0.5\right) \\ &+ \sigma\left(2 + \sin\left(x - 0.5\right) + \tanh\left(\sigma\left(y - 0.5\right)\right)\right)\operatorname{sech}^2\left(\sigma\left(y - 0.5\right)\right), \end{aligned}$$

being σ an input parameter that controls the steepness of the solution in a certain desired region, close to $y = 0.5$. The exact solution is

$$u(x,y) = 2 + \sin\left(x - 0.5\right) + \tanh\left(\sigma\left(y - 0.5\right)\right),$$

which is very anisotropic, the gradient of u does not change alike in both directions. The sine function in one direction is very smooth but the hyperbolic tangent function around $y = 0.5$ is very sharp for large σ. In fact, the greater the value of σ is, the greater the gradient of u in y-direction around 0.5 becomes, see Figure 3.11.

The ENATE scheme works with the conservative form of the transport equation,

$$\frac{\partial\left(\rho u\phi\right)}{\partial x} + \frac{\partial\left(\rho u\phi\right)}{\partial y} = S,$$

in which the conserved variable is the variable under study, $\phi(x,y) = u(x,y)$, $\rho = 1/2$ and the convective coefficients use the values of u in the previous iteration, i.e. $\rho u = u^{\text{old}}/2$.

The code was run until the normalized difference between two consecutive iterations was less than 10^{-4}. In order to compare with the FV-CF scheme [209] the transport equation has been further discretized with the latter. With $|P| \to \infty$ the source integrals do not have the exponential factor. Different comparisons were undertaken:

1. FaP using CIR+CCS is compared with FV-CF,
2. CIR+CCS is compared with Hermite+CCS in FaP,
3. FaP and REMEDIES are compared,
4. The special case $u = v$ in 3.2.2 of the *streamline approach* is computed.

First, the l_2-norm of the error is plotted in Figure 3.12 where eight numerical experiments were implemented: two levels in the gradient and four CIR/CCS combinations. Both smooth and sharp gradient simulations using a fourth-order CIR + fourth-order CCS, sixth-order CIR + fourth-order CCS show an identical behaviour. In both cases, ENATE works as a fourth-order scheme, Table 3.2, being slightly better with a smooth gradient.

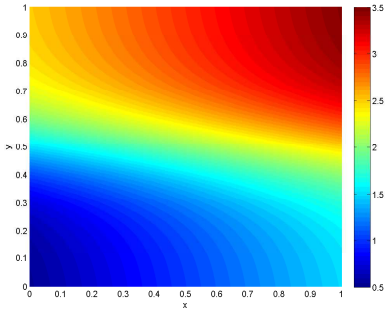

(A) $u(x, y)$ field with $\sigma = 5$.

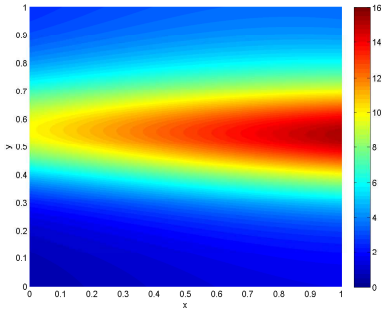

(B) $S(x, y)$ field with $\sigma = 5$.

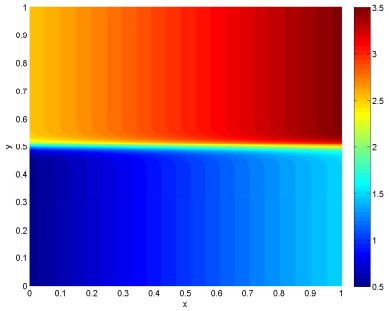

(C) $u(x, y)$ field with $\sigma = 50$.

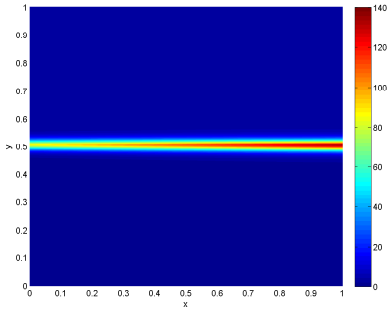

(D) $S(x, y)$ field with $\sigma = 50$.

FIGURE 3.11: Example *Nonlinear convection-only problem*, manufactured problem for the Burgers' equation.

The fourth-order CIR + sixth-order CCS and sixth-order CIR + sixth-order CCS follow the same behaviour in sharp gradient, except for the 500 $\times$ 500 mesh whose results differ from each other less than one order of magnitude. ENATE works as a sixth-order scheme. With a smooth gradient and same orders of CIR and CCS the differences become relevant beyond the 200 $\times$ 200 mesh. Rejecting results of the last Δx, fourth-order ENATE is achieved with a fourth-order CIR + sixth-order CCS and sixth-order ENATE is obtained by sixth-order CIR + sixth-order CCS. On the other hand, eighth-order CIR or CCS did not provide good results and they are not reported.

It is worth highlighting the good results obtained by ENATE with its accessories (CCS and CIR) in this nonlinear equation. In the more stringent case of $\sigma = 50$ the l_2-norm is $3 \cdot 10^{-10}$ with a mesh of 500 $\times$ 500.

ENATE provides much better results than the FV-CF scheme, even for $\sigma = 50$, case that contains a region where the solution changes very quickly. As is remarked by its authors, FV-CF becomes a second-order cell-vertex FV method when Péclet goes to infinity, as in this test. ENATE cannot provide a solution for $\sqrt{\Delta x \Delta y} > 2 \cdot 10^{-2}$ whereas FV-CF works fine for $\sqrt{\Delta x \Delta y}$ greater than this value. For large $\sqrt{\Delta x \Delta y}$, the integrals of ENATE are more sensitive to the exponentials than the FV-CF scheme.

On the other hand, the accuracy with FaP is studied using Hermite (2.51), (2.52) and (2.53) or CIR, once $\partial \mathcal{F}_x / \partial x$ and $\partial \mathcal{F}_y / \partial y$ are computed with CCS. First, the l_2-norm of the error using Hermite+CCS is plotted in Figure 3.13. Again, the order of ENATE is ruled by CCS. Only with $\sigma = 50$

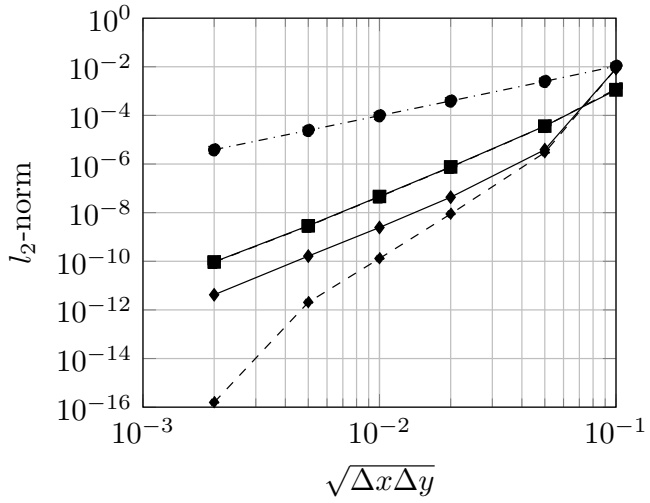

(A) Smooth gradient, $\sigma = 5$.

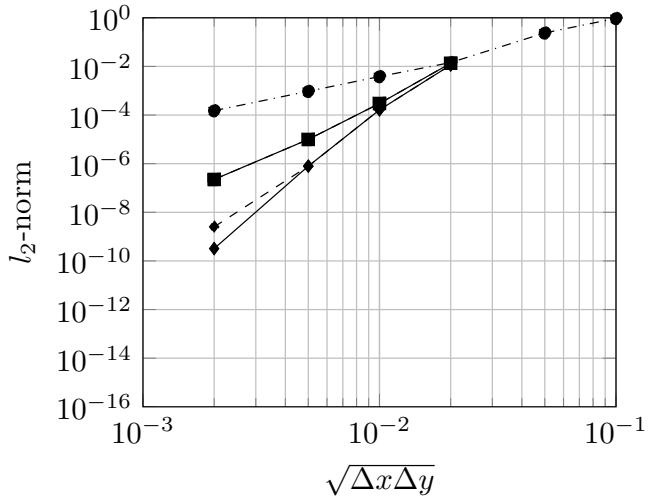

(B) Sharp gradient, $\sigma = 50$.

FIGURE 3.12: Example *Nonlinear convection-only problem*, the l_2-norm of the error for two numerical methods. • Dash dotted line, FV-CF scheme. ■ Solid line, ENATE with FaP using 4th-order CIR + 4th-order CCS. ■ Dashed line, 6th-order CIR + 4th-order CCS. ♦ Dashed line, 4th-order CIR + 6th-order CCS. ♦ Dashed line, 6th-order CIR + 6th-order CCS.

Case	σ	CIR	CCS	ENATE with FaP
1.1	5 (Smooth)	4th	4th	4th
1.2		4th	6th	4th
1.3		6th	4th	4th
1.4		6th	6th	6th
2.1	50 (Sharp)	4th	4th	4th
2.2		4th	6th	6th
2.3		6th	4th	4th
2.4		6th	6th	6th

TABLE 3.2: Example *Nonlinear convection-only problem*, orders obtained by several combinations of CCS and CIR. Case 1.2 is better than 1.1. Cases 1.3 and 2.3 is identical to 1.1 and 2.1 respectively.

some differences pop up with Cubic and Quintic in $\sqrt{\Delta x \Delta y} = 10^{-2}$ and $\sqrt{\Delta x \Delta y} = 2 \cdot 10^{-3}$, but they are not significant. Now, if Figure 3.12 is compared with 3.13, CIR and Hermite give the same accuracy but the CPU time in the case of ENATE with FaP using CIR+CCS is a bit less than Hermite+CCS. As an example, in the case of $\sqrt{\Delta x \Delta y} = 10^{-2}$ CIR runs in 11 min. and Hermite in ∼15 min. The cause is that more derivatives need to be computed, e.g., Quintic requires $\partial \mathcal{F}_x / \partial x$, $\partial^2 \mathcal{F}_x / \partial x \partial y$, $\partial^3 \mathcal{F}_x / \partial x \partial y^2$ (in y-direction).

Another analysis is the comparison of FaP vs. REMEDIES. The integrals were computed in both approaches using Hermite + CCS. In Figure 3.14 the l_2-norm of the error has been plotted. In the case with $\sigma = 5$, norms with FaP and REMEDIES were similar for Cubic Hermite + 4th-order CCS and one order of magnitude better in REMEDIES than in FaP for Quintic Hermite + 6th-order CCS. For $\sigma = 50$, slight differences are seen in the norm. Septic Hermite in both approaches and with different σ was not able to get a norm below Quintic.

Regarding CPU time, REMEDIES is faster than FaP, see Table 3.3. For instance, in the case of $\sigma = 5$, REMEDIES takes around 2 min, FaP 20 min, in $\sqrt{\Delta x \Delta y} = 5 \cdot 10^{-3}$ using Cubic Hermite + 4th-order CCS. For $\sigma = 50$ and same Hermite + CCS and spacing, REMEDIES takes 30.5 s, unlike FaP that takes 14 min.

Finally, this test allowed to compute the transport equation under the transformation of the stream-function coordinates on page 76. The integral in (3.5) was calculated by CIR. In Figure 3.15 the numerical results are compared with FaP. In both tests, if the convection-only transport equation is reduced to an ODE over a streamline and the one-dimensional fluxes of ENATE are applied, the numerical solution improves two orders of magnitude for a fourth-order ENATE, or four orders of magnitude for a sixth-order ENATE. Additionally, in the case $\sigma = 50$, the transformation is better at approximating the integrals than FaP or REMEDIES for large $\sqrt{\Delta x \Delta y}$, as well as REMEDIES.

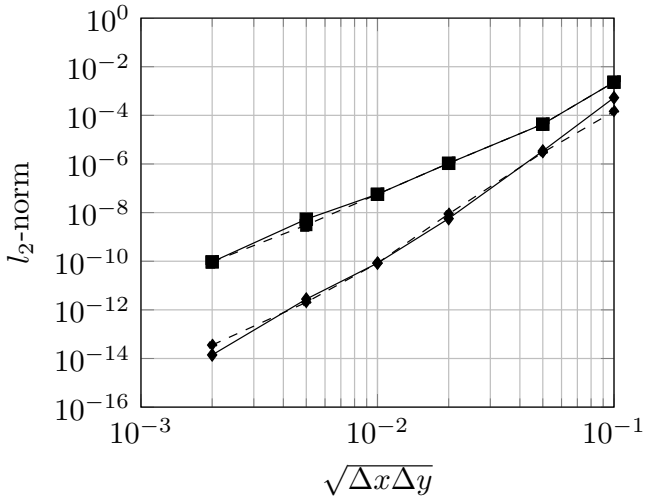

(A) Smooth gradient, $\sigma = 5$.

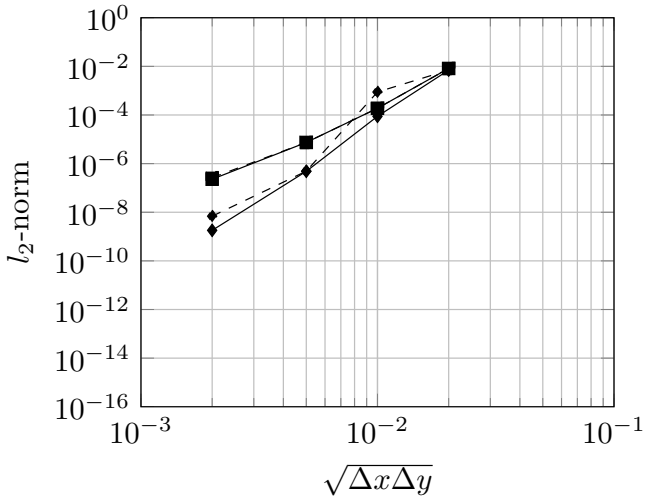

(B) Sharp gradient, $\sigma = 50$.

FIGURE 3.13: Example *Nonlinear convection-only problem*, the l_2-norm of the errors for ENATE with FaP using Hermite. ■ Solid line, Cubic Hermite + 4th-order CCS. ■ Dashed line, Quintic Hermite + 4th-order CCS. ♦ Solid line, Cubic Hermite + 6th-order CCS. ♦ Dashed line, Quintic Hermite + 6th-order CCS.

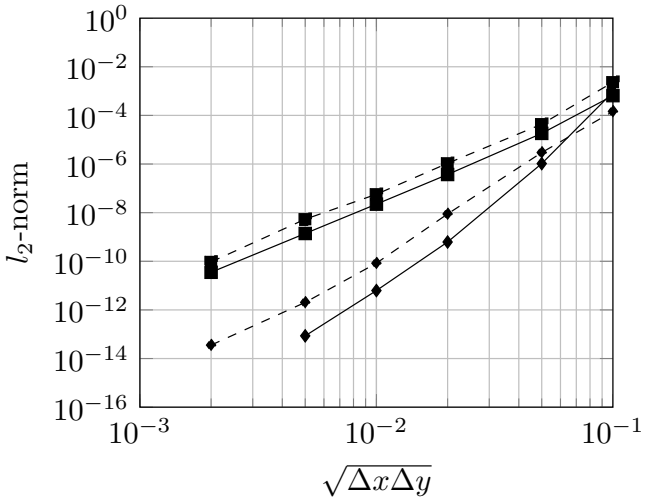

(A) Smooth gradient, $\sigma = 5$.

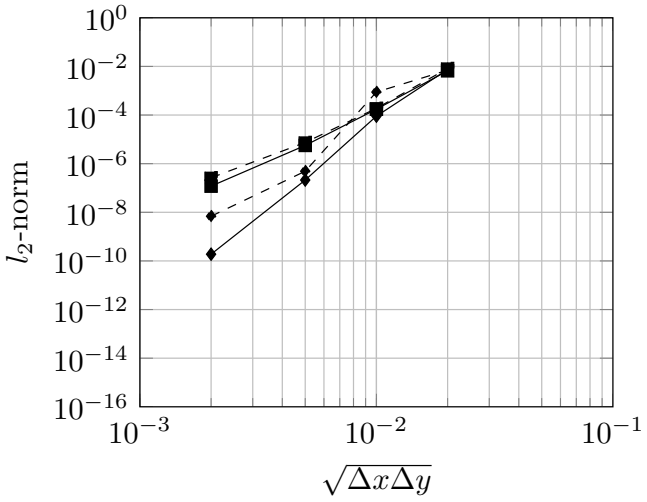

(B) Sharp gradient, $\sigma = 50$.

FIGURE 3.14: Example *Nonlinear convection-only problem*, the l_2-norm of the errors for two approaches. ■ Solid line, ENATE with REMEDIES using Cubic Hermite + 4th-order CCS. ♦ Solid line, Quintic Hermite + 6th-order CCS. ■ Dashed line, ENATE with FaP using Cubic Hermite + 4th-order CCS. ♦ Dashed line, Quintic Hermite + 6th-order CCS.

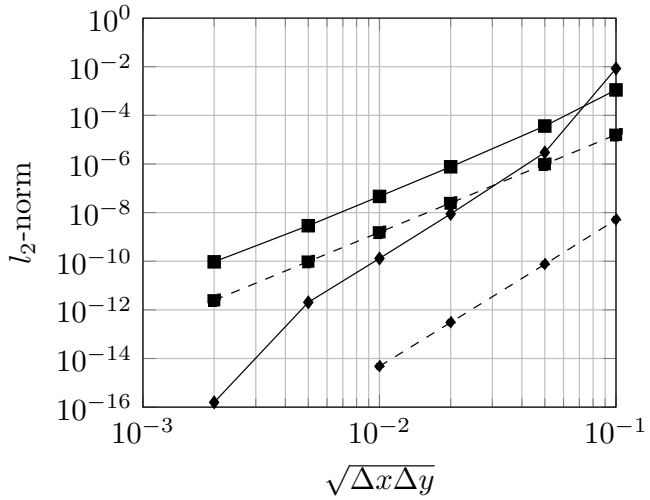

(A) Smooth gradient, $\sigma = 5$.

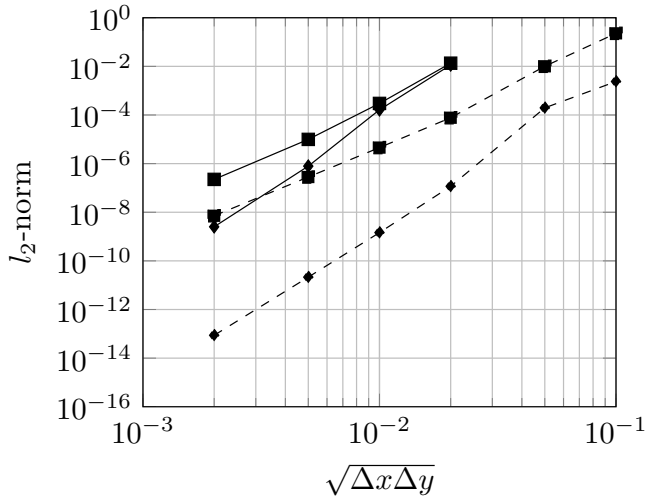

(B) Sharp gradient, $\sigma = 50$.

FIGURE 3.15: Example *Nonlinear convection-only problem*, the l_2-norm of the errors for FaP and stream-function coordinate. ■ Solid line, ENATE with FaP using 4th-order CIR + 4th-order CCS. ♦ Solid line, 6th-order CIR + 6th-order CCS. ■ Dashed line, ENATE with stream-function coordinate using 4th-order CIR. ♦ Dashed line, 6th-order CIR.

σ	$\sqrt{\Delta x \Delta y}$	Cubic + 4th-CCS		Quintic + 6th-CCS	
		REMEDIES	FaP	REMEDIES	FaP
5	0.1	0.16	0.05	0.11	4.79
	0.05	0.46	0.18	0.72	10.51
	0.02	2.61	9.44	4.67	51.61
	0.01	15.0	140.45	27.0	176.30
	0.005	118.9	1226.70	200.8	1010.55
	0.002	512.6	13110.67		
50	0.02	0.5	6.18	0.6	4.74
	0.01	2.5	102.49	4.4	145.94
	0.005	30.5	833.76	143.0	1355.53
	0.002	315.3	Oscillating		

TABLE 3.3: Example *Nonlinear convection-only problem*, comparing the FaP and REMEDIES approaches in terms of elapsed CPU time (in seconds).

3.6.3 Poisson's equation

The accuracy of ENATE either with FaP or with REMEDIES depends on many factors, particularly on the value of the Péclet number based on the interval size. As part of the assessment of REMEDIES two cases with zero Péclet, i.e., a Poisson's equation, were run. Poisson's equation is widely used in physics, and particularly in computational fluid dynamics to solve the pressure field [1, 2].

Two cases were computed that solve

$$\frac{\partial^2 \phi}{\partial x^2} + \frac{\partial^2 \phi}{\partial y^2} = -S,$$

in a squared domain of unit size. The two sources and boundary conditions are such that the solution for the first case is

$$\phi(x, y) = \exp\left(-0.5(4\pi)^2((x - 0.5)^2 + (y - 0.5)^2)\right),$$

and for the second

$$\phi(x, y) = (x^3 - y^4 + x^2 y^3) \sin 2\pi x \sin 2\pi y,$$

plotted in Figure 3.16. A uniform mesh in both coordinates was used with $\Delta x = \Delta y$. In these cases the accuracy of results will be measured by the l_2-norm of the vector difference between the computed results and the exact ones. The two cases presented were also studied by Zapata and Balam [248], where they used high-order compact schemes.

In Figure 3.17 the comparison between the two approaches, REMEDIES and FaP, is depicted. The norm is presented against the mesh size. The order of accuracy of both is the same but the actual values are slightly different with a gap of half an order of magnitude between them. The relative behaviour is a bit surprising because with cubic Hermite FaP is better than REMEDIES but it is the other way round with quintic Hermite. The differences may only be caused by the buildup of errors due to the number of arithmetic operations required to get to a converged solution, different for

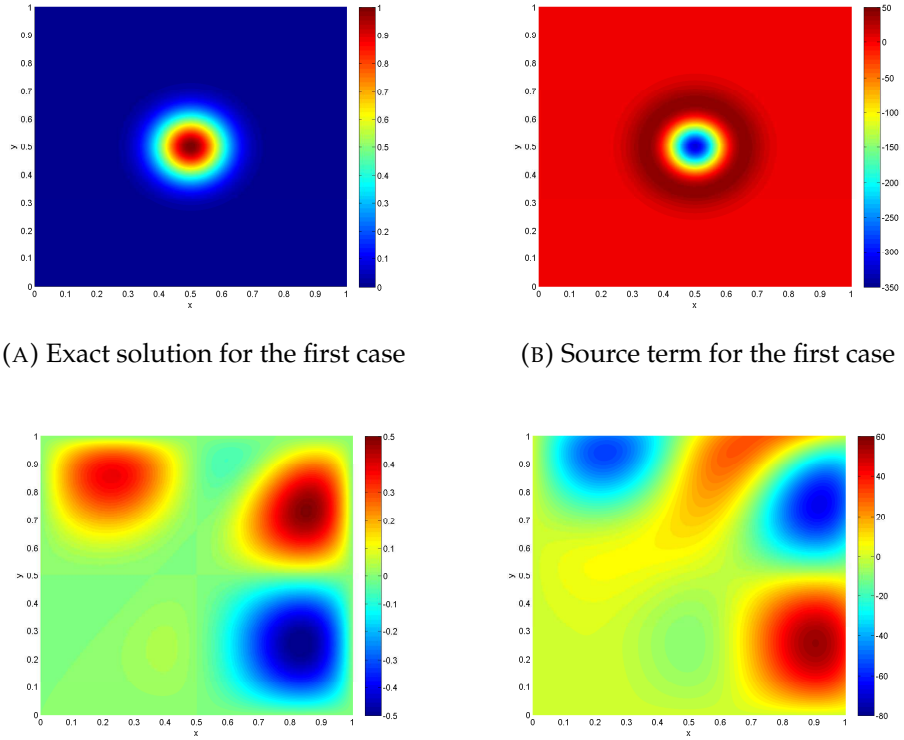

(A) Exact solution for the first case

(B) Source term for the first case

(C) Exact solution for the second case

(D) Source term for the second case

FIGURE 3.16: Example *Poisson's equation*, manufactured problems for the Poisson's equation.

each approach.

It is convenient to state the differences between the two approaches in terms of arithmetic operations. The most important one is the number of sweeps over the 2D domain required to solve the algebraic equation pertinent to either approach. FaP solves the algebraic equation resulting from the sum of equations (3.12a) and (3.13a) once discretized. REMEDIES solves the algebraic equation for $\Delta\phi_2^\star$. In the case of FaP the number of required sweeps is just four, whereas REMEDIES requires many sweeps to obtain a good estimation of $\Delta\phi_2^\star$. The CPU time not only depends on the number of sweeps per iteration but also on the number of iterations needed for convergence. CPU times have already been presented for a former test case and we anticipate that REMEDIES is faster than FaP at reaching the converged solution for many cases computed.

Figure 3.18 compares ENATE with REMEDIES with results from Zapata and Balam of similar order of accuracy. These authors present tables of l_2-norms for explicit, implicit and high-order implicit schemes, the names refer to the way the second derivatives are evaluated. In each category different approximations to the source function are considered. Those whose formal orders of accuracy are sixth, eighth and tenth respectively, named as EF3, IF3 and HIF3 in the paper, are chosen for comparison. The theoretical orders of accuracy of cubic, quintic and septic Hermite are fourth, sixth and eighth but in this case, apart from cubic, the orders were closer to the others just mentioned. Cubic Hermite is the only Hermite polynomial that conforms to the formal order of accuracy. For a short range of mesh

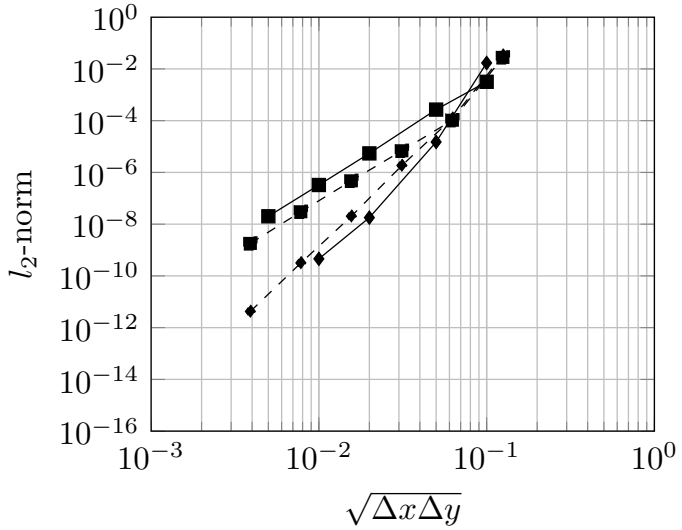

FIGURE 3.17: Example *Poisson's equation*, the l_2-norm of the error for the first Poisson problem. Solid lines are for REMEDIES and dashed lines correspond to FaP approach. ■ Cubic Hermite. ♦ Quintic Hermite.

sizes quintic Hermite is eighth-order but in the last mesh becomes sixth-order. Septic Hermite is tenth-order over an ample range of mesh sizes and follows closely the convergence results of HIF3.

The second Poisson case is depicted in Figure 3.19. Similar conclusions to those of the first Poisson case can be drawn from the comparison of REMEDIES and FaP. For cubic Hermite both approaches give very close l_2 results. For quintic Hermite the differences are more noticeable, always in favour of the β treatment. It seems that the new terms in the interpolant introduced by quintic Hermite are more important in this case and the requirements of a larger number of arithmetic operations for FaP contribute to greater discretization errors. Yet, in the final range of interval sizes both behave as sixth-order.

Figure 3.20 shows the comparison with Zapata and Balam schemes. All schemes present the formal order of accuracy except septic that is tenth order. For all interval sizes cubic Hermite is almost two orders of magnitude better than Zapata and Balam comparable scheme. Quintic Hermite is two orders of magnitude better only for small interval sizes.

The explicit schemes of Zapata and Balam require the use of TDMA or PDMA to solve the final system of equations but due to the stencil of the implicit schemes, namely 21 points for both IF3 and HIF3 in 2D, a SOR procedure is followed. ENATE only employs TDMA, for a three-point stencil in each coordinate is employed, which also makes the coding much less burdensome.

The l_2 data from Zapata and Balam are extracted directly from their paper where no information about the CPU time taken by each scheme is provided for these two cases.

In the course of this research with REMEDIES two interesting aspects

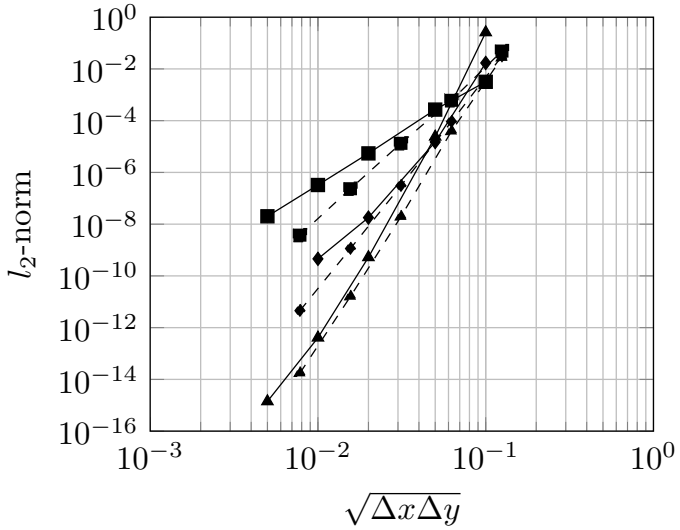

FIGURE 3.18: Example *Poisson's equation*, the l_2-norm of the error for the first Poisson problem. Solid lines are those of REMEDIES and dashed lines correspond to Zapata and Balam data of similar order of accuracy. ■ Cubic Hermite and EF3. ♦ Quintic Hermite and IF3. ▲ Septic Hermite and HIF3.

came up. First, the CPU time was strongly dependent on the Péclet number of the problem. The smaller this number is, the longer CPU time is needed to get the final solution. Poisson's problems are consequently the worst due to the number of sweeps required to obtain a reasonably good estimation of $\Delta\phi_2$. Remind that this equation is the only one that is 2D, the equations for ϕ_1 and ϕ_2 are 1D. A second aspect that emerged is the existence of a minimum number of sweeps below which the solution diverges. This happens for relatively fine meshes.

In Tables 3.4 and 3.5 the CPU time taken in the two Poisson cases with REMEDIES by the different Hermite polynomials is shown. The cases were run under the β approach for two different mesh sizes, a fine one 200×200, and a medium one 50×50. In the second Poisson case with septic Hermite the finest grid is 100×100 as with this grid the solution is already near machine accuracy.

In both tests the CPU time for a mesh of 50×50 is of the order of one second. With this mesh and in the first Poisson problem the order of magnitude of the l_2 norm ranges from 10^{-5} for cubic to 10^{-9} for septic, whereas for the second problem it goes from 10^{-7} to 10^{-12}. As seen in the tables the optimum number of sweeps is mildly dependent on both the polynomial degree and the source but it is strongly dependent on the grid size. CPU time for FaP is much longer for all meshes and Hermite polynomials, and it is not detailed. For example, FaP cubic Hermite for a mesh of 200×200 takes about 900 s, compared to 357 s with REMEDIES. This improvement in CPU time of the β approach is consistently found in all cases tested.

Hermite	200×200		50×50	
	Sweeps ×4	CPU time $[s]$	Sweeps	CPU Time $[s]$
Cubic	100	diverges	10	4.14
	200	461	20	0.65
	300	259	30	0.52
	400	199	40	0.51
	500	178	50	0.55
	600	170		
	700	251		
Quintic	100	diverges	10	5.96
	200	543	20	1.05
	300	239	30	0.73
	400	258	40	0.73
			50	0.76
Septic	100	diverges	10	7.95
	200	872	20	1.28
	300	487	30	1.07
	400	430	40	1.00
	500	393	50	1.17
	600	400		

TABLE 3.4: Example *Poisson's equation*, First Poisson problem. Number of sweeps and CPU time in seconds for two mesh sizes.

Hermite	200×200		50×50	
	Sweeps ×4	CPU time $[s]$	Sweeps	CPU Time $[s]$
Cubic	100	diverges	10	4.8
	200	508	20	1.3
	300	445	30	1.2
	400	407	40	1.26
	500	366		
	600	357		
	700	360		
Quintic	100	diverges	10	8.0
	200	777	20	1.95
	300	626	30	1.71
	400	566	40	1.78
	500	548		
	600	543		
	700	580		
Septic	70	43	10	9.6
	80	39	20	2.42
	90	39	30	2.18
	100	40	40	1.98
	200	44	50	2.25

TABLE 3.5: Example *Poisson's equation*, second Poisson problem. Number of sweeps and CPU time in seconds for two mesh sizes. The first two columns of septic Hermite are presented for a mesh of 100×100 as it is already very close to machine accuracy.

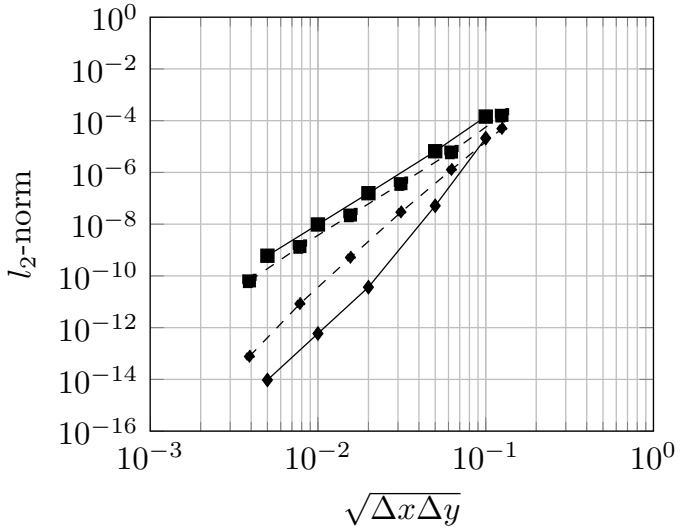

FIGURE 3.19: Example *Poisson's equation*, the l_2-norm of the error for the second Poisson problem. Solid lines are for REMEDIES and dashed lines correspond to FaP approach.

3.6.4 Convection equation with piecewise-constant BC

Let us consider the following BVP [88, 151],

$$\begin{cases} \dfrac{\partial}{\partial x}(\rho u \phi) + \dfrac{\partial}{\partial y}(\rho v \phi) = 0, & (x, y) \in (0, 1] \times (0, 1], \\ \phi(x, 0) = 1, & 0 \leq x \leq 1, \\ \phi(0, y) = 0, & 0 < y \leq 1, \end{cases}$$

with ρu and ρv positive constants. Since convection is the only transportive process, a discontinuity develops along a straight line with slope $\rho v / \rho u$. A value of 1 fills the domain below this line, and a value of 0 above it, see Fig. 3.21. Since numerical schemes have errors attached to the discretization process, the numerical ϕ will not preserve the discontinuity and there will be some spread perpendicular to this straight line.

In case of ENATE with FaP, integrals (3.17d) are zero as $S = 0$ and the fluxes (3.11) are constant in the two areas of the domain. Although ϕ shows a discontinuity across the straight line passing through the origin, over this line the sum of $\int_{x_W}^{x_C} (\partial \mathcal{F}_y / \partial y) \mathrm{d}x$ and $\int_{y_S}^{y_C} (\partial \mathcal{F}_x / \partial x) \mathrm{d}y$ is zero if the Dirac delta function contribution at x_C is neglected. In all examples shown this is assumed. Thus, ENATE with FaP yields

$$(\rho u + \rho v)\phi_C = \rho u \phi_W + \rho v \phi_S. \tag{3.40}$$

Due to the fact that the extra terms are discarded, a way to improve the accuracy of this approach results from adding an additional point to the stencil in the following manner. Shift the indices $\phi_C \to \phi_S$, $\phi_W \to \phi_C$ and

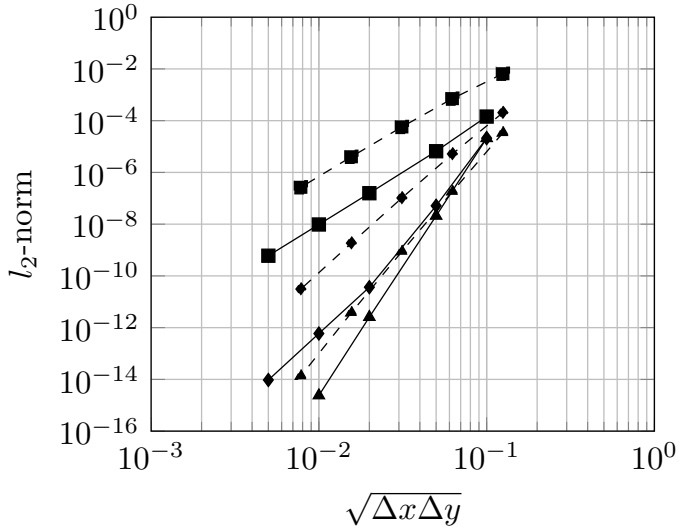

FIGURE 3.20: Example *Poisson's equation*, the l_2-norm of the error for the second Poisson problem. Solid lines are those of REMEDIES and dashed lines correspond to Zapata and Balam data of similar order of accuracy. ■ Cubic Hermite and EF3. ♦ Quintic Hermite and IF3. ▲ Septic Hermite and HIF3.

$\phi_S \to \phi_{SW}$, obtaining

$$(\rho u + \rho v)\phi_S = \rho v \phi_C + \rho u \phi_{SW}.$$

Then, changing the sense of ρv and multiply ρu by the aspect ratio of the mesh, defined as $r_a \coloneqq \Delta y / \Delta x$,

$$(r_a \rho u - \rho v)\phi_S = -\rho v \phi_C + r_a \rho u \phi_{SW}. \tag{3.41}$$

The ratio r_a should be included because if $\Delta x \neq \Delta y$ the streamline that passes through x_C will pass through x_{SW} iff $\rho v \Delta x = \rho u \Delta y$. It is easy to check that in that case the previous algebraic equation provides $\phi_{SW} = \phi_C$. If r_a is not included there will also be contribution from ϕ_S which is not correct. Scheme (3.41) that uses the streamline direction to derive the algebraic relation between nodes is the SUDS of Raithby [172], back in 1976. Finally, eqn.(3.40) + eqn.(3.41), ϕ_C links with ϕ_W, ϕ_S and ϕ_{SW}:

$$(\rho u + 2\rho v)\phi_C = \rho u \phi_W + (2\rho v - r_a \rho u)\phi_S + r_a \rho u \phi_{SW}, \tag{3.42}$$

which preserves positiveness iff $\rho v / \rho u \geq r_a / 2$. On the other hand, REMEDIES used the integrals of β computed by CIR, no assumption was made. The numerical diffusion of REMEDIES will be shown in the computations as to provide a theoretical derivation was not feasible.

In Table 3.6 the l_2-norm of the error when $\rho u = \rho v = 1$ on a uniform mesh, $\Delta x = \Delta y$, is displayed. Both FV-CF and ENATE show a behaviour of a scheme less than $1st$-order. The reason of this drop in quality of ENATE lies in two facts. Since the integrals of $S_{\{x,y\}}$ do not take part in FaP, the

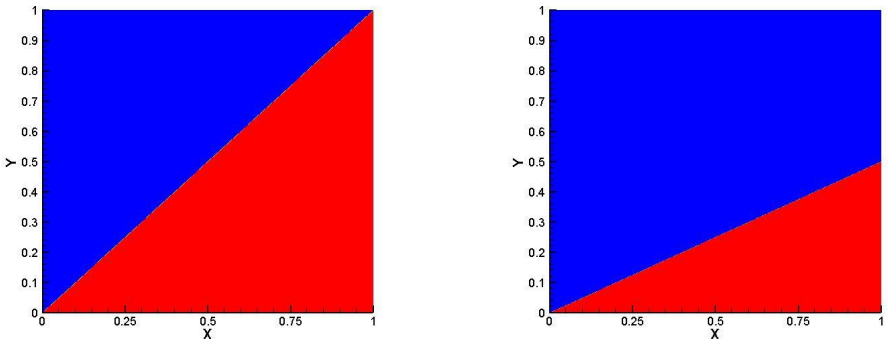

FIGURE 3.21: Example *Piecewise constant boundary condition*, exact solution over the box with $\rho u = \rho v$ (left) and $\rho u = 2\rho v$ (right). Red domain, $\phi(x, y > (\rho v/\rho u)x) = 1$. Blue domain, $\phi(x, y < (\rho v/\rho u)x) = 0$.

scheme converts into an upwind method. For REMEDIES, where the integrals of β are computed, there were no differences in using either fourth- or sixth-order CIR, because the accuracy is determined by the β derivatives. They are very inaccurate as β is a Dirac delta along the straight line of slope $\rho v/\rho u$. Notwithstanding this, the best l_2-norm is obtained with REMEDIES.

$\sqrt{\Delta x \Delta y}$	FV-CF	ENATE		
		FaP		REMEDIES
		3-point	4-point	
0.1	$1.8257 \cdot 10^{-1}$	$2.6140 \cdot 10^{-1}$	$2.1520 \cdot 10^{-1}$	$1.6777 \cdot 10^{-1}$
0.01	$1.0777 \cdot 10^{-1}$	$1.4616 \cdot 10^{-1}$	$1.2321 \cdot 10^{-1}$	$5.0664 \cdot 10^{-2}$
0.001	$6.1178 \cdot 10^{-2}$	$8.2971 \cdot 10^{-2}$	$6.9879 \cdot 10^{-2}$	$1.7137 \cdot 10^{-2}$

TABLE 3.6: Example *Piecewise constant boundary condition*, the l_2-norm of the error when $\rho u = \rho v$ for the FV-CF and ENATE scheme.

If the convection is changed, e.g. $\rho u = 1$ and $\rho v = 0.5$, the l_2-norm of the error does not change too much, Table 3.7. However, with the FV-CF scheme the computed convection direction has changed, see Fig. 3.22. If a uniform mesh is adopted with $\Delta x = \Delta y$, bottom left figure, not only is FV-CF adding numerical diffusion but it is also solving a different convection problem. If its modified equation is looked at, both interpolation and mesh produce an artificial convection direction that changes back to the real one if $r_a = \rho v/\rho u$ [120]. Regarding ENATE with FaP, an improvement of the number of points in a stencil is shown in the two top subfigures in Figure 3.22. The modified equation for the stencil (3.40) is

$$\frac{\partial}{\partial x}\left(\rho u\phi - \frac{\rho u \Delta x}{2}\frac{\partial \phi}{\partial x}\right) + r_a \frac{\partial}{\partial y}\left(\rho v\phi - \frac{\rho v \Delta y}{2}\frac{\partial \phi}{\partial y}\right) \simeq 0,$$

and for (3.42),

$$\frac{\partial}{\partial x}\left(\rho u\phi - \frac{\rho u \Delta x}{2}\frac{\partial \phi}{\partial x}\right) + \frac{2r_a}{1+r_a}\frac{\partial}{\partial y}\left(\rho v\phi\right) \simeq 0.$$

$\sqrt{\Delta x \Delta y}$	FV-CF	ENATE with REMEDIES
0.0707 ...	$1.6213 \cdot 10^{-1}$	$1.6213 \cdot 10^{-1}$
0.00707 ...	$9.0570 \cdot 10^{-1}$	$3.5737 \cdot 10^{-2}$
0.000707 ...	$5.0897 \cdot 10^{-2}$	

$\sqrt{\Delta x \Delta y}$	ENATE		
	FaP		REMEDIES
	3-point	4-point	
0.1	$2.1610 \cdot 10^{-1}$	$1.9541 \cdot 10^{-1}$	$1.5973 \cdot 10^{-1}$
0.01	$1.1652 \cdot 10^{-1}$	$8.9610 \cdot 10^{-1}$	$5.7161 \cdot 10^{-2}$
0.001	$6.5336 \cdot 10^{-2}$	$4.9686 \cdot 10^{-2}$	$2.5555 \cdot 10^{-2}$

TABLE 3.7: Example *Piecewise constant boundary condition*, the l_2-norm of the error with $\rho u \neq \rho v$ for the FV-CF and ENATE schemes.

With the information of ϕ_{SW}, numerical diffusion is made to disappear. However, FaP with $r_a \neq 1$ suffers from the same problems as FV-CF with $\Delta x = \Delta y$ due to the factors multiplying the former modified equations. It was verified that this was in fact the case, but if ρv is multiplied by $1/r_a$ in scheme (3.40) or $(1+r_a)/(2r_a)$ in scheme (3.42), we are able to get rid of this problem.

Finally, REMEDIES gives engaging results. In a mesh with $\Delta x = \Delta y$, the numerical diffusion along the discontinuity is reduced, but oscillations show up, middle left in Fig. 3.22. So ENATE with REMEDIES may be dispersive in nature. However, if the mesh is modified with $\Delta x = 2\Delta y$, we are able to get rid of those oscillations and move closer to the exact solution with small numerical diffusion. This behaviour is because specific points of the mesh lie in the discontinuity line which apparently is more adequate for obtaining more accurate β-derivatives, see Fig. 3.23. In Fig. 3.24 we plot $\phi(x, y)$ along a line perpendicular to the discontinuity from $(1, 0)$ to $(0.5, 1)$. It can be seen that a nonuniform REMEDIES reduces the numerical diffusion with small oscillations near the discontinuity. As an additional comparison the schemes above were also checked against the second-order NOTABLE scheme [148].

3.6.5 Rotating flow

We consider now a fluid flow rotating around the origin of coordinates in the absence of source. The BVP is

$$\begin{cases} \dfrac{\partial}{\partial x}\left(y\phi - \Gamma\dfrac{\partial \phi}{\partial x}\right) + \dfrac{\partial}{\partial y}\left(-x\phi - \Gamma\dfrac{\partial \phi}{\partial y}\right) = 0, & (x, y) \in (0, 1) \times (0, 1), \\ \phi(0, y) = g_1(y), \quad \partial_x \phi(1, y) = 0, & 0 \leq y \leq 1, \\ \phi(x, 1) = g_2(x), \quad \partial_y \phi(x, 0) = 0, & 0 \leq x \leq 1, \end{cases}$$

where two inlet profiles are set up. First, one linear $g_1(y) = y$, $g_2(x) = 1 - x$ and second, one with a hyperbolic tangent $g_1(y) = 0.5\,(1 + \tanh\,(10y - 5))$, $g_2(x) = 0.5\,(1 - \tanh\,(10x - 5))$. The first profile gives a smooth solution all over the domain contrary to the second one that shows a steep inner layer. As diffusion increases the layer becomes less and less steep, see Fig.

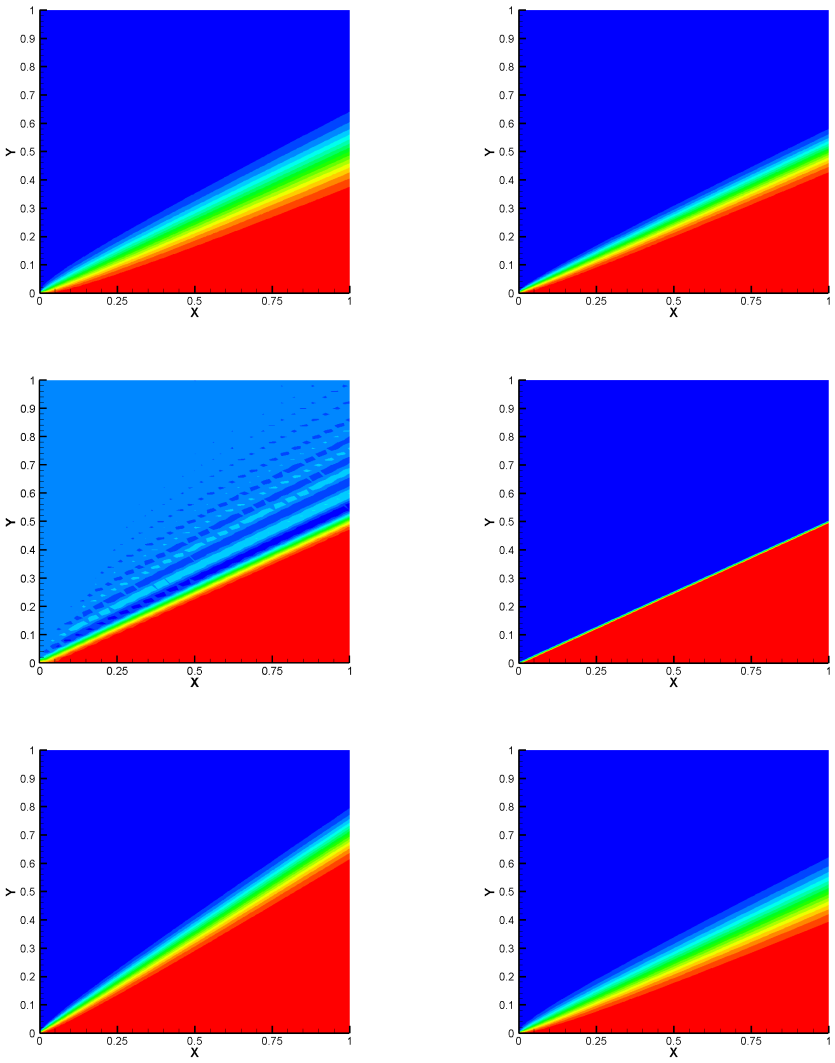

FIGURE 3.22: Example *Piecewise constant boundary condition*, numerical solutions in $\sqrt{\Delta x \Delta y} = 0.01$. **Top left**, 3-point ENATE with FaP. **Top right**, 4-point ENATE with FaP. **Middle left**, $\Delta x = \Delta y$ ENATE with REMEDIES. **Middle right**, $\Delta x \neq \Delta y$ ENATE with REMEDIES. **Bottom left**, $\Delta x = \Delta y$ FV-CF. **Bottom right**, $\Delta x \neq \Delta y$ FV-CF.

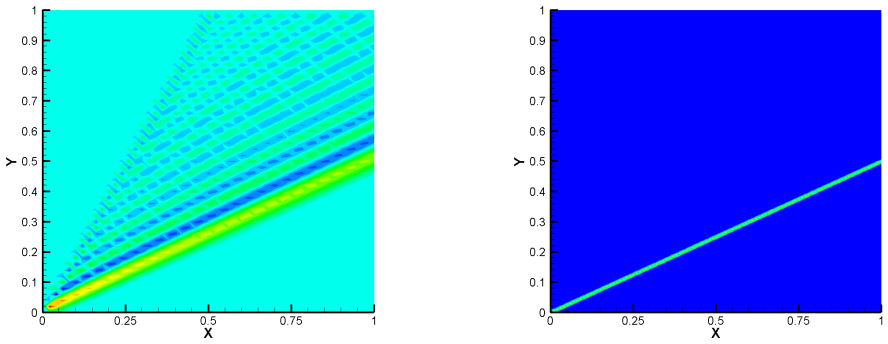

FIGURE 3.23: Example *Piecewise constant boundary condition*, numerical β field in $\sqrt{\Delta x \Delta y} = 0.01$ when $\Delta x = \Delta y$ (left) and $\Delta x = 2\Delta y$ (right).

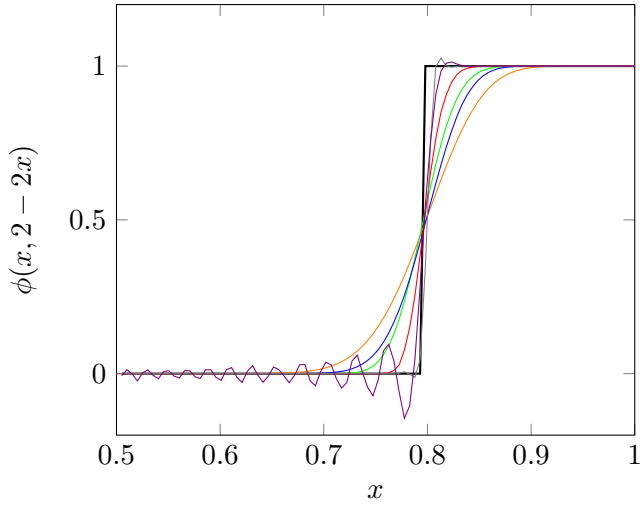

FIGURE 3.24: Example *Piecewise constant boundary condition*, profiles of the transport variable on a line $y = 2 - 2x$ in $\sqrt{\Delta x \Delta y} = 0.02$. **Black**, Exact. **Gray**, $\Delta x \neq \Delta y$ ENATE with REMEDIES. **Violet**, $\Delta x = \Delta y$ ENATE with REMEDIES. **Red**, NOTABLE. **Green**, 4-point ENATE with FaP. **Blue**, nonuniform FV-CF. **Orange**, 3-point ENATE with FaP.

3.25. The smaller the Γ values are, the closer the outlet profiles are to those at the inlet. Two diffusion coefficients were used: $\Gamma \in \{10^{-2}, 10^{-4}\}$. As no exact solution is known for this example, Richardson extrapolation is employed to obtain the reference value. Again, the FV-CF scheme in local flow adapted coordinates [210] is compared with ENATE. The results shown were carried out with Quintic Hermite spline in FaP and a Cubic Hermite spline with REMEDIES. The approaches used sixth-order CCS in case of FaP, fourth-order in case of REMEDIES and fourth-order CIR in both FaP and REMEDIES. Richardson extrapolation did not produce any conclusive result regarding the order of the scheme, although the simulations did converge. Only fourth-order CCS in FaP did not converge.

For the linear profile and for the hyperbolic profile the points used to compare schemes are $(0.5, 0.5)$ and $(0.4, 0.4)$, respectively. These points were chosen because they are where the solution starts to change rapidly

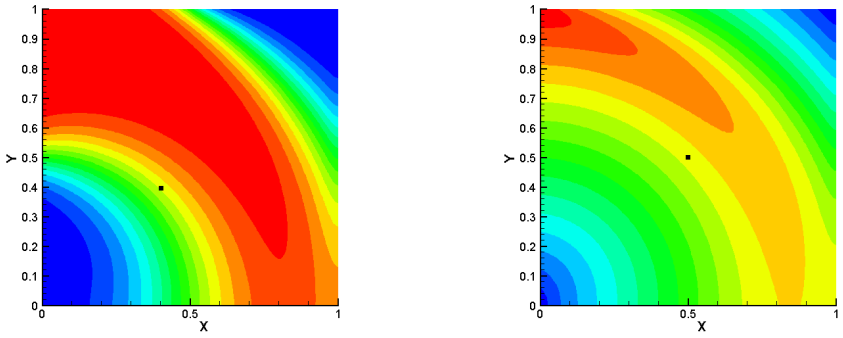

FIGURE 3.25: Example *Rotating flow*, ENATE numerical solution for $\Gamma = 10^{-2}$. Left, Hyperbolic profile; Right, Linear profile. Richardson interpolation at black square point $(0.4, 0.4)$, left; $(0.5, 0.5)$, right.

along the second diagonal. Table 3.8 shows the value of $\phi(0.5, 0.5)$ for the linear profile. In ENATE with FaP, the *Start-off* column refers to an initial solution removing the derivatives of the flux in (3.17d) whereas the *Iteration* column calculates those values of the right hand side and it keeps updating the integrals until the residuals are below a certain tolerance. Clearly, FaP achieves a mesh independent solution with only 40 nodes with $\Gamma = 10^{-2}$ or 80 nodes for $\Gamma = 10^{-4}$. REMEDIES took twice this number of nodes to attain it. In comparison, a 160 nodes FV-CF gives a similar $\phi(0.5, 0.5)$ as 20 nodes FaP with $\Gamma = 10^{-2}$, and 160 nodes FV-CF and 80 nodes FaP display the same behaviour with $\Gamma = 10^{-4}$. When the flow is convection-dominated ($\Gamma = 10^{-4}$) the numerical solution with ENATE in a 10x10 mesh blows up due to a bad resolution of the integrals. Table 3.9 presents results of the Richardson factor and order of convergence. The FV-CF scheme shows a second-order accuracy in both cases. ENATE with FaP is seventh-order with $\Gamma = 10^{-2}$ and almost sixth-order with $\Gamma = 10^{-4}$. ENATE with REMEDIES is third-order with $\Gamma = 10^{-2}$.

Γ	$\sqrt{\Delta x \Delta y}$	FV-CF	ENATE		
			FaP		REMEDIES
			Start-off	Iteration	
10^{-2}	10^{-1}	0.712002	0.698780	0.714575	0.714653
	$5 \cdot 10^{-2}$	0.713686	0.713777	0.714962	0.714973
	$2.5 \cdot 10^{-2}$	0.714608	0.715197	0.715007	0.715005
	$1.25 \cdot 10^{-2}$	0.714901	0.715097	0.715007	0.715007
	$6.25 \cdot 10^{-3}$	0.714980	0.715033	0.715007	0.715007
10^{-4}	10^{-1}	0.705217			
	$5 \cdot 10^{-2}$	0.707027	0.717594	0.706143	0.713433
	$2.5 \cdot 10^{-2}$	0.707168	0.715144	0.717198	0.708733
	$1.25 \cdot 10^{-2}$	0.707205	0.711263	0.707218	0.707199
	$6.25 \cdot 10^{-3}$	0.707215	0.709188	0.707218	0.707218

TABLE 3.8: Example *Rotating flow*, $\phi(0.5, 0.5)$ with six figures in the linear profile.

In the hyperbolic tangent case, Table 3.10 shows similar behaviour as

Γ	$\sqrt{\Delta x \Delta y}$	FV-CF	ENATE	
			FaP	REMEDIES
10^{-2}	10^{-1}	1.83 (0.87)	8.55 (3.10)	10.20 (3.35)
	$5 \cdot 10^{-2}$	3.14 (1.65)	151.60 (7.24)	13.84 (3.79)
	$2.5 \cdot 10^{-2}$	3.73 (1.90)	151.93 (7.25)	7.60 (2.93)
10^{-4}	10^{-1}	12.88 (3.69)		
	$5 \cdot 10^{-2}$	3.79 (1.92)	56.78 (5.83)	3.06 (1.62)
	$2.5 \cdot 10^{-2}$	4.00 (2.00)	56.97 (5.83)	-79.43

TABLE 3.9: Example *Rotating flow*, Richardson factor and the order of the scheme in brackets as a function of the mesh size for linear profile.

the linear one. ENATE either with FaP or with REMEDIES achieves a mesh-independent solution with 80 nodes for $\Gamma = 10^{-2}$, and with 160 nodes for $\Gamma = 10^{-4}$. Looking at Table 3.11, the FV-CF scheme shows an accuracy close to second-order although with $\Gamma = 10^{-4}$ an oscillation in the solution occurs that gives some unusual values of $RF_{\Delta x}$. ENATE with FaP is between sixth- and seventh-order with $\Gamma = 10^{-2}$ and fourth-order with $\Gamma = 10^{-4}$. Whenever the solution gets steeper in some region the order of accuracy decreases. ENATE with REMEDIES is fourth-order in both diffusion cases.

Γ	$\sqrt{\Delta x \Delta y}$	FV-CF	ENATE		
			FaP		REMEDIES
			Start-off	Iteration	
10^{-2}	10^{-1}	0.703646	0.690092	0.700945	0.701610
	$5 \cdot 10^{-2}$	0.702980	0.699863	0.701475	0.701492
	$2.5 \cdot 10^{-2}$	0.701933	0.701279	0.701480	0.701480
	$1.25 \cdot 10^{-2}$	0.701598	0.701446	0.701479	0.701479
	$6.25 \cdot 10^{-3}$	0.701509	0.701472	0.701479	0.701479
	$3.125 \cdot 10^{-3}$	0.701487	0.701478	0.701479	0.701479
10^{-4}	10^{-1}	0.751865			
	$5 \cdot 10^{-2}$	0.781566	0.723873	0.784815	0.785121
	$2.5 \cdot 10^{-2}$	0.785862	0.763420	0.785618	0.785605
	$1.25 \cdot 10^{-2}$	0.785862	0.763420	0.785618	0.785620
	$6.25 \cdot 10^{-3}$	0.785696	0.774244	0.785621	0.785621
	$3.125 \cdot 10^{-3}$	0.785642	0.780394	0.785621	0.785621

TABLE 3.10: Example *Rotating flow*, $\phi(0.4, 0.4)$ with six figures for a hyperbolic profile.

Finally, for this numerical example is not possible to compare the CPU time between FV-CF and ENATE. The reason is that both schemes were coded in different languages: FV-CF in MATLAB and ENATE in Fortran. Also, it is not appropriate to compare FaP and REMEDIES as they use different Hermite splines, but for instance, in the hyperbolic-inlet case and $\Gamma = 10^{-4}$, FaP run in 18.58 min and REMEDIES in 61.5 sec.

Γ	$\sqrt{\Delta x \Delta y}$	FV-CF	ENATE	
			FaP	REMEDIES
10^{-2}	10^{-1}	$0.64\,(-0.64)$	$121.96\,(6.93)$	$10.05\,(3.33)$
	$5 \cdot 10^{-2}$	$3.12\,(1.64)$	$115.04\,(6.85)$	$18.01\,(4.17)$
	$2.5 \cdot 10^{-2}$	$3.77\,(1.91)$	$94.68\,(6.56)$	$11.03\,(3.46)$
	$1.25 \cdot 10^{-2}$	$3.64\,(1.86)$	$90.72\,(6.50)$	-660.38
10^{-4}	10^{-1}	$6.70\,(2.74)$		
	$5 \cdot 10^{-2}$	-32.16	$18.83\,(4.23)$	$31.06\,(4.96)$
	$2.5 \cdot 10^{-2}$	$0.83\,(-0.27)$	$16.19\,(4.02)$	$18.62\,(4.22)$
	$1.25 \cdot 10^{-2}$	$3.06\,(1.61)$	$16.02\,(4.00)$	$13.90\,(3.80)$

TABLE 3.11: Example *Rotating flow*, Richardson factor and the order of the scheme in brackets as a function of the mesh size for hyperbolic profile.

3.6.6 Stommel's ocean model

Finally, this chapter is closed with an application in Geophysical Fluid Dynamics [249]: calculations of wind-driven ocean currents. We used Stommel theory [203] who proposed a transport equation for the stream-function in a convective ocean cell. Some simple models can be found in [106] and others more sophisticated in [154]. We start off with the steady Navier-Stokes (NS) equation in the Earth frame, i.e.

$$\nabla \cdot (\rho \mathbf{u}) = 0,$$
$$\nabla \cdot \left(\rho \mathbf{u} \otimes \mathbf{u} - \mu(\nabla \mathbf{u} + (\nabla \mathbf{u})^T)\right) = \rho \mathbf{f}_m - \nabla p' - 2\boldsymbol{\Omega} \times \rho \mathbf{u}.$$

The last term in the RHS of the momentum equation is the Coriolis force where $\boldsymbol{\Omega}$ is the Earth's angular velocity vector. The pressure, p', is the sum of the fluid pressure, p, the gravity contribution, $\rho g r$, and the centrifugal pressure, $-\rho \Omega^2 r_\perp^2/2$ where $r_\perp = |\mathbf{r}_\perp|$ is the perpendicular distance from the axis of rotation and $\Omega = |\boldsymbol{\Omega}|$. $\mathbf{f}_m$ is the external force per unit of mass and $\mathbf{u} \coloneqq (u, v, w)^T$ is the velocity field. The NS equations should be solved in spherical coordinates but in the phenomena studied here the curvature of the Earth can be neglected. This allows to use a local Cartesian coordinate system. This is called the *tangent-plane approximation*, see Fig. 3.26. No vertical velocity is assumed, $w = 0$, all variables are independent of z-axis, $\rho = \rho_0 =$ const., no dissipative effects are considered and a small Rossby number, what allows to drop the advection term. So, the NS equations become

$$\nabla \cdot \mathbf{u} = 0,$$
$$f_\theta \mathbf{u}^\perp = \mathbf{f}_m - \frac{1}{\rho_0} \nabla p',$$

where $\mathbf{u}^\perp \coloneqq (-v, u, 0)^T$, $f_\theta = 2\Omega \sin\theta$ and θ the latitude. In the vertical line, the centrifugal force can be neglected [221] and, therefore, we have hydrostatic pressure over z. Regarding Coriolis force, for small latitude variations

in the ocean cell, f_θ could be developed in Taylor series at a particular latitude θ_0, i.e.

$$f_\theta \simeq 2\Omega \sin\theta_0 + \frac{2\Omega\cos\theta_0}{R_E} R_E \Delta\theta = f_{\theta_0} + \left.\frac{\mathrm{d}f_\theta}{\mathrm{d}\theta}\right|_{\theta_0} y.$$

This is called the *beta-plane approximation*. On the other hand, the ocean model includes the wind force $\mathbf{f}_{\text{wind}}$ on the surface and a friction stress at the bottom proportional to the fluid velocity, i.e.

$$\mathbf{f}_m = \mathbf{f}_{\text{wind}} - \frac{R}{D}\mathbf{u}, \quad \mathbf{f}_{\text{wind}} = (f_{wx}, f_{wy}, 0)^T,$$

where R is some constant and D is the depth of the ocean at rest, constant in this model. The next step is to integrate the momentum equation from the bottom of the ocean, $z = 0$, to the surface, $z = D$. As no variable depends on z, the equation remains unchanged. Finally, we take the curl of both sides in the momentum equation,

$$f_\theta \nabla\times\mathbf{u}^\perp + \nabla f_\theta \times \mathbf{u}^\perp = \nabla\times\mathbf{f}_{\text{wind}} - \frac{R}{D}\nabla\times\mathbf{u}.$$

It can be seen that $\nabla\times\mathbf{u}^\perp = (0,0,\nabla\cdot\mathbf{u})^T = \mathbf{0}$ and $\nabla f_\theta = (0, (\mathrm{d}f_\theta/\mathrm{d}\theta)_{\theta_0}, 0)^T$ is a constant vector. If the stream-function is defined as $\mathbf{u}^\perp := \nabla\Psi$ and the vector $\nabla^\perp f_\theta := (-(\mathrm{d}f_\theta/\mathrm{d}\theta)_{\theta_0}, 0, 0)^T$, then

$$\begin{aligned}\nabla f_\theta \times \mathbf{u}^\perp &= (0,0,\nabla\cdot(\nabla^\perp f_\theta\,\Psi))^T,\\ \nabla\times\mathbf{u} &= (0,0,-\nabla^2\Psi)^T,\end{aligned}$$

and, therefore, the equation resulting in z direction is

$$\nabla\cdot\left(\nabla^\perp f_\theta\,\Psi - \frac{R}{D}\nabla\Psi\right) = (\nabla\times\mathbf{f}_{\text{wind}})_z,$$

which is clearly a transport equation for the stream function Ψ. The variation of Coriolis force is the convection-like parameter, the bottom friction acts as the diffusive term and the wind stress on the surface of the ocean cell as the source.

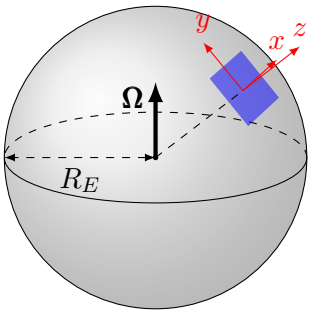

FIGURE 3.26: Example *Stommel's ocean model*, the tangent-plane approximation and Ocean cell (blue rectangle) on the Earth.

For the case to be solved, Stommel proposed a rectangular ocean area with wind force as

$$\mathbf{f}_{\text{wind}} = \left(\frac{F}{D}\cos\left(\frac{\pi}{b}y\right), 0, 0\right)^T.$$

The BVP for $\phi = \Psi(x, y)$ writes as follows:

$$\begin{cases} \dfrac{\partial}{\partial x}\left(\rho u\phi - \Gamma\dfrac{\partial\phi}{\partial x}\right) + \dfrac{\partial}{\partial y}\left(-\Gamma\dfrac{\partial\phi}{\partial y}\right) = S, & (x, y) \in (0, a) \times (0, b), \\ \phi(0, y) = 0, \quad \phi(a, y) = 0, & 0 \le y \le b, \\ \phi(x, b) = 0, \quad \phi(x, 0) = 0, & 0 \le x \le a, \end{cases}$$

where

$$\rho u = -\frac{D}{R}\left.\frac{\mathrm{d}f_\theta}{\mathrm{d}\theta}\right|_{\theta_0}, \quad \Gamma = 1, \quad S = \frac{Fb}{R\pi}\sin\left(\frac{\pi}{b}y\right).$$

The source function is zero at $y = 0$ and $y = b$ and follows the same sine function at $x = 0$ and $x = a$. Note that in the y direction there is no convection and the source only depends on y, the latitude. The model [203] uses the next set of constants:

$$D = 2 \cdot 10^2\,\mathrm{m}, \quad F = 0.3 \cdot 10^{-7}\,\mathrm{m^2 s^{-2}},$$
$$R = 0.6 \cdot 10^{-3}\,\mathrm{m s^{-1}}, \quad \left.\frac{\mathrm{d}f_\theta}{\mathrm{d}\theta}\right|_{64^\circ} = 10^{-11}\,\mathrm{m^{-1} s^{-1}},$$

and the domain is $a = 10^7$ m and $b = 2\pi \cdot 10^6$ m. The exact solution is given by

$$\phi = p\sin\left(\frac{\pi}{b}y\right)\left(\frac{\exp(q^- x) - \exp(q^+ x)}{\exp(q^- a) - \exp(q^+ a)} - \frac{\exp(q^- x) - 1}{\exp(q^- a) - 1}\right),$$

with

$$p = \frac{F}{R}\left(\exp(q^- a) - 1\right)\left(\frac{b}{\pi}\right)^3, \quad q^\pm = \frac{\rho u}{2} \pm \sqrt{\left(\frac{\rho u}{2}\right)^2 + \left(\frac{\pi}{b}\right)^2},$$

and plotted in Fig. 3.27a. It can be seen a boundary layer at $x = 0$ that mimics some western highly-concentrated streamlines in subtropical gyres [126, 155] such as the Gulf stream or the Kuroshio current, among others.

In this numerical test, only REMEDIES was computed. The reason was the long CPU time for the *cross-flux approach*. In addition, a nonuniform mesh is going to be used clustering nodes at the left boundary, what would increase substantially the execution time of ENATE with FaP. A drawback of CCS as originally devised is that it only works for a mesh of equal spacing. A modification of this numerical method dealing with a nonuniform mesh is described in Appendix E.

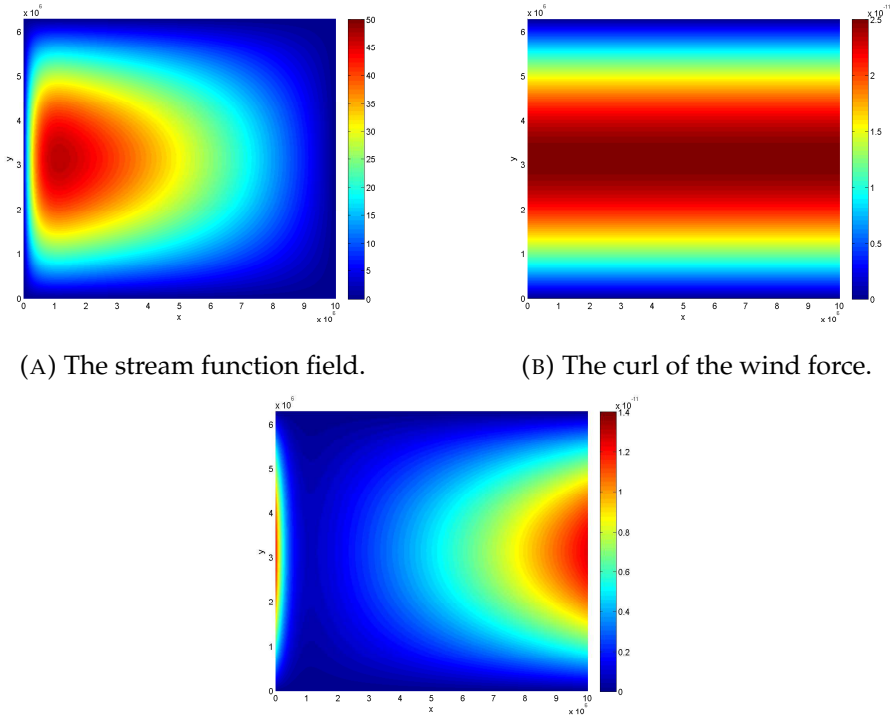

(A) The stream function field.

(B) The curl of the wind force.

(C) The β field for REMEDIES.

FIGURE 3.27: Example *Stommel's ocean model*, ocean problem for the Stommel box.

Regarding the boundary conditions, they are of Dirichlet type for the stream function. The values of β at boundaries can be shown to be

$$\beta(0, y) = \beta(a, y) = \frac{1}{2} S(y),$$
$$\beta(x, 0) = \beta(x, b) = 0.$$

The ENATE scheme with REMEDIES was run with Cubic, Quintic and Septic Hermite polynomials for different number of grid points in a uniform mesh. Convergence results are displayed in Fig. 3.28. It can be appreciated the good accuracy attained by ENATE as compared with the results with the high-order compact scheme presented in [29]. The CCS and cubic Hermite are fourth-order with cubic ENATE lying below CCS in the limited range of grid sizes where both can be compared. In terms of accuracy, quintic and septic behave close to what is theoretically predicted. Quintic is slightly better than sixth-order and septic is eighth-order, although when it approaches the machine accuracy region the order is somehow reduced.

To check the adequate behaviour of ENATE in nonuniform meshes with very large size ratio between contiguous intervals a test was carried out with the mesh divided in two zones, see Fig. 3.29. The first zone is always kept the same: 100 nodes covering $5 \cdot 10^5$ m. The second zone changes from nonuniform with smooth transition to uniform with extremely abrupt size transition. The results obtained are presented in Table 3.12. It can be observed that as the number of nodes is reduced the accuracy worsens. In the worst case, for which the size ratio where the two zones meet is around one hundred, the norms are of order 10^{-4}. That means that the ENATE

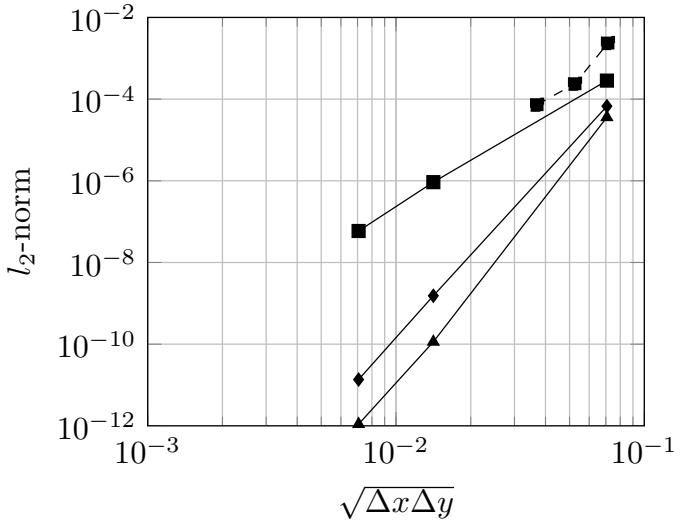

FIGURE 3.28: Example *Stommel's ocean model*, the l_2-norm of the error for the Stommel's ocean model in a $\Delta x = \Delta y$ mesh. ■ **and dashed line**, Chu & Fun combined compact difference. ■ **and solid line**, ENATE with REMEDIES using Cubic Hermite. ♦, Quintic Hermite. ▲, Septic Hermite.

Mesh	l_1	l_2	l_∞
200×100 nice	$6.31 \cdot 10^{-8}$	$7.49 \cdot 10^{-8}$	$1.44 \cdot 10^{-7}$
(100+100)×100	$5.95 \cdot 10^{-7}$	$9.50 \cdot 10^{-7}$	$3.36 \cdot 10^{-6}$
(100+50)×100	$1.15 \cdot 10^{-5}$	$1.64 \cdot 10^{-5}$	$5.27 \cdot 10^{-5}$
(100+25)×100	$2.05 \cdot 10^{-4}$	$2.72 \cdot 10^{-4}$	$6.68 \cdot 10^{-4}$

TABLE 3.12: Example *the Stommel's ocean model*, norms of some run cases in non-uniform meshes.

treatment for abrupt size transition works quite well.

Finally, other uniform meshes were studied keeping $\Delta x = 1.6\Delta y$. The l_2-norm of the error is found in Fig. 3.30. Similar orders of convergence for Hermite are obtained compared to the $\Delta x = \Delta y$ mesh test: cubic is fourth-order whereas quintic is sixth-order and septic is almost eighth-order. Even so, the accuracy compared with the uniform mesh, Fig. 3.28, increased. Regarding CPU time, Table 3.13, it was observed that an increase in the number of sweeps in the matrix solver sometimes reduces the execution time. In coarse meshes, the CPU time was almost the same for all splines. The maximum time was around 5 min. with quintic.

Mesh	Sweeps×4	CPU time [s]		
		Cubic	Quintic	Septic
320×200	450	252		
	500	244	308	307
	550	217	300	300
	600	217	329	327
	650	192		
	700	210		
160×100	75			26
	100	14.9	18.7	20.5
	150	13.6	17.9	23
	200	13.1	20.8	30
	250	12.6	29.2	
	300	13.2		
80×50	20	0.9		1.2
	25			1
	30	0.7	0.9	1
	35		0.8	0.85
	40	0.6	0.8	0.95
	45		0.7	
	50	0.76	0.8	
40×25	5	0.1	0.13	0.15
	10	0.06	0.06	0.09
	15		0.06	0.12
	20			0.15

TABLE 3.13: Example *Stommel's ocean model*, number of sweeps and CPU time in seconds for some nonuniform mesh sizes.

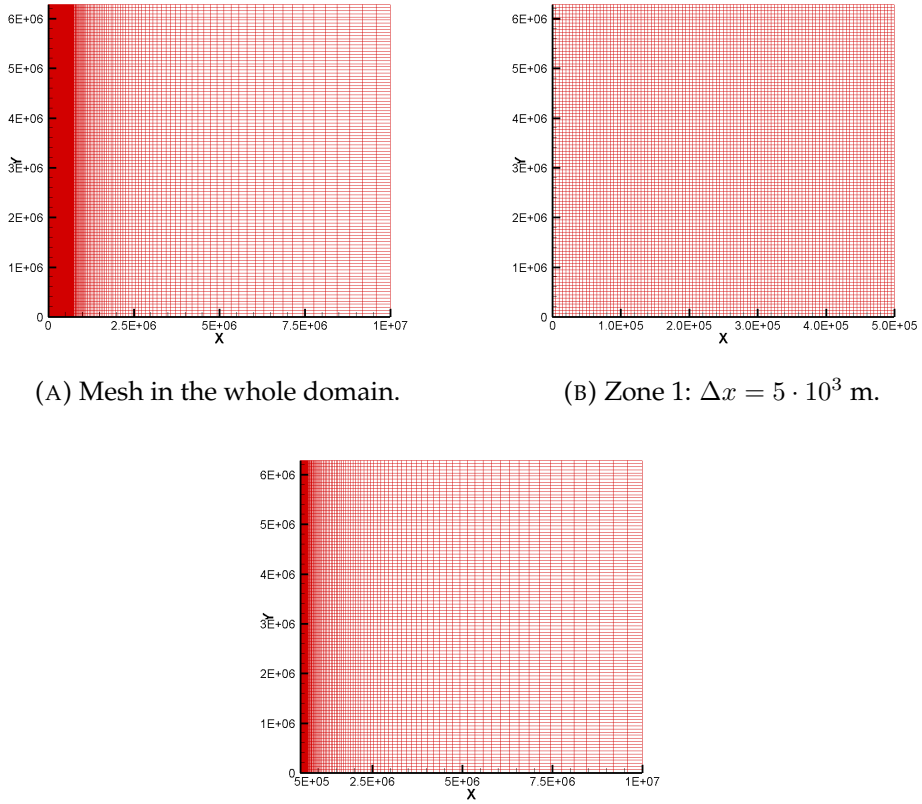

(A) Mesh in the whole domain.

(B) Zone 1: $\Delta x = 5 \cdot 10^3$ m.

(C) Zone 2: $\Delta x_o = 5 \cdot 10^3$ m, $\Delta x_f = 4 \cdot 10^5$ m.

FIGURE 3.29: Example *Stommel's ocean model*, non-uniform mesh.

3.7 In Closing

In this chapter, three approaches were devised for modelling steady-state two-dimensional problems based on the one-dimensional exponential flux.

The first formulation consists of a dimensionality reduction transforming a PDE to a first-order ODE via the stream-function coordinates. The result yielded a two-point upwind stencil where the information is propagated on streamlines. The counterpart is that it can only work for convection-only problems and that the computation of iso-ψ and iso-φ lines may become tough. An in-depth analysis may be of interest in order to know how the accuracy is reduced when a tiny diffusion exists in the problem or the streamline is too twisted. How vortex lines should be dealt with? How the boundary condition is imposed in such a situation? Although its limitations, the approach gave the best l_2-norm for the 2D Burgers' equation.

The other two formulations consist of a coordinate splitting (FaP) and an axial splitting (REMEDIES). Both approaches solve two pseudo-1D transport equations, but the first one sets the derivative of $\mathcal{F}$ in the other coordinate as pseudo-source, whereas in the latter the source S is redistributed in each axis by a β field. The new coefficients in the 2D approaches are formed by the one-dimensional ones. So, they keep a compact computational molecule, a five-point stencil, and the same numerical features. In

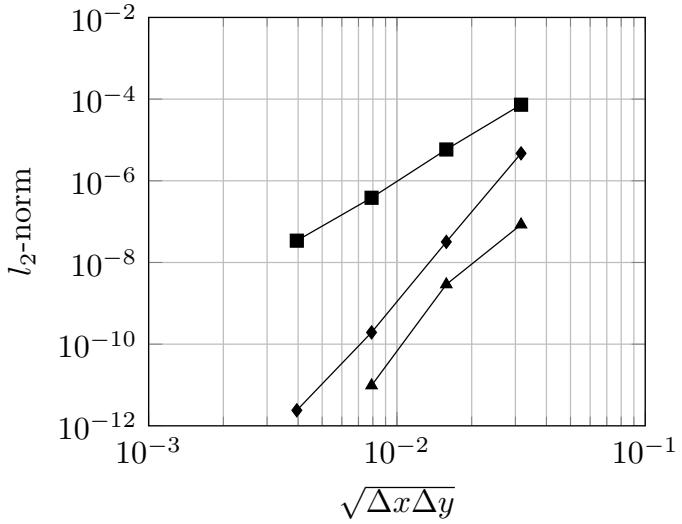

FIGURE 3.30: Example *Stommel's ocean model*, the l_2-norm of the error for the Stommel's ocean model in a $\Delta x = 1.6\Delta y$ mesh. ■ **and solid line**, ENATE with REMEDIES using Cubic Hermite. ♦, Quintic Hermite. ▲, Septic Hermite.

the numerical cases computed both FaP and REMEDIES give similar accuracy in some cases. In others REMEDIES performs better, for instance, a sixth-order REMEDIES is more accurate than a sixth-order FaP. The major improvement of REMEDIES is in the CPU time. REMEDIES is faster than FaP due to the amount of operations per iteration and the number of iterations to get convergence. The required CPU time of REMEDIES is of the order of seconds or minutes, FaP requires minutes or hours. Also, we note that REMEDIES takes more time as Péclet number gets smaller whereas with FaP is the opposite.

An example was carried out with a non-uniform mesh. Although the accuracy was slightly reduced in comparison to a uniform mesh, it gave reasonable results for expansion ratios as large as ten.

Chapter 4

Paradigm shift: time-dependent ENATE

Goals:

- To carry over the ideas of steady two-dimensional modelling to solve unsteady 1D problems

4.1 Unsteady flow problems

In the previous chapter, three approaches were developed for accurately solving the steady 2D transport equation. However, flow variables may vary temporarily due to the nature of the flow processes. Flows through pipe bends [253], separated flow [193] or vortex shedding [98, 185, 208], just to name a few, are intrinsically unsteady. In such a case, a temporal term is added to the conservation law (3.10),

$$\frac{\partial \rho\phi}{\partial t} + \nabla \cdot (\rho \mathbf{u}\phi - \Gamma \nabla\phi) = S,$$

which takes into account time-dependent phenomena in convection-diffusion problems. This chapter deals with unsteady 1D transport equations, i.e.,

$$\frac{\partial \rho\phi}{\partial t} + \frac{\partial}{\partial x}\left(\rho u\phi - \Gamma \frac{\partial \phi}{\partial x}\right) = S, \qquad x_{B1} < x < x_{B2}, \;\; t > 0, \tag{4.1a}$$

$$\phi(x,0) = \phi^0(x), \qquad x_{B1} \leq x \leq x_{B2}, \tag{4.1b}$$

$$\phi(x_{B1},t) = \phi_{B1}(t), \;\; \phi(x_{B2},t) = \phi_{B2}(t), \qquad t \geq 0. \tag{4.1c}$$

The initial value is $\phi^0(x)$ and $\phi_{B1}(t)$ and $\phi_{B2}(t)$ are the boundary values. A Dirichlet BC is assumed but it can be of any other type. A possible way to discretize this PDE may start by carrying out an integration over the control volume $[x_W, x_C]$,

$$\int_{x_W}^{x_C} \frac{\partial \rho\phi}{\partial t} \mathrm{d}x + \mathcal{F}_{x\,C} - \mathcal{F}_{x\,W} = IS_{01}|_{WC}\,,$$

After substituting the exact 1D flux, see Appendix A, one finally arrives at a first order ODE

$$\Delta x_{WC} \frac{\mathrm{d}\overline{\rho\phi}^x}{\mathrm{d}t} - A_W\phi_W + A_C\phi_C - A_E\phi_E = b_C,$$

being $\overline{\rho\phi}^x$ the spatial average of $\rho\phi$ in $[x_W, x_C]$, whereas A_i and b_C are summarized in Chapter 2. The average of a generic variable z in a coordinate ξ is defined as

$$\overline{z}^{\xi} := \frac{1}{\Delta\xi}\int_{\xi_j}^{\xi_j+\Delta\xi} z\,\mathrm{d}\xi.$$

The next step is to compute $\overline{\rho\phi}$ via any quadrature and discretize $\mathrm{d}\overline{\rho\phi}/\mathrm{d}t$. In order to avoid some simplifications in the integral evaluation and the use of time integration methods, one could solve the problem (4.1a) by using the ideas put forward in previous chapter. Consider a new spatial dimension $\eta = ct$ where c is an arbitrary velocity, constant and positive. The unsteady 1D transport equation is rewritten as follows:

$$\frac{\partial}{\partial\eta}(\rho c\phi) + \frac{\partial}{\partial x}\left(\rho u\phi - \Gamma\frac{\partial\phi}{\partial x}\right) = S.$$

Looking at this equation, one may consider the temporal term akin to a diffusionless transport phenomenon with ρc a convection-like parameter. Then, its numerical solution can be computed using the same ideas explained in steady two-dimensional modelling: the cross-flux approach and the source redistribution approach. The streamline approach will no longer be considered.

4.1.1 A note and clarification

In this section parabolic problems in time as well as elliptical in the spatial coordinate will be treated. Although the discrete equations move forward in physical time, it is necessary to update the discrete sources containing either the flux derivatives or the redistribution coefficient $\beta(x,t)$ along the whole time coordinate. Therefore, $\phi(x,t)$ at all discrete times and spatial points must be computed and available.

4.2 Unsteady cross-flux

Let us start by defining the fluxes in (x,η)-domain as

$$\boldsymbol{\mathcal{F}} = (\mathcal{F}_x, \mathcal{F}_\eta)^T := \left(\rho u\phi - \Gamma\frac{\partial\phi}{\partial x}, \rho c\phi\right)^T.$$

Mimicking the numerical background on page 81, the decomposition gives two differential equations:

$$\frac{\partial}{\partial x}\left(\rho u\phi - \Gamma\frac{\partial\phi}{\partial x}\right) = S - \frac{\partial\mathcal{F}_\eta}{\partial\eta} =: S_x, \tag{4.2a}$$

$$\frac{\partial}{\partial\eta}(\rho c\phi) = S - \frac{\partial\mathcal{F}_x}{\partial x} =: S_\eta. \tag{4.2b}$$

The interval size $\Delta\eta$ is $c\Delta t$, $\eta_n = nc\Delta t$, and the notation used for any variable z is $z(\eta_n, x_i) = z_i^n$ or $z(\eta_n, x_C) = z_C^n$. The discretization of the first

equation is the usual one,

$$-A^n_W\phi^n_W + A^n_{x\,C}\phi^n_C - A^n_E\phi^n_E = b^n_{x\,C},$$

with

$$b^n_{x\,C} = IS_{x\,01}|^n_{WC} + \left(\frac{IS_xGE_{x\,01}}{IGE_{x\,01}}\bigg|^n_{CE} - \frac{IS_xGE_{x\,01}}{IGE_{x\,01}}\bigg|^n_{WC} \right),$$

at a time level n. On the other hand, the second equation is discretized by integrating in time from η_{n-1} to η_n at a constant x-coordinate, x_C, i.e.

$$(\rho c)^n_C\phi^n_C - (\rho c)^{n-1}_C\phi^{n-1}_C = b^n_{\eta\,C},$$

with

$$b^n_{\eta\,C} = \int_{\eta_{n-1}}^{\eta_n} S_{\eta\,C}\,\mathrm{d}\eta,$$

where $S_{\eta\,C} = S_\eta(\eta, x_C)$. Finally, the two discrete equations can be added forming a four-point stencil, see Figure 4.1. Defining the vectors,

$$\begin{aligned}
\boldsymbol{\rho}\mathbf{c}^n &\coloneqq ((\rho c)^n_{B1}, \ldots, (\rho c)^n_C, \ldots, (\rho c)^n_{B2})^T,\\
\boldsymbol{\phi}^n &\coloneqq (\phi^n_{B1}, \ldots, \phi^n_W, \phi^n_C, \phi^n_E, \ldots, \phi^n_{B2})^T,\\
\mathbf{b}^n &\coloneqq \left(b^n_{\eta\,B1} + b^n_{x\,B1}, \ldots, b^n_{\eta\,C} + b^n_{x\,C}, \ldots, b^n_{\eta\,B2} + b^n_{x\,B2}\right)^T,
\end{aligned}$$

and the matrices,

$$\begin{aligned}
\mathbf{A}^n &\coloneqq \text{tridiag}(-A^n_W, A^n_{x\,C}, -A^n_E),\\
\mathbf{C}^n &\coloneqq \text{diag}(\boldsymbol{\rho}\mathbf{c}^n),\\
\mathbf{P}^n &\coloneqq \mathbf{C}^n + \mathbf{A}^n,
\end{aligned}$$

the system,

$$\mathbf{P}^n\boldsymbol{\phi}^n = \mathbf{C}^{n-1}\boldsymbol{\phi}^{n-1} + \mathbf{b}^n, \quad n \geq 1,$$

is made up to get the numerical solution of the problem (4.1a). For $n = 1$, $\boldsymbol{\phi}^0 = \phi^0(\mathbf{x})$ where $\mathbf{x} = (x_{B1}, \ldots, x_C, \ldots, x_{B2})^T$. On the other hand, $\mathbf{P}^n$ is still tridiagonal so TDMA may be used. The velocity in the transformed temporal term will always be taken as $1\,\mathrm{m/s}$ but it will be kept in the formulae out of dimensional consistency.

The procedure to compute $b^n_{x\,C}$ was explained on page 86 and $b^n_{\eta\,C}$ is computed via CCS+CIR, page 86 and 97. Regarding stability, the previous discrete equation is implicit so a diagonally dominant $\mathbf{P}^n$ matrix should be guaranteed to have a bounded solution.

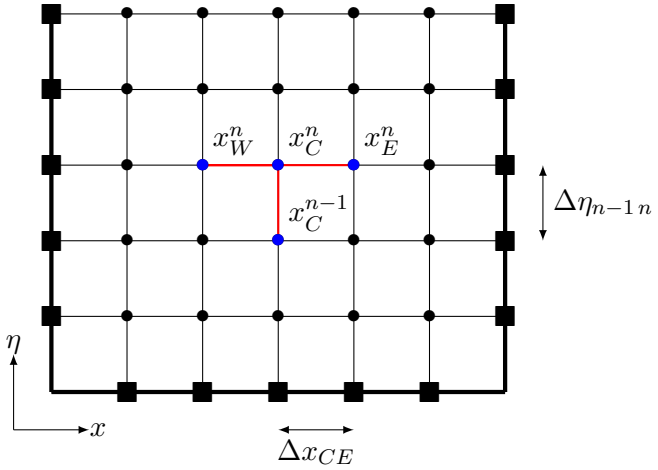

FIGURE 4.1: Space-time discrete domain, stencil in red lines. ■ Boundary and initial values, • Inner values

4.3 Unsteady redistribution coefficient

For the second approach developed in the previous chapter, the calculations follow the same path but now with different expressions. At a given computational iteration denoted by the superscript $\star$, the pseudo-ODEs that rule $\phi_1^\star$ and $\phi_2^\star$ are

$$\frac{\partial}{\partial x}\left(\rho u\phi_1^\star - \Gamma\frac{\partial\phi_1^\star}{\partial x}\right) = \frac{1}{2}S + \beta^\star =: S_x,$$
$$\frac{\partial}{\partial \eta}\left(\rho c\phi_2^\star\right) = \frac{1}{2}S - \beta^\star =: S_\eta.$$

Their numerical solutions may be achieved by taking the same discrete equations from the previous section. In order to get ϕ, $\phi_2^\star$ must be updated by its increment $\Delta\phi_2^\star$. With a bit of algebra and repeating the same steps as in page 92, assuming Γ is independent of ϕ, the discrete equation for the increment writes in matrix form

$$\widetilde{\mathbf{P}}^n\boldsymbol{\Delta\phi_2^\star}^n = \mathbf{C}^{n-1}\boldsymbol{\Delta\phi_2^\star}^{n-1} + r_a\mathbf{A}^n\left(\boldsymbol{\phi_1^\star}^n - \boldsymbol{\phi_2^\star}^n\right) + \mathbf{v}_{\boldsymbol{\phi}}^{\star\,n}, \quad n \geq 1,$$

where the principal matrix is defined as $\widetilde{\mathbf{P}}^n := \mathbf{C}^n + r_a\mathbf{A}^n$, the vectors as

$$\boldsymbol{\phi_1^\star}^n := \left(\phi_{B1}^n, \ldots, \phi_{1\,W}^{\star\,n}, \phi_{1\,C}^{\star\,n}, \phi_{1\,E}^{\star\,n}, \ldots, \phi_{B2}^n\right)^T,$$
$$\boldsymbol{\phi_2^\star}^n := \left(\phi_{B1}^n, \ldots, \phi_{2\,W}^{\star\,n}, \phi_{2\,C}^{\star\,n}, \phi_{2\,E}^{\star\,n}, \ldots, \phi_{B2}^n\right)^T,$$
$$\boldsymbol{\Delta\phi_2^\star}^n := \left(0, \ldots, \Delta\phi_{2\,W}^{\star\,n}, \Delta\phi_{2\,C}^{\star\,n}, \Delta\phi_{2\,E}^{\star\,n}, \ldots, 0\right)^T,$$

the aspect ratio as $r_a := \Delta\eta_{n-1\,n}/\max\{\Delta x_{WC}, \Delta x_{CE}\}$ and $\mathbf{v}_{\boldsymbol{\phi}}^{\star\,n}$ is related to the possible source dependence on the solution. The initial value is $\boldsymbol{\Delta\phi_2^\star}^0 = \mathbf{0}$. Finally, $\beta_C^{\star\,n}$ is updated with its increment given by

$$\boldsymbol{\Delta\beta}^{\star\,n} = \frac{\mathbf{C}^{n-1}\boldsymbol{\Delta\phi_2^\star}^{n-1} - \mathbf{C}^n\boldsymbol{\Delta\phi_2^\star}^n + \mathbf{v}_{\boldsymbol{\beta}}^{\star\,n}}{\Delta},$$

being $\Delta \coloneqq \Delta\eta_{n-1\,n}$ the step size, the vector $\boldsymbol{\Delta\beta^\star}^n \coloneqq (0,\dots,\Delta\beta_C^{\star n},\dots,0)^T$ and $\mathbf{v}_{\boldsymbol{\beta}}^{\star n}$ silimar to $\mathbf{v}_{\boldsymbol{\phi}}^{\star n}$. Either in the discrete equations for $\Delta\phi_2$ or $\Delta\beta$, if the source S is independent of the solution, $\mathbf{v}_{\boldsymbol{\phi}}^{\star n} = \mathbf{v}_{\boldsymbol{\beta}}^{\star n} = \mathbf{0}$. Otherwise,

$$\mathbf{v}_{\boldsymbol{\phi}}^{\star n} = \frac{1}{2}\left[\mathrm{diag}(\boldsymbol{\Delta x})\overline{\boldsymbol{\Delta S_2^\star}^n}^x + \mathrm{diag}(\boldsymbol{\Delta\eta})\overline{\boldsymbol{\Delta S_2^\star}^n}^\eta\right],$$
$$\mathbf{v}_{\boldsymbol{\beta}}^{\star n} = \frac{1}{2}\,\mathrm{diag}(\boldsymbol{\Delta\eta})\overline{\boldsymbol{\Delta S_2^\star}^n}^\eta.$$

where $\boldsymbol{\Delta x}$ and $\boldsymbol{\Delta\eta}$ are vectors containing the interval lengths in each interval of the domain to take into account a nonuniform mesh. $\overline{\boldsymbol{\Delta S_2^\star}^n}^x$ and $\overline{\boldsymbol{\Delta S_2^\star}^n}^\eta$, are average integrals over each interval in x- and η-direction computing with CIR. Again, being $\widetilde{\mathbf{P}}^n$ diagonally dominant is sufficient condition for stability in $\Delta\phi_2$.

4.4 Numerical Examples

Three numerical tests to assess high resolution in transient problems are provided. All of them have an exact solution so the l_2-norm is calculated in the space-time domain as well as the l_1-norm at a given time for the last one. The definitions of these norms are given on page 58 and 99.

4.4.1 Unsteady homogeneous one-dimensional convection-diffusion problem

The equation solved is an unsteady transport equation in a domain of unit length for a time $t \in (0,T]$, i.e.

$$\begin{cases} \dfrac{\partial\rho\phi}{\partial t} + \dfrac{\partial}{\partial x}\left(\rho u\phi - \Gamma\dfrac{\partial\phi}{\partial x}\right) = 0, & (x,t) \in (0,1)\times(0,T], \\ \phi(0,t) = 0, & t \in (0,T], \\ \phi(x,0) = \exp(5x)\sin(\pi x), & x \in (0,1). \end{cases}$$

with $\rho = 1$, $u = 0.1$, $T = 1$ and $\Gamma = 0.01$. The solution is $\phi(x,t) = \exp(5x - t(0,01\pi^2 + 0,25))\sin(\pi x)$ and plotted in Figure 4.2.

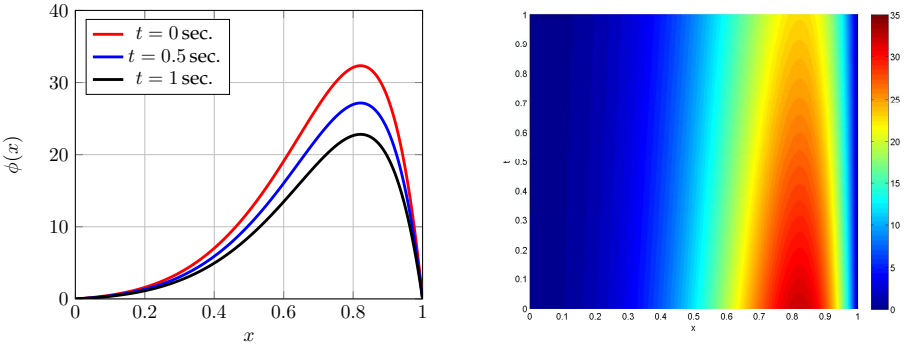

(A) Profile solution. (B) Space-time domain.

FIGURE 4.2: Example *Unsteady homogeneous one-dimensional convection-diffusion problem*, exact solution.

As explained earlier, the case has been run with both approaches, FaP and REMEDIES, as a two-dimensional convection diffusion equation with a pseudo-spatial coordinate $\eta = ct$, $c = 1$. A uniform mesh is employed in both coordinates with $\Delta\eta = \Delta x$.

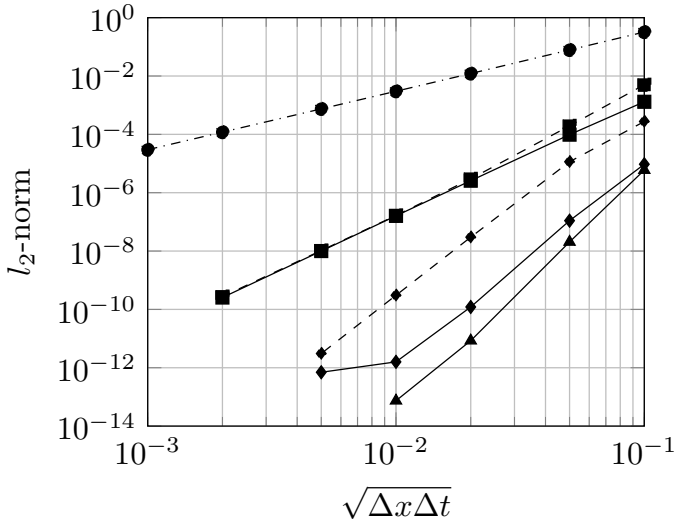

FIGURE 4.3: Example *Unsteady homogeneous one-dimensional convection-diffusion problem*, the l_2-norm of the error for ENATE comparing with a traditional numerical scheme. Solid lines are for REMEDIES and dashed lines are for FaP. • Crank-Nicolson ■ Cubic Hermite. ♦ Quintic Hermite. ▲ Septic Hermite.

In Figure 4.3 norms of FaP and REMEDIES are compared against each other as well as with a traditional scheme like Crank-Nicolson. All schemes conform to their theoretical order of accuracy: Crank-Nicolson is second order, and all mth-order Hermite polynomials are of $(m + 1)$th order of accuracy. The CPU time is always of the order of one second except for the finest meshes. Cubic-REMEDIES with a mesh of 500×500 takes 40 seconds, and Quintic-REMEDIES for a mesh of 200×200, 26.4 seconds. Only a sweep is required to estimate $\Delta\phi_2$ which makes the difference in CPU time for both approaches more noticeable, always in favour of REMEDIES.

Cubic Hermite provides the same norms for both approaches. Quintic-REMEDIES is roughly two orders of magnitude better than Quintic-FaP, both being sixth-order in most part of the graph. Roundoff errors build up for the finest mesh with Quintic-REMEDIES, and as a consequence there is barely any difference in the l_2-norm with the next coarser grid. Septic-REMEDIES is between eighth- and ninth-order.

As mentioned above it is not necessary to perform more than one sweep in the estimation of $\Delta\phi_2$. It seems that having one time coordinate makes the domain strongly connected through all points along this coordinate and allows a quick estimate of $\Delta\phi_2$. In the case of Poisson equation the connection is weaker and it takes more sweeps to get a good value. This is only due to our strategy of sweeping the 2D domain line-by-line, had we used another procedure to invert the coefficient matrix the conclusions about the

computer time associated to various Péclet numbers would have been different.

CPU time for FaP is much longer for all runs. To give an idea, for cubic Hermite and the 500×500 mesh, FaP takes about 1 hour of CPU time, two orders of magnitude more than REMEDIES.

4.4.2 Unsteady inhomogeneous one-dimensional convection problem

The equation solved is an unsteady inhomogeneous transport equation in a domain of unit length for a time $t \in (0, T]$, i.e.

$$\begin{cases} \dfrac{\partial \rho\phi}{\partial t} + \dfrac{\partial}{\partial x}(\rho u \phi) = -\dfrac{\phi}{\tau}, & (x,t) \in (0,1) \times (0,T], \\ \phi(0,t) = \exp(-t/\tau)\sin(-\pi u t), & t \in (0,T], \\ \phi(x,0) = \sin(\pi x), & x \in (0,1). \end{cases}$$

with $\rho = 1$ and $T = 1$. The exact solution is $\phi(x,t) = \exp(-t/\tau)\sin(\pi(x - ut))$ and plotted in Figure 4.11. Parameter τ is a characteristic time of decay. Four cases were studied, two values of $\tau \in \{0.05, 0.5\}$, corresponding to a quick decay and a relatively mild one, combined with two values of velocity, $u \in \{1, 10\}$. This hyperbolic equation with a relaxation source term that is relatively stiff [245] mimics the Boltzmann equation in the absence of the local equilibrium distribution [13]. Boltzmann equation is currently one of the cutting edge technique to solve Navier-Stokes equations [42, 80, 135, 194].

The source depends linearly on the solution and has to be updated in every iteration. Remind that if Péclet goes to infinity the upwind source integral is the only contribution of the right-hand side. In FaP this integral is calculated with CIR [118]. With REMEDIES, Hermite polynomial integration is used.

In our implementation the equation for $\Delta\phi_2^\star$ is employed to update the solution. $\Delta\phi_1^\star$ in the source is considered to be equal to $\Delta\phi_2^\star$ during the whole updating process. The reason is that explained on page 96.

In Figure 4.4 the convergence pattern of two cases of cubic Hermite, one with no source in the RHS of $\Delta\phi_2^\star$ equation and the other with it, is shown. Both runs start from scratch with a mesh of 500×500. The main difference between both approaches lies in the initial increase of the norm during the first iterations. When including the extra source this increase is much less pronounced what makes the convergence quicker in the initial stages. In both runs there is a noticeable change of slope when the norm reaches the region of low values. This is related to the relative importance of the neglected $\Delta\beta^\star$ terms compared to the considered ones. When the neglected integrals are much less than the terms kept in the RHS associated to $\phi_1^\star - \phi_2^\star$ the convergence is very quick, whereas it slows down considerably if they are of the same order. For a large interval of the convergence curve the two curves lie on top of each other. A criterion to decide whether including or not the $\Delta\phi_2^\star$ source can be the time taken for both approaches to reach a certain l_2-norm, for instance 10^{-6}. Well, the run with no source takes 23 s and that with source 30 s. At least in this case it is not worth to include it.

It may well be that in other computational tests the inclusion of this source makes a favourable difference.

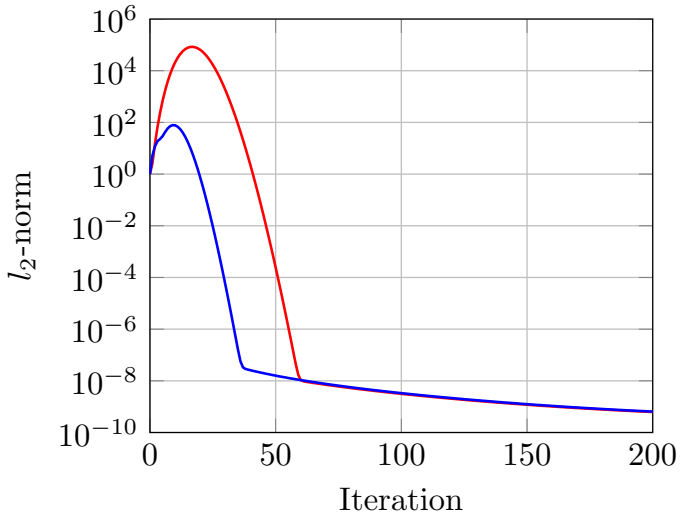

FIGURE 4.4: Example *Unsteady inhomogeneous one-dimensional convection problem*, the l_2-norm of the error versus number of iterations in REMEDIES for a 500×500 mesh. Red line with $\Delta\phi_2^{\star}$ source. Blue line without $\Delta\phi_2$ source

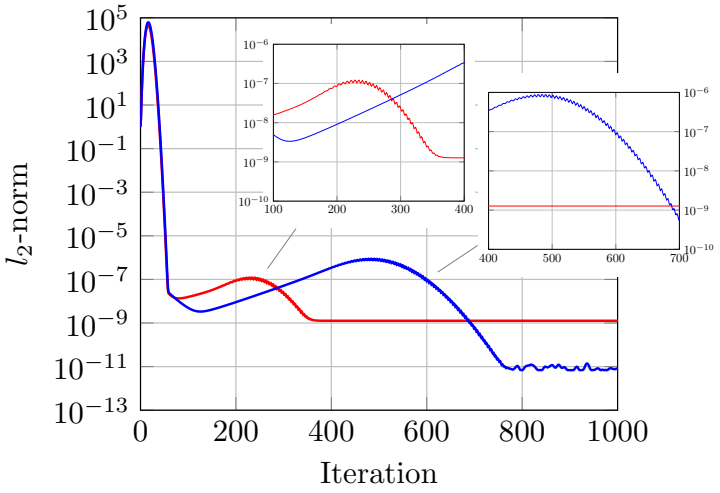

FIGURE 4.5: Example *Unsteady inhomogeneous one-dimensional convection problem*, the l_2-norm of the error versus number of iterations in REMEDIES. Red line, 100×100. Blue line, 200×200.

In this test problem the convergence pattern has some ups and downs for some combinations of meshes and Hermite polynomials. In Figure 4.5 the l_2-norm is plotted against the number of iterations for two meshes 100×100 and 200×200 with quintic Hermite. This hilly behaviour always appears for quintic and septic Hermite polynomials and relatively fine grids. Moreover, in the downward part of the convergence hill the curve is mildly oscillatory that may suggest that the process of convergence is more unstable in these cases. For very coarse grids, 10×10 and 20×20, there is a slight rise in the norm during several iterations that can barely be noticed.

In Figures 4.6 and 4.7 the l_2-norm is depicted for $\tau = 0.05$ and the two velocity cases, $u = 1$ and $u = 10$, with FaP and REMEDIES. Cubic Hermite behaves as a fourth order scheme. Quintic Hermite with FaP is sixth order but with REMEDIES is seventh-order for some intervals. Septic Hermite behaviour is pretty close to that of Quintic Hermite.

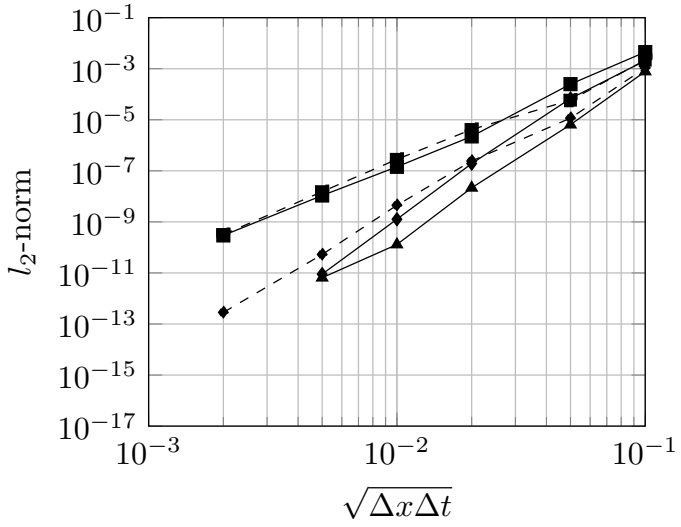

FIGURE 4.6: Example *Unsteady inhomogeneous one-dimensional convection problem*, the l_2-norm of the error for $\tau = 0.05$ and $u = 1$. ■ Cubic Hermite. ♦ Quintic Hermite. ▲ Septic Hermite. Solid line, REMEDIES. Dashed line, FaP.

The two cases for $\tau = 0.5$ are shown in figures 4.8 and 4.9. No significant differences with the previous case are seen.

In the four cases computed Cubic Hermite with FaP is better than REMEDIES, especially for the case $u = 10$, $\tau = 0.5$, where a difference of three orders of magnitude in the l_2-norm is observed. The reason for such a huge gap is still unknown. The difference is also present in the rest of cases, yet in milder form.

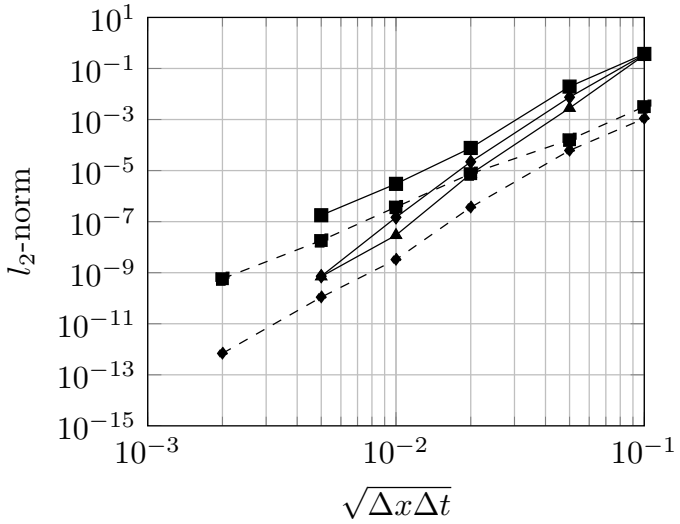

FIGURE 4.7: Example *Unsteady inhomogeneous one-dimensional convection problem*, the l_2-norm of the error for $\tau = 0.05$ and $u = 10$. ■ Cubic Hermite. ♦ Quintic Hermite. ▲ Septic Hermite. Solid line, REMEDIES. Dashed line, FaP.

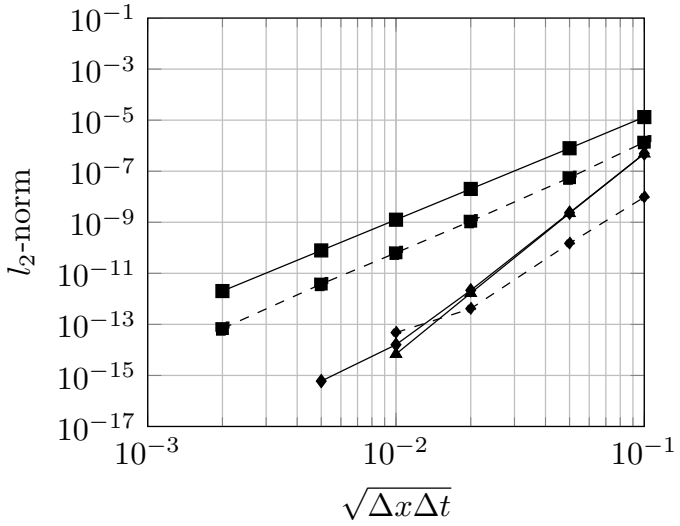

FIGURE 4.8: Example *Unsteady inhomogeneous one-dimensional convection problem*, the l_2-norm of the error for $\tau = 0.5$ and $u = 1$. ■ Cubic Hermite. ♦ Quintic Hermite. ▲ Septic Hermite. Solid line, REMEDIES. Dashed line, FaP.

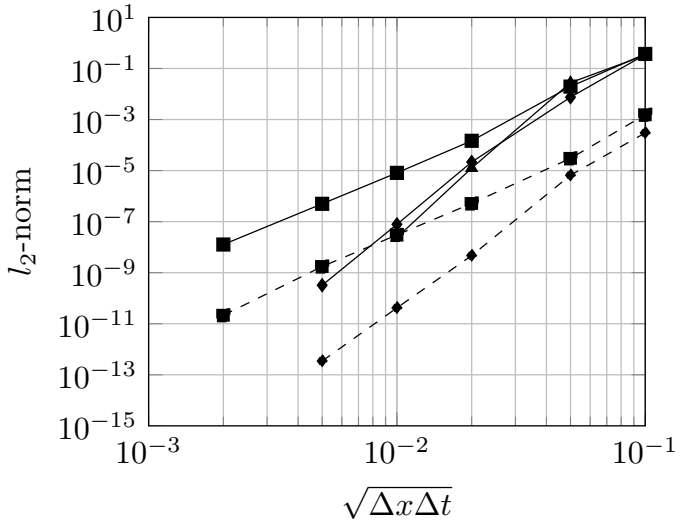

FIGURE 4.9: Example *Unsteady inhomogeneous one-dimensional convection problem*, the l_2-norm of the error for $\tau = 0.5$ and $u = 10$. ■ Cubic Hermite. ♦ Quintic Hermite. ▲ Septic Hermite. Solid line, REMEDIES. Dashed line, FaP.

4.4.3 Wave travelling problem

The last test case is one with a bit more complicated source term.

$$\begin{cases} \dfrac{\partial \phi}{\partial t} + \dfrac{\partial}{\partial x}(u\phi) = -\dfrac{1}{\tau}\phi(1-\phi), & (x,t) \in (0,1) \times (0,0.5], \\ \phi(0,t) = \phi_0(t) = 0.8 + 0.2\sin(2\pi t), & t \in (0,0.5], \\ \phi(x,0) = \phi^0(x) = 0.8, & x \in (0,1). \end{cases}$$

As in the previous example, τ is a characteristic time of decay. The solution is

$$\phi(x,t) = \begin{cases} \left[1 + \left(\dfrac{1}{\phi_0\left(t - x/u\right)} - 1\right)\exp\left(\dfrac{x}{u\tau}\right)\right]^{-1} & \text{for} \quad x < ut \\ \left[1 + \left(\dfrac{1}{\phi^0\left(x - ut\right)} - 1\right)\exp\left(\dfrac{t}{\tau}\right)\right]^{-1} & \text{for} \quad x \geq ut \end{cases}$$

This example was also chosen by ten Thije Boonkkamp and Anthonissen to assess the FV-CF scheme [209]. The solution of this case is only $\mathcal{C}^0$ across the characteristic line $x = ut$. Both the fluxes and β are discontinuous at this line what makes this a challenging test case for our approach. Additionally, it was shown in Llorente *et al.* [120] that FV-CF and ENATE were almost identical in 1D but differed considerably in 2D, and this case is a good test to assess the accuracy of our approach in comparison to FV-CF.

The exact solution decays in time except along the characteristic line that starts at $x = 0, t = 1/4$ along which ϕ is one and the source zero. This lack of decay initially transforms the sine function into a spiky function that eventually converts into a function of value one at points of the straight line $x = u(t - 1/4)$ and measure zero in the x-domain.

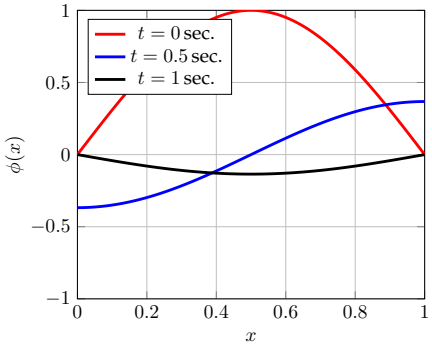

(A) Profile solution.

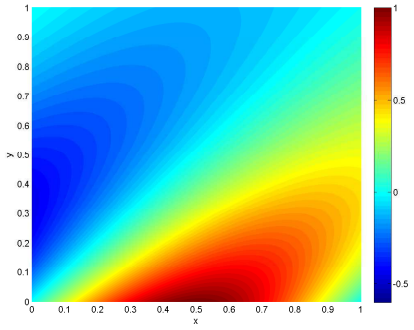

(B) Space-time domain.

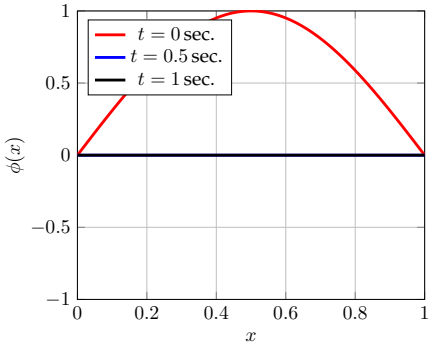

(C) Profile solution.

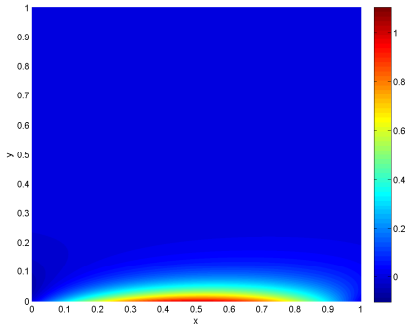

(D) Space-time domain.

FIGURE 4.10: Example *Unsteady inhomogeneous one-dimensional convection problem*, exact solution with $u = 1$. (A) and (B) with $\tau = 0.5$. (C) and (D) with $\tau = 0.05$.

The assessment of both approaches will be performed in the x-domain for $t = 0.5$. No extra source due to the solution-dependent term has been included in the $\Delta\phi_2$ equation. In Figure 4.12 comparative results with a very coarse grid are depicted. Contrary to the Euler method, both ENATE approaches follow the spiky part of the solution but with significant over- and under-shoots, especially REMEDIES. With such a coarse grid the results are not very good although they are qualitatively much better than those with Euler explicit.

In Figure 4.13 the comparison between FV-CF and ENATE is presented. The values of the parameters employed are $\tau = 0.04$ and $u = 0.95$. The l_1-norm of the error at $t = 0.5$ s was computed. As shown, FV-CF is second-order and the two ENATE versions, FaP and REMEDIES, are fourth-order. The main difference between both approaches is the source treatment. Splitting the equation (4.1a) into two quasi-one-dimensional equations seems to work fine either with FaP or REMEDIES because both approaches use high-order quadratures. In the case of FV-CF, $\partial\phi/\partial t$ is only included as pseudo-source. Then the scheme produces a first-order ODE system solved by a second-order Crank–Nicolson method, see [209] for details.

The results presented with ENATE-REMEDIES have been carried out

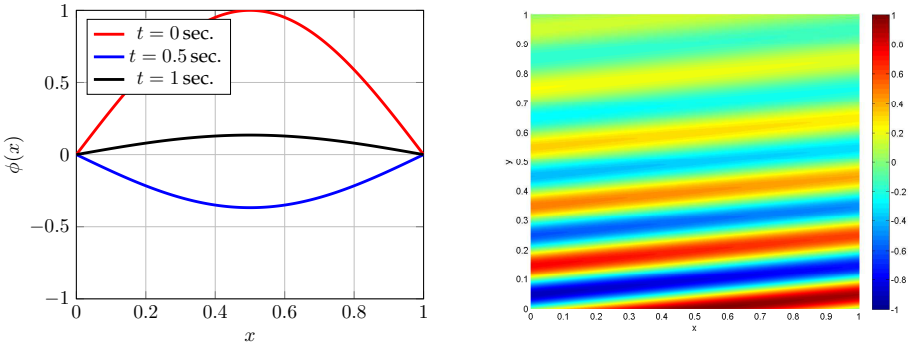

(A) Profile solution. (B) Space-time domain.

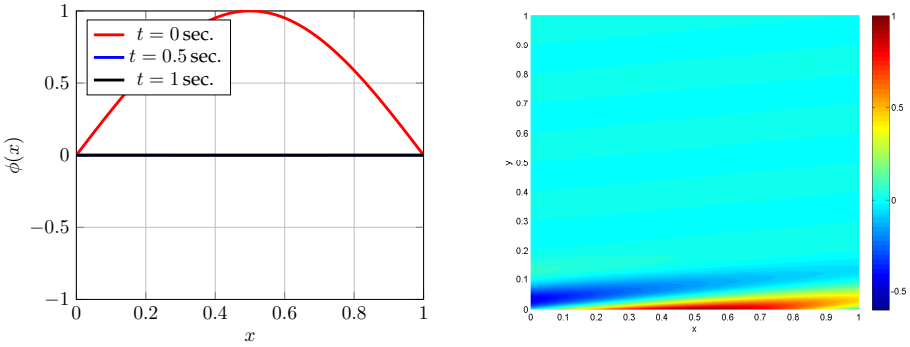

(C) Profile solution. (D) Space-time domain.

FIGURE 4.11: Example *Unsteady inhomogeneous one-dimensional convection problem*, exact solution with $u = 10$. (A) and (B) with $\tau = 0.5$. (C) and (D) with $\tau = 0.05$.

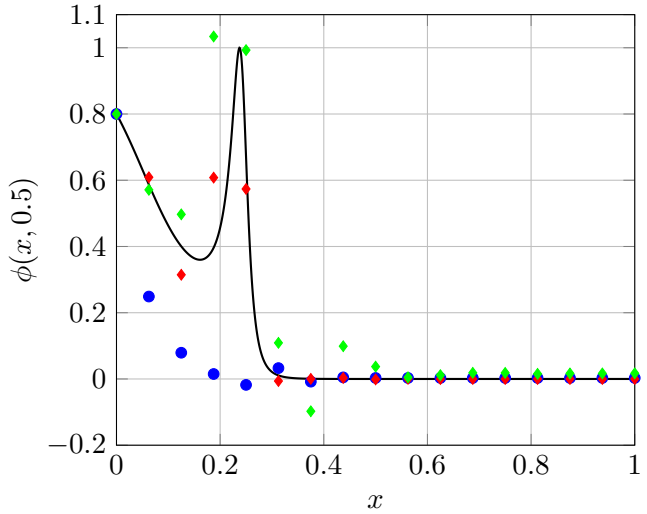

FIGURE 4.12: Example *Wave travelling problem*, exact solution at $t = 0.5$ s (black line). Numerical solutions in a mesh with $\Delta x = 0.0625$ m and time step $\Delta t = 0.0625$ s: Explicit Euler method (blue dots), ENATE with FaP (red diamonds) and ENATE with REMEDIES (green diamonds).

with Cubic Hermite for the integrals, but FaP used CIR. Compact derivatives of fourth-order are used to evaluate the first derivative of the appropriate variables. Despite the discontinuities of the latter, fourth-order compact derivative is still able to provide a reasonably good estimation of the

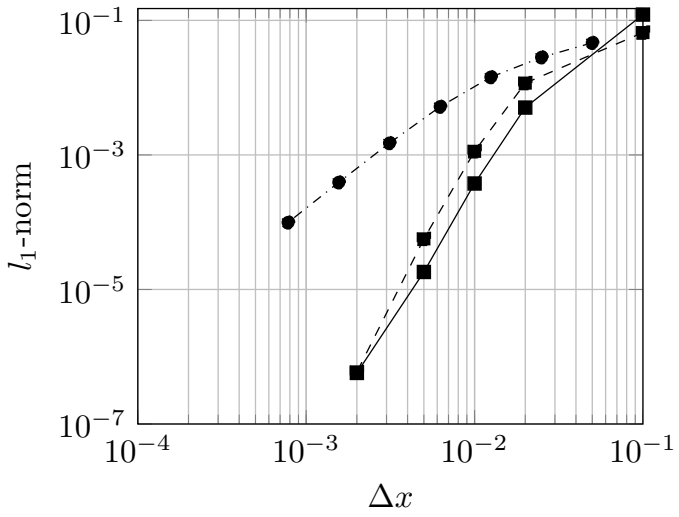

FIGURE 4.13: Example *Wave travelling problem*, the l_1-norm of the error comparing two exponential schemes. • FV-CF scheme. ■ ENATE. Solid line, REMEDIES. Dashed line, FaP.

first derivative. In fact, fourth-order CCS even provides usable values of second and third derivatives for Quintic and Septic Hermite. However, the use of compact derivatives of order higher than four caused a blowup of the calculations. When a combination of Hermite polynomials and compact derivatives of different orders is used, the order of accuracy of the results is the lower of the two, for example, Quintic Hermite (sixth-order) and fourth-order compact derivatives gives a fourth-order accuracy overall. There are huge differences in the CPU time. FaP took 50 min to reach the solution at $t = 0.5$ s with 500 nodes in the x coordinate whereas REMEDIES employed around 4 min.

4.5 In Closing

Finally, in this chapter the developed numerical techniques are focussed on solving unsteady problems. The temporal term is resolved as a convection-only problem and, therefore, the numerical approaches in the previous chapter are also applicable.

The numerical examples showed an improvement over basic discretization techniques such as Crank-Nicolson or Euler explicit. In fact, in the last one Euler was unable to catch the wave. A surprising outcome came up for the reaction problems. The accuracy of REMEDIES dropped two orders of magnitude compared to FaP in the worst case. Even so, the fast convergence of REMEDIES makes this approach a good choice for temporal phenomena since only requires just one sweep in the $\Delta\phi_2$ equation to get the solution in the convergence process.

Regarding stability, both FaP and REMEDIES are implicit methods which are unconditionally stable ensuring diagonally-dominant matrix for $\mathbf{P}^n$ in FaP and $\widetilde{\mathbf{P}}^n$ in REMEDIES.

Chapter 5

Conclusions and future research

ENATE is capable of getting the exact solution of a steady one-dimensional transport equation. In order to derive a discrete equation associated to a node in a split-up domain the continuity of the diffusive flux is enforced in the two adjacent control volumes that share the node. The result is a three-point stencil where the accuracy of the scheme depends on how well or poorly the integrals in the coefficients and discrete source are computed. Therefore, high-order results can be achieved without modifying the computational molecule. The quadrature used to calculate the integrals was Hermite polynomials. Also, it is proved that the 1D exponential flux of ENATE preserves positiveness and can interpolate smoothly from strong convection to dominant diffusion with the same formulation.

In the main part of this work, the exponential formulation of ENATE is extended to multidimensional problems, in particular, steady-state two-dimensional and unsteady-state one-dimensional. The formulation uses a short computational molecule while keeping a similar accuracy to the one-dimensional approach. One initial approach consisted in a splitting of the 2D transport equation into two pseudo-1D transport equations. In each direction the influence of the other direction comes in the source by the term $S \pm \partial \mathcal{F}_{\{y,x\}}/\partial\{y,x\}$. This contribution implies that ENATE is conservative over each one-dimensional control volume along both coordinates of the problem. The computation of these integrals requires an evaluation of the $\mathcal{F}$s derivatives via central compact schemes. Other integrals such as the average of Péclet and the integral of the source are computed via compact integration rules.

This accurate evaluation of the new pseudo-sources brings high-order resolution, as shown in the *Numerical Examples* section, but increases a great deal the CPU time due to the required number of operations per iteration. This issue gave a chance for seeking a remedy for the excessive CPU time. The second approach splits the source by an unknown field that is solved during the iterative process. Along the iterative process the numerical solution in each axis is different, so a correction equation has to be derived that forces the two solutions to be equal. Converged results were obtained with this approach in a much shorter CPU time. Moreover, as the number of operations is reduced the accuracy is often increased with respect to the first one.

Finally, we carry on extending the scope of our numerical scheme by

solving time-dependent problems. Instead of a classic methodology to reduce the PDE to a first-order ODE in time and solve it by a time integration method, it was decided to use what was previously learnt in two-dimensional problems to derive a practical implementation that gave satisfactory results.

It can be concluded that ENATE forms a robust and high-order multi-dimensional exponential scheme for convection-diffusion problems. However, additional work should go on to tackle realistic situations. Different items of ongoing work are sorted next.

5.1 High-order novel quadratures

One main aspect that makes ENATE a high-order exponential scheme is the quadratures employed. The disadvantage is that most of them, principally Hermite splines, need the computation of derivatives. Future research that ENATE should follow for it to be an efficient scheme is the derivation of novel high-order quadratures that only use the information at grid points, e.g. ϕ values. Section 3.5 on page 97 gives details of one of them: CIR. It can get the same accuracy as Hermite splines but it is derivative-free. This is achieved by the derivation of linear combinations of the integrals in each interval. Thus, to calculate

$$\int_{x_W}^{x_C} \frac{\partial \mathcal{F}_y}{\partial y} \mathrm{d}x \quad \text{and} \quad \int_{y_S}^{y_C} \frac{\partial \mathcal{F}_x}{\partial x} \mathrm{d}y,$$

instead of computing two, or more, compact derivatives and then CIR, we might use a 2D Taylor series and link those integrals in a two-dimensional stencil with ϕ. Some research in this line has started.

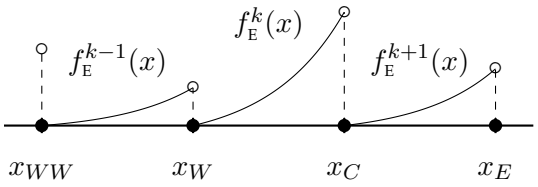

FIGURE 5.1: Integrand of $ISGE_{01}$, $f_{\mathrm{E}}(\widehat{x}) = IS_{0\widehat{x}}/\widehat{\Gamma E}$ for each interval, in the discrete domain.

Also, we might seek new quadratures for integrals such as $ISGE$. The integrals that contain the exponential factor $\overline{E}$ are piecewise continuous functions and, therefore, discontinuous at grid points, see Fig. 5.1. Hermite can deal with this type of integrals because only uses the information of the nodes of an interval, but CIR grabs adjacent information. One demand for this quadrature is that the integrand be continuous. A discontinuous CIR was derived that takes into account the jump in each grid points that the integrand produces, e.g

$$\frac{1}{10}\int_{x_{WW}}^{x_W} f_{\mathrm{E}}^{k-1}\mathrm{d}x + \int_{x_W}^{x_C} f_{\mathrm{E}}^{k}\mathrm{d}x + \frac{1}{10}\int_{x_C}^{x_E} f_{\mathrm{E}}^{k+1}\mathrm{d}x \approx \frac{3\Delta x}{5}\left[\widetilde{f}_{\mathrm{E}W} + \widetilde{f}_{\mathrm{E}C}\right],$$

where $\widetilde{f}_{\mathrm{E}W} = (f_{\mathrm{E}W}^{k-1} + 2f_{\mathrm{E}W}^{k})/3$ and $\widetilde{f}_{\mathrm{E}C} = (2f_{\mathrm{E}C}^{k} + f_{\mathrm{E}C}^{k+1})/3$. The quadrature is built by expanding in Taylor series the different functions in a k-interval

$[x_W, x_C]$, linking the functions at nodes by the jumps and expanding these jumps in Taylor series as well. However, the resolution was poor. A reason for that result is that it was assumed that the derivatives can be obtained by the Taylor expansion of f_{E}^{k+m} and this is not the case, that is, every derivative of f_{E}^{k+m} must also be expanded in Taylor series. More research is still needed in this matter.

5.2 Reaction problems

It was found in the last examples of Chapter 4 that REMEDIES lost accuracy for reaction problems where the source depends on the solution. There could be different causes, either the treatment of $\Delta\phi_2^\star$ and $\Delta\beta^\star$ via $\overline{\Delta S_2^\star}^x$ and $\overline{\Delta S_2^\star}^y$, or the resolution of the transport equations in each axis. In both cases they are based on an exponential scheme that does not take into account that the source depends linearly on the transported variable. One way to improve it would be to look for the exact solution of the PDE

$$\frac{\mathrm{d}}{\mathrm{d}x}\left(\rho u\phi - \Gamma\frac{\mathrm{d}\phi}{\mathrm{d}x}\right) = S + S_\phi\phi,$$

which represents better the nature of the problem and where neither S nor S_ϕ depend on ϕ. This type of equations can be found in combustion theory, for instance. Even if S_ϕ constant, its resolution is not straightforward. Under the same methodology of Chapter 2, the dimensionless equation would be

$$\frac{\mathrm{d}}{\mathrm{d}\widehat{x}}\left(\widehat{\rho u}\widehat{\phi} - \frac{\widehat{\Gamma}}{P_0}\frac{\mathrm{d}\widehat{\phi}}{\mathrm{d}\widehat{x}}\right) = \frac{(S + S_\phi\phi_{lb})\,\Delta x}{(\rho u)_{lb}\,\Delta\phi} + \frac{S_\phi\Delta x}{(\rho u)_{lb}}\widehat{\phi} - \frac{\phi_{lb}}{\Delta\phi}\frac{\mathrm{d}\widehat{\rho u}}{\mathrm{d}\widehat{x}}.$$

The complete solution could be written as $\widehat{\phi}(\widehat{x}) = F(\widehat{x}) + R(\widehat{x}) + \overline{\phi}^N(\widehat{x})$, assuming $F(1) = 0$. The solution $\overline{\phi}^N(\widehat{x})$ and $F(\widehat{x})$ are the homogeneous and the particular solution with $S + S_\phi\phi_{lb}$, respectively, and their formulae are written on page 21 and 26. $R(\widehat{x})$ with $R(0) = R(1) = 0$ is the solution of a transport equation with the reactive source, $S_\phi\Delta x\widehat{\phi}/\,(\rho u)_{lb}$. Integrating this equation from 0 to $\widehat{x}$ yields

$$\frac{\mathrm{d}\mathbf{r}}{\mathrm{d}\widehat{x}} + \mathbf{M}\mathbf{r} = \mathbf{s}, \quad \mathbf{r}(0) = \mathbf{0},$$

where

$$\mathbf{r} \coloneqq \left(\int_0^{\widehat{x}} S_\phi R\,\mathrm{d}\widehat{x}', R\right)^T, \quad \mathbf{M} \coloneqq \begin{pmatrix} 0 & -S_\phi \\ \dfrac{\Delta x^2}{\Gamma} & -P \end{pmatrix},$$
$$\mathbf{s} \coloneqq \left(0, -\frac{\Delta x^2}{\Gamma}\int_0^{\widehat{x}} S_\phi\left[F + \overline{\phi}^N\right]\mathrm{d}\widehat{x}'\right)^T.$$

The resulting is a first-order ODE system whose solution method is well-known. After considerable algebraic manipulation, it is likely that we may achieve an exponential scheme with a three-point stencil where the coefficients are modified by some integrals of S_ϕ that vanish in the limit case

of $S_\phi \to 0$, recovering the original exponential scheme. The same strategy was carried out in [211] but for constant coefficients. Additionally, it will be needed to check if the quadratures described in this thesis can still be used for these new integrals and yet give high-accuracy results.

5.3 Complex geometry

Cartesian mesh always offers the best results but is inefficient for complex geometry or flow features where some node clustering is required. ENATE can be used with nonuniform meshes where the clustering is done across the domain, although there might be some interest in performing only a local refinement in a certain area. A mesh similar to that in Figure 5.2 may be present. In such a case, we need to transform the cartesian transport equation to a (ξ, η) transport equation. Under this transformation, the Jacobian,

$$\mathcal{J} = \frac{\partial x}{\partial \xi}\frac{\partial y}{\partial \eta} - \frac{\partial x}{\partial \eta}\frac{\partial y}{\partial \xi},$$

is clearly discontinuous making the resulting equation difficult to handle numerically. In fact, we have four values of $\mathcal{J}$ at the same point depending on the interval. A way to remove this problem is the use of the transport equation locally rather than globally. To decompose and force the continuity of the flux around a central point, and apply REMEDIES since it does not take into account the normal flux derivative in the source as FaP. Even so, it is not clear how to evaluate integrals and derivatives, as they are discontinuous along the iso-ξ and -η lines.

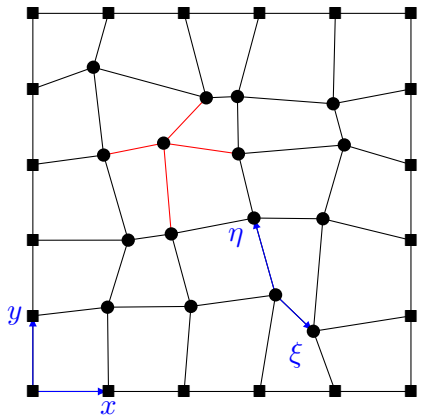

FIGURE 5.2: Random mesh. Black circle, inner points; Black square, boundary points. Red lines, computational molecule. Blue lines, coordinate basis.

For complex geometries with obstacles two methodologies can be followed. One way is the use of unstructured mesh as it offers the best adaptability but suffers from the same problems as the random mesh. On the other hand, an immersed boundary method can be used. This method requires to localize a Lagrangian point of an internal body or complex boundary what is a bit challenging for programming. There are two issues: 1) it is not clear how to proceed with REMEDIES to calculate β at nodes on the internal boundaries, 2) how to link an internal boundary node with a mesh

node when the internal body or complex boundary does not contain a mesh node. Some progress is being made right now in this issue.

5.4 Navier-Stokes simulations

One application that we may not be overlooked is the discretization of the Navier-Stokes (NS) equations. According to the previous numerical examples, REMEDIES might work properly with this set of nonlinear equations with a reasonable computational time. The convective terms in the momentum equation would be frozen similar to that on page 54.

One important aspect of NS is the Velocity-Pressure coupling. A SIMPLE technique for ENATE was derived in order to calculate a pressure-correction equation, as well as the velocity corrections. However, this idea of coupling was rejected because some source integrals had to be dropped out to get adequate discrete equations what would impair the accuracy. Another well-known coupling technique is the pressure Poisson equation obtained form the NS equations,

$$\frac{\partial^2 p}{\partial x^2}+\frac{\partial^2 p}{\partial y^2}=-\rho\left[\left(\frac{\partial u}{\partial x}\right)^2+2\frac{\partial u}{\partial x}\frac{\partial v}{\partial y}+\left(\frac{\partial v}{\partial y}\right)^2\right]=:-S_p,$$

derived by taking the divergence of the momentum equation. On page 109 a Poisson's equation was computed, so similar results would be expected. As it is pointed out in this chapter, the ENATE scheme must progress to new quadratures, free of the derivative of the integrand. For the Poisson's equation, ENATE needs to compute the integral

$$\int_{x_W}^{x_C}\int_{x_W}^{x} f\,\mathrm{d}x'\mathrm{d}x,$$

in which f can be either S_p or the distribution field β_p for REMEDIES. One quadrature that could meet our demands, and similar to CIR, could be

$$\frac{1}{10}\int_{x_{WW}}^{x_W}\int_{x_{WW}}^{x} f\,\mathrm{d}x'\mathrm{d}x+\int_{x_W}^{x_C}\int_{x_W}^{x} f\,\mathrm{d}x'\mathrm{d}x+\frac{1}{10}\int_{x_C}^{x_E}\int_{x_C}^{x} f\,\mathrm{d}x'\mathrm{d}x\approx\frac{\Delta x^2}{5}\left[2f_W+f_C\right]$$

which is order 5. It was checked that this quadrature works fine for a smooth function, e.g $f(x)=\sin x$. So, its implementation in Poisson's equation is in progress. Finally, the ENATE scheme applied to the NS equations is associated to a collocated arrangement of the variables on the grid, but also a staggered arrangement, see [103], is being considered due to its strong velocity-pressure coupling.

Capítulo 5

Conclusiones y trabajo futuro

ENATE es capaz de obtener la solución exacta de una ecuación de transporte unidimensional en estado estacionario. Para deducir una ecuación discreta asociada a un nodo en un dominio dividido se impone la continuidad del flujo difusivo en dos volúmenes de control adyacentes que comparten un mismo nodo. El resultado es una plantilla de tres puntos donde la precisión del esquema depende de como de bien o mal se calculan las integrales en los coeficientes y la fuente discreta. Por lo tanto, se pueden lograr resultados de alto orden sin modificar dicha molécula computacional. La cuadratura utilizada para calcular las integrales son polinomios de Hermite. Además, se ha comprobado que el flujo exponencial 1D de ENATE conserva la positividad y puede interpolar suavemente desde una convección fuerte hasta una difusión dominante con la misma formulación.

En lo referente a la parte principal de este trabajo, se extendió la formulación exponencial de ENATE a problemas multidimensionales, en particular, bidimensionales estacionarios y unidimensionales transitorios. Esta formulación utiliza una molécula computacional corta manteniendo una precisión similar al esquema unidimensional. Un enfoque inicial consistió en la división de la ecuación de transporte 2D en dos ecuaciones de transporte pseudo-1D. En cada dirección coordenada la influencia de la otra dirección viene dada por el término $S \pm \partial \mathcal{F}_{\{y,x\}}/\partial\{y,x\}$. Esta contribución implica que ENATE es conservativa sobre cada volumen de control unidimensional en ambas coordenadas del problema. El cálculo de estas integrales requiere una evaluación de las derivadas de $\mathcal{F}$ a través de un esquema compacto central. Otras integrales como el Péclet promedio y la integral de la fuente se calculan mediante las reglas de la integración compacta.

Esta evaluación precisa de las nuevas pseudo-fuentes proporciona una resolución de alto orden, como se muestra en la sección *Numerical Examples*, pero aumenta mucho el tiempo de CPU debido al alto número de operaciones por iteración. Este problema brindó la oportunidad de buscar una solución para el excesivo tiempo de CPU. El segundo enfoque divide la fuente en un campo desconocido que se resuelve durante el proceso iterativo. A lo largo del proceso iterativo, la solución numérica en cada eje es diferente, por lo que se debe deducir una ecuación correctora que obligue a las dos soluciones a ser iguales. Los resultados convergidos se obtuvieron con este enfoque en un tiempo de CPU mucho más corto. Además, a medida que se reduce el número de operaciones, la precisión aumenta con respecto a la primera.

Finalmente, seguimos ampliando el alcance de nuestro esquema numérico resolviendo problemas dependientes del tiempo. En lugar de una metodología

clásica para reducir una PDE a un ODE de primer orden en tiempo y resolverlo mediante un método de integración temporal, se decidió usar lo que se aprendió previamente en problemas bidimensionales para deducir una implementación práctica que dio resultados satisfactorios.

Se puede concluir que ENATE es un esquema exponencial multidimensional robusto y de alto orden para problemas de convección-difusión. Sin embargo, se debe continuar trabajando para abordar situaciones realistas. A continuación se ordenan diferentes elementos de trabajo en curso.

5.1 Novedosas cuadraturas de alto orden

Un aspecto principal que convierte a ENATE en un esquema exponencial de alto orden son las cuadraturas empleadas. La desventaja es que la mayoría de ellas, principalmente los polinomios de Hermite, necesitan el cálculo de derivadas. Una investigación futura que ENATE debería seguir para que sea un esquema eficiente es la deducción de nuevas cuadraturas de alto orden que solo usen la información en puntos de la malla, es decir, solo valores de ϕ. La Sección 3.5 en la página 97 da detalles de uno de ellos: CIR. Esta cuadratura puede obtener la misma precisión que Hermite, pero sin utilizar las derivadas. Esto se logra mediante un empleo de combinaciones lineales de las integrales en cada intervalo. Por lo tanto, para calcular

$$\int_{x_W}^{x_C} \frac{\partial \mathcal{F}_y}{\partial y} \mathrm{d}x \quad \text{y} \quad \int_{y_S}^{y_C} \frac{\partial \mathcal{F}_x}{\partial x} \mathrm{d}y,$$

en lugar de calcular dos o más derivadas compactas y luego CIR, podríamos usar una serie de Taylor 2D y vincular estas integrales sobre una plantilla bidimensional de ϕs. Se han iniciado algunas investigaciones en esta línea.

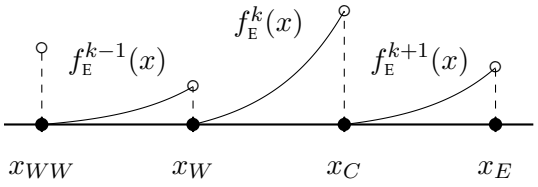

FIGURA 5.1: Integrando de $ISGE_{01}$, $f_{\mathrm{E}}(\widehat{x}) = IS_{0\widehat{x}}/\widehat{\Gamma}\overline{E}$ para un intervalo de referencia, en el dominio discreto.

Además, se podrían buscar nuevas cuadraturas para integrales como $ISGE$. Las integrales que contienen el factor exponencial $\overline{E}$ son funciones continuas a trozos y, por lo tanto, discontinuas en los puntos de la malla, ver Fig. 5.1. Hermite puede manejar este tipo de integrales porque solo usa la información de los nodos de un intervalo, pero CIR toma información adyacente. Un requisito para la cuadratura CIR es que el integrando sea continuo. Se obtuvo un CIR discontinuo que tiene en cuenta el salto que produce el integrando en cada punto de la malla, p.ej.

$$\frac{1}{10}\int_{x_{WW}}^{x_W} f_{\mathrm{E}}^{k-1}\mathrm{d}x + \int_{x_W}^{x_C} f_{\mathrm{E}}^{k}\mathrm{d}x + \frac{1}{10}\int_{x_C}^{x_E} f_{\mathrm{E}}^{k+1}\mathrm{d}x \approx \frac{3\Delta x}{5}\left[\widetilde{f}_{\mathrm{E}W} + \widetilde{f}_{\mathrm{E}C}\right],$$

donde $\widetilde{f}_{\mathrm{E}W} = (f_{\mathrm{E}W}^{k-1} + 2f_{\mathrm{E}W}^{k})/3$ y $\widetilde{f}_{\mathrm{E}C} = (2f_{\mathrm{E}C}^{k} + f_{\mathrm{E}C}^{k+1})/3$. La cuadratura anterior se construye expandiendo en serie de Taylor las diferentes funciones en

un intervalo k $[x_w, x_C]$, vinculando las funciones en los nodos por los saltos y expandiendo también estos saltos en la serie Taylor. Sin embargo, el resultado fue malo. Una razón para este resultado es que se asumió que las derivadas podían ser obtenidas mediante la expansión de Taylor de f_{E}^{k+m} y no es el caso, es decir, cada derivada de f_{E}^{k+m} también debe expandirse en serie de Taylor. Todavía se necesita más investigación en este asunto.

5.2 Problemas de reacción

En los últimos ejemplos del Capítulo 4 se encontró que REMEDIES perdió precisión para problemas de reacción donde la fuente depende de la solución. Podría haber diferentes causas, ya sea el tratamiento de $\Delta\phi_2^\star$ y $\Delta\beta^\star$ a través de $\overline{\Delta S_2^\star}^x$ y $\overline{\Delta S_2^\star}^y$, o la resolución de las ecuaciones de transporte en cada eje. En ambos casos las ecuaciones se basan en un esquema exponencial que no tiene en cuenta que la fuente depende linealmente de la variable de transporte. Una forma de mejorarlo sería buscar la solución exacta a la PDE

$$\frac{\mathrm{d}}{\mathrm{d}x}\left(\rho u\phi - \Gamma\frac{\mathrm{d}\phi}{\mathrm{d}x}\right) = S + S_\phi\phi,$$

que representa mejor la naturaleza del problema y donde ni S ni S_ϕ dependen de ϕ. Este tipo de ecuaciones se pueden encontrar en la teoría de la combustión, por ejemplo. Incluso con S_ϕ constante, su resolución no es sencilla. Bajo la misma metodología que en el Capítulo 2, la ecuación adimensional sería

$$\frac{\mathrm{d}}{\mathrm{d}\widehat{x}}\left(\widehat{\rho u}\widehat{\phi} - \frac{\widehat{\Gamma}}{P_0}\frac{\mathrm{d}\widehat{\phi}}{\mathrm{d}\widehat{x}}\right) = \frac{(S + S_\phi\phi_{lb})\,\Delta x}{(\rho u)_{lb}\,\Delta\phi} + \frac{S_\phi\Delta x}{(\rho u)_{lb}}\widehat{\phi} - \frac{\phi_{lb}}{\Delta\phi}\frac{\mathrm{d}\widehat{\rho u}}{\mathrm{d}\widehat{x}}.$$

La solución completa podría escribirse como $\widehat{\phi}(\widehat{x}) = F(\widehat{x}) + R(\widehat{x}) + \overline{\phi}^N(\widehat{x})$, suponiendo que $F(1) = 0$. La solución $\overline{\phi}^N(\widehat{x})$ y $F(\widehat{x})$ son la solución homogénea y particular con $S + S_\phi\phi_{lb}$, respectivamente, y sus fórmulas están escritas en la página 21 y 26. $R(\widehat{x})$ con $R(0) = R(1) = 0$ es la solución de una ecuación de transporte con la fuente reactiva, $S_\phi\Delta x\widehat{\phi}/\,(\rho u)_{lb}$. La integración de esta ecuación de 0 a $\widehat{x}$ produce

$$\frac{\mathrm{d}\mathbf{r}}{\mathrm{d}\widehat{x}} + \mathbf{M}\mathbf{r} = \mathbf{s}, \quad \mathbf{r}(0) = \mathbf{0},$$

donde

$$\mathbf{r} \coloneqq \left(\int_0^{\widehat{x}} S_\phi R\,\mathrm{d}\widehat{x}', R\right)^T, \quad \mathbf{M} \coloneqq \begin{pmatrix} 0 & -S_\phi \\ \dfrac{\Delta x^2}{\Gamma} & -P \end{pmatrix},$$
$$\mathbf{s} \coloneqq \left(0, -\frac{\Delta x^2}{\Gamma}\int_0^{\widehat{x}} S_\phi\left[F + \overline{\phi}^N\right]\mathrm{d}\widehat{x}'\right)^T.$$

El resultado es un sistema ODE de primer orden cuya solución es bien conocida. Después de una considerable manipulación algebraica, es probable que podamos lograr un esquema exponencial con una plantilla de tres

puntos donde los coeficientes son modificados por algunas integrales de S_ϕ que desaparecen en el caso límite de $S_\phi \to 0$, recuperando el esquema exponencial original. La misma estrategia se desarrollo en [211] pero para coeficientes constantes. Además, será necesario verificar si las cuadraturas descritas en esta tesis todavía pueden ser utilizadas para estas nuevas integrales y aún así dar resultados de alta precisión.

5.3 Geometría compleja

La malla cartesiana siempre ofrece los mejores resultados, pero es ineficiente para geometrías complejas o características de flujo donde se requiere algún agrupamiento de nodos. ENATE puede ser usado con mallas no uniformes donde el agrupamiento se realiza en todo el dominio, aunque puede haber algún interés en realizar solo un refinamiento local en un área determinada. Se puede encontrar una malla similar a la de la Figura 5.2. En tal caso, necesitamos transformar la ecuación de transporte cartesiana en una ecuación de transporte (ξ, η). Bajo esta transformación, el Jacobiano,

$$\mathcal{J} = \frac{\partial x}{\partial \xi}\frac{\partial y}{\partial \eta} - \frac{\partial x}{\partial \eta}\frac{\partial y}{\partial \xi},$$

es claramente discontinuo, lo que hace que la ecuación resultante sea difícil de manejar numéricamente. De hecho, tenemos cuatro valores de $\mathcal{J}$ en el mismo punto, dependiendo del intervalo. Una forma de eliminar este problema es el uso de la ecuación de transporte localmente en lugar de globalmente. La idea sería descomponer y forzar la continuidad del flujo alrededor de un punto central, y aplicar REMEDIES ya que no tiene en cuenta la derivada de flujo normal en la fuente como FaP. Aun así, no está claro cómo evaluar integrales y derivadas, ya que son discontinuas a lo largo de las líneas iso-ξ y -η.

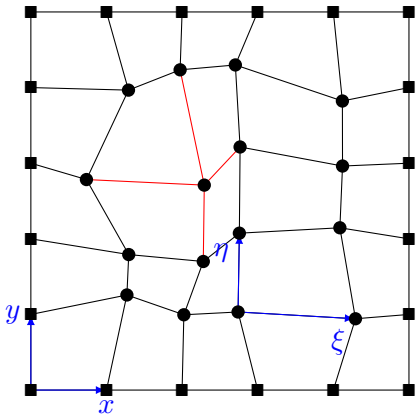

FIGURA 5.2: Malla aleatoria Círculo negro, puntos internos; Cuadrado negro, puntos del contorno. Líneas rojas, molécula computacional. Líneas azules, bases de coordenadas.

Para geometrías complejas con obstáculos pueden seguirse dos metodologías. Una forma es el uso de mallas no estructuradas, ya que ofrece la mejor adaptabilidad pero sufre los mismos problemas que las mallas aleatorias.

Por otro lado, se puede utilizar un método de inmersión de malla. Este método requiere localizar un punto lagrangiano de un cuerpo interno, lo que supone un desafío para la programación. Hay dos problemas: 1) no está claro cómo proceder con REMEDIES para calcular β en los nodos del cuerpo interno, 2) cómo vincular un nodo de contorno interno con un nodo de malla cuando el cuerpo interno o el contorno complejo no contiene un nodo de malla. Se están haciendo algunos progresos en este momento.

5.4 Simulaciones con Navier-Stokes

Una aplicación que no podemos pasar por alto es la discretización de las ecuaciones de Navier-Stokes (NS). Según los ejemplos numéricos anteriores, REMEDIES podría funcionar correctamente con este conjunto de ecuaciones no lineales con un tiempo de cálculo razonable. Los términos convectivos en la ecuación de momento se calcularían explicitamente de forma similar a la de la página 54.

Un aspecto importante de NS es el acoplamiento Velocidad-Presión. Se dedujo una técnica SIMPLE para ENATE para calcular una ecuación de corrección de presión, así como las correcciones de velocidad. Sin embargo, esta idea de acoplamiento fue rechazada porque algunas integrales de la fuente tuvieron que ser eliminadas para obtener ecuaciones discretas adecuadas lo que perjudicaría a la precisión. Otra técnica de acoplamiento bien conocida es la ecuación de Poisson de presión obtenida directamente de las ecuaciones NS,

$$\frac{\partial^2 p}{\partial x^2} + \frac{\partial^2 p}{\partial y^2} = -\rho \left[\left(\frac{\partial u}{\partial x} \right)^2 + 2 \frac{\partial u}{\partial x} \frac{\partial v}{\partial y} + \left(\frac{\partial v}{\partial y} \right)^2 \right] =: -S_p,$$

tomando la divergencia de la ecuación de cantidad de movimiento. En la página 109 se calculó una ecuación de Poisson, por lo que se esperarían resultados similares. Como se señala en este capítulo, el esquema ENATE debe progresar a nuevas cuadraturas que no necesiten la derivada del integrando. Para la ecuación de Poisson, ENATE necesita calcular la integral

$$\int_{x_W}^{x_C} \int_{x_W}^{x} f \, \mathrm{d}x' \mathrm{d}x,$$

en el que f puede ser S_p o el campo de distribución β_p para REMEDIES. Una cuadratura que podría satisfacer nuestras demandas, y similar a CIR, podría ser

$$\frac{1}{10} \int_{x_{WW}}^{x_W} \int_{x_{WW}}^{x} f \, \mathrm{d}x' \mathrm{d}x + \int_{x_W}^{x_C} \int_{x_W}^{x} f \, \mathrm{d}x' \mathrm{d}x + \frac{1}{10} \int_{x_C}^{x_E} \int_{x_C}^{x} f \, \mathrm{d}x' \mathrm{d}x \approx \frac{\Delta x^2}{5} \left[2 f_W + f_C \right]$$

la cual es de orden 5. Se verificó que esta cuadratura funciona bien para una función suave, por ejemplo, $f(x) = \sin x$. Su implementación en la ecuación de Poisson está en progreso. Finalmente, el esquema ENATE aplicado a las ecuaciones NS está asociado a una disposición colocalizada de las variables en la malla, pero también se está considerando una disposición escalonada, ver [103], debido al fuerte acoplamiento velocidad-presión.

Appendix A

Deduction of the total flux formula within a reference interval

A.1 Introduction

This appendix shows how to derive the expression for $\mathcal{F}$ when the values of ϕ at points are known. Let us start with equation (2.26) that says

$$\Gamma\frac{\mathrm{d}\phi}{\mathrm{d}x} = \rho u\Delta\phi\left(\frac{1}{P}\frac{\mathrm{d}F}{\mathrm{d}\widehat{x}} + (1-F(1))\frac{1}{P}\frac{\mathrm{d}\overline{\phi}^N}{\mathrm{d}\widehat{x}}\right),$$

where $\mathrm{d}\overline{\phi}^N/\mathrm{d}\widehat{x}$ is described by equation (2.27a) and $\mathrm{d}F/\mathrm{d}\widehat{x}$ by (2.27b). If they are substituted into the diffusive flux, considering equation (2.20),

$$\Gamma\frac{\mathrm{d}\phi}{\mathrm{d}x} = \rho u\Delta\phi\Bigg(\widehat{\phi}(\widehat{x}) + \frac{1}{P_0}\frac{1}{\widehat{\rho u}(\widehat{x})}\frac{1}{IGE_{01}} + \frac{\phi_{lb}}{\Delta\phi}\Bigg[1 - \frac{1}{\widehat{\rho u}(\widehat{x})}\frac{ILE_{01}}{IGE_{01}}\Bigg] - \frac{1}{\widehat{\rho u}(\widehat{x})}\left[\widetilde{IS}_{0\widehat{x}} - \frac{\widetilde{ISGE}_{01}}{IGE_{01}}\right]\Bigg).$$

Taking the first equation in (2.2a), some terms cancel out,

$$\Gamma\frac{\mathrm{d}\phi}{\mathrm{d}x} = \rho u\Delta\phi\Bigg(\frac{\phi}{\Delta\phi} + \frac{\Gamma_{lb}}{\rho u\Delta x}\frac{1}{IGE_{01}} - \frac{\phi_{lb}}{\Delta\phi}\frac{1}{\widehat{\rho u}(\widehat{x})}\frac{ILE_{01}}{IGE_{01}} - \frac{1}{\widehat{\rho u}(\widehat{x})}\left[\widetilde{IS}_{0\widehat{x}} - \frac{\widetilde{ISGE}_{01}}{IGE_{01}}\right]\Bigg).$$

If $\rho u\Delta\phi$ multiplies the whole bracket, the hats of $\widetilde{IS}_{0\widehat{x}}$ and $\widetilde{ISGE}_{01}$ disappear by (2.24a) $-$ (2.24b), then

$$\Gamma\frac{\mathrm{d}\phi}{\mathrm{d}x} = \rho u\phi + \frac{\Gamma_{lb}}{\Delta x}\frac{\Delta\phi}{IGE_{01}} - (\rho u)_{lb}\phi_{lb}\frac{ILE_{01}}{IGE_{01}} - IS_{0\widehat{x}} + \frac{ISGE_{01}}{IGE_{01}}.$$

Since $\mathcal{F} = \rho u\phi - \Gamma\mathrm{d}\phi/\mathrm{d}x$, the total flux reads

$$\mathcal{F}(\widehat{x}) = -\frac{\Gamma_{lb}}{\Delta x}\frac{\phi_{rb}-\phi_{lb}}{IGE_{01}} + (\rho u)_{lb}\phi_{lb}\frac{ILE_{01}}{IGE_{01}} + IS_{0\widehat{x}} - \frac{ISGE_{01}}{IGE_{01}},$$

or grouping ϕ terms,

$$\mathcal{F}(\widehat{x}) = (\rho u)_{lb}\left(\widetilde{k} + \frac{ILE_{01}}{IGE_{01}}\right)\phi_{lb} - (\rho u)_{lb}\widetilde{k}\,\phi_{rb} + IS_{0\widehat{x}} - \frac{ISGE_{01}}{IGE_{01}}. \quad \text{(A.1)}$$

In a reference interval, the left boundary (lb) is $\widehat{x} = 0$ and the right boundary (rb) is $\widehat{x} = 1$.

A.2 Decomposition of $\mathcal{F}(\widehat{x})$

The flux (A.1) can be interpreted as a sum of two fluxes,

$$\mathcal{F}(\widehat{x}) = \mathcal{F}^{\phi} + \mathcal{F}^{S}(\widehat{x}).$$

A constant homogeneous flux,

$$\begin{aligned}
\mathcal{F}^{\phi} &= (\rho u)_{lb}\left(\widetilde{k} + \frac{ILE_{01}}{IGE_{01}}\right)\phi_{lb} - (\rho u)_{lb}\widetilde{k}\,\phi_{rb} \\
&= (\rho u)_{lb}\frac{ILE_{01}}{IGE_{01}}\left[\left(\widetilde{k}\frac{IGE_{01}}{ILE_{01}} + 1\right)\phi_{lb} - \widetilde{k}\frac{IGE_{01}}{ILE_{01}}\phi_{rb}\right] \\
&= (\rho u)_{lb}\frac{ILE_{01}}{IGE_{01}}\left[\left(\frac{1}{P_0 ILE_{01}} + 1\right)\phi_{lb} - \frac{1}{P_0 ILE_{01}}\phi_{rb}\right] \\
&= (\rho u)_{lb}\frac{ILE_{01}}{IGE_{01}}\left[\frac{\exp(\overline{P})}{\exp(\overline{P}) - 1}\phi_{lb} - \frac{1}{\exp(\overline{P}) - 1}\phi_{rb}\right] \\
&= \frac{(\rho u)_{lb}}{\overline{P}}\frac{ILE_{01}}{IGE_{01}}\left[\frac{-\overline{P}}{\exp(-\overline{P}) - 1}\phi_{lb} - \frac{\overline{P}}{\exp(\overline{P}) - 1}\phi_{rb}\right],
\end{aligned}$$

related to the ϕ values at the edges of the interval, and a nonhomogeneous flux

$$\mathcal{F}^{S}(\widehat{x}) = IS_{0\widehat{x}} - \frac{ISGE_{01}}{IGE_{01}},$$

which depends on the source.

Appendix B

Hermite's interpolation for exponential integrals

B.1 Coefficients a_i for the interpolator

The approximation of the integral

$$\int_0^1 f_{\text{E}}(\widehat{x})\mathrm{d}\widehat{x} \approx \frac{\exp\overline{P}}{\overline{P}}\Sigma_1 - \frac{1}{\overline{P}}\Sigma_2, \tag{B.1}$$

with $f_{\text{E}}(\widehat{x}) \coloneqq g(\widehat{x})/\overline{E}(\widehat{x})$ is determined by the a_i values in

$$\Sigma_1 = \sum_{i=0}^{m} a_i \frac{i!}{\overline{P}^i}, \quad \Sigma_2 = \sum_{i=0}^{m}\left(a_i \sum_{j=0}^{i} \frac{i!}{\overline{P}^j (i-j)!}\right). \tag{B.2}$$

These a_i are the coefficients of the Hermite polynomial that interpolates $g(\widehat{x})$. The function $g(\widehat{x})$ is arbitrary, page 49. For a quick implementation in a subroutine, the set of variables defined as

$$\begin{aligned}
\theta_{00} =& g(0),\\
\theta_{01} =& g(1),\\
\theta_{10} =& \left.\frac{\mathrm{d}g}{\mathrm{d}\widehat{x}}\right|_0 - \theta_{00}\left(P(0)-\overline{P}\right),\\
\theta_{11} =& \left.\frac{\mathrm{d}g}{\mathrm{d}\widehat{x}}\right|_1 - \theta_{01}\left(P(1)-\overline{P}\right),\\
\theta_{20} =& \left.\frac{\mathrm{d}^2 g}{\mathrm{d}\widehat{x}^2}\right|_0 - \left(\left.\frac{\mathrm{d}g}{\mathrm{d}\widehat{x}}\right|_0 + \theta_{10}\right)\left(P(0)-\overline{P}\right) - \theta_{00}\left.\frac{\mathrm{d}P}{\mathrm{d}\widehat{x}}\right|_0,\\
\theta_{21} =& \left.\frac{\mathrm{d}^2 g}{\mathrm{d}\widehat{x}^2}\right|_1 - \left(\left.\frac{\mathrm{d}g}{\mathrm{d}\widehat{x}}\right|_1 + \theta_{11}\right)\left(P(1)-\overline{P}\right) - \theta_{01}\left.\frac{\mathrm{d}P}{\mathrm{d}\widehat{x}}\right|_1,\\
\theta_{30} =& \left.\frac{\mathrm{d}^3 g}{\mathrm{d}\widehat{x}^3}\right|_0 - 2\left(\left.\frac{\mathrm{d}^2 g}{\mathrm{d}\widehat{x}^2}\right|_0 - \theta_{00}\left.\frac{\mathrm{d}P}{\mathrm{d}\widehat{x}}\right|_0 + \frac{1}{2}\theta_{20}\right)\left(P(0)-\overline{P}\right)\\
&- \left.\frac{\mathrm{d}g}{\mathrm{d}\widehat{x}}\right|_0\left(3\left.\frac{\mathrm{d}P}{\mathrm{d}\widehat{x}}\right|_0 - \left(P(0)-\overline{P}\right)^2\right) - \theta_{00}\left.\frac{\mathrm{d}^2 P}{\mathrm{d}\widehat{x}^2}\right|_0,\\
\theta_{31} =& \left.\frac{\mathrm{d}^3 g}{\mathrm{d}\widehat{x}^3}\right|_1 - 2\left(\left.\frac{\mathrm{d}^2 g}{\mathrm{d}\widehat{x}^2}\right|_1 - \theta_{01}\left.\frac{\mathrm{d}P}{\mathrm{d}\widehat{x}}\right|_1 + \frac{1}{2}\theta_{21}\right)\left(P(1)-\overline{P}\right)\\
&- \left.\frac{\mathrm{d}g}{\mathrm{d}\widehat{x}}\right|_1\left(3\left.\frac{\mathrm{d}P}{\mathrm{d}\widehat{x}}\right|_1 - \left(P(1)-\overline{P}\right)^2\right) - \theta_{01}\left.\frac{\mathrm{d}^2 P}{\mathrm{d}\widehat{x}^2}\right|_1,
\end{aligned}$$

are grouped in the vector $\boldsymbol{\theta}$ of the linear system $\mathbf{Ha} = \boldsymbol{\theta}$, being $\mathbf{H}$ the dense matrix of the interpolation. An example is written on page 51. Inverting the matrix gives the vector $\mathbf{a} = (a_0, a_1, \ldots, a_m)^T$ which is gathered in the next subsections.

B.1.1 Cubic Hermite Spline

$$\begin{pmatrix} a_0 \\ a_1 \\ a_2 \\ a_3 \end{pmatrix} = \begin{pmatrix} 1 & 0 & 0 & 0 \\ 0 & 0 & 1 & 0 \\ -3 & 3 & -2 & -1 \\ 2 & -2 & 1 & 1 \end{pmatrix} \begin{pmatrix} \theta_{00} \\ \theta_{01} \\ \theta_{10} \\ \theta_{11} \end{pmatrix}. \tag{B.3}$$

B.1.2 Quintic Hermite Spline

$$\begin{pmatrix} a_0 \\ a_1 \\ a_2 \\ a_3 \\ a_4 \\ a_5 \end{pmatrix} = \begin{pmatrix} 1 & 0 & 0 & 0 & 0 & 0 \\ 0 & 0 & 1 & 0 & 0 & 0 \\ 0 & 0 & 0 & 0 & 1/2 & 0 \\ -10 & 10 & -6 & -4 & -3/2 & 1/2 \\ 15 & -15 & 8 & 7 & 3/2 & -1 \\ -6 & 6 & -3 & -3 & -1/2 & 1/2 \end{pmatrix} \begin{pmatrix} \theta_{00} \\ \theta_{01} \\ \theta_{10} \\ \theta_{11} \\ \theta_{20} \\ \theta_{21} \end{pmatrix}. \tag{B.4}$$

B.1.3 Septic Hermite Spline

$$\begin{pmatrix} a_0 \\ a_1 \\ a_2 \\ a_3 \\ a_4 \\ a_5 \\ a_6 \\ a_7 \end{pmatrix} = \begin{pmatrix} 1 & 0 & 0 & 0 & 0 & 0 & 0 & 0 \\ 0 & 0 & 1 & 0 & 0 & 0 & 0 & 0 \\ 0 & 0 & 0 & 0 & 1/2 & 0 & 0 & 0 \\ 0 & 0 & 0 & 0 & 0 & 0 & 1/6 & 0 \\ -35 & 35 & -20 & -15 & -5 & 5/2 & -2/3 & -1/6 \\ 84 & -84 & 45 & 39 & 10 & -7 & 1 & 1/2 \\ -70 & 70 & -36 & -34 & -15/2 & 13/2 & -2/3 & -1/2 \\ 20 & -20 & 10 & 10 & 2 & -2 & 1/6 & 1/6 \end{pmatrix} \begin{pmatrix} \theta_{00} \\ \theta_{01} \\ \theta_{10} \\ \theta_{11} \\ \theta_{20} \\ \theta_{21} \\ \theta_{30} \\ \theta_{31} \end{pmatrix}. \tag{B.5}$$

B.2 Alternative final formulation

Formula (B.1) with (B.2) could be tough to handle, but it can be simplified further. Let us substitute the sums Σ_1 and Σ_2,

$$\int_0^1 f_{\mathrm{E}}(\widehat{x})\mathrm{d}\widehat{x} \approx \frac{\exp \overline{P}}{\overline{P}} \sum_{i=0}^{m} a_i \frac{i!}{\overline{P}^i} - \frac{1}{\overline{P}} \sum_{i=0}^{m} \left(a_i \sum_{j=0}^{i} \frac{i!}{\overline{P}^j (i-j)!} \right),$$

and remove common factor,

$$\int_0^1 f_{\mathrm{E}}(\widehat{x})\mathrm{d}\widehat{x} \approx \sum_{i=0}^{m} \left(a_i \frac{i!}{\overline{P}^i} \left(\frac{\exp \overline{P}}{\overline{P}} - \frac{1}{\overline{P}} \sum_{j=0}^{i} \frac{\overline{P}^{i-j}}{(i-j)!} \right) \right).$$

Taking out the coefficient a_0 and inverts the term that multiplies the a_i,

$$\int_0^1 f_{\text{E}}(\widehat{x})\mathrm{d}\widehat{x} \approx \frac{a_0}{\dfrac{\overline{P}}{\exp\overline{P}-1}} + \sum_{i=1}^{m} \frac{a_i}{\dfrac{\overline{P}}{\dfrac{i!}{\overline{P}^i}\left(\exp\overline{P} - \displaystyle\sum_{j=0}^{i}\frac{\overline{P}^{i-j}}{(i-j)!}\right)}}.$$

Similarly, taking out the first term of the second sum,

$$\int_0^1 f_{\text{E}}(\widehat{x})\mathrm{d}\widehat{x} \approx \frac{a_0}{\dfrac{\overline{P}}{\exp\overline{P}-1}} + \sum_{i=1}^{m} \frac{a_i}{\dfrac{\overline{P}}{\dfrac{i!}{\overline{P}^i}\left(\exp\overline{P} - \displaystyle\sum_{j=1}^{i}\frac{\overline{P}^{i-j}}{(i-j)!}\right)-1}},$$

and inverting the rest in the same way,

$$\int_0^1 f_{\text{E}}(\widehat{x})\mathrm{d}\widehat{x} \approx \frac{a_0}{\dfrac{\overline{P}}{\exp\overline{P}-1}} + \sum_{i=1}^{m} \frac{a_i}{\dfrac{\overline{P}}{\dfrac{i}{\overline{P}}-1}}.$$
$$\frac{}{\dfrac{(i-1)!}{\overline{P}^{i-1}}\left(\exp\overline{P} - \displaystyle\sum_{j=1}^{i}\frac{\overline{P}^{i-j}}{(i-j)!}\right)}$$

If one takes again the steps up to get rid of the second sum, a recurrence relation is obtained as follows:

$$\int_0^1 f_{\text{E}}(\widehat{x})\mathrm{d}\widehat{x} \approx \frac{a_0}{\dfrac{\overline{P}}{\exp\overline{P}-1}} + \sum_{i=1}^{m} \frac{a_i}{\dfrac{\overline{P}}{\dfrac{i}{\overline{P}}-1}}.$$
$$\cfrac{}{\cfrac{i-1}{\overline{P}}-1}$$
$$\cfrac{}{\vdots}$$
$$\cfrac{}{\cfrac{3}{\overline{P}}-1}$$
$$\cfrac{}{\cfrac{2}{\overline{P}}-1}$$
$$\cfrac{}{\cfrac{1}{\overline{P}}-1}$$
$$\cfrac{}{\exp\overline{P}-1}$$

So, the final expression can be shorted to

$$\int_0^1 f_{\text{E}}(\widehat{x})\mathrm{d}\widehat{x} \approx \sum_{i=0}^{m} \frac{a_i}{B_i(\overline{P})},$$

where the first function, $B_0(z)$, is the Bernoulli function and the $B_i(z)$ are built from it:

$$B_i(z) \coloneqq \begin{cases} \dfrac{z}{\exp z - 1}, & \text{If } \ i = 0, \\ \dfrac{z}{\dfrac{i}{B_{i-1}(z)} - 1}, & \text{Otherwise,} \end{cases}$$

Several limit cases are

$$B_i(z) \simeq \begin{cases} 1 + i, & \text{If } \ z = 0, \\ 0, & \text{If } \ z \to +\infty, \\ |z|, & \text{If } \ z \to -\infty. \end{cases}$$

The ratio of two different B-functions is

$$\frac{B_j(z)}{B_i(z)} \simeq \begin{cases} \dfrac{1+j}{1+i}, & \text{If } \ z = 0, \\ 0, & \text{If } \ z \to +\infty \ \text{ and } \ j < i, \\ \dfrac{i!}{j!} z^{j-i}, & \text{If } \ z \to +\infty \ \text{ and } \ j > i, \\ 1, & \text{If } \ z \to -\infty. \end{cases}$$

B.2.1 Special case in $ISGE_{01}/IGE_{01}$

Assume a case where P and Γ are piecewise constant. In that case $IGE_{01} = (\exp P - 1)/P = 1/B_0(P)$ and, therefore, the next ratio of integrals can be approximated as

$$\frac{ISGE_{01}}{IGE_{01}} \approx a_0 + \sum_{i=1}^{m} \frac{B_0(P)}{B_i(P)} a_i.$$

The coefficients a_i depend on both the order of the Hermite spline employed and the g-function, that in that case is $g(\widehat{x}) = IS_{0\widehat{x}}$.

Cubic Hermite

System (B.3) yields the set:

$$\begin{aligned} a_0 &= 0, \\ a_1 &= \Delta x\, S(0), \\ a_2 &= 3\, IS_{01} - 2\Delta x\, S(0) - \Delta x\, S(1), \\ a_3 &= -2\, IS_{01} + \Delta x\, S(0) + \Delta x\, S(1). \end{aligned}$$

Then, the complete source (2.32) is

$$b_C = IS_{01}|_{WC} + \left[\frac{B_0(P)}{B_1(P)}a_1 + \frac{B_0(P)}{B_2(P)}a_2 + \frac{B_0(P)}{B_3(P)}a_3\right]_{CE} - \left[\frac{B_0(P)}{B_1(P)}a_1 + \frac{B_0(P)}{B_2(P)}a_2 + \frac{B_0(P)}{B_3(P)}a_3\right]_{WC}.$$

Substituting the particular values of the a_i coefficients and collecting terms containing $S_C = S(0)|_{CE} = S(1)|_{WC}$ provides

$$\Delta x_{CE} S_C \left[\frac{B_0(P)}{B_1(P)} - 2\frac{B_0(P)}{B_2(P)} + \frac{B_0(P)}{B_3(P)}\right]_{CE} + \Delta x_{WC} S_C \left[\frac{B_0(P)}{B_2(P)} - \frac{B_0(P)}{B_3(P)}\right]_{WC}.$$

Likewise with S_W,

$$-\Delta x_{WC} S_W \left[\frac{B_0(P)}{B_1(P)} - 2\frac{B_0(P)}{B_2(P)} + \frac{B_0(P)}{B_3(P)}\right]_{WC},$$

and S_E,

$$-\Delta x_{CE} S_E \left[\frac{B_0(P)}{B_2(P)} - \frac{B_0(P)}{B_3(P)}\right]_{CE}.$$

The terms related to the integrals of the source over the intervals associated to x_C are

$$\left[1 - 3\frac{B_0(P)}{B_2(P)} + 2\frac{B_0(P)}{B_3(P)}\right]_{WC} IS_{01}|_{WC},$$

and

$$\left[3\frac{B_0(P)}{B_2(P)} - 2\frac{B_0(P)}{B_3(P)}\right]_{CE} IS_{01}|_{CE}.$$

Thus, the complete contribution with cubic Hermite splines is

$$\begin{aligned} b_C = &- \gamma_1|_{WC}\, S_W + (\gamma_1|_{CE} + \gamma_2|_{WC})\, S_C - \gamma_2|_{CE}\, S_E \\ &+ \zeta_1|_{WC}\, IS_{01}|_{WC} + \zeta_2|_{CE}\, IS_{01}|_{CE}, \end{aligned}$$

where the new coefficients in the pop-up stencil of S and IS_{01} are defined as

$$\gamma_1 \coloneqq \Delta x \left[\frac{B_0(P)}{B_1(P)} - 2\frac{B_0(P)}{B_2(P)} + \frac{B_0(P)}{B_3(P)}\right], \quad \gamma_2 \coloneqq \Delta x \left[\frac{B_0(P)}{B_2(P)} - \frac{B_0(P)}{B_3(P)}\right],$$
$$\zeta_1 \coloneqq 1 - 3\frac{B_0(P)}{B_2(P)} + 2\frac{B_0(P)}{B_3(P)}, \quad \zeta_2 \coloneqq 1 - \zeta_1,$$

and the source integrals over $[x_W, x_C]$ and $[x_C, x_E]$ can again be approximated with cubic Hermite splines or compact integration rules CIR. In the limit cases these coefficients give

$$\gamma_1 = \gamma_2 = \begin{cases} \dfrac{\Delta x}{12}, & \text{If } P = 0. \\ 0, & \text{If } |P| \to \infty, \end{cases}$$

and

$$\zeta_1 = \begin{cases} \frac{1}{2}, & \text{If } P = 0, \\ 1, & \text{If } P \to +\infty, \\ 0, & \text{If } P \to -\infty, \end{cases} \quad \zeta_2 = \begin{cases} \frac{1}{2}, & \text{If } P = 0, \\ 0, & \text{If } P \to +\infty, \\ 1, & \text{If } P \to -\infty. \end{cases}$$

Quintic Hermite

Following the procedure indicated in the previous subsection but now for quintic splines, the general source term is obtained as

$$\begin{aligned} b_C = IS_{01}|_{WC} &+ \left[\frac{B_0(P)}{B_1(P)}a_1 + \frac{B_0(P)}{B_2(P)}a_2 + \frac{B_0(P)}{B_3(P)}a_3 + \frac{B_0(P)}{B_4(P)}a_4 + \frac{B_0(P)}{B_5(P)}a_5\right]_{CE} \\ &- \left[\frac{B_0(P)}{B_1(P)}a_1 + \frac{B_0(P)}{B_2(P)}a_2 + \frac{B_0(P)}{B_3(P)}a_3 + \frac{B_0(P)}{B_4(P)}a_4 + \frac{B_0(P)}{B_5(P)}a_5\right]_{WC}, \end{aligned}$$

with the a_i:

$$\begin{aligned} &a_0 = 0, \quad a_1 = \Delta x\, S(0), \quad a_2 = \frac{1}{2}\Delta x \left.\frac{\mathrm{d}S}{\mathrm{d}\widehat{x}}\right|_0, \\ &a_3 = 10\, IS_{01} - 6\,\Delta x\, S(0) - 4\,\Delta x\, S(1) - \frac{3}{2}\,\Delta x \left.\frac{\mathrm{d}S}{\mathrm{d}\widehat{x}}\right|_0 + \frac{1}{2}\,\Delta x \left.\frac{\mathrm{d}S}{\mathrm{d}\widehat{x}}\right|_1, \\ &a_4 = -15\, IS_{01} + 8\,\Delta x\, S(0) + 7\,\Delta x\, S(1) + \frac{3}{2}\Delta x \left.\frac{\mathrm{d}S}{\mathrm{d}\widehat{x}}\right|_0 - \Delta x \left.\frac{\mathrm{d}S}{\mathrm{d}\widehat{x}}\right|_1, \\ &a_5 = 6\, IS_{01} - 3\,\Delta x\, S(0) - 3\,\Delta x\, S(1) - \frac{1}{2}\,\Delta x \left.\frac{\mathrm{d}S}{\mathrm{d}\widehat{x}}\right|_0 + \frac{1}{2}\,\Delta x \left.\frac{\mathrm{d}S}{\mathrm{d}\widehat{x}}\right|_1. \end{aligned}$$

Collecting terms containing S_C,

$$\begin{aligned} &\Delta x_{CE} S(x_C) \left[\frac{B_0(P)}{B_1(P)} - 6\frac{B_0(P)}{B_3(P)} + 8\frac{B_0(P)}{B_4(P)} - 3\frac{B_0(P)}{B_5(P)}\right]_{CE} \\ &+\Delta x_{WC} S(x_C) \left[4\frac{B_0(P)}{B_3(P)} - 7\frac{B_0(P)}{B_4(P)} + 3\frac{B_0(P)}{B_5(P)}\right]_{WC}, \end{aligned}$$

and those of S_W,

$$-\Delta x_{CE} S_E \left[4\frac{B_0(P)}{B_3(P)} - 7\frac{B_0(P)}{B_4(P)} + 3\frac{B_0(P)}{B_5(P)}\right]_{CE},$$

and S_E,

$$-\Delta x_{WC} S_W \left[\frac{B_0(P)}{B_1(P)} - 6\frac{B_0(P)}{B_3(P)} + 8\frac{B_0(P)}{B_4(P)} - 3\frac{B_0(P)}{B_5(P)}\right]_{WC}.$$

As quintic splines are employed there are additional terms related to the source derivative at the nodes. Those having $\mathrm{d}S/\mathrm{d}x$ at C are

$$\begin{aligned} &\Delta x_{CE}^2 \left.\frac{\mathrm{d}S}{\mathrm{d}x}\right|_C \left[\frac{1}{2}\frac{B_0(P)}{B_2(P)} - \frac{3}{2}\frac{B_0(P)}{B_3(P)} + \frac{3}{2}\frac{B_0(P)}{B_4(P)} - \frac{1}{2}\frac{B_0(P)}{B_5(P)}\right]_{CE} \\ &+\Delta x_{WC}^2 \left.\frac{\mathrm{d}S}{\mathrm{d}x}\right|_C \left[-\frac{1}{2}\frac{B_0(P)}{B_3(P)} + \frac{B_0(P)}{B_4(P)} - \frac{1}{2}\frac{B_0(P)}{B_5(P)}\right]_{WC}. \end{aligned}$$

Recall that $\mathrm{d}^n/\mathrm{d}\widehat{x}^n = \Delta x^n \mathrm{d}^n/\mathrm{d}x^n$. Those that multiply the source derivative at the adjacent nodes are

$$-\Delta x_{CE}^2 \left.\frac{\mathrm{d}S}{\mathrm{d}x}\right|_E \left[-\frac{1}{2}\frac{B_0(P)}{B_3(P)} + \frac{B_0(P)}{B_4(P)} - \frac{1}{2}\frac{B_0(P)}{B_5(P)}\right]_{CE},$$

and

$$-\Delta x_{WC}^2 \left.\frac{\mathrm{d}S}{\mathrm{d}x}\right|_W \left[\frac{1}{2}\frac{B_0(P)}{B_2(P)} - \frac{3}{2}\frac{B_0(P)}{B_3(P)} + \frac{3}{2}\frac{B_0(P)}{B_4(P)} - \frac{1}{2}\frac{B_0(P)}{B_5(P)}\right]_{WC},$$

The terms containing the integrals are

$$\left[1 - 10\frac{B_0(P)}{B_3(P)} + 15\frac{B_0(P)}{B_4(P)} - 6\frac{B_0(P)}{B_5(P)}\right]_{WC} IS_{01}|_{WC}\,,$$

and

$$\left[10\frac{B_0(P)}{B_3(P)} - 15\frac{B_0(P)}{B_4(P)} + 6\frac{B_0(P)}{B_5(P)}\right]_{CE} IS_{01}|_{CE}\,.$$

The complete source term with quintic Hermite is

$$\begin{aligned} b_C = &- \gamma_1|_{WC}\, S_W + (\gamma_1|_{CE} + \gamma_2|_{WC})\, S_C - \gamma_2|_{CE}\, S_E \\ &- \delta_1|_{WC} \left.\frac{\mathrm{d}S}{\mathrm{d}x}\right|_W + (\delta_1|_{CE} + \delta_2|_{WC}) \left.\frac{\mathrm{d}S}{\mathrm{d}x}\right|_C - \delta_2|_{CE} \left.\frac{\mathrm{d}S}{\mathrm{d}x}\right|_E \\ &+ \zeta_1|_{WC}\, IS_{01}|_{WC} + \zeta_2|_{CE}\, IS_{01}|_{CE}\,, \end{aligned}$$

where the coefficients are

$$\begin{aligned} \gamma_1 &\coloneqq \Delta x \left[\frac{B_0(P)}{B_1(P)} - 6\frac{B_0(P)}{B_3(P)} + 8\frac{B_0(P)}{B_4(P)} - 3\frac{B_0(P)}{B_5(P)}\right], \\ \gamma_2 &\coloneqq \Delta x \left[4\frac{B_0(P)}{B_3(P)} - 7\frac{B_0(P)}{B_4(P)} + 3\frac{B_0(P)}{B_5(P)}\right], \\ \delta_1 &\coloneqq \Delta x^2 \left[\frac{1}{2}\frac{B_0(P)}{B_2(P)} - \frac{3}{2}\frac{B_0(P)}{B_3(P)} + \frac{3}{2}\frac{B_0(P)}{B_4(P)} - \frac{1}{2}\frac{B_0(P)}{B_5(P)}\right], \\ \delta_2 &\coloneqq \Delta x^2 \left[-\frac{1}{2}\frac{B_0(P)}{B_3(P)} + \frac{B_0(P)}{B_4(P)} - \frac{1}{2}\frac{B_0(P)}{B_5(P)}\right], \\ \zeta_1 &\coloneqq 1 - 10\frac{B_0(P)}{B_3(P)} + 15\frac{B_0(P)}{B_4(P)} - 6\frac{B_0(P)}{B_5(P)}, \quad \zeta_2 \coloneqq 1 - \zeta_1, \end{aligned}$$

and their limits

$$\gamma_1 = \gamma_2 = \begin{cases} \dfrac{\Delta x}{10}, & \text{If } P = 0, \\ 0, & \text{If } |P| \to \infty, \end{cases}$$

and

$$\delta_1 = \begin{cases} \dfrac{\Delta x^2}{120}, & \text{If } P = 0, \\ 0, & \text{If } |P| \to \infty, \end{cases} \qquad \delta_2 = \begin{cases} -\dfrac{\Delta x^2}{120}, & \text{If } P = 0, \\ 0, & \text{If } |P| \to \infty. \end{cases}$$

The limits of ζ_1 and ζ_2 are the same as in cubic Hermite.

Septic Hermite

If septic splines are used, the source contribution is

$$\begin{aligned} b_C = IS_{01}|_{WC} + &\left[\frac{B_0(P)}{B_1(P)}a_1 + \frac{B_0(P)}{B_2(P)}a_2 + \frac{B_0(P)}{B_3(P)}a_3 \right. \\ &\left. + \frac{B_0(P)}{B_4(P)}a_4 + \frac{B_0(P)}{B_5(P)}a_5 + \frac{B_0(P)}{B_6(P)}a_6 + \frac{B_0(P)}{B_7(P)}a_7\right]_{CE} \\ &- \left[\frac{B_0(P)}{B_1(P)}a_1 + \frac{B_0(P)}{B_2(P)}a_2 + \frac{B_0(P)}{B_3(P)}a_3 \right. \\ &\left. + \frac{B_0(P)}{B_4(P)}a_4 + \frac{B_0(P)}{B_5(P)}a_5 + \frac{B_0(P)}{B_6(P)}a_6 + \frac{B_0(P)}{B_7(P)}a_7\right]_{WC}, \end{aligned}$$

being the a_i:

$$\begin{aligned} a_0 =& 0, \quad a_1 = \Delta x\, S(0), \quad a_2 = \frac{1}{2}\Delta x \left.\frac{\mathrm{d}S}{\mathrm{d}\widehat{x}}\right|_0, \quad a_3 = \frac{1}{6}\Delta x^2 \left.\frac{\mathrm{d}^2S}{\mathrm{d}\widehat{x}^2}\right|_0, \\ a_4 =& 35\, IS_{01} - 20\,\Delta x\, S(0) - 15\,\Delta x\, S(1) - 5\Delta x \left.\frac{\mathrm{d}S}{\mathrm{d}\widehat{x}}\right|_0 + \frac{5}{2}\Delta x \left.\frac{\mathrm{d}S}{\mathrm{d}\widehat{x}}\right|_1 \\ &- \frac{2}{3}\Delta x \left.\frac{\mathrm{d}^2S}{\mathrm{d}\widehat{x}^2}\right|_0 - \frac{1}{6}\Delta x \left.\frac{\mathrm{d}^2S}{\mathrm{d}\widehat{x}^2}\right|_1, \\ a_5 =& -84\, IS_{01} + 45\,\Delta x\, S(0) + 39\,\Delta x\, S(1) + 10\Delta x \left.\frac{\mathrm{d}S}{\mathrm{d}\widehat{x}}\right|_0 - 7\Delta x \left.\frac{\mathrm{d}S}{\mathrm{d}\widehat{x}}\right|_1 \\ &+ \Delta x \left.\frac{\mathrm{d}^2S}{\mathrm{d}\widehat{x}^2}\right|_0 + \frac{1}{2}\Delta x \left.\frac{\mathrm{d}^2S}{\mathrm{d}\widehat{x}^2}\right|_1, \\ a_6 =& 70\, IS_{01} - 36\,\Delta x\, S(0) - 34\,\Delta x\, S(1) - \frac{15}{2}\Delta x \left.\frac{\mathrm{d}S}{\mathrm{d}\widehat{x}}\right|_0 + \frac{13}{2}\Delta x \left.\frac{\mathrm{d}S}{\mathrm{d}\widehat{x}}\right|_1 \\ &- \frac{2}{3}\Delta x \left.\frac{\mathrm{d}^2S}{\mathrm{d}\widehat{x}^2}\right|_0 - \frac{1}{2}\Delta x \left.\frac{\mathrm{d}^2S}{\mathrm{d}\widehat{x}^2}\right|_1, \\ a_7 =& -20\, IS_{01} + 10\,\Delta x\, S(0) + 10\,\Delta x\, S(1) + 2\Delta x \left.\frac{\mathrm{d}S}{\mathrm{d}\widehat{x}}\right|_0 - 2\Delta x \left.\frac{\mathrm{d}S}{\mathrm{d}\widehat{x}}\right|_1 \\ &+ \frac{1}{6}\Delta x \left.\frac{\mathrm{d}^2S}{\mathrm{d}\widehat{x}^2}\right|_0 + \frac{1}{6}\Delta x \left.\frac{\mathrm{d}^2S}{\mathrm{d}\widehat{x}^2}\right|_1. \end{aligned}$$

Collecting terms containing S_C,

$$\begin{aligned} &\Delta x_{CE} S_C \left[\frac{B_0(P)}{B_1(P)} - 20\frac{B_0(P)}{B_4(P)} + 45\frac{B_0(P)}{B_5(P)} - 36\frac{B_0(P)}{B_6(P)} + 10\frac{B_0(P)}{B_7(P)}\right]_{CE} \\ &+\Delta x_{WC} S_C \left[15\frac{B_0(P)}{B_4(P)} - 39\frac{B_0(P)}{B_5(P)} + 34\frac{B_0(P)}{B_6(P)} - 10\frac{B_0(P)}{B_7(P)}\right]_{WC}. \end{aligned}$$

Those pertaining to S_E are

$$-\Delta x_{CE} S_E \left[15\frac{B_0(P)}{B_4(P)} - 39\frac{B_0(P)}{B_5(P)} + 34\frac{B_0(P)}{B_6(P)} - 10\frac{B_0(P)}{B_7(P)}\right]_{CE},$$

and those to S_W,

$$-\Delta x_{WC} S_W \left[\frac{B_0(P)}{B_1(P)} - 20\frac{B_0(P)}{B_4(P)} + 45\frac{B_0(P)}{B_5(P)} - 36\frac{B_0(P)}{B_6(P)} + 10\frac{B_0(P)}{B_7(P)}\right]_{WC}.$$

Likewise for $\mathrm{d}S/\mathrm{d}x$ at x_C,

$$\Delta x_{CE}^2 \left.\frac{\mathrm{d}S}{\mathrm{d}x}\right|_C \left[\frac{1}{2}\frac{B_0(P)}{B_2(P)} - 5\frac{B_0(P)}{B_4(P)} + 10\frac{B_0(P)}{B_5(P)} - \frac{15}{2}\frac{B_0(P)}{B_6(P)} + 2\frac{B_0(P)}{B_7(P)}\right]_{CE}$$
$$+\Delta x_{WC}^2 \left.\frac{\mathrm{d}S}{\mathrm{d}x}\right|_C \left[-\frac{5}{2}\frac{B_0(P)}{B_4(P)} + 7\frac{B_0(P)}{B_5(P)} - \frac{13}{2}\frac{B_0(P)}{B_6(P)} + 2\frac{B_0(P)}{B_7(P)}\right]_{WC},$$

at x_E,

$$-\Delta x_{CE}^2 \left.\frac{\mathrm{d}S}{\mathrm{d}x}\right|_E \left[-\frac{5}{2}\frac{B_0(P)}{B_4(P)} + 7\frac{B_0(P)}{B_5(P)} - \frac{13}{2}\frac{B_0(P)}{B_6(P)} + 2\frac{B_0(P)}{B_7(P)}\right]_{CE},$$

and at x_W,

$$-\Delta x_{WC}^2 \left.\frac{\mathrm{d}S}{\mathrm{d}x}\right|_W \left[\frac{1}{2}\frac{B_0(P)}{B_2(P)} - 5\frac{B_0(P)}{B_4(P)} + 10\frac{B_0(P)}{B_5(P)} - \frac{15}{2}\frac{B_0(P)}{B_6(P)} + 2\frac{B_0(P)}{B_7(P)}\right]_{WC},$$

Septic requires another order up of the derivative, so picking up terms with $\mathrm{d}^2S/\mathrm{d}x^2$ at x_C,

$$\Delta x_{CE}^3 \left.\frac{\mathrm{d}^2S}{\mathrm{d}x^2}\right|_C \left[\frac{1}{6}\frac{B_0(P)}{B_3(P)} - \frac{2}{3}\frac{B_0(P)}{B_4(P)} + \frac{B_0(P)}{B_5(P)} - \frac{2}{3}\frac{B_0(P)}{B_6(P)} + \frac{1}{6}\frac{B_0(P)}{B_7(P)}\right]_{CE}$$
$$+\Delta x_{WP}^3 \left.\frac{\mathrm{d}^2S}{\mathrm{d}x^2}\right|_C \left[\frac{1}{6}\frac{B_0(P)}{B_4(P)} - \frac{1}{2}\frac{B_0(P)}{B_5(P)} + \frac{1}{2}\frac{B_0(P)}{B_6(P)} - \frac{1}{6}\frac{B_0(P)}{B_7(P)}\right]_{WC},$$

at x_E,

$$-\Delta x_{CE}^3 \left.\frac{\mathrm{d}^2S}{\mathrm{d}x^2}\right|_E \left[\frac{1}{6}\frac{B_0(P)}{B_4(P)} - \frac{1}{2}\frac{B_0(P)}{B_5(P)} + \frac{1}{2}\frac{B_0(P)}{B_6(P)} - \frac{1}{6}\frac{B_0(P)}{B_7(P)}\right]_{CE},$$

and at x_W,

$$-\Delta x_{WC}^3 \left.\frac{\mathrm{d}^2S}{\mathrm{d}x^2}\right|_W \left[\frac{1}{6}\frac{B_0(P)}{B_3(P)} - \frac{2}{3}\frac{B_0(P)}{B_4(P)} + \frac{B_0(P)}{B_5(P)} - \frac{2}{3}\frac{B_0(P)}{B_6(P)} + \frac{1}{6}\frac{B_0(P)}{B_7(P)}\right]_{WC}.$$

The terms containing the integrals are

$$\left[1 - 35\frac{B_0(P)}{B_4(P)} + 84\frac{B_0(P)}{B_5(P)} - 70\frac{B_0(P)}{B_6(P)} + 20\frac{B_0(P)}{B_7(P)}\right]_{WC} IS_{01}|_{WC},$$

and

$$\left[35\frac{B_0(P)}{B_4(P)} - 84\frac{B_0(P)}{B_5(P)} + 70\frac{B_0(P)}{B_6(P)} - 20\frac{B_0(P)}{B_7(P)}\right]_{CE} IS_{01}|_{CE}.$$

Finally, the complete source contribution is

$$\begin{aligned} b_C = &- \gamma_1|_{WC}\, S_W + (\gamma_1|_{CE} + \gamma_2|_{WC}) S_P - \gamma_2|_{CE}\, S_E \\ &- \delta_1|_{WC} \left.\frac{\mathrm{d}S}{\mathrm{d}x}\right|_W + (\delta_1|_{CE} + \delta_2|_{WC}) \left.\frac{\mathrm{d}S}{\mathrm{d}x}\right|_C - \delta_2|_{CE} \left.\frac{\mathrm{d}S}{\mathrm{d}x}\right|_E \\ &- \epsilon_1|_{WC} \left.\frac{\mathrm{d}^2S}{\mathrm{d}x^2}\right|_W + (\epsilon_1|_{CE} + \epsilon_2|_{WC}) \left.\frac{\mathrm{d}^2S}{\mathrm{d}x^2}\right|_C - \epsilon_2|_{CE} \left.\frac{\mathrm{d}^2S}{\mathrm{d}x^2}\right|_E \\ &+ \zeta_1|_{WC}\, IS_{01}|_{WC} + \zeta_2|_{CE}\, IS_{01}|_{CE}, \end{aligned}$$

together with

$$\gamma_1 \coloneqq \Delta x \left[\frac{B_0(P)}{B_1(P)} - 20\frac{B_0(P)}{B_4(P)} + 45\frac{B_0(P)}{B_5(P)} - 36\frac{B_0(P)}{B_6(P)} + 10\frac{B_0(P)}{B_7(P)}\right],$$
$$\gamma_2 \coloneqq \Delta x \left[15\frac{B_0(P)}{B_4(P)} - 39\frac{B_0(P)}{B_5(P)} + 34\frac{B_0(P)}{B_6(P)} - 10\frac{B_0(P)}{B_7(P)}\right]$$
$$\delta_1 \coloneqq \Delta x^2 \left[\frac{1}{2}\frac{B_0(P)}{B_2(P)} - 5\frac{B_0(P)}{B_4(P)} + 10\frac{B_0(P)}{B_5(P)} - \frac{15}{2}\frac{B_0(P)}{B_6(P)} + 2\frac{B_0(P)}{B_7(P)}\right],$$
$$\delta_2 \coloneqq \Delta x^2 \left[-\frac{5}{2}\frac{B_0(P)}{B_4(P)} + 7\frac{B_0(P)}{B_5(P)} - \frac{13}{2}\frac{B_0(P)}{B_6(P)} + 2\frac{B_0(P)}{B_7(P)}\right],$$
$$\epsilon_1 \coloneqq \Delta x^3 \left[\frac{1}{6}\frac{B_0(P)}{B_3(P)} - \frac{2}{3}\frac{B_0(P)}{B_4(P)} + \frac{B_0(P)}{B_5(P)} - \frac{2}{3}\frac{B_0(P)}{B_6(P)} + \frac{1}{6}\frac{B_0(P)}{B_7(P)}\right],$$
$$\epsilon_2 \coloneqq \Delta x^3 \left[\frac{1}{6}\frac{B_0(P)}{B_4(P)} - \frac{1}{2}\frac{B_0(P)}{B_5(P)} + \frac{1}{2}\frac{B_0(P)}{B_6(P)} - \frac{1}{6}\frac{B_0(P)}{B_7(P)}\right],$$
$$\zeta_1 \coloneqq 1 - 35\frac{B_0(P)}{B_4(P)} + 84\frac{B_0(P)}{B_5(P)} - 70\frac{B_0(P)}{B_6(P)} + 20\frac{B_0(P)}{B_7(P)}, \quad \zeta_2 \coloneqq 1 - \zeta_1,$$

In the limit cases,

$$\gamma_1 = \gamma_2 = \begin{cases} \dfrac{3\Delta x}{28}, & \text{If } P = 0, \\ 0, & \text{If } |P| \to \infty, \end{cases} \qquad \epsilon_1 = \epsilon_2 = \begin{cases} \dfrac{\Delta x^3}{1680}, & \text{If } P = 0, \\ 0, & \text{If } |P| \to \infty, \end{cases}$$

and

$$\delta_1 = \begin{cases} \dfrac{\Delta x^2}{84}, & \text{If } P = 0, \\ 0, & \text{If } |P| \to \infty, \end{cases} \qquad \delta_2 = \begin{cases} -\dfrac{\Delta x^2}{84}, & \text{If } P = 0, \\ 0, & \text{If } |P| \to \infty. \end{cases}$$

Likewise, limits for ζ_1 and ζ_2 are as in Cubic.

Appendix C

Simplifying integrals

C.1 Introduction

In ENATE, only ILE_{01} has a simpler version

$$ILE_{01} = \int_0^1 \frac{\widehat{\rho u}}{\widehat{\overline{\Gamma}}\overline{E}} \mathrm{d}\widehat{x} = \frac{\exp \overline{P} - 1}{P_0},$$

while others keep their original formulation such as

$$ISGE_{01} = \int_0^1 \frac{\Delta x}{\widehat{\overline{\Gamma}}\overline{E}} \left[\int_0^{\widehat{x}} S \, \mathrm{d}\widehat{x}' \right] \mathrm{d}\widehat{x},$$

or

$$IGE_{01} = \int_0^1 \frac{\mathrm{d}\widehat{x}}{\widehat{\overline{\Gamma}}\overline{E}}.$$

However, some simplifications of the above integrals could be made via integration by parts.

C.2 Integration-by-parts generalization

Let us consider two functions, $f = f(x)$ and $g = g(x)$. Integration by parts states that

$$\int f \, \mathrm{d}g = fg - \int g \, \mathrm{d}f,$$

or replacing $\mathrm{d}f = (\mathrm{d}f/\mathrm{d}x)\mathrm{d}x$ and $\mathrm{d}g = (\mathrm{d}g/\mathrm{d}x)\mathrm{d}x$,

$$\int f \frac{\mathrm{d}g}{\mathrm{d}x} \mathrm{d}x = fg - \int g \frac{\mathrm{d}f}{\mathrm{d}x} \mathrm{d}x.$$

With the help of another function $h = h(x)$ such that $h = \mathrm{d}g/\mathrm{d}x$, and consequently $g = \int h \mathrm{d}x$, then the integral of the product of two functions is given by

$$\int fh \, \mathrm{d}x = f \int h \, \mathrm{d}x - \int \frac{\mathrm{d}f}{\mathrm{d}x} \left[\int h \, \mathrm{d}x \right] \mathrm{d}x.$$

The previous formula could be seen as a generalization of integration by parts. We are interested in calculating the definite integral in the interval

$[a,b]$, at the lower limit a,

$$\int^a fh\,\mathrm{d}x = f(a)\int^a h\,\mathrm{d}x - \int^a \frac{\mathrm{d}f}{\mathrm{d}x}\left[\int^x h\,\mathrm{d}x'\right]\mathrm{d}x,$$

where x' is a dummy variable, the integral in the interval $[a,b]$ reads

$$\int_a^b fh\,\mathrm{d}x = f(b)\int^b h\,\mathrm{d}x - f(a)\int^a h\,\mathrm{d}x - \int_a^b \frac{\mathrm{d}f}{\mathrm{d}x}\left[\int^x h\,\mathrm{d}x'\right]\mathrm{d}x.$$

Bear in mind that

$$\int_a^b \frac{\mathrm{d}f}{\mathrm{d}x}\left[\int_a^x h\,\mathrm{d}x'\right]\mathrm{d}x = \int_a^b \frac{\mathrm{d}f}{\mathrm{d}x}\left[\int^x h\,\mathrm{d}x'\right]\mathrm{d}x - [f(b)-f(a)]\int^a h\,\mathrm{d}x,$$

so the inner product of $f(x)h(x)$ within $[a,b]$ can be calculated as

$$\int_a^b fh\,\mathrm{d}x = f(b)\int_a^b h\,\mathrm{d}x - \int_a^b \frac{\mathrm{d}f}{\mathrm{d}x}\left[\int_a^x h\,\mathrm{d}x'\right]\mathrm{d}x.$$

If $f(x)$ is an nth degree polynomial, then by repeating integration by parts to the second term,

$$\int_a^b fh\,\mathrm{d}x = \sum_{k=0}^{n}(-1)^k\left.\frac{\mathrm{d}^k f}{\mathrm{d}x^k}\right|_b \underbrace{\int_a^b\cdots\int_a^x}_{k+1} h\,(\mathrm{d}x)^{k+1}.$$

C.3 Simple version of IGE_{01}

The simplification for the integral IGE_{01} is accomplished with $f = 1/\overline{E}$ and $h = 1/\widehat{\Gamma}$, i.e.,

$$\begin{aligned} IGE_{01} &= \int_0^1 \frac{d\widehat{x}}{\widehat{\Gamma}} + \int_0^1 \frac{P}{\overline{E}}\left[\int_0^{\widehat{x}} \frac{d\widehat{x}'}{\widehat{\Gamma}}\right]\mathrm{d}\widehat{x} \\ &= IG_{01} + \int_0^1 \frac{P}{\overline{E}} IG_{0\widehat{x}}\,\mathrm{d}\widehat{x} \\ &= 1 + \int_0^1 \frac{P\,\widehat{x}}{\overline{E}}\mathrm{d}\widehat{x} \quad (\Gamma = \text{const.})\,. \end{aligned}$$

If ILE_{01} is integrated by parts with $f = \widehat{\rho u}$ and $h = 1/\widehat{\Gamma}\overline{E}$ then

$$ILE_{01} = \widehat{\rho u}(1) IGE_{01} - \int_0^1 \frac{\mathrm{d}\widehat{\rho u}}{\mathrm{d}\widehat{x}} IGE_{0\widehat{x}}\mathrm{d}\widehat{x}$$

is an integral equation for IGE_{01}. In terms of the ratio ILE_{01}/IGE_{01},

$$\frac{ILE_{01}}{IGE_{01}} = 1 + \int_0^1 \frac{\mathrm{d}\widehat{\rho u}}{\mathrm{d}\widehat{x}}\left[1 - \frac{IGE_{0\widehat{x}}}{IGE_{01}}\right]\mathrm{d}\widehat{x}.$$

Due to the conservation of mass in 1D, $\mathrm{d}\rho u/\mathrm{d}x = 0$, $IGE_{01} = ILE_{01}$. Assume without loss of generality that $\mathrm{d}\rho u/\mathrm{d}x \neq 0$ and

$$IGE_{0\widehat{x}} = \alpha \frac{\exp \overline{P} - \exp \int_{\widehat{x}}^{1} P \mathrm{d}\widehat{x}'}{P_0} + \beta,$$

where α and β are constant to be determined. By substituting it in the integral equation and cancelling out the terms,

$$\alpha = \frac{1}{\widehat{\rho u}(1)} \text{ and } \beta = \frac{\widehat{\rho u}(1) - 1}{\widehat{\rho u}(1)} \frac{\exp \overline{P}}{P_0} - \frac{1}{P_0 \widehat{\rho u}(1)} \int_0^1 \frac{\mathrm{d}\widehat{\rho u}}{\mathrm{d}\widehat{x}} \frac{1}{\overline{E}} \mathrm{d}\widehat{x}.$$

By integrating by parts again,

$$IGE_{01} = \frac{1 + \widehat{\rho u}(1)}{\widehat{\rho u}(1)} \frac{\exp \overline{P} - 1}{P_0} - \frac{1}{\widehat{\rho u}(1)} \int_0^1 \frac{\widehat{\rho u}^2}{\widehat{\Gamma}\overline{E}} \mathrm{d}\widehat{x}.$$

The previous integral could be approximated by Hermite. Recall that IGE_{01} must be positive, so the integral should meet

$$\int_0^1 \frac{\widehat{\rho u}^2}{\widehat{\Gamma}\overline{E}} \mathrm{d}\widehat{x} < (1 + \widehat{\rho u}(1)) \frac{\exp \overline{P} - 1}{P_0}.$$

C.4 Simple version of $ISGE_{01}$

Taking $f = \Delta x \int_0^{\widehat{x}} S \, \mathrm{d}\widehat{x}'$ and $h = 1/(\widehat{\Gamma}\overline{E})$, then

$$\begin{aligned} ISGE_{01} &= \Delta x \int_0^1 S \, \mathrm{d}\widehat{x} \int_0^1 \frac{\mathrm{d}\widehat{x}}{\widehat{\Gamma}\overline{E}} - \Delta x \int_0^1 S \left[\int_0^{\widehat{x}} \frac{\mathrm{d}\widehat{x}'}{\widehat{\Gamma}\overline{E}} \right] \mathrm{d}\widehat{x} \\ &= IS_{01} IGE_{01} - \Delta x \int_0^1 S \, IGE_{0\widehat{x}} \, \mathrm{d}\widehat{x}, \end{aligned}$$

or in terms of the ratio $ISGE_{01}/IGE_{01}$,

$$\frac{ISGE_{01}}{IGE_{01}} = \Delta x \int_0^1 S \left[1 - \frac{IGE_{0\widehat{x}}}{IGE_{01}} \right] \mathrm{d}\widehat{x}.$$

If S and P are constants, then

$$\frac{ISGE_{01}}{IGE_{01}} = \Delta x S \frac{\exp P - P - 1}{P(\exp P - 1)},$$

which is the expected value. If the term into the brackets is defined as $w(\widehat{x}) \coloneqq 1 - IGE_{0\widehat{x}}/IGE_{01}$, then $w(\widehat{x})$ has the next properties:

1. $w(0) = 1$ and $w(1) = 0$,
2. $w(\widehat{x}) \leq 1$ since $1/(\widehat{\Gamma}\overline{E}) > 0$,
3. $w(\widehat{x}) \simeq 0$ as $P \to +\infty$ and $w(\widehat{x}) \simeq 1$ as $P \to -\infty$,
4. $\dot{w}(\widehat{x}) = -1/(IGE_{01} \, \widehat{\Gamma}\overline{E}) < 0$.

A dot over $w(\widehat{x})$ stands for $\mathrm{d}w/\mathrm{d}\widehat{x}$. $w(\widehat{x})$ has no local maximum since $\dot{w}(\widehat{x}) \neq 0$, so $0 \leq w(\widehat{x}) \leq 1$. Since the discrete source b_C is the balance of $ISGE_{01}/IGE_{01}$ within $[x_C, x_E]$ and $[x_W, x_C]$ plus IS_{01} within $[x_W, x_C]$, then

$$b_C = \Delta x \int_0^1 S \frac{IGE_{0\widehat{x}}}{IGE_{01}} \,\mathrm{d}\widehat{x}\bigg|_{WC} + \Delta x \int_0^1 S \left[1 - \frac{IGE_{0\widehat{x}}}{IGE_{01}}\right] \mathrm{d}\widehat{x}\bigg|_{CE},$$

or in a compact way: b_C is defined by the integral from x_W to x_E of the source times the Green's function $G(\widehat{x})$ of the convection-diffusion problem, i.e.,

$$G(\widehat{x}) = \begin{cases} 1 - w(\widehat{x}) & \text{within } [x_W, x_C] \\ w(\widehat{x}) & \text{within } [x_C, x_E] \end{cases},$$

whose properties are:

1. $G(1)|_{WC} = G(0)|_{CE}$,
2. $0 \leq G(\widehat{x}) \leq 1$ within $[x_W, x_E]$,
3. $G(\widehat{x}) \simeq 1$ within $[x_W, x_C]$ and $G(\widehat{x}) \simeq 0$ within $[x_C, x_E]$ as $P \to +\infty$,
4. $G(\widehat{x}) \simeq 0$ within $[x_W, x_C]$ and $G(\widehat{x}) \simeq 1$ within $[x_C, x_E]$ as $P \to -\infty$,
5. $\dot{G}(1)\Big|_{WC} - \dot{G}(0)\Big|_{CE} = \dfrac{\Gamma_0/\Gamma_1}{IGE_{01}}\bigg|_{WC} + \dfrac{\exp \overline{P}}{IGE_{01}}\bigg|_{CE} > 0.$

In the special case that Péclet number is constant, the jump in the derivative writes

$$\dot{G}(1)\Big|_{WC} - \dot{G}(0)\Big|_{CE} = \begin{cases} 2 & \text{If } P = 0, \\ |P| & \text{If } P \to \pm\infty. \end{cases}.$$

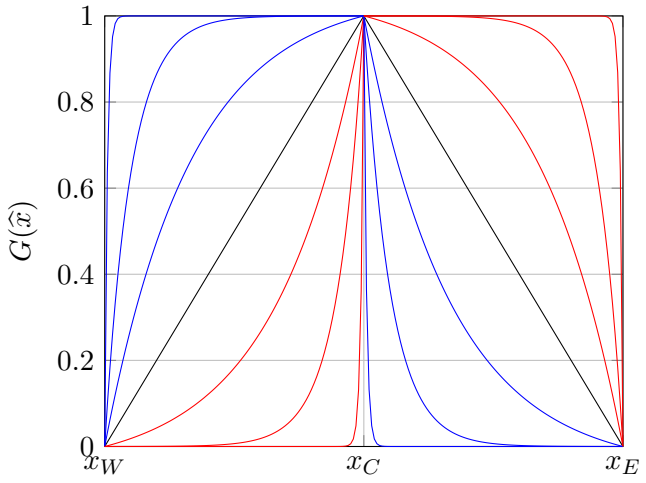

FIGURE C.1: The Green's function over two adjacent intervals for a constant Péclet regime. Black line, $P = 0$. Blue lines, $P \in \{3, 10, 100\}$. Red lines, $P \in \{-3, -10, -100\}$.

Appendix D

Compact Integration Rules

D.1 Derivation of the rule

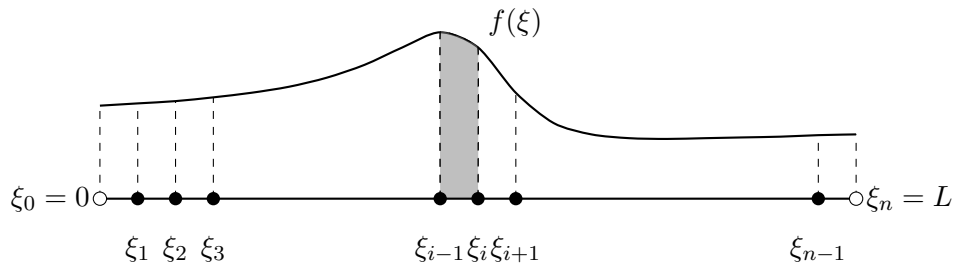

FIGURE D.1: Domain of $f(\xi)$ splits in n intervals of equal length ($\Delta\xi = L/n$).

In this appendix, we show the derivation of a derivative-free quadrature, unlike Hermite splines, to calculate the integral in an interval of a real function $f(\xi)$, smooth and continuous over the domain $[0, L]$. The function can be given analytically or as a data set at evenly distributed nodes. This quadrature fits well for IS_{01} and $\overline{P}$ in the ENATE scheme. For a clear derivation, we shall use a standard notation instead of the FV notation: ξ_i for ξ_C and so on.

Looking the Figure D.1, the integral in each interval, gray area, is put in terms of a linear combination of adjacent integrals in the left-hand side (LHS), and $f(\xi_{i+k})$, $k \in \mathbb{Z}$, in the right-hand side (RHS). The number of k's will depend on the order of accuracy sought. The quadrature is named "**C**ompact **I**ntegration **R**ules", CIR, and is analogous to the compact differentiation [108].

The generic linear combination of definite integrals centered at (ξ_{i-1}, ξ_i) for internal points is given by

$$\sum_{k=-m_1}^{m_2} \alpha_k \int_{\xi_{i+k-1}}^{\xi_{i+k}} f \, \mathrm{d}\xi = \Delta\xi \sum_{k=-q_1}^{q_2} a_k f(\xi_{i+k}) + \tau_i, \tag{D.1}$$

where $m_{1,2} \in \mathbb{N}_0$ and $q_{1,2} \in \mathbb{N}_0$ are the lower/upper bounds of the stencil for the definite integrals and the function values, respectively. If we define the vector of integrals at every interval as

$$\overline{\mathbf{f}} = \frac{1}{\Delta\xi} \left(\int_{\xi_0}^{\xi_1} f \, \mathrm{d}\xi, \int_{\xi_1}^{\xi_2} f \, \mathrm{d}\xi, \cdots, \int_{\xi_{n-1}}^{\xi_n} f \, \mathrm{d}\xi \right)^T,$$

and the integrand at nodes,

$$\mathbf{f} = (f_0,\ f_1,\ \cdots,\ f_n)^T,$$

the CIR method ends up by solving the linear system

$$\mathbf{M}\bar{\mathbf{f}} = \mathbf{Q}\mathbf{f} + \boldsymbol{\tau}, \tag{D.2}$$

where $\mathbf{M}$ is an n-by-n band-matrix that stores the parameters α_k and $\mathbf{Q}$ is an n-by-$(n+1)$ band-matrix of a_k's. Note that if $m_1 = m_2 = 0$, $\mathbf{M}$ is a diagonal matrix and the quadrature is explicit. The development of CIR will be described in detail for some special cases of equation (D.1). In particular, symmetry in the LHS will be assumed with $\alpha_0 = 1$. The detailed analysis will be restricted to a matrix of five diagonals in the LHS, $m_1 = m_2 = 2$, and six diagonals in the RHS, $q_1 = 3$ and $q_2 = 2$, that is

$$\begin{aligned}&\beta\int_{\xi_{i-3}}^{\xi_{i-2}} f\,\mathrm{d}\xi + \alpha\int_{\xi_{i-2}}^{\xi_{i-1}} f\,\mathrm{d}\xi + \int_{\xi_{i-1}}^{\xi_i} f\,\mathrm{d}\xi + \alpha\int_{\xi_i}^{\xi_{i+1}} f\,\mathrm{d}\xi + \beta\int_{\xi_{i+1}}^{\xi_{i+2}} f\,\mathrm{d}\xi \\ &= \Delta\xi\left[af(\xi_{i-3}) + bf(\xi_{i-2}) + cf(\xi_{i-1}) + df(\xi_i) + ef(\xi_{i+1}) + gf(\xi_{i+2})\right] + \tau_i.\end{aligned} \tag{D.3}$$

The last term is the error made in the linear combination, it is not the error in the evaluation of the integral $\int_{\xi_{i-1}}^{\xi_i} f\,\mathrm{d}\xi$. Throughout the appendix we will characterize each scheme by its local truncation error, τ_i, defined as the leading order of the error in the linear combination. The integrals of every interval have the same order of truncation error as the linear combination. As shown later, the global truncation error of the integral over the whole domain is one order of accuracy less. In the wavenumber analysis and the results section as we are mainly interested in the errors in the integral of the whole domain, the rules will be named according to the global truncation error.

The system of equations has a coefficient matrix that could be tri- or penta- diagonal depending on whether β is zero or not. On the other hand $\{a, b, c, d, e, g\}$ are linked with $\{\alpha, \beta\}$ when matching the Taylor series coefficients until the desired order of accuracy. The truncation error is related to the first term of the Taylor series that cannot be made zero by the chosen coefficients.

The notation used for the integral and the integrand is

$$\int_{\xi_0}^{\xi_{i+k}} f\,\mathrm{d}\xi = F_{i+k}, \quad f(\xi_{i+k}) = f_{i+k}, \quad k \in \mathbb{Z}.$$

In a uniform mesh the Taylor expansion centered at ξ_i of the above variables is given by

$$f_{i+k} = f_i + k\Delta x f_i^{(1)} + \frac{k^2\Delta\xi^2}{2!}f_i^{(2)} + \cdots, \tag{D.4a}$$

$$F_{i+k} = F_i + k\Delta x f_i + \frac{k^2\Delta\xi^2}{2!}f_i^{(1)} + \frac{k^3\Delta\xi^3}{3!}f_i^{(2)} + \cdots, \tag{D.4b}$$

where $f_i^{(l)}$ is a l-order (≥ 1) derivative. Equation (D.4b) is related to a definite integral within $[\xi_i, \xi_{i+k}]$ if $k > 0$ or $[\xi_{i+k}, \xi_i]$ if $k < 0$. In equation (D.3),

the integration limits go from ξ_{i+k-1} to ξ_{i+k}. So, in that case, the integrals of the vector $\overline{\mathbf{f}}$ are computed as $\overline{f}_{i+k} = (F_{i+k} - F_{i+k-1})/\Delta\xi$ in order to cancel out F_i.

D.1.1 Local third-order family

Let us begin with a simple low order rule where we match the f_i and the $f_i^{(1)}$ terms as shown below.

$$\begin{aligned}
&\beta\left(\Delta\xi f_i + \frac{\left(2^2-3^2\right)\Delta\xi^2}{2!}f_i^{(1)}\right) + \alpha\left(\Delta\xi f_i + \frac{\left(1-2^2\right)\Delta\xi^2}{2!}f_i^{(1)}\right)\\
+&\left(\Delta\xi f_i - \frac{\Delta\xi^2}{2!}f_i^{(1)}\right) + \alpha\left(\Delta\xi f_i + \frac{\Delta\xi^2}{2!}f_i^{(1)}\right) + \beta\left(\Delta\xi f_i + \frac{\left(2^2-1\right)\Delta\xi^2}{2!}f_i^{(1)}\right)\\
&\approx \Delta\xi\left[a\left(f_i - 3\Delta\xi f_i^{(1)}\right) + b\left(f_i - 2\Delta\xi f_i^{(1)}\right) + c\left(f_i - \Delta\xi f_i^{(1)}\right)\right.\\
&\left. + df_i + e\left(f_i + \Delta\xi f_i^{(1)}\right) + g\left(f_i + 2\Delta\xi f_i^{(1)}\right)\right].
\end{aligned}$$

Taking the first two terms of each expansion, a set of two equations is obtained by equating the factors that multiply f_i and $f_i^{(1)}$ to zero:

$$\begin{aligned}
a + b + c + d + e + g =& 1 + 2\alpha + 2\beta,\\
3^1a + 2^1b + c - e - 2^1g =& 1!\frac{1 + 2\left(2^1-1\right)\alpha + \left(1-2^3+3^2\right)\beta}{2!}.
\end{aligned}$$

As there are eight coefficients and only two equations to be satisfied there are six arbitrary values. As an example, one can take $a = b = e = g = 0$ then $c = d = (1 + 2\alpha + 2\beta)/2$ where α and β are still arbitrary. The local truncation error is

$$\tau_i = -\left(\frac{1 - 10\alpha - 46\beta}{2}\right)\frac{\Delta\xi^3}{3!}f_i^{(2)}.$$

The local order of accuracy is the power of the interval size contained in the local truncation error. In this rule the local truncation error is proportional to $\Delta\xi^3$ so the order of accuracy is 3.

There is a number of values of $\{\alpha, \beta\}$ that make this term zero, those that satisfy $10\alpha + 46\beta = 1$. In those cases the order of accuracy increases two orders of magnitude,

$$\tau_i = -\left(\frac{38\alpha - 502\beta - 11}{6}\right)\frac{\Delta\xi^5}{5!}f_i^{(4)}.$$

The same increase happens for rules of any odd order of the local truncation error for a certain combination of α and β. Incidentally, if $\alpha = \beta = 0$ the integral is explicit and the Trapezoidal rule over each interval $[\xi_{i-1}, \xi_i]$ is recovered, i.e.,

$$\int_{\xi_{i-1}}^{\xi_i} f\,\mathrm{d}\xi \approx \frac{\Delta\xi}{2}\left(f_{i-1} + f_i\right).$$

Following this procedure we can obtain the integral in all intervals into which the whole domain has been split. The integral from 0 to L can be

calculated by the integration additive property. For instance, by taking the trapezoidal rule for each interval and summing up for the whole domain the composite Trapezoidal rule is obtained,

$$\int_0^L f \,\mathrm{d}\xi = \frac{\Delta\xi}{2}\left(f_0 + 2\sum_{i=1}^{n-1} f_i + f_n\right) - \frac{\Delta\xi^2 L}{12} f^{(2)}_{\xi^\star},$$

where $\xi^\star$ is some point within $[0, L]$. The last term of the expression has been rearranged as an average of values of the second derivative, $f_i^{(2)}$, at each interval $[\xi_{i-1}, \xi_i)$,

$$\sum_{i=1}^{n} -\frac{\Delta\xi^3}{12} f_i^{(2)} = -\frac{\Delta\xi^2 \Delta\xi\, n}{12} \frac{\sum_{i=1}^{n} f_i^{(2)}}{n} = -\frac{\Delta\xi^2 L}{12} f^{(2)}_{\xi^\star}.$$

The order of accuracy for the integral over the whole domain is 2.

D.1.2 Local fifth-, seventh- and ninth-order family

Similarly, the set of equations to be satisfied for several orders of accuracy of the local truncation error is presented in this subsection. The coefficients have to satisfy up to equation (D.6) for 5^{th}-order, up to equation (D.7) for 7^{th}-order, and up to equation (D.8) for 9^{th}-order.

$$a + b + c + d + e + g = 1 + 2\alpha + 2\beta, \tag{D.5}$$

$$\begin{aligned}
3^1 a + 2^1 b + c - e - 2^1 g &= 1! \frac{1 + 2\left(2^1 - 1\right)\alpha + \left(1 - 2^3 + 3^2\right)\beta}{2!}, \\
3^2 a + 2^2 b + c + e + 2^2 g &= 2! \frac{1 + 2^3\alpha + \left(3^3 - 1\right)\beta}{3!}, \\
3^3 a + 2^3 b + c - e - 2^3 g &= 3! \frac{1 + 2\left(2^3 - 1\right)\alpha + \left(1 - 2^5 + 3^4\right)\beta}{4!}, \\
3^4 a + 2^4 b + c + e + 2^4 g &= 4! \frac{1 + 2^5\alpha + \left(3^5 - 1\right)\beta}{5!}, \\
3^5 a + 2^5 b + c - e - 2^5 g &= 5! \frac{1 + 2\left(2^5 - 1\right)\alpha + \left(1 - 2^7 + 3^6\right)\beta}{6!}, \\
3^6 a + 2^6 b + c + e + 2^6 g &= 6! \frac{1 + 2^7\alpha + \left(3^7 - 1\right)\beta}{7!}, \\
3^7 a + 2^7 b + c - e - 2^7 g &= 7! \frac{1 + 2\left(2^7 - 1\right)\alpha + \left(1 - 2^9 + 3^8\right)\beta}{8!}.
\end{aligned} \tag{D.6, D.7, D.8}$$

A family rule which has a fifth-order local τ_i can be given by the following set of coefficients:

$$a = g = 0, \qquad b = e = \frac{10\alpha + 46\beta - 1}{24}, \qquad c = d = \frac{14\alpha - 22\beta + 13}{24}.$$

It should be mentioned that the same values of α and β that made the third-order local truncation error vanish, also cause the pair $\{b, e\}$ to become zero in the fifth-order family. As seen before, this particular pair of values of $\{\alpha, \beta\}$ leads the rule to fifth-order accuracy. In the same way, when taking $\beta = 0$ and $\alpha = 1/10$, a fifth-order rule with a two-point stencil in the RHS is

obtained,

$$\frac{1}{10}\int_{\xi_{i-2}}^{\xi_{i-1}} f\,\mathrm{d}\xi + \int_{\xi_{i-1}}^{\xi_i} f\,\mathrm{d}\xi + \frac{1}{10}\int_{\xi_i}^{\xi_{i+1}} f\,\mathrm{d}\xi \approx \frac{3\Delta\xi}{5}\left[f_{i-1}+f_i\right]. \tag{D.9}$$

When $\alpha = 11/38$ the fifth-order local truncation error goes to zero and a seventh-order accuracy is attained with a four-point stencil in the RHS by

$$\begin{aligned}&\frac{11}{38}\int_{\xi_{i-2}}^{\xi_{i-1}} f\,\mathrm{d}\xi + \int_{\xi_{i-1}}^{\xi_i} f\,\mathrm{d}\xi + \frac{11}{38}\int_{\xi_i}^{\xi_{i+1}} f\,\mathrm{d}\xi \\ &\approx \frac{\Delta\xi}{38}\left[3f_{i-2}+27f_{i-1}+27f_i+3f_{i+1}\right].\end{aligned} \tag{D.10}$$

Leaving α and β as free parameters, the seventh-order family becomes

$$\begin{aligned}a = g &= -\frac{38\alpha - 502\beta - 11}{1440}, \qquad b = e = \frac{238\alpha + 418\beta - 31}{480}, \\ c = d &= \frac{382\alpha - 158\beta + 401}{720}.\end{aligned}$$

Finally, solving the whole system of equations, a ninth-order family with only one free parameter β is obtained as follows:

$$\begin{aligned}a = g &= \frac{3\,(478\beta - 3)}{5420}, \qquad b = e = \frac{3\,(4426\beta + 199)}{5420}, \\ c = d &= \frac{24\,(83\beta + 42)}{1355}, \qquad \alpha = \frac{1726\beta + 191}{542}.\end{aligned}$$

Taking $\beta = 0$ a ninth-order scheme with a six-point stencil in the RHS can be obtained,

$$\begin{aligned}&\frac{191}{542}\int_{\xi_{i-2}}^{\xi_{i-1}} f\,\mathrm{d}\xi + \int_{\xi_{i-1}}^{\xi_i} f\,\mathrm{d}\xi + \frac{191}{542}\int_{\xi_i}^{\xi_{i+1}} f\,\mathrm{d}\xi \\ &\approx \frac{\Delta\xi}{5420}\left[-9f_{i-3}+597f_{i-2}+4032f_{i-1}+4032f_i+597f_{i+1}-9f_{i+2}\right].\end{aligned} \tag{D.11}$$

For the $(l+1)$th-order families the local truncation error can be written as

$$\begin{aligned}\tau_i = \Big[&1 + 2^{l+1}\alpha + \left(3^{l+1}-1\right)\beta \\ &- (l+1)\left(3^l a + 2^l b + c + e + 2^l g\right)\Big]\frac{\Delta\xi^{l+1}}{(l+1)!}f_i^{(l)},\end{aligned} \tag{D.12}$$

and listed in Table D.1 for different values of weights and parameters.

Ninth order can be achieved with a RHS stencil of six points. If greater accuracy is sought one can increase the stencil, the number of neighbour integrals considered or both, to let more Taylor coefficients match in the left- and right-hand sides of equation (D.1). Furthermore, the study of family rules need not be limited to odd orders. For instance, to derive a local

fourth-order family the system of equations is

$$\begin{aligned} a+b+c+d+e+g &= 1+2\alpha+2\beta, \\ 3^1a+2^1b+c-e-2^1g &= 1!\frac{1+2\left(2^1-1\right)\alpha+\left(1-2^3+3^2\right)\beta}{2!}, \\ 3^2a+2^2b+c+e+2^2g &= 2!\frac{1+2^3\alpha+\left(3^3-1\right)\beta}{3!}. \end{aligned}$$

Taking $\beta = 0$ and $a = e = g = 0$, the family rule with free α becomes

$$b = \frac{10\alpha-1}{12}, \quad c = \frac{2(1-\alpha)}{3}, \quad d = \frac{22\alpha+5}{12},$$

with the truncation error being

$$\tau_i = (1-10\alpha)\frac{\Delta\xi^4}{4!}f_i^{(3)}.$$

If $\alpha = 1/10$ the rule (D.9) is recovered.

a, g	b, e	c, d	α	β	τ_i
		$\frac{1}{2}$			$-\frac{\Delta\xi^3}{12}f_i^{(2)}$
		$\frac{1+2\alpha+2\beta}{2}$	α	β	$-\left(\frac{1-10\alpha-46\beta}{2}\right)\frac{\Delta\xi^3}{3!}f_i^{(2)}$
	$\frac{10\alpha+46\beta-1}{24}$	$\frac{14\alpha-22\beta+13}{24}$	α	β	$-\left(\frac{38\alpha-502\beta-11}{6}\right)\frac{\Delta\xi^5}{5!}f_i^{(4)}$
		$\frac{3}{5}$	$\frac{1}{10}$		$-\frac{\Delta\xi^5}{100}f_i^{(4)}$
$-\frac{38\alpha-502\beta-11}{1440}$	$\frac{238\alpha+418\beta-31}{480}$	$\frac{382\alpha-158\beta+401}{720}$	α	β	$-\left(\frac{191-542\alpha+1726\beta}{12}\right)\frac{\Delta\xi^7}{7!}f_i^{(6)}$
	$\frac{3}{38}$	$\frac{27}{38}$	$\frac{11}{38}$		$-\frac{3\Delta\xi^7}{5320}f_i^{(6)}$
$\frac{3(478\beta-3)}{5420}$	$\frac{3(4426\beta+199)}{5420}$	$\frac{24(83\beta+42)}{1355}$	$\frac{1726\beta+191}{542}$	β	$-\frac{216(3762\beta-137)}{1355}\frac{\Delta\xi^9}{9!}f_i^{(8)}$
$-\frac{9}{5420}$	$\frac{597}{5420}$	$\frac{1008}{1355}$	$\frac{191}{542}$		$-\frac{29592}{1355}\frac{\Delta\xi^9}{9!}f_i^{(8)}$

TABLE D.1: Summary of parameters, weights and local truncation errors for eqn.(D.3). No entry value means that the parameter is equal to zero.

D.1.3 CIR at Boundaries

The whole background for internal points has been provided, but it is necessary, in closing the algebraic system, to treat the integrals of $f(\xi)$ at both boundaries using the same strategy of matching Taylor series terms. A general boundary rule centered at (ξ_{p-1}, ξ_p) close to ξ_0 could be

$$\sum_{k=-m_{c1}}^{m_{c2}} \alpha_k \int_{\xi_{p+k-1}}^{\xi_{p+k}} f \, \mathrm{d}\xi = \Delta\xi \sum_{k=0}^{q_c} a_k f(\xi_k) + \tau_p,$$

where m_{c2}, $q_c \in \mathbb{N}_0$ and $\{m_{c1} \in \mathbb{N}_0 | \, 0 \leq m_{c1} \leq p-1\}$. The equivalent rule close to ξ_n reads

$$\sum_{k=-m_{c1}}^{m_{c2}} \alpha_k \int_{\xi_{p-k-1}}^{\xi_{p-k}} f \, \mathrm{d}\xi = \Delta\xi \sum_{k=0}^{q_c} a_k f(\xi_{n-k}) + \tau_p,$$

where $\{m_{c1} \in \mathbb{N}_0 | \, 0 \leq m_{c1} \leq n-p\}$. Note that α's and a's are the same for both rules and might be identical or not to the internal ones. The set $\{a_k\}$ links with $\{\alpha_k\}$ via similar expansion (D.4) centered at ξ_p. With similar particularizations as before, boundary CIRs at ξ_0, $p=1$, and ξ_n, $p=n$, have the form

$$\begin{aligned}
&\int_{\xi_0}^{\xi_1} f \, \mathrm{d}\xi + \alpha \int_{\xi_1}^{\xi_2} f \, \mathrm{d}\xi \\
&= \Delta\xi \left[a f_0 + b f_1 + c f_2 + d f_3 + e f_4 + g f_5 + k f_6 \right] + \tau_1, \\
&\alpha \int_{\xi_{n-2}}^{\xi_{n-1}} f \, \mathrm{d}\xi + \int_{\xi_{n-1}}^{\xi_n} f \, \mathrm{d}\xi \\
&= \Delta\xi \left[a f_n + b f_{n-1} + c f_{n-2} + d f_{n-3} + e f_{n-4} + g f_{n-5} + k f_{n-6} \right] + \tau_n,
\end{aligned}$$

where the local truncation error is

$$\begin{aligned}
\tau_{1,n} = \Big[1 + \left(2^{l+1} - 1 \right) \alpha - (l+1) \Big(& b + 2^l c \\
& + \; 3^l d + 4^l e + 5^l g + 6^l k \Big) \Big] \frac{\Delta\xi^{l+1}}{(l+1)!} f_{1,n}^{(l)}.
\end{aligned}$$

For the 9^{th}-order rule and any other with a large stencil in the RHS, an additional boundary expression should be added at ξ_1 and ξ_{n-1} since some points of the stencil in (D.11) are outside the domain. For instance, close to the left boundary the integral $\int_{\xi_1}^{\xi_2} f \, \mathrm{d}\xi$ would require $f(\xi_{-1})$. For this case we have

$$\begin{aligned}
&\alpha_{-1} \int_{\xi_0}^{\xi_1} f \, \mathrm{d}\xi + \int_{\xi_1}^{\xi_2} f \, \mathrm{d}\xi + \alpha_1 \int_{\xi_2}^{\xi_3} f \, \mathrm{d}\xi \\
&= \Delta\xi \left[a f_0 + b f_1 + c f_2 + d f_3 + e f_4 + g f_5 \right] + \tau_2, \\
&\alpha_1 \int_{\xi_{n-3}}^{\xi_{n-2}} f \, \mathrm{d}\xi + \int_{\xi_{n-2}}^{\xi_{n-1}} f \mathrm{d}\xi + \alpha_{-1} \int_{\xi_{n-1}}^{\xi_n} f \, \mathrm{d}\xi \\
&= \Delta\xi \left[a f_n + b f_{n-1} + c f_{n-2} + d f_{n-3} + e f_{n-4} + g f_{n-5} \right] + \tau_{n-1},
\end{aligned}$$

with the truncation error being

$$\begin{aligned}
\tau_{2,n-1} = \Big[1 + \left(2^9 - 1 \right) \alpha_{-1} + \alpha_1 & \\
- 9 \left(2^8 a + b + d + 2^8 e + 3^8 g \right) \Big] & \frac{\Delta\xi^9}{9!} f_{2,n-1}^{(8)}.
\end{aligned}$$

All parameters and weights are provided in Table D.2 and D.3 for boundary points. As a remark, a 5^{th}-order boundary rule yields Simpson's rule for the integral between ξ_0 and ξ_2. Some of the rules are also provided in Table D.2 with a free α but adding this new degree of freedom enlarges the stencil of the RHS by one node. Notice that the ninth-order rule for nodes adjacent to boundary has broken the symmetry to get a shorter stencil in the RHS.

Local order	α	a	b	c	d	e	g	k
3	α	$\frac{1-\alpha}{2}$	$\frac{1+3\alpha}{2}$					
		$\frac{1}{2}$	$\frac{1}{2}$					
5	α	$\frac{9-\alpha}{24}$	$\frac{13\alpha+19}{24}$	$\frac{13\alpha-5}{24}$	$\frac{1-\alpha}{24}$			
	1	$\frac{1}{3}$	$\frac{4}{3}$	$\frac{1}{3}$				
7	α	$\frac{475-27\alpha}{1440}$	$\frac{637\alpha+1427}{1440}$	$\frac{7(73\alpha-57)}{720}$	$\frac{241-129\alpha}{720}$	$\frac{77\alpha-173}{1440}$	$\frac{27-11\alpha}{1440}$	
	$\frac{27}{11}$	$\frac{281}{990}$	$\frac{1028}{495}$	$\frac{196}{165}$	$-\frac{52}{495}$	$\frac{1}{90}$		
9	$-\frac{1375}{56097}$	$\frac{71036879}{212046660}$	$\frac{5684564}{5890185}$	$-\frac{13273643}{23560740}$	$\frac{19246592}{53011665}$	$-\frac{3823643}{23560740}$	$\frac{253964}{5890185}$	$-\frac{1085521}{212046660}$

TABLE D.2: Parameter and weights for boundary rule at ξ_0 and ξ_n. No entry value means that the parameter is equal to zero.

α_{-1}	α_1	a	b	c	d	e	g
$\frac{5}{32}$	$\frac{4357}{6112}$	$\frac{2337}{61120}$	$\frac{33687}{61120}$	$\frac{3897}{3820}$	$\frac{258}{955}$	$-\frac{693}{61120}$	$\frac{9}{12224}$

TABLE D.3: Parameter and weights for 9^{th}-order boundary rule at ξ_1 and ξ_{n-1}.

D.1.4 Global truncation error

The global truncation error can be estimated as the sum of all the elements of the vector that results from $\mathbf{M}^{-1}\tau$, that is,

$$\tau = \mathbf{1}^T\mathbf{M}^{-1}\boldsymbol{\tau},$$

being $\mathbf{1} = (1, 1, \cdots, 1)^T$. The vector of local truncation errors at each point of the mesh $\{\xi_i\}$ is written as

$$\tau = \Delta\xi^{l+1}\text{diag}(\boldsymbol{\lambda})\mathbf{f}^{(\mathbf{l})},$$

where $\boldsymbol{\lambda} = (\lambda_1, \lambda_2, \cdots, \lambda_n)^T$ is the vector of constants, that are equal for inner points, and $\mathbf{f}^{(\mathbf{l})} = (f_1^{(l)}, f_2^{(l)}, \cdots, f_n^{(l)})^T$ is the vector of lth-derivative values. So

$$\tau = \Delta\xi^{l+1}\boldsymbol{\lambda}^{\star}\cdot\mathbf{f}^{(\mathbf{l})} \quad \text{with} \quad \boldsymbol{\lambda}^{\star} = \mathbf{1}^T\mathbf{M}^{-1}\text{diag}(\boldsymbol{\lambda}).$$

It can be rearranged as a weighted average of values for the lth derivative at ξ_i,

$$\tau = \Delta\xi^l\Delta\xi\, n\,\frac{\boldsymbol{\lambda}^{\star}\cdot\mathbf{1}}{n}\,\frac{\boldsymbol{\lambda}^{\star}\cdot\mathbf{f}^{(\mathbf{l})}}{\boldsymbol{\lambda}^{\star}\cdot\mathbf{1}} = \Delta\xi^l L\,\overline{\lambda^{\star}}\,f_a^{(l)},$$

the truncation error for the integral of the whole domain is $\mathcal{O}\left(\Delta\xi^l\right)$ whereas for the integrals of the intervals is $\mathcal{O}\left(\Delta\xi^{l+1}\right)$.

D.2 CIR as linear multistep method

In this section an analogy between CIR and linear multistep methods for ODE is established. It will be theoretically shown that if CIR is cast as a linear multistep method it is not stable but when used as originally proposed, that is, a system of equations, it can provide very accurate solutions

without stability problems in the iterative matrix solver, at least for the numerical tests proposed. CIR can compute the 1D integral

$$F(\xi) = \int_{\xi_0}^{\xi} f(\xi')\,\mathrm{d}\xi',$$

being ξ' the integration variable. In a general case, the integrand f may depend on F, thus dealing with an integral equation

$$F(\xi) = \int_{\xi_0}^{\xi} f(\xi', F(\xi'))\,\mathrm{d}\xi'.$$

As will be shown CIR can also be interpreted as a linear multistep method applied to the first-order ODE

$$\frac{\mathrm{d}F}{\mathrm{d}\xi} = f(\xi, F(\xi)), \quad F(\xi_0) = 0.$$

In a linear multistep method $\mathrm{d}F/\mathrm{d}\xi$ is approximated as a linear combination of the discrete integrals $\{F_i\}$ at equally spaced mesh points $\{\xi_i\}$ and the RHS is computed by a linear combination of f values at the same points.

$$\sum_{s=0}^{w} \lambda_s F_{i+s} = \Delta\xi \sum_{s=0}^{w} \mu_s f_{i+s}.$$

Coefficients λ_s and μ_s are determined by Taylor expansion matching, numerical integration, or interpolation. If the integrals in equation (D.3) are separated as

$$\int_{\xi_{i+k-1}}^{\xi_{i+k}} f\,\mathrm{d}\xi = F_{i+k} - F_{i+k-1}, \quad k \in \{0, \pm 1, \pm 2\},$$

and the F-terms are grouped with a previous shift of indices, e.g. $F_{i-3} \to F_i$ and so on, then the recurrence relation reads

$$\begin{aligned}
&\beta F_{i+5} + (\alpha - \beta)\, F_{i+4} + (1-\alpha) F_{i+3} - (1-\alpha) F_{i+2} \\
&-(\alpha - \beta) F_{i+1} - \beta F_i = \Delta\xi \Big[g f_{i+5} + e f_{i+4} + d f_{i+3} \\
&+ c f_{i+2} + b f_{i+1} + a f_i \Big].
\end{aligned} \tag{D.13}$$

Then, the λ_s and μ_s coefficients are

$$\begin{aligned}
\{\lambda_s | s = 0, \ldots, 5\} &= \{-\beta, -(\alpha - \beta), -(1-\alpha), 1-\alpha, \alpha - \beta, \beta\}, \\
\{\mu_s | s = 0, \ldots, 5\} &= \{a, b, c, d, e, g\}.
\end{aligned}$$

Equation (D.13) is a 5-step method which will be implicit in a general nonlinear case where f depends on F, as long as $g \neq 0$. In the limit case of $\beta = 0$, the method is 3-step, i.e.,

$$\begin{aligned}
&\alpha F_{i+3} + (1-\alpha) F_{i+2} - (1-\alpha) F_{i+1} - \alpha F_i \\
&= \Delta\xi \Big[e f_{i+3} + d f_{i+2} + c f_{i+1} + b f_i \Big],
\end{aligned} \tag{D.14}$$

where

$$\{\lambda_s | s = 0, \ldots, 3\} = \{-\alpha, -(1-\alpha), 1-\alpha, \alpha\},$$
$$\{\mu_s | s = 0, \ldots, 3\} = \{b, c, d, e\}.$$

To keep the same number of points in the left- and right-hand side, $a = g = 0$ has been taken. Additionally, if $e \neq 0$ then (D.14) is an implicit method. The coefficients $\{\alpha, \beta\}$ and parameters $\{a, b, c, d, e, g\}$ are those in Table D.1. As any CIR scheme can be cast as a linear multistep method one may wonder at this point if there is any reason to implement CIR as a multistep method instead of a tri/penta-diagonal system. Of course, this will depend on the characteristics of multistep CIR, so in the following subsections the consistency and stability of a multistep CIR of three or five steps will be checked.

D.2.1 Consistency

A linear multistep method is consistent if the truncation error defined as

$$\tau_i = \frac{\sum_{s=0}^{w} \left(\lambda_s F_{i+s} - \Delta\xi \mu_s F'_{i+s}\right)}{\Delta\xi \sum_{s=0}^{w} \mu_s},$$

tends to zero when the space length $\Delta\xi$ tends to zero as well. τ_i is divided by $\Delta\xi \sum_{s=0}^{w} \mu_s$ in order to normalize the error. In terms of the first, $\rho(r) = \sum_{s=0}^{w} \lambda_s r^s$, and second, $\sigma(r) = \sum_{s=0}^{w} \mu_s r^s$, characteristic polynomials the condition reads

$$\rho(1) = 0 \qquad \text{and} \qquad \left.\frac{\mathrm{d}\rho}{\mathrm{d}r}\right|_1 = \sigma(1) \neq 0. \tag{D.15}$$

For the 5-step CIR these two polynomials are

$$\rho_5(r) = \beta r^5 + (\alpha - \beta)\, r^4 + (1-\alpha) r^3 - (1-\alpha) r^2 - (\alpha - \beta) r - \beta,$$
$$\sigma_5(r) = g r^5 + e r^4 + d r^3 + c r^2 + b r + a,$$

whereas for the 3-step CIR

$$\rho_3(r) = \alpha r^3 + (1-\alpha) r^2 - (1-\alpha) r - \alpha,$$
$$\sigma_3(r) = e r^3 + d r^2 + c r + b.$$

The first condition in (D.15) is met because terms containing α and β cancel out, whereas the second condition yields the equation (D.5). Therefore a 3-step CIR is consistent if $\alpha \neq -1/2$ and so is 5-step CIR is if $\alpha + \beta \neq -1/2$. As none of the CIR schemes put forward in the previous section, e.g. (D.9), (D.10) and (D.11), have negative values of $\{\alpha, \beta\}$, the condition is satisfied.

D.2.2 Stability

Aside from consistency, stability plays an important role in the numerical analysis. The theory of linear multistep method distinguishes two types of stabilities: Zero- and A-stability. A method is called zero-stable if the

numerical solution

$$\sum_{s=0}^{w} \lambda_s F_{i+s} = 0,$$

remains bounded as $i \to \infty$, or roughly speaking, round-off errors do not grow up. That is checked by the roots of the first characteristic polynomial which must lie within a unit circle with at most a simple root on the edge of the disk. For instance, the polynomial $\rho_3(r)$ can be factorized as

$$\rho_3(r) = (r-1)\left(\alpha r^2 + r + \alpha\right).$$

The first root has $|r_0| = 1$. If r_1, r_2 are the roots of $\alpha r^2 + r + \alpha$, then

$$\begin{cases} r_1 + r_2 = -1/\alpha, \\ r_1 r_2 = 1. \end{cases}$$

The second equation of the system tells that if one solution, e.g., $|r_1| \leq 1$ then $|r_2| \geq 1\ \forall \alpha$. Similarly with the 5-step CIR,

$$\rho_5(r) = (r-1)\left(\beta r^4 + \alpha r^3 + r^2 + \alpha r + \beta\right),$$

one root is on the unit disk and the others obey

$$\begin{cases} r_1 + r_2 + r_3 + r_4 = -\alpha/\beta, \\ r_1 r_2 + r_2 r_3 + r_3 r_4 + r_4 r_1 + r_1 r_3 + r_2 r_4 = 1/\beta, \\ r_1 r_2 r_3 + r_2 r_3 r_4 + r_1 r_2 r_4 + r_1 r_3 r_4 = -\alpha/\beta, \\ r_1 r_2 r_3 r_4 = 1, \end{cases}$$

where at least one root will be outside the disk. Therefore, the CIR method as a linear multistep method is not stable, it is mandatory that the integrals related to CIR be solved by a tri/pentadiagonal matrix system.

D.2.3 Build an ODE solver with CIR

As seen in previous section, CIR, written as a multistep method does not have good stability properties but written as a system of equations is able to numerically approximate ODEs. Let us consider for instance the nonhomogeneous linear BVP

$$\begin{cases} \dfrac{\mathrm{d}F}{\mathrm{d}\xi} + pF = q, \quad \xi_0 \leq \xi \leq \xi_n, \\ F(\xi_0) = F_{\text{BC}}, \end{cases} \tag{D.16}$$

being F_{BC} a given value at the boundary, $p = p(\xi)$ and $q = q(\xi)$ two given functions. The CIR method can be applied to $\mathrm{d}F/\mathrm{d}\xi$ with, e.g., rule (D.9) in the following manner

$$\frac{1}{10}\int_{\xi_{i-2}}^{\xi_{i-1}} \frac{\mathrm{d}F}{\mathrm{d}\xi}\mathrm{d}\xi + \int_{\xi_{i-1}}^{\xi_i} \frac{\mathrm{d}F}{\mathrm{d}\xi}\mathrm{d}\xi + \frac{1}{10}\int_{\xi_i}^{\xi_{i+1}} \frac{\mathrm{d}F}{\mathrm{d}\xi}\mathrm{d}\xi = \frac{3\Delta\xi}{5}\left(\left.\frac{\mathrm{d}F}{\mathrm{d}\xi}\right|_{i-1} + \left.\frac{\mathrm{d}F}{\mathrm{d}\xi}\right|_{i}\right),$$

and then

$$\frac{F_{i-1}-F_{i-2}}{10}+F_i-F_{i-1}+\frac{F_{i+1}-F_i}{10}=\frac{3\Delta\xi}{5}\left(q_{i-1}+q_i\right)-\frac{3\Delta\xi}{5}\left(p_{i-1}F_{i-1}+p_iF_i\right).$$

Grouping the terms F_{i-1} and F_i, a four-point stencil for the discrete solution $\{F_i\}$ at inner points reads

$$-\frac{1}{10}F_{i-2}+\left(\frac{3\Delta\xi}{5}p_{i-1}-\frac{9}{10}\right)F_{i-1}+\left(\frac{3\Delta\xi}{5}p_i+\frac{9}{10}\right)F_i+\frac{1}{10}F_{i+1}=\frac{3\Delta\xi}{5}\left(q_{i-1}+q_i\right).$$

As for the boundary schemes, the boundary expressions are employed with order 5 and $\alpha=1$ in table D.2,

$$\left(\frac{\Delta\xi}{3}p_0-1\right)F_0+\frac{4\Delta\xi}{3}p_1F_1+\left(\frac{\Delta\xi}{3}p_2+1\right)F_2=\frac{\Delta\xi}{3}\left(q_0+4q_1+q_2\right),$$
$$\left(\frac{\Delta\xi}{3}p_{n-2}-1\right)F_{n-2}+\frac{4\Delta\xi}{3}p_{n-1}F_{n-1}+\left(\frac{\Delta\xi}{3}p_n+1\right)F_n=\frac{\Delta\xi}{3}\left(q_{n-2}+4q_{n-1}+q_n\right),$$

Thus, the numerical solution is achieved by solving

$$\mathbf{M}\mathbf{v}=\Delta\xi\mathbf{M}_2\mathbf{q}+\mathbf{v}_{\text{BC}},\quad \mathbf{M}=\mathbf{M}_1+\Delta\xi\mathbf{M}_2\,\text{diag}(\mathbf{p}),$$

where the vectors are defined as $\mathbf{v}=(F_0,F_1,\ldots,F_n)^T$, $\mathbf{v}_{\text{BC}}=(F_{\text{BC}},0,\ldots,0)^T$, $\mathbf{p}=(p_0,p_1,\ldots,p_n)^T$, $\mathbf{q}=(q_0,q_1,\ldots,q_n)^T$ and the matrices

$$\mathbf{M}_1=\begin{pmatrix}
1 & 0 & 0 & \cdots & \cdots & \cdots & 0\\
-1 & 0 & 1 & \ddots & \ddots & \ddots & \vdots\\
-\frac{1}{10} & -\frac{9}{10} & \frac{9}{10} & \frac{1}{10} & \ddots & \ddots & \vdots\\
0 & -\frac{1}{10} & -\frac{9}{10} & \frac{9}{10} & \frac{1}{10} & \ddots & \vdots\\
\vdots & \ddots & \ddots & \ddots & \ddots & \ddots & 0\\
\vdots & \ddots & \ddots & -\frac{1}{10} & -\frac{9}{10} & \frac{9}{10} & \frac{1}{10}\\
0 & \cdots & \cdots & 0 & -1 & 0 & 1
\end{pmatrix},$$

$$\mathbf{M}_2=\begin{pmatrix}
0 & 0 & 0 & \cdots & \cdots & \cdots & 0\\
\frac{1}{3} & \frac{4}{3} & \frac{1}{3} & \ddots & \ddots & \ddots & \vdots\\
0 & \frac{3}{5} & \frac{3}{5} & 0 & \ddots & \ddots & \vdots\\
\vdots & 0 & \frac{3}{5} & \frac{3}{5} & 0 & \ddots & \vdots\\
\vdots & \ddots & \ddots & \ddots & \ddots & \ddots & 0\\
\vdots & \ddots & \ddots & 0 & \frac{3}{5} & \frac{3}{5} & 0\\
0 & \cdots & \cdots & 0 & \frac{1}{3} & \frac{4}{3} & \frac{1}{3}
\end{pmatrix}.$$

Should greater accuracy be required, e.g., the rule with $\alpha=27/11$ could be used. The $\mathbf{M}_1$, $\mathbf{M}_2$ banded matrices would change to

$$\mathbf{M}_1 = \begin{pmatrix} 1 & 0 & 0 & \cdots & \cdots & \cdots & 0 \\ -1 & -\frac{16}{11} & \frac{27}{11} & \ddots & \ddots & \ddots & \vdots \\ -11 & -27 & 27 & 11 & \ddots & \ddots & \vdots \\ 0 & -11 & -27 & 27 & 11 & \ddots & \vdots \\ \vdots & \ddots & \ddots & \ddots & \ddots & \ddots & 0 \\ \vdots & \ddots & \ddots & -11 & -27 & 27 & 11 \\ 0 & \cdots & \cdots & 0 & -\frac{27}{11} & \frac{16}{11} & 1 \end{pmatrix},$$

$$\mathbf{M}_2 = \begin{pmatrix} 0 & \cdots & \cdots & \cdots & \cdots & \cdots & 0 \\ \frac{281}{990} & \frac{1028}{495} & \frac{196}{165} & -\frac{52}{495} & \frac{1}{90} & \ddots & \vdots \\ 3 & 27 & 27 & 3 & 0 & 0 & \vdots \\ 0 & 3 & 27 & 27 & 3 & \ddots & \vdots \\ \vdots & \ddots & \ddots & \ddots & \ddots & \ddots & 0 \\ \vdots & 0 & 0 & 3 & 27 & 27 & 3 \\ 0 & \cdots & \frac{1}{90} & -\frac{52}{495} & \frac{196}{165} & \frac{1028}{495} & \frac{281}{990} \end{pmatrix}.$$

Two numerical cases are proposed. The first one is a homogeneous, $q(\xi) = 0$, linear BVP with variable coefficient, $p(\xi) = 2\xi$, and boundary condition $F(0) = 1$ whose exact solution is the Gaussian function, $F(\xi) = e^{-\xi^2}$. The other case is a stiff problem with $p(\xi) = 1000$, $q(\xi) = 3000 - 2000e^{-\xi}$ and $F(0) = 0$. Its exact solution takes the form

$$F(\xi) = 3 - \frac{997e^{-1000\,\xi} + 2000e^{-\xi}}{999},$$

and describes a process with two characteristic length scales as shown below in Figure D.3a.

In both cases the l_2-norm of the vector difference between the numerical solution and the exact one was computed. The system of equations for both cases was calculated in Matlab with one of Lapack solvers for banded matrices. The numerical solution of CIR was compared with two versions of a Predict-Evaluate-Correct-Evaluate (PECE) multistep method. This method was also coded in Matlab.

- Predictor with an Adams-Bashforth four-, five-step (AB4, AB5)
- Corrector with an Adams-Moulton three-, four-step (AM3, AM4)

Clearly, 4th-order CIR is slightly better than AB4-AM3 and both reach 4th-order accuracy. In contrast, the AB5-AM4 method is 5th-order, whereas 6th-order CIR attains the theoretical order of accuracy.

The initial strong variation of the stiff problem makes the CIR schemes not so practical in this case if $\Delta\xi$ is constant. Due to the two distinct characteristic lengths a function $\Delta\xi = \Delta\xi(\xi)$ is needed, but CIR is derived with $\Delta\xi$ constant. The solution is to define a break point, ξ_b thereby a constant $\Delta\xi_1$ is used within the interval $[\xi_0, \xi_b]$ whereas a constant $\Delta\xi_2$ is adopted in the interval $[\xi_b, \xi_n]$, being $\Delta\xi_1 < \Delta\xi_2$. The link between the two zones is ξ_b where the equations for the boundaries are employed.

As in the Gaussian problem, system CIR achieves 4th-, 6th-order accuracy, see Figure D.3b. $\overline{\Delta\xi}$ stands for average interval length. For the variable step-size PECE method with tolerance 10^{-4}, $\Delta\xi_{\text{min}} = 10^{-5}$ and $\Delta\xi_{\text{max}} = 10^{-2}$, the l_2-norm was $4.41 \cdot 10^{-5}$ with $\overline{\Delta\xi} = 1.4 \cdot 10^{-3}$. For the same $\overline{\Delta\xi}$ the 4th-order CIR gives a l_2-norm of 10^{-8} and the sixth-order, 10^{-12}.

As already commented CIR cast as multistep method is unstable. It was verified for both ODE problems that this was in fact the case.

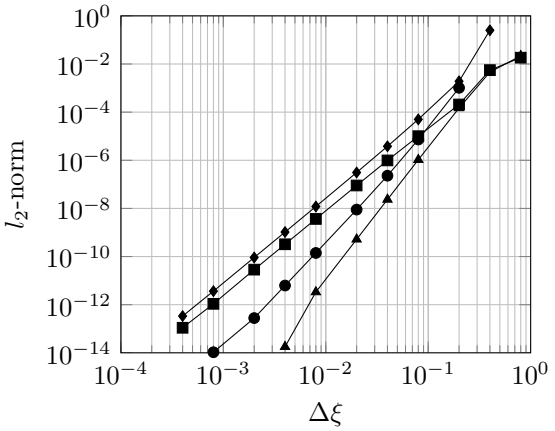

FIGURE D.2: Linear ODE $\mathrm{d}F/\mathrm{d}\xi + 2\xi F = 0$; $F(0) = 1$. **Black Square**, 4th-order rules; **Black Triangle**, 6th-order rules; **Black Diamond**, AB4-AM3; **Black Circle**, AB5-AM4.

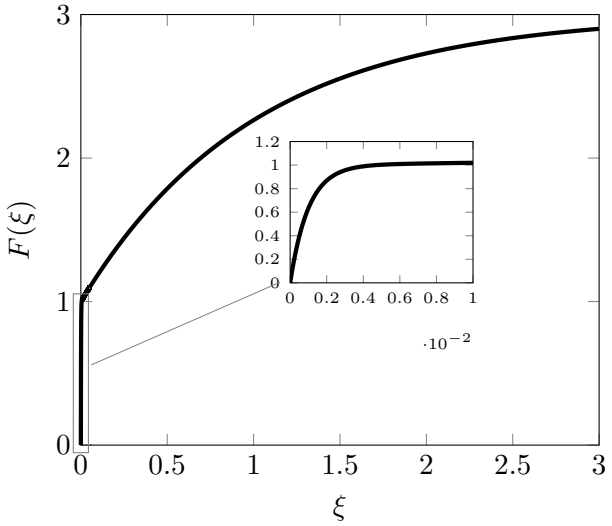

(A) Exact solution.

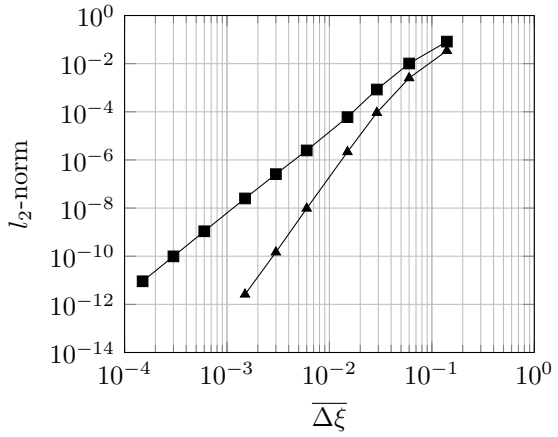

(B) **Black Square**, 4th-order rules; **Black Triangle**, 6th-order rules.

FIGURE D.3: Linear ODE $\mathrm{d}F/\mathrm{d}\xi + 1000F = 3000 - 2000e^{-\xi}$; $F(0) = 0$.

Appendix E

Compact derivation for nonuniform meshes

E.1 Introduction

Let us consider a mesh with nonuniform interval sizes. We are interested in obtaining the point values of the first derivative if the values of the function are known at the same locations. For that purpose implicit formulations will be employed where a linear combination of derivatives is related to a linear combination of the values of the function via Taylor series matching. This technique is also known as compact derivation.

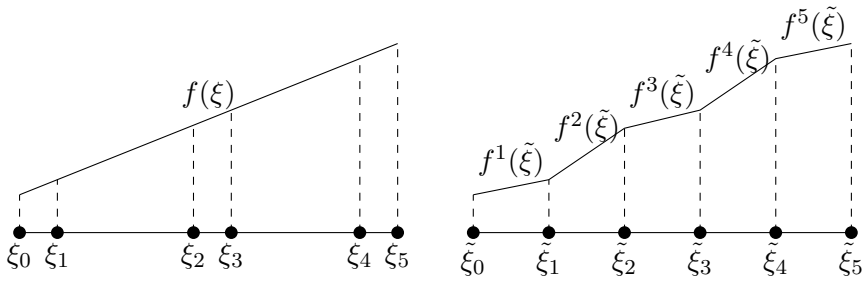

FIGURE E.1: Nonuniform mesh (left) vs Uniform mesh (right).

When deriving the coefficients of a compact derivative a constant interval size is usually assumed. In order to employ a uniform mesh where the coefficients of the linear combination are easier to derive, a mapping is constructed between the original nonuniform mesh and a uniform one, related to one another with the Jacobian, $\mathcal{J}$, of the mapping. A traditional way of defining the interval sizes in a nonuniform mesh is via an expansion/contraction ratio, defined as the ratio between the sizes of two consecutive intervals. If such is the case, the Jacobian is constant in each interval and discontinuous at the interval edges which causes the derivatives of the function in the uniform mesh to be discontinuous at the same place, even though the original derivatives were continuous. That is,

$$\frac{\partial}{\partial \xi} = \frac{1}{\mathcal{J}} \frac{\partial}{\partial \tilde{\xi}}$$

E.2 Inner Coefficients

In the uniform mesh we seek to link a linear combination of the derivatives of the function around the location $\tilde{\xi}_i$ to a linear combination of the function values around $\tilde{\xi}_i$,

$$\alpha f_{i-1}^{(1)k} + f_i^{(1)k+1} + \beta f_{i+1}^{(1)k+2} = \frac{1}{\Delta\tilde{\xi}} \left[a f_{i+2} + b f_{i+1} + c f_i + d f_{i-1} + e f_{i-2} \right] . \quad \text{(E.1)}$$

The notation adopted is that $f_i^{(l)k+1}$ represents the lth-derivative at $\tilde{\xi}_i$ of the function f^{k+1} defined in the interval $[\tilde{\xi}_i, \tilde{\xi}_{i+1}]$. We use piecewise C^∞ functions, one for each interval, that come from the mapping of a function that is C^∞ over the whole domain. The jump in the derivatives at the interval boundaries is associated to the ratio between Jacobians of the two consecutive mappings. The jump in the mth-derivative is this ratio to the mth power.

Note that f_i is the same at both sides of the edge but $f^{(1)}$ is not, that is why it must be specified to which function (interval) the derivative belongs. In the following, we will construct compact formulations for the derivatives **at the right** of the discontinuity. We will match coefficients at point ξ_i for $(k+1)$-functions. The Taylor series expansion of f_{i+2} is

$$\begin{aligned} f_{i+2} =& f_{i+1} + \Delta\tilde{\xi} f_{i+1}^{(1)k+2} + \frac{\Delta\tilde{\xi}^2}{2!} f_{i+1}^{(2)k+2} + \frac{\Delta\tilde{\xi}^3}{3!} f_{i+1}^{(3)k+2} + \cdots \\ =& f_{i+1} + \Delta\tilde{\xi} \left(\frac{\mathcal{J}_{k+2}}{\mathcal{J}_{k+1}} \right) f_{i+1}^{(1)k+1} + \frac{\Delta\tilde{\xi}^2}{2!} \left(\frac{\mathcal{J}_{k+2}}{\mathcal{J}_{k+1}} \right)^2 f_{i+1}^{(2)k+1} \\ & + \frac{\Delta\tilde{\xi}^3}{3!} \left(\frac{\mathcal{J}_{k+2}}{\mathcal{J}_{k+1}} \right)^3 f_{i+1}^{(3)k+1} + \cdots . \end{aligned}$$

In the second expression all terms belong to the $(k+1)$-function which is C^∞, so we can develop each term in its Taylor series:

$$\begin{aligned} f_{i+1} &= f_i + \Delta\tilde{\xi} f_i^{(1)k+1} + \frac{\Delta\tilde{\xi}^2}{2!} f_i^{(2)k+1} + \frac{\Delta\tilde{\xi}^3}{3!} f_i^{(3)k+1} + \cdots , \\ f_{i+1}^{(1)k+1} &= f_i^{(1)k+1} + \Delta\tilde{\xi} f_i^{(2)k+1} + \frac{\Delta\tilde{\xi}^2}{2!} f_i^{(3)k+1} + \cdots , \\ f_{i+1}^{(2)k+1} &= f_i^{(2)k+1} + \Delta\tilde{\xi} f_i^{(3)k+1} + \frac{\Delta\tilde{\xi}^2}{2!} f_i^{(4)k+1} + \cdots , \\ f_{i+1}^{(3)k+1} &= f_i^{(3)k+1} + \Delta\tilde{\xi} f_i^{(4)k+1} + \frac{\Delta\tilde{\xi}^2}{2!} f_i^{(5)k+1} + \cdots . \end{aligned}$$

Collecting like terms we obtain

$$\begin{aligned} f_{i+2} =& f_i + \Delta\tilde{\xi} \left(1 + \frac{\mathcal{J}_{k+2}}{\mathcal{J}_{k+1}} \right) f_i^{(1)k+1} + \frac{\Delta\tilde{\xi}^2}{2!} \left(1 + \frac{\mathcal{J}_{k+2}}{\mathcal{J}_{k+1}} \right)^2 f_i^{(2)k+1} \\ & + \frac{\Delta\tilde{\xi}^3}{3!} \left(1 + \frac{\mathcal{J}_{k+2}}{\mathcal{J}_{k+1}} \right)^3 f_i^{(3)k+1} + \cdots . \end{aligned}$$

On the other hand,

$$\begin{aligned}
f_{i+1} =& f_i + \Delta\tilde{\xi} f_i^{(1)k+1} + \frac{\Delta\tilde{\xi}^2}{2!} f_i^{(2)k+1} + \frac{\Delta\tilde{\xi}^3}{3!} f_i^{(3)k+1} + \cdots, \\
f_{i-1} =& f_i - \Delta\tilde{\xi} f_i^{(1)k} + \frac{\Delta\tilde{\xi}^2}{2!} f_i^{(2)k} - \frac{\Delta\tilde{\xi}^3}{3!} f_i^{(3)k} + \cdots \\
=& f_i - \Delta\tilde{\xi} \frac{\mathcal{J}_k}{\mathcal{J}_{k+1}} f_i^{(1)k+1} + \frac{\Delta\tilde{\xi}^2}{2!} \left(\frac{\mathcal{J}_k}{\mathcal{J}_{k+1}}\right)^2 f_i^{(2)k+1} \\
& - \frac{\Delta\tilde{\xi}^3}{3!} \left(\frac{\mathcal{J}_k}{\mathcal{J}_{k+1}}\right)^3 f_i^{(3)k+1} + \cdots .
\end{aligned}$$

Finally

$$\begin{aligned}
f_{i-2} =& f_{i-1} - \Delta\tilde{\xi} f_{i-1}^{(1)k-1} + \frac{\Delta\tilde{\xi}^2}{2!} f_{i-1}^{(2)k-1} - \frac{\Delta\tilde{\xi}^3}{3!} f_{i-1}^{(3)k-1} + \cdots \\
=& f_{i-1} - \Delta\tilde{\xi} \frac{\mathcal{J}_{k-1}}{\mathcal{J}_k} f_{i-1}^{(1)k} + \frac{\Delta\tilde{\xi}^2}{2!} \left(\frac{\mathcal{J}_{k-1}}{\mathcal{J}_k}\right)^2 f_{i-1}^{(2)k} \\
& - \frac{\Delta\tilde{\xi}^3}{3!} \left(\frac{\mathcal{J}_{k-1}}{\mathcal{J}_k}\right)^2 f_{i-1}^{(3)k} + \cdots .
\end{aligned}$$

Each term of the final expression has to be written in terms of f^{k+1} at ξ_i, f_{i-1} has already been obtained so for the rest,

$$\begin{aligned}
f_{i-1}^{(1)k} =& f_i^{(1)k} - \Delta\tilde{\xi} f_i^{(2)k} + \frac{\Delta\tilde{\xi}^2}{2!} f_i^{(3)k} - \cdots \\
=& \frac{\mathcal{J}_k}{\mathcal{J}_{k+1}} f_i^{(1)k+1} - \Delta\tilde{\xi} \left(\frac{\mathcal{J}_k}{\mathcal{J}_{k+1}}\right)^2 f_i^{(2)k+1} + \frac{\Delta\tilde{\xi}^2}{2!} \left(\frac{\mathcal{J}_k}{\mathcal{J}_{k+1}}\right)^3 f_i^{(3)k+1} - \cdots .
\end{aligned}$$

Likewise for $f_{i-1}^{(2)k}$. Collecting all terms,

$$\begin{aligned}
f_{i-2} =& f_i - \Delta\tilde{\xi} \frac{\mathcal{J}_k + \mathcal{J}_{k-1}}{\mathcal{J}_{k+1}} f_i^{(1)k+1} + \frac{\Delta\tilde{\xi}^2}{2!} \left(\frac{\mathcal{J}_k + \mathcal{J}_{k-1}}{\mathcal{J}_{k+1}}\right)^2 f_i^{(2)k+1} \\
& - \frac{\Delta\tilde{\xi}^3}{3!} \left(\frac{\mathcal{J}_k + \mathcal{J}_{k-1}}{\mathcal{J}_{k+1}}\right)^3 f_i^{(3)k+1} + \cdots .
\end{aligned}$$

Summing up. The expansions for the RHS are

$$
\begin{aligned}
f_{i+2} =& f_i + \Delta\tilde{\xi}\left(1+\frac{\mathcal{J}_{k+2}}{\mathcal{J}_{k+1}}\right) f_i^{(1)k+1} + \frac{\Delta\tilde{\xi}^2}{2!}\left(1+\frac{\mathcal{J}_{k+2}}{\mathcal{J}_{k+1}}\right)^2 f_i^{(2)k+1} \\
&+ \frac{\Delta\tilde{\xi}^3}{3!}\left(1+\frac{\mathcal{J}_{k+2}}{\mathcal{J}_{k+1}}\right)^3 f_i^{(3)k+1} + \cdots, \\
f_{i+1} =& f_i + \Delta\tilde{\xi} f_i^{(1)k+1} + \frac{\Delta\tilde{\xi}^2}{2!} f_i^{(2)k+1} + \frac{\Delta\tilde{\xi}^3}{3!} f_i^{(3)k+1} + \cdots, \\
f_i =& f_i, \\
f_{i-1} =& f_i - \Delta\tilde{\xi}\frac{\mathcal{J}_k}{\mathcal{J}_{k+1}} f_i^{(1)k+1} + \frac{\Delta\tilde{\xi}^2}{2!}\left(\frac{\mathcal{J}_k}{\mathcal{J}_{k+1}}\right)^2 f_i^{(2)k+1} \\
&- \frac{\Delta\tilde{\xi}^3}{3!}\left(\frac{\mathcal{J}_k}{\mathcal{J}_{k+1}}\right)^3 f_i^{(3)k+1} + \cdots, \\
f_{i-2} =& f_i - \Delta\tilde{\xi}\frac{\mathcal{J}_k + \mathcal{J}_{k-1}}{\mathcal{J}_{k+1}} f_i^{(1)k+1} + \frac{\Delta\tilde{\xi}^2}{2!}\left(\frac{\mathcal{J}_k + \mathcal{J}_{k-1}}{\mathcal{J}_{k+1}}\right)^2 f_i^{(2)k+1} \\
&- \frac{\Delta\tilde{\xi}^3}{3!}\left(\frac{\mathcal{J}_k + \mathcal{J}_{k-1}}{\mathcal{J}_{k+1}}\right)^3 f_i^{(3)k+1} + \cdots.
\end{aligned}
$$

whereas for the LHS,

$$
\begin{aligned}
f_{i-1}^{(1)k} =& \frac{\mathcal{J}_k}{\mathcal{J}_{k+1}} f_i^{(1)k+1} - \Delta\tilde{\xi}\left(\frac{\mathcal{J}_k}{\mathcal{J}_{k+1}}\right)^2 f_i^{(2)k+1} \\
&+ \frac{\Delta\tilde{\xi}^2}{2!}\left(\frac{\mathcal{J}_k}{\mathcal{J}_{k+1}}\right)^3 f_i^{(3)k+1} + \cdots, \\
f_i^{(1)k+1} =& f_i^{(1)k+1}, \\
f_{i+1}^{(1)k+2} =& \frac{\mathcal{J}_{k+2}}{\mathcal{J}_{k+1}}\left(f_i^{(1)k+1} + \Delta\tilde{\xi} f_i^{(2)k+1} + \frac{\Delta\tilde{\xi}^2}{2!} f_i^{(3)k+1} + \cdots\right).
\end{aligned}
$$

The different compact derivatives will be obtained by matching terms in both sides for f_i and $f_i^{(m)k+1}$ up to the desired order. The equations for the factors in the linear combination given in scheme (E.1) are

$$
\begin{aligned}
& a + b + c + d + e = 0, \\
& a\left(1+\frac{\mathcal{J}_{k+2}}{\mathcal{J}_{k+1}}\right) + b - d\frac{\mathcal{J}_k}{\mathcal{J}_{k+1}} - e\frac{\mathcal{J}_k + \mathcal{J}_{k-1}}{\mathcal{J}_{k+1}} = \alpha\frac{\mathcal{J}_k}{\mathcal{J}_{k+1}} + 1 + \beta\frac{\mathcal{J}_{k+2}}{\mathcal{J}_{k+1}}, \\
& \frac{a}{2!}\left(1+\frac{\mathcal{J}_{k+2}}{\mathcal{J}_{k+1}}\right)^2 + \frac{b}{2!} + \frac{d}{2!}\left(\frac{\mathcal{J}_k}{\mathcal{J}_{k+1}}\right)^2 + \frac{e}{2!}\left(\frac{\mathcal{J}_k + \mathcal{J}_{k-1}}{\mathcal{J}_{k+1}}\right)^2 = -\alpha\left(\frac{\mathcal{J}_k}{\mathcal{J}_{k+1}}\right)^2 + \beta\frac{\mathcal{J}_{k+2}}{\mathcal{J}_{k+1}}, \\
& \frac{a}{3!}\left(1+\frac{\mathcal{J}_{k+2}}{\mathcal{J}_{k+1}}\right)^3 + \frac{b}{3!} - \frac{d}{3!}\left(\frac{\mathcal{J}_k}{\mathcal{J}_{k+1}}\right)^3 - \frac{e}{3!}\left(\frac{\mathcal{J}_k + \mathcal{J}_{k-1}}{\mathcal{J}_{k+1}}\right)^3 = \frac{\alpha}{2!}\left(\frac{\mathcal{J}_k}{\mathcal{J}_{k+1}}\right)^3 + \frac{\beta}{2!}\frac{\mathcal{J}_{k+2}}{\mathcal{J}_{k+1}}.
\end{aligned}
$$

The coefficients until $f_i^{(3)k+1}$ have been written. If the coefficients are such that they satisfy up to $f_i^{(l)k+1}$ the truncation error is of the order of $\Delta\tilde{\xi}^l$. In general the equation that equalizes the terms containing $f_i^{(l)k+1}$ derivative

in both linear combinations is

$$\frac{a}{l!}\left(1+\frac{\mathcal{J}_{k+2}}{\mathcal{J}_{k+1}}\right)^l+\frac{b}{l!}+(-1)^l\frac{d}{l!}\left(\frac{\mathcal{J}_k}{\mathcal{J}_{k+1}}\right)^l+(-1)^l\frac{e}{l!}\left(\frac{\mathcal{J}_k+\mathcal{J}_{k-1}}{\mathcal{J}_{k+1}}\right)^l$$
$$=(-1)^{l+1}\frac{\alpha}{(l-1)!}\left(\frac{\mathcal{J}_k}{\mathcal{J}_{k+1}}\right)^l+\frac{\beta}{(l-1)!}\frac{\mathcal{J}_{k+2}}{\mathcal{J}_{k+1}}.$$

E.3 Boundary coefficients

For the node at the left boundary of the complete domain we have

$$f_0^{(1)1}+\alpha f_1^{(1)2}=\frac{1}{\Delta\tilde{\xi}}(af_0+bf_1+cf_2+df_3). \tag{E.2}$$

The equations that link all factors to f_0 and $f_0^{(1)1}$ are

$$\begin{aligned}
f_0 =& f_0,\\
f_1 =& f_0+\Delta\tilde{\xi}f_0^{(1)1}+\frac{\Delta\tilde{\xi}^2}{2!}f_0^{(2)1}+\frac{\Delta\tilde{\xi}^3}{3!}f_0^{(3)1}+\cdots,\\
f_2 =& f_0+\Delta\tilde{\xi}\left(1+\frac{\mathcal{J}_2}{\mathcal{J}_1}\right)f_0^{(1)1}+\frac{\Delta\tilde{\xi}^2}{2!}\left(1+\frac{\mathcal{J}_2}{\mathcal{J}_1}\right)^2f_0^{(2)1}\\
&+\frac{\Delta\tilde{\xi}^3}{3!}\left(1+\frac{\mathcal{J}_2}{\mathcal{J}_1}\right)^3f_0^{(3)1}+\cdots,\\
f_3 =& f_0+\Delta\tilde{\xi}\left(1+\frac{\mathcal{J}_2}{\mathcal{J}_1}+\frac{\mathcal{J}_3}{\mathcal{J}_1}\right)f_0^{(1)1}+\frac{\Delta\tilde{\xi}^2}{2!}\left(1+\frac{\mathcal{J}_2}{\mathcal{J}_1}+\frac{\mathcal{J}_3}{\mathcal{J}_1}\right)^2f_0^{(2)1}\\
&+\frac{\Delta\tilde{\xi}^3}{3!}\left(1+\frac{\mathcal{J}_2}{\mathcal{J}_1}+\frac{\mathcal{J}_3}{\mathcal{J}_1}\right)^3f_0^{(3)1}+\cdots,\\
f_0^{(1)1} =& f_0^{(1)1},\\
f_1^{(1)2} =& \frac{\mathcal{J}_2}{\mathcal{J}_1}\left(f_0^{(1)1}+\Delta\tilde{\xi}f_0^{(2)1}+\frac{\Delta\tilde{\xi}^2}{2!}f_0^{(3)1}+\cdots\right).
\end{aligned}$$

According to the linear combination (E.2), the equations to be satisfied from f_0 to $f_0^{(4)1}$ are

$$\begin{aligned}
&a+b+c+d=0,\\
&b+c\left(1+\frac{\mathcal{J}_2}{\mathcal{J}_1}\right)+d\left(1+\frac{\mathcal{J}_2}{\mathcal{J}_1}+\frac{\mathcal{J}_3}{\mathcal{J}_1}\right)=1+\alpha\frac{\mathcal{J}_2}{\mathcal{J}_1},\\
&\frac{b}{2!}+\frac{c}{2!}\left(1+\frac{\mathcal{J}_2}{\mathcal{J}_1}\right)^2+\frac{d}{2!}\left(1+\frac{\mathcal{J}_2}{\mathcal{J}_1}+\frac{\mathcal{J}_3}{\mathcal{J}_1}\right)^2=\alpha\frac{\mathcal{J}_2}{\mathcal{J}_1},\\
&\frac{b}{3!}+\frac{c}{3!}\left(1+\frac{\mathcal{J}_2}{\mathcal{J}_1}\right)^3+\frac{d}{3!}\left(1+\frac{\mathcal{J}_2}{\mathcal{J}_1}+\frac{\mathcal{J}_3}{\mathcal{J}_1}\right)^3=\frac{\alpha}{2!}\frac{\mathcal{J}_2}{\mathcal{J}_1},\\
&\frac{b}{4!}+\frac{c}{4!}\left(1+\frac{\mathcal{J}_2}{\mathcal{J}_1}\right)^4+\frac{d}{4!}\left(1+\frac{\mathcal{J}_2}{\mathcal{J}_1}+\frac{\mathcal{J}_3}{\mathcal{J}_1}\right)^4=\frac{\alpha}{3!}\frac{\mathcal{J}_2}{\mathcal{J}_1},
\end{aligned}$$

and the lth-derivative for $f_0^{(l)1}$ is

$$\frac{b}{l!}+\frac{c}{l!}\left(1+\frac{\mathcal{J}_2}{\mathcal{J}_1}\right)^l+\frac{d}{l!}\left(1+\frac{\mathcal{J}_2}{\mathcal{J}_1}+\frac{\mathcal{J}_3}{\mathcal{J}_1}\right)^l=\frac{\alpha}{(l-1)!}\frac{\mathcal{J}_2}{\mathcal{J}_1}.$$

For the right boundary

$$f_n^{(1)n+1}+\alpha f_{n-1}^{(1)n}=\frac{1}{\Delta\tilde{\xi}}(af_n+bf_{n-1}+cf_{n-2}+df_{n-3}). \tag{E.3}$$

The terms are

$$\begin{aligned}
f_n =& f_n,\\
f_{n-1} =& f_n-\Delta\tilde{\xi}\frac{\mathcal{J}_n}{\mathcal{J}_{n+1}}f_n^{(1)n+1}+\frac{\Delta\tilde{\xi}^2}{2!}\left(\frac{\mathcal{J}_n}{\mathcal{J}_{n+1}}\right)^2 f_n^{(2)n+1}\\
&-\frac{\Delta\tilde{\xi}^3}{3!}\left(\frac{\mathcal{J}_n}{\mathcal{J}_{n+1}}\right)^3 f_n^{(3)n+1}+\cdots,\\
f_{n-2} =& f_n-\Delta\tilde{\xi}\frac{\mathcal{J}_n+\mathcal{J}_{n-1}}{\mathcal{J}_{n+1}}f_n^{(1)n+1}+\frac{\Delta\tilde{\xi}^2}{2!}\left(\frac{\mathcal{J}_n+\mathcal{J}_{n-1}}{\mathcal{J}_{n+1}}\right)^2 f_n^{(2)n+1}\\
&-\frac{\Delta\tilde{\xi}^3}{3!}\left(\frac{\mathcal{J}_n+\mathcal{J}_{n-1}}{\mathcal{J}_{n+1}}\right)^3 f_n^{(3)n+1}+\cdots,\\
f_{n-3} =& f_n-\Delta\tilde{\xi}\frac{\mathcal{J}_n+\mathcal{J}_{n-1}+\mathcal{J}_{n-2}}{\mathcal{J}_{n+1}}f_n^{(1)n+1}+\frac{\Delta\tilde{\xi}^2}{2!}\left(\frac{\mathcal{J}_n+\mathcal{J}_{n-1}+\mathcal{J}_{n-2}}{\mathcal{J}_{n+1}}\right)^2 f_n^{(2)n+1}\\
&-\frac{\Delta\tilde{\xi}^3}{3!}\left(\frac{\mathcal{J}_n+\mathcal{J}_{n-1}+\mathcal{J}_{n-2}}{\mathcal{J}_{n+1}}\right)^3 f_n^{(3)n+1}+\cdots,\\
f_n^{(1)n+1} =& f_n^{(1)n+1},\\
f_{n-1}^{(1)n} =& \frac{\mathcal{J}_n}{\mathcal{J}_{n+1}}f_n^{(1)n+1}-\Delta\tilde{\xi}\left(\frac{\mathcal{J}_n}{\mathcal{J}_{n+1}}\right)^2 f_n^{(2)n+1}+\frac{\Delta\tilde{\xi}^2}{2!}\left(\frac{\mathcal{J}_n}{\mathcal{J}_{n+1}}\right)^3 f_n^{(3)n+1}+\cdots.
\end{aligned}$$

The equations for the coefficients in (E.3) from f_n to $f_n^{(4)n+1}$ are

$$\begin{aligned}
&a+b+c+d=0,\\
&-b\frac{\mathcal{J}_n}{\mathcal{J}_{n+1}}-c\left(\frac{\mathcal{J}_n+\mathcal{J}_{n-1}}{\mathcal{J}_{n+1}}\right)-d\left(\frac{\mathcal{J}_n+\mathcal{J}_{n-1}+\mathcal{J}_{n-2}}{\mathcal{J}_{n+1}}\right)=1+\alpha\frac{\mathcal{J}_n}{\mathcal{J}_{n+1}},\\
&\frac{b}{2!}\left(\frac{\mathcal{J}_n}{\mathcal{J}_{n+1}}\right)^2+\frac{c}{2!}\left(\frac{\mathcal{J}_n+\mathcal{J}_{n-1}}{\mathcal{J}_{n+1}}\right)^2+\frac{d}{2!}\left(\frac{\mathcal{J}_n+\mathcal{J}_{n-1}+\mathcal{J}_{n-2}}{\mathcal{J}_{n+1}}\right)^2=-\alpha\left(\frac{\mathcal{J}_n}{\mathcal{J}_{n+1}}\right)^2,\\
&-\frac{b}{3!}\left(\frac{\mathcal{J}_n}{\mathcal{J}_{n+1}}\right)^3-\frac{c}{3!}\left(\frac{\mathcal{J}_n+\mathcal{J}_{n-1}}{\mathcal{J}_{n+1}}\right)^3-\frac{d}{3!}\left(\frac{\mathcal{J}_n+\mathcal{J}_{n-1}+\mathcal{J}_{n-2}}{\mathcal{J}_{n+1}}\right)^3=\frac{\alpha}{2!}\left(\frac{\mathcal{J}_n}{\mathcal{J}_{n+1}}\right)^3,\\
&\frac{b}{4!}\left(\frac{\mathcal{J}_n}{\mathcal{J}_{n+1}}\right)^4+\frac{c}{4!}\left(\frac{\mathcal{J}_n+\mathcal{J}_{n-1}}{\mathcal{J}_{n+1}}\right)^4+\frac{d}{4!}\left(\frac{\mathcal{J}_n+\mathcal{J}_{n-1}+\mathcal{J}_{n-2}}{\mathcal{J}_{n+1}}\right)^4=-\frac{\alpha}{3!}\left(\frac{\mathcal{J}_n}{\mathcal{J}_{n+1}}\right)^4,
\end{aligned}$$

and the lth-derivative for $f_n^{(l)n+1}$ is

$$\begin{aligned}
&(-1)^l\frac{b}{l!}\left(\frac{\mathcal{J}_n}{\mathcal{J}_{n+1}}\right)^l+(-1)^l\frac{c}{l!}\left(\frac{\mathcal{J}_n+\mathcal{J}_{n-1}}{\mathcal{J}_{n+1}}\right)^l\\
&+(-1)^l\frac{d}{l!}\left(\frac{\mathcal{J}_n+\mathcal{J}_{n-1}+\mathcal{J}_{n-2}}{\mathcal{J}_{n+1}}\right)^l=(-1)^{l+1}\frac{\alpha}{(l-1)!}\left(\frac{\mathcal{J}_n}{\mathcal{J}_{n+1}}\right)^l.
\end{aligned}$$

Bibliography

1. Abdallah, S. Numerical solutions for the incompressible Navier-Stokes equations in primitive variables using a non-staggered grid, II. *Journal of Computational Physics* **70,** 193–202 (1987).
2. Abdallah, S. Numerical solutions for the pressure Poisson equation with Neumann boundary conditions using a non-staggered grid, I. *Journal of Computational Physics* **70,** 182–192 (1987).
3. Adison, H. *Principles and Practice of Finite Volume Method* ISBN: 9781632404176 (ML Books International, 2015).
4. Airbus. *Photo gallery*
5. Angermann, L. & Wang, S. A super-convergent unsymmetric finite volume method for convection-diffusion equations. *Journal of Computational and Applied Mathematics* **358,** 179–189 (2019).
6. Anthonissen, M. J. H. & ten Thije Boonkkamp, J. H. M. *A compact high order finite volume scheme for advection-diffusion-reaction equations* in *Numerical Analysis and Applied Mathematics (Proceedings ICNAAM 2009)* Crete, Sept. 18–22, 2009 (eds Simos, T. E., Psihoyios, G. & Tsitouras, C.) (Greece, 2009).
7. Babuska, I., Andersson, B., Guo, B., Melenk, J. M. & Oh, H. S. Finite element method for solving problems with singular solutions. *Journal of Computational and Applied Mathematics* **74,** 51–70 (1996).
8. Baeza, A., Burger, R., Mulet, P. & Zorio, D. On the Efficient Computation of Smoothness Indicators for a Class of WENO Reconstructions. *Journal of Scientific Computing* **80,** 1240–1263 (2019).
9. Bank, R. E., Burgler, J. F., Fichtner, W. & Smith, R. K. Some upwinding techniques for finite element approximations of convection-diffusion equations. *Numerische Mathematik* **58,** 185–202 (1990).
10. Beck, A. D. *et al.* High-order discontinuous Galerkin spectral element methods for transitional and turbulent flow simulations. *International Journal for Numerical Methods in Fluids* **76,** 522–548 (2014).
11. Belytschko, T., Krongauz, Y., Organ, D., Fleming, M. & Krysl, P. Meshless methods: An overview and recent developments. *Computer Methods in Applied Mechanics and Engineering* **139,** 3–47 (1996).
12. Berger, M. J., Aftosmis, M. J. & Murman, S. M. Analysis of Slope Limiters on Irregular Grids. *AIAA Journal* **302,** 1–22 (2005).
13. Bhatnagar, P., Gross, E. & Krook, M. A Model for Collision Processes in Gases. I. Small Amplitude Processes in Charged and Neutral One-Component Systems. *Physical Review* **94,** 511–525 (1954).
14. Bianchini, R. & Gosse, L. A truly two-dimensional discretization of drift-diffusion equations on cartesian grids. *SIAM Journal on Numerical Analysis* **56,** 2845–2870 (2018).

15. Black, K. A conservative spectral element method for the approximation of compressible fluid flow. *Kybernetika* **35,** 133–146 (1999).
16. Boris, J. P. & Book, D. L. Flux-corrected transport. I. SHASTA, a fluid transport algorithm that works. *Journal of Computational Physics* **11,** 38–69 (1973).
17. Brennen, C. E. *Fundamentals of Multiphase Flow* ISBN: 9780511807169 (Cambringe University Press, 2014).
18. Broersen, D. & Stevenson, R. A robust Petrov-Galerkin discretisation of convection-diffusion equations. *Computers & Mathematics with Applications* **68,** 1605–1618 (2014).
19. Bruno, O. P. & Jimenez, E. Higher-Order Linear-Time Unconditionally Stable Alternating Direction Implicit Methods for Nonlinear Convection-Diffusion Partial Differential Equation Systems. *ASME Journal of Fluids Engineering* **136,** 060904 (2014).
20. Burden, R. & Faires, J. *Numerical Analysis* ISBN: 9781305253667 (Cengage Learning, Inc, 2016).
21. Butcher, J. C. *Numerical Methods for Ordinary Differential Equations* ISBN: 9781119121503 (Wiley, 2016).
22. Butterweck, M. & Pozorski, J. Inverse method for viscous flow design using stream-function coordinates. *Acta Mechanica* **224,** 353–361 (2013).
23. Cada, M. & Torrilhon, M. *Compact third order limiter functions for Finite-Volume-Methods* tech. rep. (Swiss Federal Institute of Technology, Zurich, 2008).
24. Canuto, C. G., Hussaini, M. Y., Quarteroni, A. & Zang, T. A. *Spectral Methods. Fundamentals in Single Domains* ISBN: 9783540307259 (Springer, 2006).
25. Carslaw, H. S. & Jaeger, J. C. *Conduction of Heat in Solids* ISBN: 9780198533030 (Oxford University Press, 1959).
26. Castro-Orgaz, O. & Hager, W. H. *Shallow Water Hydraulics* ISBN: 9783030130732 (Springer, 2019).
27. Celik, I. & Zhang, V. M. Calculation of Numerical Uncertainty Using Richardson Extrapolation. Application to Some Simple Turbulent Flow Calculations. *ASME Journal of Fluids Engineering* **117,** 439–445 (1995).
28. Chen, N. X., Zhang, F. X. & Dong, M. Stream-function-coordinate (SFC) method for 2d and 3d aerodynamic inverse design in turbomachinery. *Inverse Problems in Engineering* **1,** 207–229 (1995).
29. Chu, P. C. & Fan, C. A Three-Point Combined Compact Difference Scheme. *Journal of Computational Physics* **140,** 370–399 (1998).
30. Chu, V. H. & Gao, C. False diffusion produced by flux limiters. *Computational Thermal Sciences: An International Journal* **5,** 503–520 (2013).
31. Collatz, L. *The Numerical Treatment of Differential Equations* ISBN: 9783662054567 (Springer, 1960).

32. Cook, A. W. & Cabot, W. H. A high-wavenumber viscosity for high-resolution numerical methods. *Journal of Computational Physics* **195,** 594–601 (2004).
33. Cui, M. A high-order compact exponential scheme for the fractional convection-diffusion equation. *Journal of Computational and Applied Mathematics* **255,** 404–416 (2014).
34. Cui, M. Compact exponential scheme for the time fractional convection-diffusion reaction equation with variable coefficients. *Journal of Computational and Applied Mathematics* **280,** 143–163 (2015).
35. Da Veiga, L. B. *et al.* Basic principles of virtual element methods. *Mathematical models & methods in applied sciences* **23,** 199–2014 (2019).
36. Dai, R., Zhang, J. & Wang, Y. Higher order ADI method with completed Richardson extrapolation for solving unsteady convection-diffusion equations. *Computers & Mathematics with Applications* **71,** 431–442 (2016).
37. Darian, H. M., Esfahanian, V. & Hejranfar, K. A shock-detecting sensor for filtering of high-order compact finite difference schemes. *Journal of Computational Physics* **230,** 494–514 (2011).
38. Davidson, P. A. *An Introduction to Magnetohydrodinamics* ISBN: 9780511626333 (Cambridge University Press, 2001).
39. De G. Allen, D. N. & Southwell, R. V. Relaxation Methods applied to determine the motion, in two dimensions, of viscous fluid past a fixed cylinder. *The Quartely Journal of Mechanics and Applied Mathematics* **8,** 129–145 (1955).
40. De Las Casas Gomez, A. & de La Cueva, A. V. *El Canal Imperial de Aragon* ISBN: 8495306093 (Caja de Ahorrros de la Inmaculada de Aragon, 1999).
41. De Vahl Davis, G. & Mallinson, G. D. An evaluation of upwind and central difference approximations by a study of recirculating flow. *Computers & Fluids* **4,** 29–43 (1976).
42. Delbosc, N., Summers, J., Khan, A., Kapur, N. & Noakes, C. Optimized implementation of the Lattice Boltzmann Method on a graphics processing unit towards real-time fluid simulation. *Computers & Mathematics with Applications* **67,** 462–475 (2014).
43. Delsaute, B. & Dupret, F. A Petrov-Galerkin method for convection-dominated problems. *International Journal for Numerical Methods in Fluids* **56** (2008).
44. Di Pietro, D. A. & Ern, A. *Mathematical Aspects of Discontinuous Galerkin Methods* ISBN: 9783642229794 (Springer, 2012).
45. Diskin, B. & Thomas, J. L. Comparison of Node-Centered and Cell-Centered Unstructured Finite Volume Discretizations: Inviscid Fluxes. *AIAA Journal* **94,** 836–854 (2011).
46. Diskin, B., Thomas, J., Nishikawa, E. N. H. & White, J. Comparison of Node-Centered and Cell-Centered Unstructured Finite-Volume Discretizations Part I: Viscous Fluxes. *AIAA Journal* **48,** 1–20 (2010).

47. Do Amaral, H. M. C. & dos Santos, R. G. *High Order Compact Method using Exponential Diffference Schemes in the solution of the convective diffusion equation* in *Proceedings of the XL Ibero-American Congress on Computational Methods in Engineering, ABMEC* Natal, RN, Nov. 3–5, 2019 (Brazil, 2019).

48. Dolejsi, V. & Feistauer, M. *Discontinuous Galerkin Method: Analysis and Applications to Compressible Flow* ISBN: 9783319192666 (Springer, 2015).

49. El-Mistikawy, T. M. & Werle, M. J. Numerical method for boundary layers with blowing - The exponential box scheme. *AIAA Journal* **16,** 749–751 (1978).

50. Etheridge, D. & Sandberg, M. *Building Ventilation: Theory and Measurement* ISBN: 9780471960874 (Wiley, 1996).

51. Fan, P. The standard upwind compact difference schemes for incompressible flow simulations. *Journal of Computational Physics* **322,** 74–112 (2016).

52. Fatehi, R. & Manzari, M. Error estimation in smoothed particle hydrodynamics and a new scheme for second derivatives. *Computers & Mathematics with Applications* **61,** 482–498 (2011).

53. Fatemi, E., Jerome, J. W. & Osher, S. Solution of hydrodynamic device model using high-order nonoscillatory shock capturing algorithms. *IEEE Transactions on Computer-Aided Design of Integrated Circuits and Systems* **10,** 232–244 (1991).

54. Fernandez-Pato, A., Navas-Montilla, A., Llorente-Lazaro, V. J., Garcia-Palacin, J. I. & Navascues-Alcay, S. *Convivir con el agua*

55. Ferziger, J. H. & Peric, M. *Computational Methods for Fluid Dynamics* 3rd ed. ISBN: 9783642560262 (Springer-Verlag, 2002).

56. Fiedler, M. *Special Matrices and Their Applications in Numerical Mathematics* ISBN: 9780486783482 (Martinus Nijhoff, 1986).

57. Fornberg, B. Generation of Finite Difference Formulas on Arbitrarily Spaced Grids. *Mathematics of Computation* **51,** 699–706 (1988).

58. Fu, Y., Tian, Z. F. & Liu, Y. A Compact Exponential Scheme for Solving 1D Unsteady Convection-Diffusion Equation with Neumann Boundary Conditions. *arXiv: Fluid Dynamics* (2018).

59. Garg, S. & Pant, M. Meshfree Methods: A Comprehensive Review of Applications. *International Journal of Computational Methods* **15,** 1830001 (2018).

60. Gartland, E. C. Uniform High-Order Difference Schemes for a Singularly Perturbed Two-Point Boundary Value Problem. *Mathematics of Computation* **48,** 551–564 (1987).

61. Garzon-Alvarado, D. A., Galeano, C. H. & Mantilla, J. M. Computational examples of reaction-convection-diffusion equations solution under the influence of fluid flow: First example. *Applied Mathematical Modelling* **36,** 5029–5045 (2012).

62. Gaskell, P. H. & Lau, A. K. C. Curvature compensated convective transport: SMART, A new boundedness preserving transport algorithm. *International Journal for Numerical Methods in Fluids* **8,** 617–641 (1988).

63. Gassner, G. J., Winters, A. R. & Kopriva, D. A. A well balanced and entropy conservative discontinuous Galerkin spectral element method for the shallow water equations. *Applied Mathematics and Computations* **272,** 291–308 (2016).
64. Ge, Y., Tian, Z. F. & Zhang, J. An exponential high-order compact ADI method for 3D unsteady convection-diffusion problems. *Numerical Methods for Partial Differential Equations* **29,** 186–205 (2013).
65. Gingold, R. A. & Monaghan, J. J. Smoothed particle hydrodynamics: theory and application to non-spherical stars. *Monthly Notices of the Royal Astronomical Society* **181,** 375–389 (1977).
66. Giraldo, F. X. & Restelli, M. A study of spectral element and discontinuous Galerkin methods for the Navier-Stokes equations in nonhydrostatic mesoscale atmospheric modeling: Equation sets and test cases. *Journal of Computational Physics* **227,** 3849–3877 (2008).
67. Godunov, S. K. A difference method for numerical calculation of discontinuous solutions of the equations of hydrodynamics. *Matematicheskii Sbornik* **47,** 271–306 (1959).
68. Gomez, H., Colominas, I., Navarrina, F. & Casteleiro, M. A hyperbolic model for convection-diffusion transport problems in CFD: Numerical analysis and applications. *Revista de la Real Academia de Ciencias Exactas, Físicas y Naturales. Serie A. Matemáticas* **102,** 319–334 (2008).
69. Gomez-Gesteira, M., Rogers, B. D., Dalrymple, R. A. & Crespo, A. J. C. State-of-the-art of classical SPH for free-surface flows. *Journal of Hydraulic Research* **48,** 6–27 (2010).
70. Gosse, L. Aliasing and two-dimensional well-balanced for drift-diffusion equations on square grids. *Mathematics of Computation* **89,** 139–168 (2019).
71. Gottlieb, S., Ketcheson, D. & Shu, C. W. *Strong Stability Preserving Runge-Kutta and Multistep Time Discretizations* ISBN: 9789814289269 (World Scientific, 2011).
72. Greenberg, J. M. & Leroux, A. Y. A Well-Balanced Scheme for the Numerical Processing of Source Terms in Hyperbolic Equation. *SIAM Journal on Numerical Analysis* **33,** 1–16 (1996).
73. Griffiths, D. F. & Lorenz, J. An analysis of the petrov-galerkin finite element method. *Computer Methods in Applied Mechanics and Engineering* **14,** 39–64 (1978).
74. Griffiths, G. W. & Schiesser, W. E. Linear Advection Equation. *Analysis of Partial Diferential Equations*, 7–45 (2012).
75. Guermond, J. L., Minev, P. & Shen, J. An overview of projection methods for incompressible flows. *Computers methods in applied mechanics and engineering* **195,** 6011–6045 (2004).
76. Hamdan, M. H. & Barron, R. M. Applications of von Mises coordinates in porous media flow. *Journal of Computational and Applied Mathematics* **39,** 353–361 (1992).
77. Harten, A. High Resolution Schemes for Hyperbolic Conservation Laws. *Journal of Computational Physics* **135,** 260–278 (1997).

78. Harten, A. & Osher, S. Uniformly High-Order Accurate Nonoscillatory Schemes. I. *SIAM Journal on Numerical Analysis* **24,** 279–309 (1987).

79. Harten, A., Engquist, B., Osher, S. & Chakravarthy, S. R. Uniformly high order accurate essentially non-oscillatory schemes, III. *Journal on Computational Physics* **71,** 231–303 (1987).

80. Haussmann, M. *et al.* Large-eddy simulation coupled with wall models for turbulent channel flows at high Reynolds numbers with a lattice Boltzmann method - Application to Coriolis mass flowmeter. *Computers & Mathematics with Applications* **78,** 3285–3302 (2019).

81. Holmes, M. H. *Introduction to Numerical Methods in Differential Equations* ISBN: 9780387308913 (Springer, 2000).

82. Horn, R. A. & Johnson, C. R. *Topics in Matrix Analysis* ISBN: 9780521839402 (Cambridge University Press, 1991).

83. Huang, C. WENO scheme with new smoothness indicator for Hamilton-Jacobi equation. *Applied Mathematics and Computation* **290,** 21–32 (2016).

84. Huang, C. & Chen, L. L. A simple smoothness indicator for the WENO scheme with adaptive order. *Journal of Computational Physics* **352,** 498–515 (2018).

85. Huang, L. C. *The exponential scheme for computation of natural convection flow in enclosures* tech. rep. (Lawrence Berkeley Laboratory, University of California, USA, 1988).

86. Hughes, T. J. R., Engel, G., Mazzei, L. & Larson, M. G. The Continuous Galerkin Method Is Locally Conservative. *Journal of Computational Physics* **163,** 467–488 (2000).

87. Hundsdorfer, W. & Verwer, J. G. *Numerical Solution of Time-Dependent Advection-Diffusion-Reaction Equations* ISBN: 9783540034407 (Springer, 2003).

88. Hwang, Y. H. Higher-order Exponential Difference Schemes for the Computations of the Steady Convection-Diffusion Equation. *Journal of Computational Physics* **129,** 134–159 (1996).

89. Il'in, A. M. Differencing scheme for a differential equation with a small parameter affecting the highest derivative. *Mathematical Notes of the Academy of Sciences of the USSR* **6,** 596–602 (1969).

90. Irisarri, D. Virtual element method stabilization for convection-diffusion-reaction problems using the link-cutting condition. *Calcolo* **54,** 141–154 (2017).

91. Irisarri, D. & Hauke, G. Stabilized virtual element methods for the unsteady incompressible Navier-Stokes equations. *Calcolo* **56,** 37–58 (2019).

92. Jeffrey, A. & Dai, H. *Handbook of Mathematical Formulas and Integrals* 4th ed. ISBN: 9780123742889 (Elsevier, 2008).

93. Jiang, G. S. & Shu, C. W. Weighted Essentially Non-oscillatory Schemes. *Journal of Computational Physics* **126,** 202–228 (1996).

94. Kantner, M. Generalized Scharfetter-Gummel schemes for electro-thermal transport in degenerate semiconductors using the Kelvin formula for the Seebeck coefficienti. *Journal of Computational Physics* **402,** 109091 (2020).
95. Karaa, S. A high-order ADI method for parabolic problems with variable coefficients. *International Journal of Computer Mathematics* **86,** 109–120 (2009).
96. Karaa, S. & Zhang, J. High order ADI method for solving unsteady convection–diffusion problems. *Journal of Computational Physics* **198,** 1–9 (2004).
97. Keller, J. J. Inverse Euler equations. *Zeitschrift für angewandte Mathematik und Physik* **49,** 363–383 (1998).
98. Khaledi, H. A. & Andersson, H. On vortex shedding from a hexagonal cylinder. *Physics Letters A* **375,** 4007–4021 (2011).
99. Khosla, P. K. & Rubin, S. G. A diagonally dominant second-order accurate implicit scheme. *Computers & Fluids* **2,** 207–209 (1974).
100. Koprucki, T. & Gartner, K. *Discretization scheme for drift-diffusion equations with strong diffusion enhancement* in *2012 12th International Conference on Numerical Simulation of Optoelectronic Devices (NUSOD)* (2012), 103–104.
101. Koprucki, T., Rotundo, N., Farrell, P., Doan, D. H. & Fuhrmann, J. On thermodynamic consistency of a Scharfetter-Gummel scheme based on a modified thermal voltage for drift-diffusion equations with diffusion enhancement. *Optical and Quantum Electronics* **47,** 1327–1332 (2015).
102. Korzilius, S. P., Kruisbrink, A. C. H., Yue, T., Schilders, W. H. A. & Anthonissen, M. J. H. *Momentum conserving methods that reduce particle clustering in SPH* in *9th International Smoothed Particle Hydrodynamics European Research Interest Community Workshop* Paris, June 3–5, 2014 (eds Violeau, D., Herault, A. & Joly, A.) (France, 2014).
103. Kumar, N., ten Thije Boonkkamp, J. H. M. & Koren, B. *Flux Approximation Scheme for the Incompressible Navier-Stokes Equations Using Local Boundary Value Problems* in *Numerical Mathematics and Advanced Applications ENUMATH 2015* (eds Karasozen, B., Manguoglu, M., Tezer-Sezgin, M., Goktepe, S. & Ugur, O.) (Springer International Publishing, Cham, 2016), 43–51.
104. Kuzmin, D. *A Guide to Numerical Methods for Transport Equations* (University Erlangen-Nuremberg, 2010).
105. Law, C. K. *Combustion Physics* ISBN: 9780511754517 (Cambridge University Press, 2006).
106. Ledoux, R. *Understanding the dynamics of wind-driven ocean circulation* B.S. Thesis (University of Groningen, 2015).
107. Lee, W. & Kim, D. W. Localized axial Green's function method for the convection–diffusion equations in arbitrary domains. *Journal of Computational Physics* **275,** 390–414 (2014).
108. Lele, S. K. Compact finite difference schemes with Spectral-like resolution. *Journal of Computational Physics* **103,** 16–42 (1992).

109. Leonard, B. P. A stable and accurate convective modelling procedure based on quadratic upstream interpolation. *Computer Methods in Applied Mechanics and Engineering* **19,** 59–98 (1979).

110. Leonard, B. P. Simple high accuracy resolution program for convective modelling of discontinuities. *International Journal for Numerical Methods in Fluids* **8,** 1291–1318 (1988).

111. Leonard, B. P. & Drummond, J. E. Why you should not use "hybrid", "power-law" or related exponential schemes for convective modelling - There are much better alternatives. *Journal for Numerical Methods in Fluids* **20,** 421–442 (1995).

112. LeVeque, R. J. *Finite-Volume Method for Hyperbolic Problems* ISBN: 9780511791253 (Cambridge University Press, 2002).

113. Li, S. & Liu, W. K. *Meshfree Particle Methods* ISBN: 9783540714712 (Springer, 2004).

114. Li, W., Pan, J. & Ren, Y. X. The discontinuous Galerkin spectral element methods for compressible flows on two-dimensional mixed grids. *Journal of Computational Physics* **364,** 314–346 (2018).

115. Liu, X., Zhang, S., Zhang, H. & Shu, C. W. A new class of central compact schemes with spectral-like resolution I: Linear schemes. *Journal of Computational Physics* **248,** 235–256 (2013).

116. Liu, X., Zhang, S., Zhang, H. & Shu, C. W. A new class of central compact schemes with spectral-like resolution II: Hybrid weighted nonlinear schemes. *Journal of Computational Physics* **284,** 133–154 (2015).

117. Liu, X. D., Osher, S. & Chan, T. Weighted Essentially Non-oscillatory Schemes. *Journal of Computational Physics* **115,** 200–212 (1994).

118. Llorente, V. J. & Pascau, A. Compact Integration Rules as a quadrature method with some applications. *Computers & Mathematics with Applications* **79,** 1241–1265 (2020).

119. Llorente, V. J., Rubio, G., Pascau, A., Ferrer, E. & Arici, M. Comparison of the ENATE approach and discontinuous Galerkin spectral element method in 1D nonlinear transport equations. *Computer Assisted Methods in Engineering and Science* **23,** 133–146 (2017).

120. Llorente, V. J., ten Thije Boonkkamp, J. H. M., Pascau, A. & Anthonissen, M. J. H. Similarities and differences of two exponential schemes for convection-diffusion problems: The FV-CF and ENATE schemes. *Applied Mathematics and Computation* **365,** 124700 (2020).

121. Lucy, L. L. A numerical approach to the testing of the fission hypothesis. *Astronomical Journal* **82,** 1013–1024 (1977).

122. Luo, C., Dlugogorski, B. Z., Moghtaderi, B. & Kennedy, E. M. Modified exponential schemes for convection-diffusion problems. *Communications in Nonliner Science and Numerical Simulation* **13,** 369–379 (2008).

123. MacKinnon, R. J. & Johnson, R. W. Differential-equation-based representation of truncation errors for accurate numerical simulation. *International Journal for Numerical Methods in Fluids* **13,** 739–757 (1991).

124. Malizia, F. & Blocken, B. Bicycle aerodynamics: History, state-of-the-art and future perspectives. *Journal of Wind Engineering & Industrial Aerodynamics* **200,** 104134 (2020).

125. Marchi, C. H. *et al.* Polynomial interpolation with repeated Richardson extrapolation to reduce discretization error in CFD. *Applied Mathematical Modelling* **40,** 8872–8885 (2016).

126. Marshall, J. & Nurser, G. On the recirculation of the subtropical gyre. *Quarterly Journal of the Royal Meteorological Society* **114,** 1517–1534 (1988).

127. Martin, M. H. A new approach to problems in two dimensional flow. *Quarterly of Applied Mathematics* **8,** 137–150 (1950).

128. Martin, M. H. The flow of a viscous fluid, I. *Archive for Rational Mechanics and Analysis* **41,** 266–286 (1971).

129. Matsumoto, D. *et al.* Erosion and sedimentation during the September 2015 flooding of the Kinu River, central Japan. *Scientific Reports* **6,** 34168 (2016).

130. Mattheij, R. M. M., Rienstra, S. W. & ten Thije Boonkkamp, J. H. M. *Partial Differential Equations: Modeling, Analysis, Computation* ISBN: 9780898715941 (Society for Industrial and Applied Mathematics, 2005).

131. Mehta, R. C. Numerical simulation of supersonic flow past reentry capsules. *Shock Waves* **15,** 31 (2006).

132. Mengolini, M., Benedetto, M. F. & Aragon, A. M. An engineering perspective to the virtual element method and its interplay with the standard finite element method. *Computer Methods in Applied Mechanics and Engineering* **350,** 995–1023 (2019).

133. Mickens, R. E. *Nonstandard Finite Difference Models of Differential Equations* ISBN: 9789810214586 (World Scientific, 1993).

134. Mickens, R. E. Nonstandard Finite Difference Schemes for Differential Equations. *Journal of Difference Equations and Applications* **8,** 823–847 (2002).

135. Mierke, D., en, C. J. & Rung, T. An efficient algorithm for the calculation of sub-grid distances for higher-order LBM boundary conditions in a GPU simulation environment. *Computers & Mathematics with Applications* **79,** 66–87 (2020).

136. Miller, J. J. H. *Computational methods for boundary and interior layers in several dimensions* ISBN: 9780906783924 (Boole Press, 1991).

137. Mishra, N. & Yedida, S. V.S. S. Efficient exponential compact higher order difference scheme for convection dominated problems. *Mathematics and Computers in Simulation* **82,** 617–628 (2011).

138. Mohamed, N., Mohamed, S. A. & Seddek, L. F. Exponential higher-order compact scheme for 3D steady convection-diffusion problem. *Applied Mathematics and Computation* **232,** 1046–1061 (2014).

139. Mojtabi, A. & Deville, M. O. One-dimensional linear advection-diffusion equation: Analytical and finite element solutions. *Computers & Fluids* **107,** 189–195 (2015).

140. Monaghan, J. J. Simulating Free Surface Flows with SPH. *Journal of Computational Physics* **110,** 399–406 (1994).

141. Montecinos-Guzman, G. *Numerical methods for advection-diffusion-reaction equations and medical applications* PhD thesis (Universita degli Studi di Trento, 2014).

142. Morton, K. W. *Numerical Solution of Convection-Diffusion Problems* 1st ed. ISBN: 9780412564406 (CRC Press LLC, 1995).

143. Moukalled, F., Mangani, L. & Darwish, M. *The Finite Volume Method in Computational Fluid Dynamics. An advanced Introduction with OpenFOAM and Matlab* ISBN: 9783319168746 (Springer, 2016).

144. NASA. *Visible Earth*

145. NASA. *Supersonic Flight*

146. Pascau, A. An exact discretization for a transport equation with piecewise-constant coefficients and arbitrary source. *Computers & Fluids* **75,** 42–50 (2013).

147. Pascau, A. & Arici, M. An accurate discretization for an inhomogeneous transport equation with arbitrary coefficients and source. *Computers & Fluids* **125,** 101–115 (2016).

148. Pascau, A., Perez, C. & Sanchez, D. A well-behaved scheme to model strong convection in a general transport equation. *International Journal of Numerical Methods for Heat & Fluid Flow* **5,** 75–87 (1995).

149. Pasmanter, R. A. Exact and Approximate Solutions of the Convection-Diffusion Equation. *The Quarterly Journal of Mechanics and Applied Mathematics* **38,** 1–26 (1985).

150. Patankar, S. V. *Numerical Heat Transfer and Fluid Flow* ISBN: 9780070487405 (McGraw-Hill book company, 1980).

151. Patel, M. K., Markatos, N. C. & Cross, M. Method of reducing false-diffusion errors in convection-diffusion problems. *Applied Mathematical Modelling* **9,** 302–306 (1985).

152. Patidar, K. C. Nonstandard finite difference methods: recent trends and further developments. *Journal of Difference Equations and Applications* **22,** 817–849 (2016).

153. Patriarca, M., Farrel, P., Fuhrmann, J. & Koprucki, T. Highly accurate quadrature-based Scharfetter-Gummel schemes for charge transport in degenerate semiconductors. *Computer Physics Communications* **235,** 40–49 (2019).

154. Pedlosky, J. *Geophysical Fluid Dynamics* ISBN: 9780387963877 (Springer, 1987).

155. Pedlosky, J. The Dynamics of the Oceanic Subtropical Gyres. *Science* **248,** 316–322 (1990).

156. Perea, J. J. & Cordero, J. M. *A New Kernel-Functions Family to Improve the Accuracy and Stability in SPH Simulations* in *Congress on Numerical Methods in Engineering CMN2017* Valencia, July 3–5, 2017 (Spain, 2017).

157. Perez-Guerrero, J. S., Pimentel, L. C. G., Skaggs, T. H. & van Genuchten, M. T. Analytical solution of the advection-diffusion transport equation using a change-of-variable and integral transform technique. *International Journal of Heat and Mass Transfer* **52,** 3297–3304 (2009).

158. Perot, J. B. Discrete Conservation Properties of Unstructured Mesh Schemes. *Annual Review of Fluid Mechanics* **43,** 299–318 (2011).

159. Peyret, R. & Taylor, T. D. *Computational Methods for Fluid Flow* ISBN: 9783642859526 (Springer, 1983).

160. Philip, J. R. Some exact solutions of convection-diffusion and diffusion equations. *Water Resources Research* **30,** 3545–3551 (1994).

161. Pinelli, A., Naqavi, I. Z., Piomelli, U. & Favier, J. Immersed-boundary methods for general finite-difference and finite-volume Navier-Stokes solvers. *Journal of Computational Physics* **229,** 9073–9091 (2010).

162. Piprek, J. *Handbook of Optoelectronic Device Modeling and Simulation: Lasers, Modulators, Photodetectors, Solar Cells, and Numerical Methods, Vol. 2 (Series in Optics and Optoelectronics)* ISBN: 9781498749565 (CRC Press, 2017).

163. Pletcher, R. H., Tannehill, J. C. & Anderson, D. A. *Computational Fluid Mechanics and Heat Transfer* ISBN: 9781591690375 (CRC Press, 2012).

164. Polyakov, S. V. Exponential difference schemes with double integral transformation for solving convection-diffusion equations. *Mathematical Models and Computer Simulations* **5,** 338–340 (2013).

165. Polyakov, S. V. Exponential schemes for solving evolutionary equations on non-regular grids. *Scientific Notes of Kazan State University, Physics and Mathematics* **149,** 121–131 (2007).

166. Polyakov, S. V., Karamzin, Y. N., Kudryashova, T. A. & Tsybulin, I. Exponential difference schemes for solving boundary-value problems for convection-diffusion type equations. *Mathematical Models and Computer Simulations* **9,** 71–82 (2017).

167. Powers, D. *Boundary Value Problems and Partial Differential Equations* 6th ed. ISBN: 9780123747198 (Academic Press, 2009).

168. Prandtl, L. & Betz, A. *Vier Abhandlungen zur Hydrodynamik und Aerodynamik* ISBN: 9783941875753 (Universitätsverlag Göttingen, 2010).

169. Prasanna-Kumar, S. S., Patnaik, B. S. V. & Liu, G. R. A new kernel function for SPH with applications to free surface flows. *International Journal for Numerical Methods in Enigeering* **111,** 383–400 (2017).

170. Prosperetti, A. & Tryggvason, G. *Computational Methods for Multiphase Flow* ISBN: 9780521847643 (Cambridge University Press, 2007).

171. Rahman, S., Yusoff, M. Z. & Hasini, H. Comparison of cell centered and cell vertex scheme in the calculation of high speed compressible flows. *AIP Conference Proceedings* **1440,** 178–189 (2012).

172. Raithby, G. D. Skew upstream differencing schemes for problems involving fluid flow. *Computer Methods in Applied Mechanics and Engineering* **9,** 153–164 (1976).

173. Ramos, J. I. Exponentially-fitted methods on layer-adapted meshes. *Applied Mathematics and Computation* **167,** 1311–1330 (2005).

174. Ramos, J. I. On diffusive methods and exponentially fitted techniques. *Applied Mathematics and Computation* **103,** 69–96 (1999).

175. Reddy, J. N. & Gartling, D. K. *The Finite Element Method in Heat Transfer and Fluid Dynamics* ISBN: 9781420085983 (CRC Press, 2010).

176. Reed, W. H. & Hill, T. R. Triangular mesh methods for the neitron transport equation. *Los Alamos Report LA-UR-73-479* (1973).

177. Roos, H. G. Ten ways to generate the Il'in and related schemes. *Journal of Computational and Applied Mathematics* **53,** 43–59 (1994).

178. Roos, H. G., Stynes, M. & Tobiska, L. *Robust Numerical Methods for Singularly Perturbed Differential Equations* ISBN: 9783540344667 (Springer, 2008).

179. Rose, M. J. Commercial vehicle fuel economy - The correlation between aerodynamic drag and fuel consumption of a typical truck. *Journal of Wind Engineering and Industrial Aerodynamics* **9,** 89–100 (1981).

180. Rubin, S. G. & Khosla, P. K. Polynomial interpolation methods for viscous flow calculations. *Journal of Computational Physics* **24,** 217–244 (1977).

181. Rubio-Calzado, G. *Truncation error estimation in the Discontinuous Galerkin Spectral Element Method* PhD thesis (Universidad Politecnica de Madrid, 2015).

182. Sacco, R. Exponentially fitted shape functions for advection-dominated flow problems in two dimensions. *Journal of Computational and Applied Mathematics* **67,** 161–165 (1996).

183. Saleem, R. A. A. & Kozlowski, T. Development of High-Resolution Total Variation Diminishing Scheme for Linear Hyperbolic Problems. *Journal of Computational Engineering* **2015,** 1–11 (2015).

184. Samimy, M., Breuer, K. S., Leal, L. G. & Steen, P. H. *A Gallery of Fluid Motion* ISBN: 9780521827737 (Cambridge University Press, 2003).

185. Santos, M. L., Pfeil, M. S. & Coutinho, A. L.G. A. *Vortex shedding by LES 3D numerical simulation* in *Proceedings of the XXXVIII Iberian Latin-American Congress on Computational Methods in Engineering* Florianopolis,Santa Catarina, Nov. 5–8, 2017 (eds Faria, P. O., Lopez, R. H., Miguel, L. F. F., Gomes, W. J. S. & Noronha, M.) (Brazil, 2017).

186. Sayevand, K., Machado, J. T. & Moradi, V. A new non-standard finite difference method for analyzing the fractional Navier-Stokes equations. *Computers & Mathematics with Applications* **78,** 1681–1694 (2019).

187. Schäfer, M. *Computational Engineering - Introduction to Numerical Methods* ISBN: 9783540306856 (Springer-Verlag, 2006).

188. Scharfetter, D. L. & Gummel, H. K. Large-signal analysis of a silicon Read diode oscillator. *IEEE Transactions on Electron Devices* **16,** 64–77 (1969).

189. Seibold, B. *M-Matrices in Meshless Finite Difference Methods* PhD thesis (University of Kaiserslautern, 2006).

190. Sen, S. A new family of (5,5)CC-4OC schemes applicable for unsteady Navier–Stokes equations. *Journal of Computational Physics* **251,** 251–271 (2013).

191. Sengupta, K., Mashayek, F. & Jacobs, G. B. Large-Eddy Simulation Using a Discontinuous Galerkin Spectral Element Method. *AIAA Journal* **402,** 1–12 (2007).

192. Sengupta, T. *High Accuracy Computing Methods. Fluid Flows and Wave Phenomena* ISBN: 9781139151825 (Cambridge University Press, 2013).

193. Serra, M., Crouzat, S., Simon, G. & Vetel, J. Material spike formation in highly unsteady separated flows. *Journal of Fluids Mechanics* **883,** 1–27 (2020).

194. Sharman, K., Straka, R. & Tavares, F. Lattice Boltzmann Methods for Industrial Applications. *Industrial & Engineering Chemistry Research* **58,** 16205–16234 (2019).

195. Shu, C. W. in *High-Order Methods for Computational Physics. Lecture Notes in Computational Science and Engineering* (eds Barth, T. J. & Deconinck, H.) 439–582 (Springer, Berlin, 1999).

196. Shu, C. W. & Osher, S. Efficient implementation of essentially non-oscillatory shock-capturing schemes. *Journal Computational Physics* **77,** 439–471 (1988).

197. Shu, C. W. & Osher, S. Efficient implementation of essentially non-oscillatory shock-capturing schemes, II. *Journal Computational Physics* **83,** 32–78 (1989).

198. Shu, S. W. Numerical experiments on the accuracy of ENO and modified ENO schemes. *Journal of Scientific Computing* **5,** 127–149 (1990).

199. Simmonds, J. G. *A Brief on Tensor Analysis* ISBN: 9780387940885 (Springer, 1994).

200. Spalding, D. B. A novel finite difference formulation for differential expressions involving both first and second derivatives. *International Journal for Numerical Methods in Engineering* **4,** 551–559 (1972).

201. Spekreijse, S. Multigrid Solution of Monotone Second-Order Discretizations of Hyperbolic Conservation Laws. *Mathematics of Computation* **49,** 135–155 (1987).

202. Spurk, J. H. & Aksel, N. *Fluid Mechanics* ISBN: 9783540735366 (Springer, 2008).

203. Stommel, H. Transactions of the American Geophysical Union. *Transactions, American Geophysical Union* **29,** 202–206 (1948).

204. Stynes, M. Convection-diffusion-reaction problems, SDFEM/SUPG and a priori meshes. *International Journal of Computing Science and Mathematics* **1,** 412–431 (2007).

205. Swanson, R. C. & Radespie, R. Cell Centered and Cell Vertex Multigrid Schemes for the Navier-Stokes Equations. *AIAA Journal* **29,** 697–703 (1991).

206. Sweby, P. K. High Resolution Schemes Using Flux Limiters for Hyperbolic Conservation Laws. *SIAM Journal on Numerical Analysis* **21,** 995–1011 (1984).

207. Takakura, Y. Direct-expansion forms of ADER schemes for conservation laws and their verification. *Journal of Computational Physics* **219,** 855–878 (2006).

208. Teimourian, A., Yazdi, S. G. & Hacisevki, H. Vortex Shedding: A Review on Flat Plate. *Fluid Dynamics* **53,** 212–221 (2018).

209. Ten Thije Boonkkamp, J. H. M. & Anthonissen, M. J. H. The Finite Volume-Complete Flux Scheme for Advection-Diffusion-Reaction Equations. *Journal of Scientific Computing* **46,** 47–70 (2011).

210. Ten Thije Boonkkamp, J. H. M., Anthonissen, M. J. H. & Kwant, R. *A Two-Dimensional Complete Flux Scheme in Local Flow Adapted Coordinates* in *Finite Volumes for Complex Applications VIII - Hyperbolic, Elliptic and Parabolic Problems. FVCA 2017* (eds Cances, C. & Omnes, P.) (Springer International Publishing, Cham, 2017), 437–445.

211. Ten Thije Boonkkamp, J. H. M., Kumar, B. V. R., Kumar, S. & Parpaei, M. *Complete Flux Scheme for Conservation Laws Containing a Linear Source* in *Numerical Mathematics and Advanced Applications ENUMATH 2015* (eds Karasozen, B., Manguoglu, M., Tezer-Sezgin, M., Goktepe, S. & Ugur, O.) (Springer International Publishing, Cham, 2016), 23–31.

212. Thiart, G. D. Finite difference scheme for the numerical solution of fluid flow and heat transfer problems on non staggered grids. *Numerical Heat Transfer, Part B: Fundamentals* **17,** 43–62 (1990).

213. Thiart, G. D. Improved Finite-Difference scheme for the solution of Convection-Diffusion problems with the SIMPLEN algorithm. *Numerical Heat Transfer, Part B: Fundamentals* **18,** 81–95 (1990).

214. Thomas, J. W. *Numerical Partial Differential Equations: Finite Difference Methods* ISBN: 9780387979991 (Springer, 1995).

215. Thomee, V. From finite differences to finite elements A short history of numerical analysis of partial differential equations. *Journal of Computational and Applied Mathematics* **128,** 1–54 (2001).

216. Tian, Z. F. & Dai, S. Q. High-order compact exponential finite difference methods for convection–diffusion type problems. *Journal of Computational Physics* **220,** 952–974 (2007).

217. Tian, Z. F. & Ge, Y. B. A fourth-order compact ADI method for solving two-dimensional unsteady convection-diffusion problems. *Journal of Computational and Applied Mathematics* **198,** 268–286 (2007).

218. Tian, Z. F. & Yu, P. X. A high-order exponential scheme for solving 1D unsteady convection–diffusion equations. *Journal of Computational and Applied Mathematics* **235,** 2477–2491 (2011).

219. Turner, M. J., Clough, R. W., Martin, H. C. & Topp, L. J. Stiffness and Deflection Analysis of Complex Structures. *Journal of Aeronautical Sciences* **9,** 805–823 (1956).

220. Tyler, J. *Analysis and Implementation of High-Order Compact Finite Difference Schemes* MA thesis (Brigham Young University, All Theses and Dissertations., Nov. 2007).

221. Vallis, G. *Atmospheric and Oceanic Fluid Dynamics. Fundamentals and Large-Scale Circulation* ISBN: 9781107588417 (Springer, 2017).

222. Van Leer, B. Towards the ultimate conservative difference scheme V: A second-order sequel to Godunov's method. *Journal of Computational Physics* **32,** 101–136 (1979).

223. Van Leer, B. Upwind-difference Methods for Aerodynamic Problems Governed by the Euler Equations. *Lectures in Applied Mathematics (Part 2)* **22,** 327–336 (1985).

224. Van den Berkmortel, S. *Extension of the finite volume-complete flux scheme to linear source terms* B.S. Thesis (Eindhoven University of Technology, 2016).

225. Van't Hof, B., ten Thije Boonkkamp, J. H. M. & Mattheij, R. M. M. Discretization of the stationary convection-diffusion-reaction equation. *Numerical Methods for Partial Differential Equations* **14,** 607–625 (1998).

226. Varga, R. S. *Matrix Iterative Analysis* ISBN: 9783540663218 (Springer-Verlag Berlin Heidelberg, 2000).

227. Versteeg, H. K. & Malalasekera, W. *An Introduction to Computational Fluid Dynamics. The finite volume method* 2nd ed. ISBN: 9780131274983 (Pearson Education Limited, 2007).

228. Violeau, D. *Fluid Mechanics and the SPH Method: Theory and Applications* ISBN: 9780199655526 (Oxford University Press, 2012).

229. Virag, Z. & Trincas, G. An improvement of the exponential differencing scheme for solving the convection-diffusion equation. *Advances in Engineering Software* **19,** 1–20 (1994).

230. Visbal, M. R. & Gaitonde, D. V. High-Order-Accurate Methods for Complex Unsteady Subsonic Flows. *AIAA Journal* **37,** 1231–1239 (1999).

231. Von Mises, R. E. Bemerkungen zur Hydrodynamik. *Zeitschrift für Angewandte Mathematik und Mechanik* **6,** 421–442 (1927).

232. Wang, C. A New Way to Generate an Exponential Finite Difference Scheme for 2D Convection-Diffusion Equations. *Journal of Applied Mathematics* **2014,** 457938 (2014).

233. Wang, Q. W., Wei, J. G. & Tao, W. Q. An improved numerical algorithm for solution of convective heat transfer problems on nonstaggered grid system. *Heat and Mass Transfer* **33,** 273–280 (1998).

234. Wang, Y. M. & Wang, T. Error analysis of a high-order compact ADI method for two-dimensional fractional convection-subdiffusion equations. *Calcolo* **53,** 301–330 (2016).

235. Wesseling, P. *Principles of Computational Fluid Dynamics* ISBN: 9783540678533 (Springer, 2001).

236. Wilcox, D. C. *Turbulence Modelling for CFD* ISBN: 9781928729082 (DCW Industries, 2006).

237. Windisch, G. *M-matrices in Numerical Analysis* ISBN: 9783663108184 (Springer, 1989).

238. Wong, H. H. & Raithby, G. D. Improved finite-difference methods based on a critical evaluation of the approximation errors. *Numerical Heat Transfer* **2,** 139–163 (1979).

239. Wu, S., Peng, B. & Tian, Z. F. Exponential compact ADI method for a coupled system of convection-diffusion equations arising from the 2D unsteady magnetohydrodynamic (MHD) flows. *Applied Numerical Mathematics* **146,** 89–122 (2019).

240. Wu, X., Liang, J. & Zhao, Y. A new smoothness indicator for third-order WENO scheme. *International Journal for Numerical Methods in Fluids* **81,** 451–459 (2015).

241. Yaghoubi, A. & Najafi, H. S. Comparison between standard and non-standard finite difference methods for solving first and second order ordinary differential equations. *International Journal of Applied Mathematical Research* **4,** 316–324 (2015).

242. Yang, H., Habchi, S. & Przekwas, A. General strong conservation formulation of Navier-Stokes equations in nonorthogonal curvilinear coordinates. *AIAA Journal* **32,** 936–941 (1994).

243. Yang, X. F., Peng, S. L. & Liu, M. B. A new kernel function for SPH with applications to free surface flows. *Applied Mathematical Modelling* **38,** 3822–3833 (2014).

244. Yapici, K. A comparison study on high-order bounded schemes: Flow of PTT-linear fluid in a lid-driven square cavity. *Korea-Australia rheology journal* **24,** 11–21 (2012).

245. Yong, W. in *Advances in the Theory of Shock Waves. Progress in Nonlinear Differential Equations and Their Applications* (eds Freistuhler, H. & Szepessy, A.) 259–305 (Springer, Boston, MA, 2001).

246. Zabadal, J., Ribeiro, V., van der Laan, F., Borges, V. & Melo, P. Exact solutions to advection-diffusion problems using differential constraints: Applications in heat exchangers design. *International Fournal of Mathematical Models and Methods in Applied Sciences* **6,** 811–818 (2012).

247. Zahran, Y. H. Third order TVD scheme for hyperbolic conservation laws. *Bulletin of the Belgian Mathematical Society, Simon Stevin* **14,** 259–275 (2005).

248. Zapata, M. U. & Balam, R. I. High-order implicit finite difference schemes for the two-dimensional Poisson equation. *Applied Mathematics and Computation* **309,** 222–244 (2017).

249. Zeitlin, V. *Geophysical Fluid Dynamics: Understanding (almost) everything with rotating shallow water models* ISBN: 9780198804338 (Oxford University Press, 2018).

250. Zhai, S., Gui, D., Huang, P. & Feng, X. A novel high-order ADI method for 3D fractional convection–diffusion equations. *International Communications in Heat and Mass Transfer* **66,** 212–217 (2015).

251. Zhang, D., Jiang, C., Liang, D. & Cheng, L. A review on TVD schemes and a refined flux-limiter for steady-state calculations. *Journal of Computational Physics* **302,** 114–154 (2015).

252. Zhang, L., Wang, L. & Ding, X. Exact Finite Difference Scheme and Nonstandard Finite Difference Scheme for Burgers and Burgers-Fisher Equations. *Journal of Applied Mathematics* **2014,** 597926 (2014).

253. Zhang, P., Gros, Y., Roberts, R. M. & Benard, A. *Modeling of Turbulent Flow with Particle Deposition in Curved Pipes* in *Proceedings of the 7th International Conference on Multiphase Flow* Tampa, Florida, May 30–June 4, 2010 (USA, 2010).

254. Zhang, S. & Shu, C. W. A New Smoothness Indicator for the WENO Schemes and Its Effect on the Convergence to Steady State Solutions. *Journal of Scientific Computing* **31,** 273–305 (2007).

255. Zhang, Y. T. & Shu, C. W. Chapter 5 - ENO and WENO Schemes. *Handbook of Numerical Analysis* **17,** 103–122 (2016).

256. Zhao, S., Lardjane, N. & Fedioun, I. Comparison of improved finite-difference WENO schemes for the implicit large eddy simulation of turbulent non-reacting and reacting high-speed shear flows. *Computers & Fluids* **95,** 74–87 (2014).

257. Zienkiewicz, O. C. Achievements and some unsolved problems od finite element method. *International Journal for Numerical Methods in Engineering* **47,** 9–28 (2000).

258. Zienkiewicz, O. C. & Cheung, Y. K. *The Finite Element Method in Structural and Continuum Mechanics. Numerical solution of problems in structural and continuum mechanics* (McGraw-Hill, 1967).

259. Zienkiewicz, O. C., Taylor, R. L. & Nithiarasu, P. *The finite element method for fluid dynamics* ISBN: 9781856176354 (Elsevier, 2005).

260. Zoppou, C. & Knight, J. H. Analytical solution of a spatially variable coefficient advection-diffusion equation in up to three dimensions. *Applied Mathematical Modelling* **23,** 667–685 (1999).

261. Zwillinger, D. *Handbook of Differential Equations* ISBN: 9780127843964 (Academic Press, 1997).